JOURNAL OF ACOUSTICAL SOCIETY OF INDIA

Volume 41   Number 1   January 2014

A Quarterly Publication of the JASI
http://www.acousticsindia.org

The Journal of Acoustical Society of India is a refereed journal of the Acoustical Society of India (ASI). The ASI is a non-profit national society founded in 31st July, 1971. The primary objective of the society is to advance the science of acoustics by creating an organization that is responsive to the needs of scientists and engineers concerned with acoustics problems all around the world.

Manuscripts of articles, technical notes and letter to the editor should be submitted to the Chief Editor. Copies of articles on specific topics listed above should also be submitted to the respective Associate Scientific Editor. Manuscripts are refereed by at least two referees and are reviewed by Publication Committee (all editors) before acceptance. On acceptance, revised articles with the text and figures scanned as separate files on a diskette should be submitted to the Editor by express mail. Manuscripts of articles must be prepared in strict accordance with the author instructions.

All information concerning subscription, new books, journals, conferences, etc. should be submitted to Chief Editor:

Acoustics, Ultrasonics & Vibration Section, CSIR-National Physical Laboratory, Dr. KS Krishnan Road, New Delhi 110 012, Tel: +91.11.4560.8317, Fax: +91.11.4560.9310, e-mail: mahavir@nplindia.org

Annual subscription price including mail postage is Rs. 2000/= for institutions, companies and libraries and Rs. 2000/= for individuals who are not ASI members. The Journal of Acoustical Society of India will be sent to ASI members free of any extra charge. Requests for specimen copies and claims for missing issues as well as address changes should be sent to the Editorial Office:

Acoustics, Ultrasonics & Vibration Section, CSIR-National Physical Laboratory, Dr. KS Krishnan Road, New Delhi 110 012, Tel: +91.11.4560.8317, Fax: +91.11.4560.9310, e-mail: mahavir@nplindia.org

Journal of Acoustical Society of India (JASI)

A quarterly publication of the Acoustical Society of India

Volume 41, Number 1, January 2014

EDITORIAL

ARTICLES

INFORMATION

How to Measure STC Ratings (ASTC Measurements)

When we are testing a noise issue between units in a multi-unit housing complex or between closed office spaces, I often get the question "Can we just turn on some loud music in one room, and listen in the next room?" Good question. Although this can help confirm that there is an issue with inadequate sound isolation, it doesn't exactly give us enough information to help provide a solution.

To ascertain the level of sound isolation of an existing assembly, there are two approaches. If the original drawings are available, we can look up the designed assembly and determine the intended sound isolation by comparing the assembly to existing lab tested assemblies. These lab tested assemblies provide a single number rating called the Sound Transmission Class (STC) which tells us how much sound the assembly is supposed to block. The higher the STC rating is the better the sound isolation. Although the STC of the designed assembly provides a good starting point for investigating the problem, existing buildings aren't always constructed exactly as designed. Because of this, a field test will provide more accurate information on how the assembly performs.

A field test provides the Apparent Sound Transmission Class (ASTC) which is typically 5-8 points lower than the STC rating. Testing according to recognized standards is the best methodology to make sure that the test is done in a repeatable and reliable way. This involves using an amplified speaker to produce broadband noise in one room (source) according to specific internationally recognized standard, usually ASTM E336. The sound level is then measured in the source room and the adjacent room (receiver). We then determine the reverberation time in the receiver which allows us to calculate the sound absorption and along with the source and receiver measurements, the resulting ASTC of the assembly. If the field tested assembly is significantly lower than expected, we know that it wasn't constructed as designed. If the assembly tests as we expect it, we know that the assembly wasn't designed to provide enough sound isolation for the current use of the space. Regardless of the results, in an existing building, an ASTC test is a useful tool for diagnosing a noise transmission issue between spaces.

At acoustics by design, we can help you measure or predict the STC rating of an assembly. Our engineers want you to get it right from the beginning, so your building has the right amount of sound isolation.

Mahavir Singh

Operational Modal Analysis of a Tyre Using a Pu Probe Based Scanning Technique

E. Tijs[1], B. Makwana[2], O. Peksel[1], S. Amarnath[2], D. Bekke[2] and Mahavir Singh[3]
[1]Microflown Technologies, Tivolilaan 205, 6824 BV, Arnhem, the Netherlands
[2]Apollo Tyres, Colosseum 2, 7521 PT, Enschede, the Netherlands
[3]CSIR-National Physical Laboratory, New Delhi
e-mail: tijs@microflown.com or mahavir@nplindia.org

ABSTRACT

Tyre vibration can be studied with several experimental and simulation techniques. An important goal for a tyre manufacturer is to "tune" the resonant frequency of the tyre sub-system to reduce the structure-borne noise in the car interior. In this paper, a novel measurement technique is applied to determine the operational tyre deflection shapes under different conditions; i.e. free condition, loaded condition, and rolling condition. The vibrational behaviour of a tyre is studied using a PU probe, which comprises a sound pressure and a particle velocity sensor, and a scanning technique. The relative phase information is obtained using a static reference sensor. The experimental data can be used to validate simulated mode-shapes and resonant frequencies.

1. INTRODUCTION

As road noise is of increasing concern in urban environments, the development of more silent tyres is pursued. For these investigations it is necessary to characterize the noise radiated. During experimental investigations, vibrations are measured often as they are the origin of sound radiated. Such studies can be rather involved because rubber can behave non-linearly and there can be asymmetrical mode shapes. Moreover, vibration patterns depend on the loading conditions and the way the tyre is excited. Excitation forces exists in normal, lateral, and in front direction, which causes vibrations in axial or in radial direction, see figure 1.

Several methods exist to measure vibrations. For example, accelerometers can measure in three directions. However, they have to be attached to the surface, which can alter the stiffness and damping of the tyre, and tests with rolling tyres are impossible. Alternatively, vibrations can be measured contact free with Laser Doppler Vibrometers. Disadvantages of this approach are that often the tyre needs to be painted and complicated set ups with mirrors are required to measure difficult to reach areas. For the investigations described in this paper, the usage of another non contact method that involves particle velocity sensors is investigated.

In the very near field, the normal component of the structural velocity is similar to the normal particle velocity [4]. Therefore, particle velocity sensors can be used to measure structural vibrations in the vicinity of objects. Such vibration tests have a high signal-to-noise ratio because [5]:
- particle velocity levels, due to the vibration of the surface itself, are high due to near field effects.
- particle velocity levels, due to background noise, usually are low because many objects have a high impedance. The incoming and reflected sound waves are nearly equal of strength but opposite in phase, thus they interfere destructively.

Fig. 1. Possible excitation directions and vibration directions.

- Particle velocity sensors are directional, and can be pointed towards the vibrating surface.

Very near field assumptions apply if two conditions are met; i.e. distance h to the surface should be much smaller its typical size L, and wavelength λ should be much larger than the size of the vibrating surface L: $2\pi \cdot h << L << \lambda$; [4-5]. In this paper, this particle velocity sensor based method is used for three vibration tests:

- a test in unloaded, free conditions,

- a test in loaded conditions where a non rotating tyre is pressed against a flat surface,

- a test in loaded conditions on a roller bench.

In the next chapters, these tests are described, and the results are presented and analyzed. During the first two tests, a shaker is used to excite the tyre in normal, lateral, or in front direction. The excitation during the latter test on the roller bench closely resembles the real conditions on the road.

Usually, vibration measurements require many measurement points. Here, a method called Scan & Paint is used to map sound fields quickly and with high resolution [6 7]. It involves a probe that is swept across a surface while a video of the measurement setup is captured. The probe position is obtained from the video with dedicated software. The tracking procedure is automated, which speeds up the post-process procedure.

2. TYRE MEASUREMENTS UNDER FREE CONDITIONS

In the first test, the operational deflection shape is measured of a tyre in unloaded conditions. The tyre is suspended in elastics, and a stinger is glued to the surface and attached to a shaker that excites the tyre in normal or in lateral direction. An accelerometer is used on a fixed position as phase reference during this measurement. The tyre vibration is measured with a probe containing a particle velocity sensor that is swept across the surface of the tyre. The position of the probe is determined by tracking a colour marker on the probe with a video camera, which is positioned at a distance from the set up. The path of the probe during the measurement is shown in figure 2 left.

There are many modes, and only a few of them are shown. Figure 2 and 3 show examples of the measured operational deflection shapes (ODS) for several frequencies. The complexity of the modes increases with frequency. The numbers of the colour scales have been removed for confidentiality reasons. Red areas are surfaces with a high velocity level and a positive phase. Green areas indicate surfaces with low levels. Blue areas indicate a high levels, but with a negative phase.

3. TYRE MEASUREMENTS UNDER LOADED CONDITIONS

In the second test, the axle of tyre is loaded. Again a stinger was used to excite the tyre in normal direction. For lateral and front excitation the arrangement shown in figure 4 is used, which enables a similar excitation
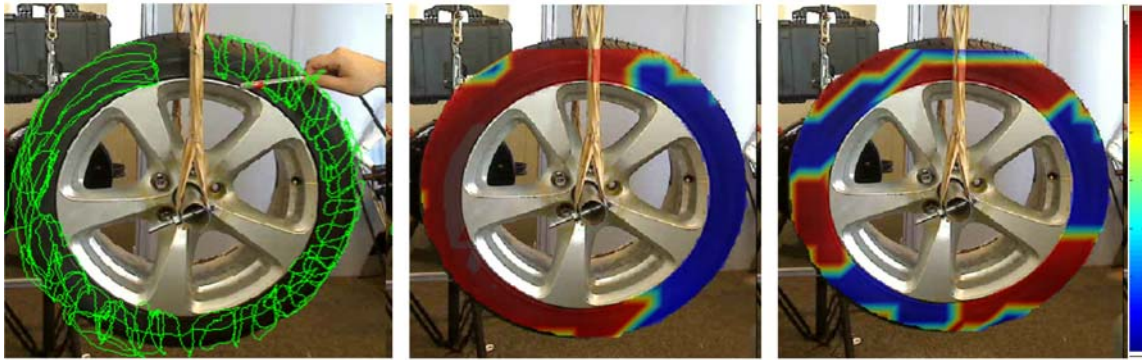
Fig. 2. Side view. Left: Scanned path of the probe. Middle: ODS at 53 Hz. Right: ODS at 199 Hz.

top rear view   bottom front view   top front view   top rear view   bottom front view   top front view
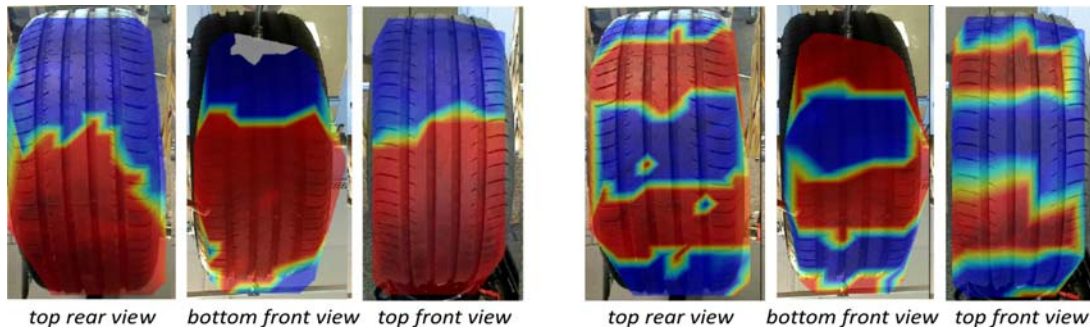
Fig. 3. Operational deflection shapes for three views for 88 Hz (left) and three view for 281 Hz (right).

as in reality. The shaker is connected to the tyre's supporting plate, which is suspended freely on bearing balls. Vibration measurements were performed for all excitation directions with the same procedure as described in the previous chapter.
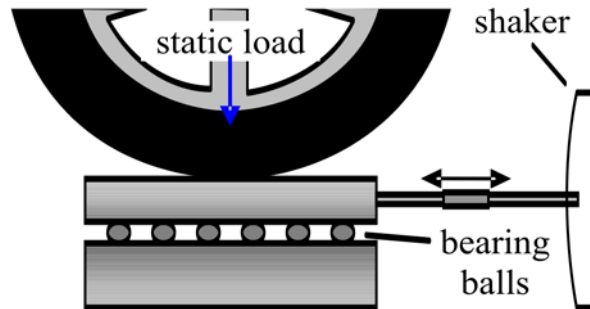
Fig. 4. Measurement arrangement to excite in lateral or front direction.

Only during some tests an additional vibration sensor was used as a phase reference, which allows calculation of the operational deflection shapes. For the other measurements it was only possible to calculate the velocity levels (only an absolute level, no sign). In addition, the load on the tyre could only be controlled accurately on one of the two set ups used.

Figure 5 shows examples of vibration patterns captured with a 4000 N load and front excitation. The absolute particle velocity levels are shown (no directional information). Red areas are surfaces with high velocity levels, blue areas vibrate little. Figure 6 shows operational deflection shapes with normal excitation and a load of approximately 3000 N. In this figure, blue areas do have a high velocity, but a negative phase.

Red areas are surfaces with a high velocity level and positive phase, green areas vibrate little. In both figures intricate mode shapes can be identified. Compared to the free suspension case, the shape and frequency of the modes is altered due to the load applied.
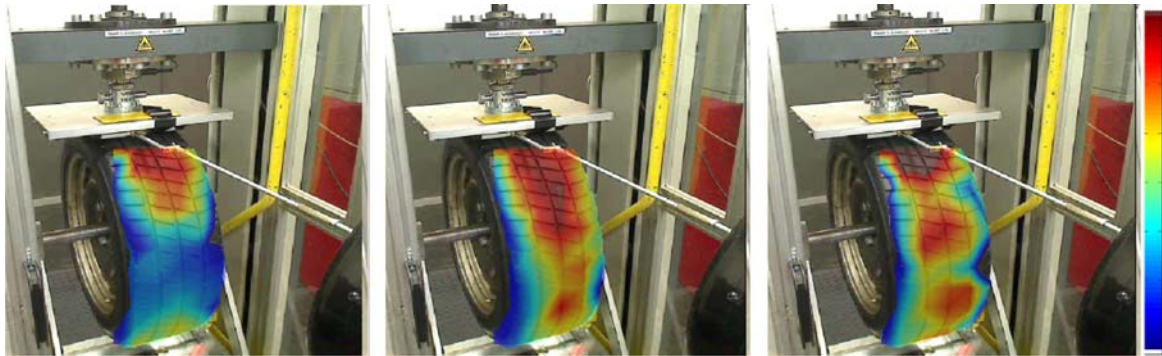
Fig. 5. Velocity levels for a 4000 N load and front excitation. Left: 59 Hz. Middle: 94 Hz. Right: 211 Hz.

65 Hz   *340 Hz*   *404 Hz*   *469 Hz*   *727 Hz*
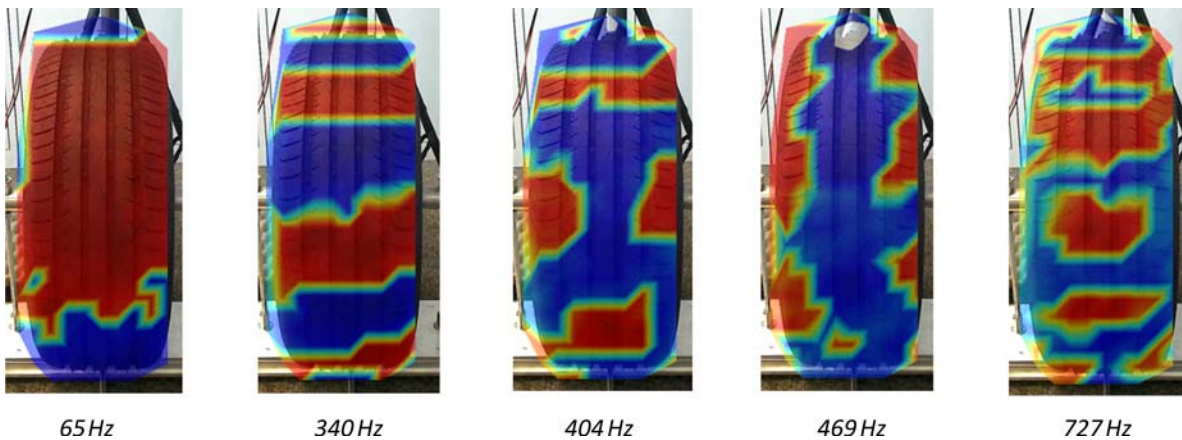
Fig. 6. ODS examples for a load of approximately 3000 N and normal excitation.

4. TYRE MEASUREMENTS UNDER ROLLING CONDITIONS

In the third test, the tyre was installed on a roller bench where the loading and excitation conditions are similar to the real conditions on a car. As mentioned before, particle velocity probes are affected little by background noise if they are placed in the vicinity of the test object. Consequently, no anechoic room is required to perform the test. Compared to laser based tests, not only the vibration is measured, but also the sound radiated. In [1] a procedure was described to calculate the sound pressure for different angles using different transfer paths. Such an approach might be supplementary to, or even partly replace past by noise tests. The advantage of roller bench tests are that conditions can be controlled well (temperature control, no rain, and there is no influence of a test vehicle).

Airflows near a rolling tyre can affect the particle velocity sensor. In 2009, similar vibration tests were performed [1]. However, at that time the development of wind caps was still in an early phase. Tests could not be performed close to the tyre because the airflow was too high. Meanwhile, better wind caps have become available. Here, a commercially available wind screen was used consisting of an open cell foam covered by cloth and loose fibres. No sensor overloads were experienced with this wind cap, which allows measurements near the tyre. A distance of ~50 mm was chosen between the centre of the particle velocity

probe and the tyre to keep a safe distance from the rotating tyre because the wind cap already has a radius of 30 mm. As the distance decreases, a higher spatial resolution is achieved and the influence of background noise reduces. Measurements with two tyre types were performed at 45 km/h and 60 km/h. The tyre load was 4000 N. An extension pole for the sensor was used for the safety of the test engineer, see figure 7.

Figure 8 and 9 show examples of vibration patterns measured. Red areas show high velocity levels, blue areas show low levels. At most frequencies the sound radiated around the tyre pavement interface exceeds the velocity levels of the side wall. However, for some modes the level of side wall vibrations of the tyre are substantial, see e.g. figure 8 left and middle. Especially such frequencies are of interest when optimizing the dynamic stiffness of the tyre.

Fig. 7. Tyre on the roller bench. The surface is scanned using an extension pole.

Fig. 8. Measured vibration pattern for tyre 1 at 45 km/h. Left: 80 Hz. Middle: 375 Hz. Right: 425 Hz.

Fig. 9. Measured vibration pattern for tyre 2 at 60 km/h. Left: 475 Hz. Middle: 530 Hz. Right: 750 Hz.

The preliminary tests demonstrate the feasibility of measuring tyre vibrations on a roller bench without overloading the particle velocity sensor. However, there are some recommendations for future measurements. The maximum speed during these tests was 60 km/h, as this is the limit of the su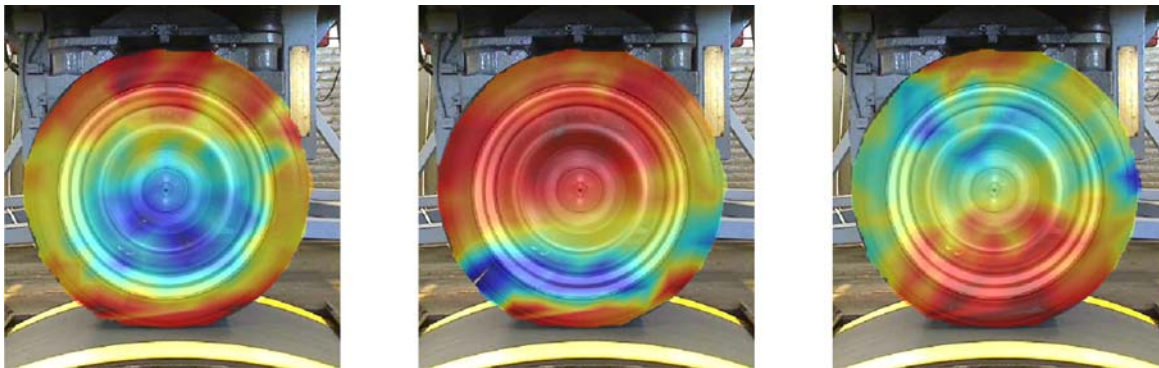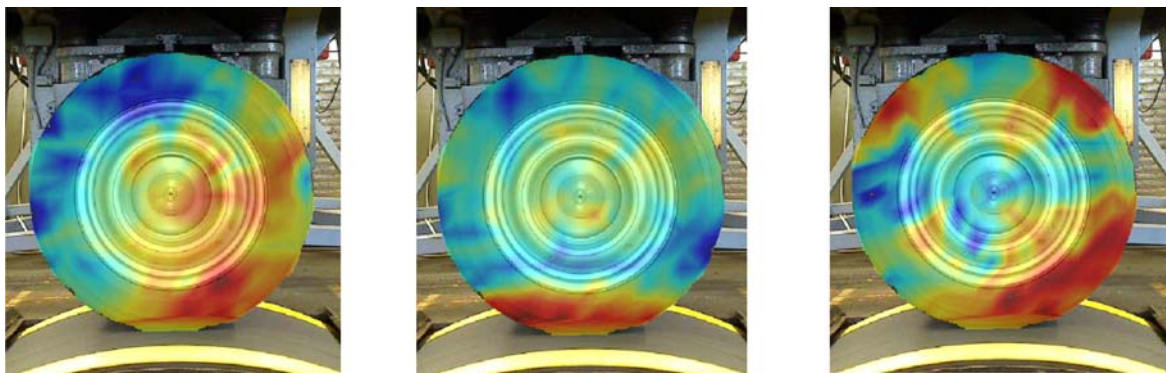bstrate mounted on the rollers. Different substrates might be used to evaluate higher speeds. Further more, no cleat was used (i.e. a strip mounted on the roll to impact the tyre). With such a cleat, the tyre would have been excited even more, and the modes might have been visible more clearly. In addition, no additional sensor was used as phase reference. With this sensor not only the velocity levels can be computed, but also the operational deflection shapes.

5. CONCLUSIONS

A methodology to measure vibrations based on particle velocity sensors has been investigated. Advantages of this method are that vibrations can be measured easily without touching the tyre. Three conditions have been tested, i.e. a tyre in unloaded conditions, a tyre in loaded conditions, and a tyre on a roller bench. Whereas test results of the first two conditions can provide useful information about the dynamic response of the tyre and can be used to validate simulations, the roller bench test is a better representation of the actual conditions. Compared to other investigations, tests could be performed close to the tyre because the latest windscreen model has been used, which can cope with higher airflow speeds. For small distances to the vibrating object, the influence of background noise is low and a high spatial resolution can be achieved. No sensor overloads due to airflow were experienced, even though the tyre sensor distance was only 5 cm.

Intricate mode shapes could be identified in all test conditions. For some tests the velocity levels were calculated. For others, also the operational defection shapes (velocity level times the sign of the phase) could be calculated when an additional sensor was used as a phase reference.

In future investigations, more tyre types might be evaluated and results of different loading conditions might be compared. On the roller bench, the maximum speed was only 60 km/h because this was the maximum of the equipment installed at that time. Higher speeds might be tested in the future. Furthermore, a cleat might be used to excite the tyre stronger, to increase vibration levels.

6. REFERENCES

[1] H.E. DE BREE, D.A. BEKKE and J.H. DE VRIES, 2009. *A source path contribution analysis on tire noise using particle velocity sensors*, Daga, Rotterdam, the Netherlands.

[2] P. KINDT, F. DE CONINCK, P. SAS and W. DESMET, 2006. *Analysis of tire/road noise caused by road impact excitations*, ISMA, Leuven, Belgium.

[3] U. SANDBERG and J. A. EJSMONT, *Tyre/Road Noise Reference Book*, Informex, Kisa, Sweden, ISBN **91**, 631-2610-9.

[4] H-E. DE BREE, V. SVETOVOY, R. RAANGS and R. VISSER, 2004. *The very near field, theory, simulations and measurements, of sound pressure and particle velocity in the very near field*, ICSV 11, International Congress on Sound and Vibration, St. Petersburg, Russia.

[5] H-E. DE BREE and W. DRUYVESTEYN, 2005. *A particle velocity sensor to measure the sound from a structure in the presence of background noise*, Forum Acusticum conference, Budapest, Hungary.

[6] E.H.G. TIJS, H-E. DE BREE and S. STELTENPOOL, 2009. *A novel acoustic pressure-velocity based method to access acoustic leakages of an acoustic enclosure in non anechoic conditions*, Euronoise, the 8th European Conference on Noise Control, Edinburgh, Scotland.

[7] D.F. COMESAÑA, S. STELTENPOOL, G.C. POUSA, H-E. DE BREE and K. R. HOLLAND, 2013. *Scan and Paint: Theory and Practice of a Sound Field Visualization Method*, ISRN Mechanical Engineering, Article ID 241958.

Sonoporation Device Adapted for Real-Time Microscope Visualization: Investigation of the Interactions between Bubbles, Cells and Medium Flow

Labelle Pauline[1], Fouqueray Manuela[1], Ngo Jacqueline[1], Der Loughian Christelle[3], Vanbelle Christophe[2], Rieu Jean-Paul[3], Inserra Claude[1] and Béra Jean-Christophe[1]

[1]*Inserm, U1032, LabTau, Lyon, F-69003, France ; Université de Lyon, Lyon, F-69003, France ; Université de Lyon1, Lyon, F-69003, France*

[2]*SFR Santé Lyon-Est, Centre Commun d'Imagerie de Lyon-Est, Lyon, France*

[3]*Université Lyon 1, Institut Lumière Matière, CNRS, UMR 5306, F-69622 Villeurbanne,*
e-mail: pauline.labelle@inserm.fr

ABSTRACT

Sonoporation appears as a promising alternative transfection technique. In order to control the biological effectshowever, mechanisms linked to acoustic cavitation need to beclarified. In this goal, a sonoporation device adapted for real-time microscope visualization and dedicated to adherent cells was designed. A regulation process on inertial cavitation level was used to ensure reproducible biologic effects,and a sonoporation rate of 19% has been obtained on adherent HT29 cells. Subsequently this device was used to investigate interactions between bubbles, cell and medium flow.Macroscope observations show large spatial-scale vortices in the entire well. They suggest an Eckart streaming that could enhance mixing of molecules within the entire well. A microscope study on a lipid bilayer membrane placed at the bottom of the well attests the presence of bubbles and shows some cracks and impacts generated by cavitation. Finally, another microscope study with cells at the bottom of the well shows that acoustic cavitation generates cell detachment and maybe brings molecules near the cell detachment zone.

1. INTRODUCTION

Ultrasound can enhance cell membrane permeability and create transient pores[1][2] : this phenomenon is called sonoporation. It is a promising alternative transfection technique to transfer molecules or genetic material into cells. It is generally admitted that acoustic cavitation, and especially inertial cavitation[3][4], is the main mechanism involved in pore formation. Most sonoporation experiments are performed with suspended cells[5][6] and therefore do not allow the visualization in the well during sonication. To get a better understanding of physical phenomena acting between cells, bubbles and medium flow during sonication, we designed a sonoporation device adapted for real-time microscope visualization and dedicated to adherent cells sonoporation. Because of the stochastic behaviour of acoustic cavitation[5], especially for acoustic intensities used for sonoporation, a regulation process on inertial cavitation level was implemented in order to increase acoustic cavitation and biological effects reproducibility[7][8]. The first step of this work is to validate oursonoporation device in terms of sonoporation rate and cell mortality. Indeed for the following

of the study, a significant sonoporation rate coupled to low cell mortality is necessary to ensure that the device parameters are well adapted to sonoporation. To get information on sonoporation process in our device three experiments are performed. First the macroscopic flow in the entire well is investigated to understand how the molecules behave in the medium flow. Then, a lipid bilayer membrane (which corresponds to a simple model of cell membrane) is placed at the bottom of the well to check if bubbles are present at the bottom and if these bubbles are responsible for damages. Indeed, in a previous study[9], microscopic defects have been observed on a lipid bilayer during sonication without checking the presence of bubble near the lipid bilayer. Finally, cells are placed at the bottom of the well to get information on cell detachment and sonoporation during sonication.

2. SONOPORATION DEVICE

Two plane piezoelectric transducers (Ferroperm PZ 26, frequency 426.5 kHz, dimensions 18 x 3 mm) are placed face to face on two sides of a culture well (Labtek, 2 wells, dimensions 20 x 20 mm, volume 2 mL). The transducers, electrically matched to 50 Ω, generate a continuous sinusoidal wave provided by a function generator (HP 33120 A) successively amplified by a variable gain amplifier (AD 603) and a power amplifier (24 V, 4.8 A, 50 MHz, Kalmus with an Alimentation (PS 3010, HQ Power)). The electrical power delivered by the generator is ranged between 0 and 8W, which correspond to maximum acoustic intensities of6.8 W/cm². The sonicated media is composed by 2 mL of ultrapure water (or cell medium for experiments with cells) at ambient temperature. A needle hydrophone (Onda HNR-0500) placed on another side of the well listens to the acoustic noise in the exposure medium. A good coupling is ensured by the use of an ultrasound transmission gel (Aquasonic) between the hydrophone and the well. The received signal is digitized (acquisition card PXI-1031, 14 bit resolution, 32 MHz sampling frequency, National Instrument), transferred to a computer and analyzed by Labview software.The experimental set-up is presented on Figure 1. Well, transducers and hydrophone are fixed in a microscope stage for visualization. A picture of this microscope stage is presented on Figure 2.
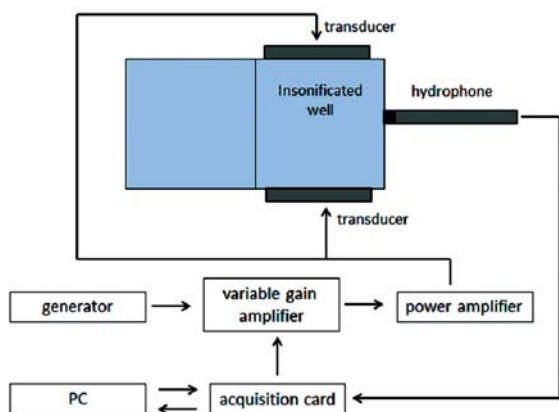
Fig. 1. Experimental setup
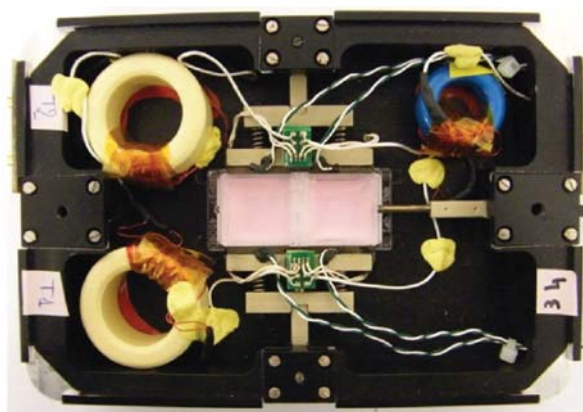
Fig. 2. Picture of the microscope stage containing well, transducers and hydrophone

The non-referenced inertial cavitation level is defined as the average level of an instantaneous spectrum in dB within the range of 0.1 to 7.1 MHz. Before sonication, the reference noise is measured as the mean value of the inertial cavitation obtained when the excitation signal is off. The inertial cavitation level is determined by the subtraction of the non-referenced inertial cavitation level and the reference noise. In the following experiment, a fixed cavitation index method is used: the enter setting is a cavitation index and the gain of variable gain amplifier is modulated regarding the difference between the cavitation index setting

and the measured cavitation index. The variable gain amplifier update is done within a feedback loop with 5 ms delay. This method is detailed in[8].

3. SYSTEM VALIDATION

For the device validation, HT29 adherent cells (human colorectal adenocarcinoma cell line) have been chosen.Sonoporation experiments consist in the internalization of siRNA coupled with the fluorochrome Alexa488. Sonoporation rate and mortality are measured with a flow cytometer (FACS Calibur; Becton, Dickinson and Company, NJ). The protocol of sonication consists in continuous excitation during about 2 minutes, for cavitation index 28 and 30. Cells are sonicated at ambient temperature. Adherent and suspension (detached) cells are treated separately and sonoporation and mortality results are presented on Figure 3.
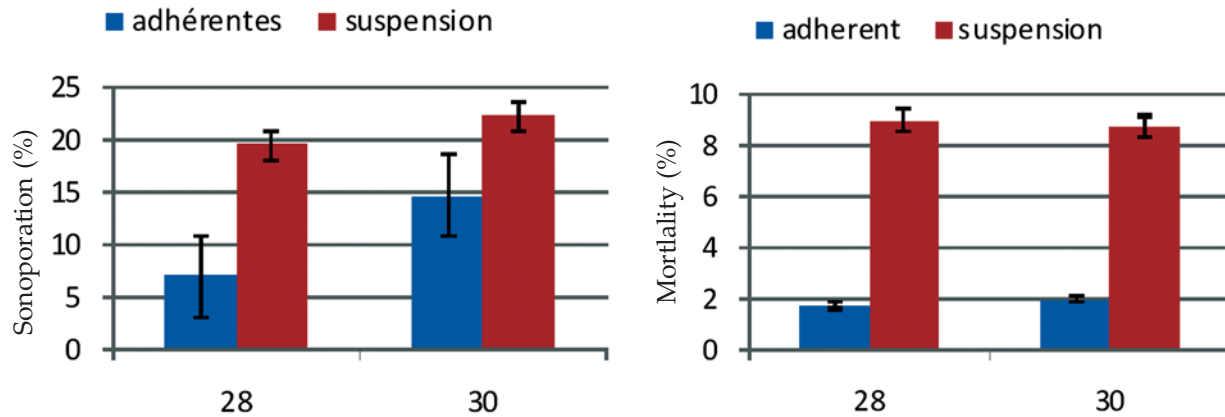
Fig. 3. Sonoporation and mortality rate obtained for cavitation index
28 and 30 on adherent and suspension cells.

Sonoporation rate is more important at cavitation index 30 than at 28 for both adherent and suspension cells. A sufficient sonoporation rate of around 15% is obtained for adherent cells at cavitation index 30. Mortality for both adherent and suspension cells is weak: around 2% for adherent cells (which is logical because dead cells are no longer adherent) and around 9% for suspension cells. It suggests cell detachment: indeed if only dead cells were detached, mortality of suspension cells should be very high. With this significant sonoporation rate, this system can thus be used for sonoporation experiment visualization. However, couldsonoporation rate on adherent cells be limited by cell detachment?

4. BUBBLE-CELL-MEDIUM INTERACTIONS

Considering that adherent cell sonoporation has been validated,different physical questions arise: how the molecules to be internalized behave in the medium flow? Are cavitation bubbles located in the vicinity of the bottom of the culture well? And can we expect single cell sonoporation visualization? In order to answer these questions, microscope and macroscope visualizations are performed.

4.1 How the molecules to be internalized behave in the medium flow?

In order to get information on the transport of molecules to be internalized, the macroscopic flow of the entire well is investigated by using a Leica MacroFluoTM. For this experiment 10 μL of micro particles of 2 μm (concentration = 10^{-2} g.L^{-1}, $\lambda_{excitation}$=505 nm and?emission=515 nm, Invitrogen) are addedto ultrapure water in the well.Videos of the macroscopic flow are performed for several cavitation indexes between 10 and 24.

Large spatial-scale (compared to the acoustic wavelength) vortices have been observed in the entire well. An example of these vortices is presented on Figure 4.
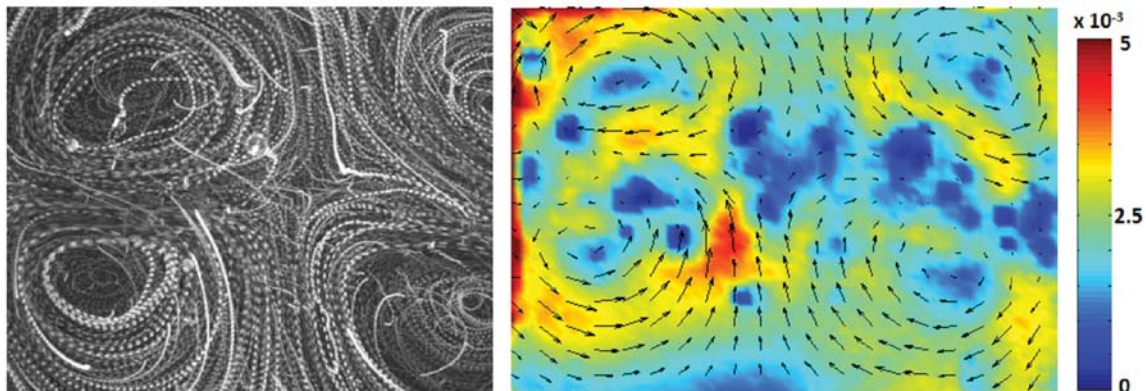
Fig. 4. Example of flow motion in the entire well (view from above, transducers are placed on right and left side of pictures): a/ projections of all images of a video during sonication and b/ displacement vectors and velocity amplitude (color bar) in m/s after Particle Image Velocimetry treatment for the same video. The mean velocity near the bottom of the well is around 3 mm/s.

They suggest an Eckart streaming that could enhance mixing of molecules within the entire well. To determine if these vortices are responsible for cell detachment, the velocity of the flow is calculated and the shear stress generated by the flow at the bottom of the well is approximated by: $\tau = \mu V / _h$,

wereμ is the dynamic viscosity of the fluid, V the flow velocity of the fluid along the boundary and h the height above the boundary. By comparing the maximum shear stress generated by our flow with the shear stress needed for cell detachment [10], it appears that the vortices at the bottom do not generate cell detachment.

4.2 Are cavitation bubbles located in the vicinity of the bottom of the culture well ?

Concerning the location of cavitating bubbles near the bottom of the well, experiments on a lipid bilayer (DLPC + fluorophore NBD (5%)) membrane are performed. The effects of cavitation bubbles on the membrane are observed by using a microscope (Nikon Eclipse TE2000E). Bubbles are observed at the bottom of the well
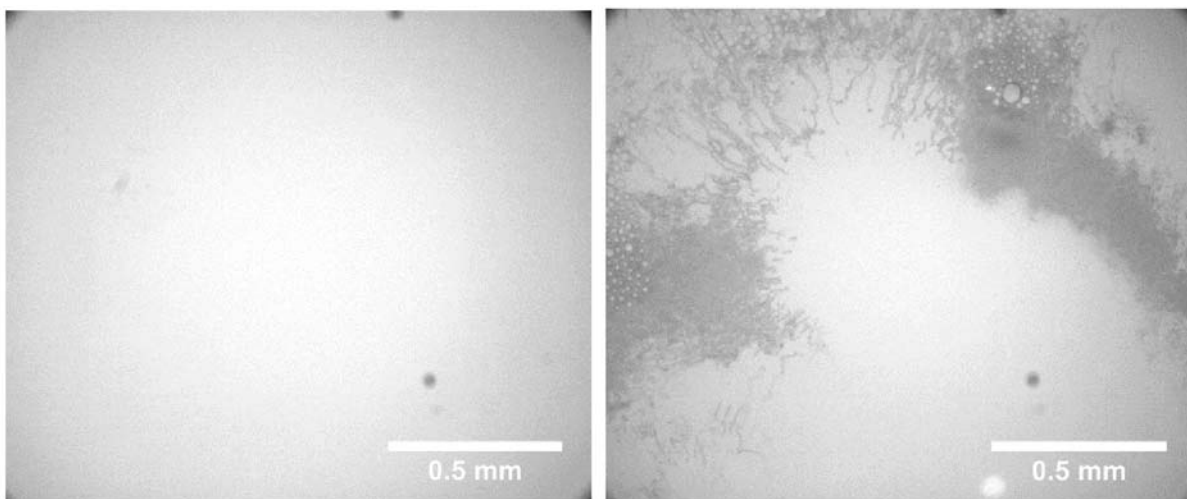
Fig. 5. Example of impacts or cracks generated by cavitation bubble on a bilayer membrane.a/ Before ultrasound excitation and b/ after 30 s of sonication for a cavitation index of 28.

during sonication and they generate permanent and non-permanent damages on the membrane as impacts and cracks. An example is presented on Figure 5showing the membrane before and after a 30 second sonication.

Damages are not spread on all the bilayer membrane but seem to be located.As small cavitation bubbles are located on pressure antinode and bigger one on pressure node, we hypothesize that the damages on the bilayer could be linked to the acoustic field at the bottom of the well.

4.3 Can we expect cell sonoporation visualization ?

A preliminary experiment on bubble-cell interactions is implemented during a sonoporation experiment under a confocal microscope (Zeiss Confocal Laser Scanning Microscopy 780). Cellmembranes have been colored in red usingVybrant® DID and siRNAmolecules which are coupled with Alexa488 appear in green. Pictures of the bottom of the well are taken before and after an ultrasound excitation of 2 minutes with a cavitation index of 24.An example of these pictures is presented on Figure 6.
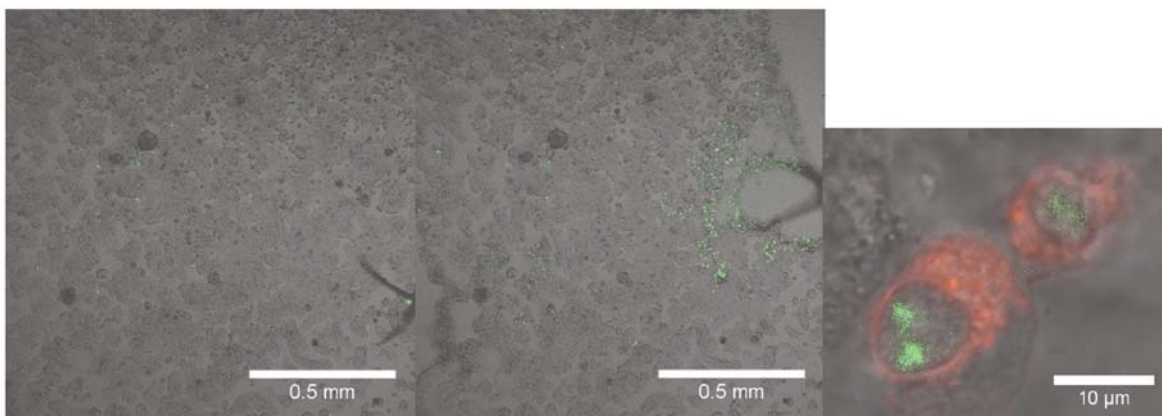
Fig. 6. Observation of cell detachment and molecules displacement due to acoustic excitation.a/ before ultrasound excitation and b/ aftera 2 minute ultrasound excitationwith cavitation index 24. Cell detachment is observed (at the top on the right) and molecules are brought near this cell detachment zone.c/ sonoporation observation: molecules (in green) are in the cell (cytoplasm in red).

After ultrasound excitation, cell detachment is observed. In this case most of cells are still present on the picture after sonication.The internalized molecule (siRNA, in green) is uniformly spread at the beginning of the shot. However, after excitation,molecules are brought near the zone where cell detachment happens.Some cells present in the same zone after sonication aresonoporated. Indeed a zoom and a z-scan in this zone confirmed the sonoporation of the two cells presented on Figure 6c: molecules (in green) are inside the cell (cytoplasm in red).

5. CONCLUSION

A sonoporation system adapted to microscope visualization in real time and dedicated to adherent cells was designed. Experiments to get a better understanding of physical mechanisms acting on cells, bubbles and medium flow are in progress. This sonoporation device is validated in term of sonoporation rate but the process is also responsible for cell detachment. During sonication, four vortices are observed in the entire well and the resulting flow motion allows mixing. It is not this flow motion at the bottom of the well which leads to cell detachment. Cavitation bubbles are observed on lipid bilayer surface and these bubbles generate permanent damages on the membrane as impacts and cracks. Cell detachment and mixing of the medium are confirmed by experiments on adherent cells under microscope: internalized molecules are brought near cell detachment zone and transfected cells are present.

6. REFERENCES

[1] M.W. MILLER, D.L. MILLER and A.A. BRAYMAN,1996. A review of in vitro bioeffects of inertial ultrasonic cavitation from a mechanistic perspective, *Ultrasound in Medicine and Biology*, **22** (9), 1131-1154.

[2] K. NG and Y. LIU, 2002. Therapeutic ultrasound: its application in drug delivery, *Medical Research Review*, **22**(2), 204-223.

[3] J. SUNDARAM, B. MELLEIN and S. MITRAGOTRI, 2003. An experimental and theoretical analysis of ultrasound-induced permeabilization of cell membranes, *Biophysicaljournal*, **84** (5), 3087-3101.

[4] L. RESLAN, J.-L. MESTAS, S. HERVEAU, J.-C. BÉRA and C. DUMONTET, 2010. Transfection of cells in suspension by ultrasound cavitation, *Journal of Controlled Release*, **142** (2), 251-258.

[5] T.G. LEIGHTON, 1995. Bubble population phenomena in acoustic cavitation , *Ultrasonics Sonochemistry*, **2** (2), S123-S136.

[6] Y. QIU, C. ZHANG, J. TU and D. ZHANG, 2012.Microbubble-induced sonoporation involved in ultrasound-mediated DNA transfection in vitro at low acoustic pressures, *Journal of Biomechanics.*, **45** (8), 1339-1345.

[7] A. SABRAOUI, C. INSERRA, B. GILLES, J.-C. BÉRA and J.-L. MESTAS, 2011. Feedback loop process to control acoustic cavitation, *Ultrasonics Sonochemistry*, **18** (2), 589-594.

[8] C. DESJOUY, A. POIZAT, B. GILLES, C. INSERRA and J.C. BERA, 2013. Control of inertial acoustic cavitation in pulsed sonication using a real-time feedback loop system , *The Journal of the Acoustical Society of America*, **134** (2), 1640-1646.

[9] M.S. MALGHANI, 1998. Generation and growth of bilayer defects induced by ultrasound, *The Journal of the Acoustical Society of America*, **103** (3), 1682-1685.

[10] M.M. PEEL and P.A. DIMILLA, 1999. Effect of cell-cell interactions on the observable strength of adhesion of sheets of cells, *Annals of Biomedical Engineering*, **27** (2), 236-246.

Audio Novelty-Based Segmentation of Music Concerts

Dalia El Badawy, Patrick Marmaroli and HervéLissek
Laboratory of Electromagnetism and Acoustics (LEMA),
Swiss Federal Institute of Technology in Lausanne (EPFL) - Station 11, 1015 Lausanne
e-mail: patrick.marmaroli@epfl.ch

ABSTRACT

The Swiss Federal Institute of Technology in Lausanne (EPFL) is in the process of digitizing an exceptional collection of audio and video recordings of the Montreux Jazz Festival (MJF) concerts. Since 1967, five thousand hours of both audio and video have been recorded with about 60% digitized so far. In order to make these archives easily manageable, ensure the correctness of the supplied metadata, and facilitate copyright management, one of the desired tasks is to know exactly how many songs are present in a given concert, and identify them individually, even in very problematic cases (such as medleys or long improvisational periods). However, due to the sheer amount of recordings to process, it is a quite cumbersome and time consuming task to have a person listen to each concert and identify every song. Consequently, it is essential to automate the process. To that end, this paper describes a strategy for automatically detecting the most important changes in an audio file of concert; for MJF concerts, those changes correspond to song transitions, interludes, or applause. The presented method belongs to the family of audio novelty-based segmentation methods. The general idea is to first divide a whole concert into short frames, each of a few milliseconds length, from which well-chosen audio features are extracted. Then, a similarity matrix is computed which provides information about the similarities between each pair of frames. Next, a kernel is correlated along the diagonal of the similarity matrix to determine the audio novelty scores. Finally, peak detection is used to find significant peaks in the scores which are suggestive of a change. The main advantage of such a method is that no training step is required as opposed to most of the classical segmentation algorithms. Additionally, relatively few audio features are needed which leads to a reduction in the amount of computation and run time. It is expected that such a pre-processing shall speed up the song identification process: instead of having to listen to hours of music, the algorithm will produce markings to indicate where to start listening. The presented method is evaluated using real concert recordings that have been segmented by hand; and its performance is compared to the state-of-the-art.

1. INTRODUCTION

At EPFL, *the Montreux Jazz Digital Projectaims* at digitizing the archives of the Montreux Jazz Festival(MJF) concerts. A few figures: since 1967, 5000 hours of audio and video are stored on 10000 magnetic tapes. These archives contain approximately 40000 songs. The safeguarding of this heritage has begun in 2010 and will continue until early 2015 when 100% of the archives (1.2 Petabytes) will be processed and stored. In order to improve these archives, make them easily manageable, facilitate copyright management and helpwith quality control, several applications are desired such as thedetection ofaudio events.In particular, it is required to know exactly whichsongs were sung in a given concert and even songs in a medley. However, dueto the

---

sheer amount of recordings available, it is quite cumbersome and timeconsuming to listen to each concert and note down the songs; it is thereforerequired to automate the process.

Detection of song changes using stochastic models is described in [1]; however, it is assumed that there are pauses between the songs which is not always the case for the MJF concerts. Related methods for semantic audio segmentation which deals with finding the constituents of a song like the intro, chorus, and bridge are described in [2], [3], [4], and[5]. Inthis paper, we describe a methodology to automatically segment MJFaudio file concerts in order to aid human listeners and speedup the process of songs identification. Audio novelty scores presented in [4] are used for detection of song changes instead of structures within the same song.

Theproposed approach isdescribed in Section Error! Reference source not found.. Section 3 presents the experiments we carried out and the performance results. Finally, the conclusion and suggestions for future work are presented in Section 4.

2. CONCERT SEGMENTATION

A concert recording generally contains several acoustic events including the songs, applause, and interludes. The first step in segmenting aconcert into those separate events is to represent the audio recording in a format suitable for analysis. This is done by extracting the socalled audio features from the raw audio signal. Then, these audio features which describe the signal are used by the segmentation module to generate a proper segmentation.

2.1 Audio features

Audio feature vectors are compsuted from small successive frames ofsize N_f(in samples) with an overlap of N_o (in samples). The number of frames contained in a signal of length N is given by the formula:

$$M = \left\lfloor \frac{N - N_f}{N_f - N_o} \right\rfloor + 1 \tag{1}$$

where stands for the floor function. In order to avoid edge effects when transforming it to the frequency domain, each frame is weighted by a Hann window (defined in[6] p. 397 for instance).

2.2 Segmentation

Once the audio is reduced to feature vectors (one per frame); the segmentation process can begin. The method used here follows [4]. The idea is tocalculate the similarity between two successive frames; if they are different,then a change is possibly detected. So first, a distance measure is required.

2.2.1 Distance Measure

A distance measure is used to quantify the similarity (or dissimilarity) between two feature vectors. One such measure is the cosine similarity, whichfor two feature vectors x_i and x_j is calculated as follows:

$$d_{ij} = \frac{<\mathbf{x}_i, \mathbf{x}_j>}{||\mathbf{x}_i|| \, ||\mathbf{x}_j||} \tag{2}$$

where <.,.> denotes the inner product and $\|.\|$ the Euclidean norm. The values range between   with 1 for parallel vectors and -1 for antiparallel. Itis a suitable measure because it is not affected by the energy levels where ifthe energy is low in two feature vectors, they can still have a high similarityscore [4].

2.2.2 Similarity Matrix

Using the distance measure, the similarity between each pair of frames can be computed and placed in a similarity matrix of size $M \times M$ where:

$$\mathbf{S}[i, j] = d_{ij}, \ \forall (i, j) \in \{1, 2, ..., M\}^2 \tag{3}$$

Figure 1 shows an audio excerpt and its corresponding similarity matrix. As indicated on the figure, the excerpt contains the ending and beginning of two different songs separated by applause.The checkerboard patterns where the changes occur are visible in the center of the similarity matrix.

2.2.3 Novelty Score

A novelty score is computed at each frame where the frames with high scores indicate a change and thus the audio should be segmented there. To calculate the score, a "checkerboard kernel" H_K of size $K \times K$, $\forall K \in \{2,3,...M\}$, is used. An example of such a kernel when $K = 4$ is provided below:

$$\mathbf{H}_4 = \begin{pmatrix} 1 & 1 & -1 & -1 \\ 1 & 1 & -1 & -1 \\ -1 & -1 & 1 & 1 \\ -1 & -1 & 1 & 1 \end{pmatrix} \tag{4}$$

Then, the 2D cross-correlation, , between the kernel and the similarity matrix at each frame is calculated as follows:

$$\mathrm{r}(m) = \mathbf{corr}\left(\mathbf{H}_K, \mathbf{S}_K^m\right) \tag{5}$$

where $\mathbf{S}_K^m$ is the part of the similarity matrix with the same size of the kernel and centered at coordinates :

$$\mathbf{S}_m^K = \mathbf{S}\left(\left[m - \frac{K}{2} + 1,...,m + \frac{K}{2}\right], \left[m - \frac{K}{2} + 1,...,m + \frac{K}{2}\right]\right) \tag{6}$$
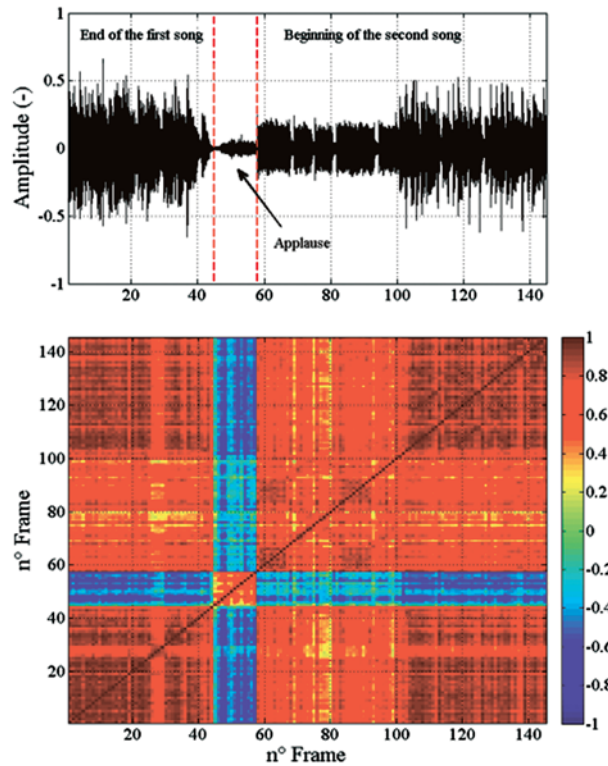

Fig. 1. top: waveform of a song change, bottom: corresponding similarity matrix

Thus, r is high at locations where the checkerboard patterns of the matrix match up with those of the kernel i.e. the positive and negative parts of the kernel multiply their respective positive and negative parts on the matrix.

Note that *K* here determines the extent of boundary detection: smaller kernels detect changes on a lower level like individual musical notes. The kernel is correlated only along the diagonal of the similarity matrix to get a score along the time dimension. Then, the scores are normalized to between 0 and 1. Using the generated novelty score at each frame, peak detection is used (with a threshold value) to find the local maxima and thus determine the positions of change.

Only peaks above a threshold areconsidered as song changes. In our algorithm, the threshold is adjusted automatically to the data. The hypothesis is that when a change occurs, the indicative peak is much higher than the other scores or weaker peaks in the same audio window. Therefore, the threshold is chosen according to the standard deviation of the scores in that window:

$$\Lambda = \mu + \lambda\sigma \tag{7}$$

where μ, respectively σ, are the mean and standard deviation of the cross-correlation values, $\mathbf{r} = [r(1), r(2), ..., r(M)]$, in the audio file, and λ is a scalar.

2.2.4 Evaluation

In order to evaluate the performance of the segmentation, two measures canbe used: recall and precision. Given the ground truth i.e. correct segmentation, *recallis* the ratioof the number correctly detected boundaries to the number of boundaries inthe ground truth (it measures how good the system is at finding the required boundaries and equals 1 if all the correct boundaries have been found). Whereas *precisionis* the ratio of the number of correctly detected boundariesto all detected boundaries regardless they are right or wrong (it equals 1 if only correct boundaries were found):

$$recall = \frac{\text{number of correct boundaries}}{\text{number of ground truth boundaries}} \qquad precision = \frac{\text{number of correct boundaries}}{\text{number of all boundaries}}$$

3. EXPERIMENT

The dataset consists of 50MJF concerts. All wave files are mono and sampled at 48 kHz. The total duration is of 60 hours 43 minutes 32 seconds. There was a total of 1132 manuallyplaced segments (song, applause, interlude) that served as the ground truthfor evaluating the system.A subset of this dataset was used for tuning the parameters (frame size, kernel size, detection threshold, audio features). It consisted of 5 randomly chosen concerts of total duration 6hours 29 minutes 1 second with 99 manual segments.Audio features that have been compared arethe spectrum, MFCC, chroma features, and their combinations; however, the spectrum gave the best results.Finally, the parameters giving us the best results are summarized in **Error! Reference source not found..**

Note that in [**Error! Reference source not found**.], the checkerboard kernel was tapered using a Gaussian function.From our experience, not using a Gaussian weighting provides a slightly better result.

Table 1. Parameter values for the experiment.

Frame size (in samples)	*NF*	8192 (170 ms)
Overlap (in samples)	N_0	0
Threshold parameter	λ	4.5
Kernel size (in number of frames)	*K*	64
Audio features	**x**	Lower spectrum (50 first coefficients) by using the MIRToolbox[7].

The segmentation results were evaluated with atolerance of 10 secondsaround the manual ground truth segmentation. We get a recall of 78.7%which is more than 8% higher than reported in [1]; while the precision is 23.3%. On inspecting some of the manual segmentations, itcould be argued that some segments should actually start earlier or latersince it is subjective; this affects the recall. However, for the precision, whenlistening to the extra added segments, it is usually the case that the beatstopped and started; or there is a sudden silence; or even a short impulse sound like a whistle.

4. CONCLUSION

This study was concerned with song change detection for the MontreuxJazz Festival concerts. The algorithm that has been developed is based on audio novelty detection. Several audio features were tried; the best was found to be the lowerfrequency spectrum. Other parameters like the frame size and whether toweight the checkerboard kernel were optimized. Finally, the algorithm wastested on 50 MJF concerts and achieved a recall value of 78.7%.

Suggestions for further improvement include overlapping the windowsfrom which frames are extracted since it could be the case that a change between the windows is missed; also, overlapping the frames themselves couldbe useful. Moreover, for MJF concerts, it is interesting to note that thereare 3 main audio events: music, speech, and applause which may occur between songs or even during a song. This extra knowledge can by all meansbe leveraged to improve the song change detection system. For instance,salient features for speech or applause can be used to detect their respectiveevents which usually occur before or after songs and thus improve the songdetection accuracy.

Future work includes matching the detected segments in the end to theirrespective events. And also, if a database of songs is available, each songcan be matched to get its title and other metadata. Furthermore, it is alsopossible to utilize the video as well where during a song; the camera is mostlikely focused on the performers then switches to the audience at the endduring the applause; so the scene changes can be a useful addition.

5. REFERENCES

[1] T. PLOTZ, G.A. FINK, P. HUSEMANN, S. KANIES, K. LIENEMANN, T. MARSCHALL, M. MARTIN, L. SCHILLINGMANN, M. STEINRUCKEN and H. SUDEK, 2006. Automatic detection of song changes in music mixes using stochastic models. In *Proceedings of the International Conference on Pattern Recognition* (*ICPR*), **3**, 665-668.

[2] P. ROMANO, G. PRANDI, A. SARTI and S. TUBARO, 2009. Musical audio semantic segmentation exploiting analysis of prominent spectral energy peaks and multi-feature refinement.In *Proceedings of the IEEE International Conference on Acoustics, Speech and Signal Processing* (*ICASSP*), 1965-1968.

[3] M. LEVY, M. SANDLER and M. CASEY, 2006. Extraction of high-level musical structure from audio data and its application to thumbnail generation. In *Proceedings of the IEEE International Conference on Acoustics, Speech and Signal Processing* (*ICASSP*), **5** (5), 5.

[4] J. FOOTE, 2000. Automatic audio segmentation using a measure of audio novelty. In P*roceedings of the IEEE International Conference on Multimedia and Expo* (*ICME*), **1**, 452-455.

[5] SAMERABDALLAH, KATY NOLAND, MARK SANDLER and MARK S, 2005. Theory and evaluation of a bayesian music structure extractor. In *Proceedings of the Sixth International Conference on Music Information Retrieval* (*ISMIR*), 420-425.

[6] S. SALIVAHANAN, A. VALLAVARAJ and C. GNANAPRIYA, 2007. *Digital signal processing*. Tata McGraw-HIll Education.

[7] OLIVIER LARTILLOT and PETRITOIVIAINEN, 2007. A Matlab toolbox for musical feature extraction from audio.In *Proceedings of the 10thInternational Conference on Digital Audio Effects* (*DAFx*), 237-244.

Experimental Evaluation of Sound Absorption Coefficient of Perforated Wood Panels

Mahavir Singh and Gurbir Singh

AUV Standards, CSIR-National Physical Laboratory, New Delhi 110 012
e-mail: mahavir.acoustics@gmal.com

ABSTRACT

For sound control in closed spaces, perforated wood-based panels are widely used as walls and ceilings covering for their sound absorption properties in the low frequency range. Despite the high interest in these products, accurate estimation models of their properties are still unavailable. This paper reports the sound absorption properties determined for drilled plywood intended for interiors covering. The drilling percentage was fixed at 1.5, while different cavity sizes were arranged behind the specimens to evaluate their influence on the sound absorption. Tests were performed by means of the impedance tube method. The experimental data obtained can be used for the development of new estimation models with increased accuracy.

1. INTRODUCTION

Sound absorption in enclosures constitutes a relevant topic for many building applications, in particular with respect to large scale structures like public buildings, offices, shopping centres or dining spaces. Such environments, in fact, are often characterized by high noise levels, especially when crowded.

Depending on the building typology, many sources contribute to increase the overall noise: people's voice (Fig. 1), movements, air-conditioning systems etc. Poor acoustics of enclosed spaces can deeply rebound on their usability, particularly with respect to the speech intelligibility.

To mention some example, high levels of noise in classrooms make students prematurely tired getting worse the efficiency of learning [2]; speech communication between diners in college halls is recognized to be generally poor [3], while the quality of communication in food courts of shopping centres is strongly affected by ambient noise [4]; finally, poor acoustics in offices can affect the working quality and cause increased stress to workers [1].

Focusing on offices, a recent study performed by Jensen and Arens [5] indicated that acoustic discomfort is perceived by workers as a critical issue in these environments.

That study consisted in a survey performed on over 23.000 occupants of office workstations, which rated nine factors of their environment (acoustic comfort, thermal comfort, air quality, lightning, cleanliness etc.). The collected answers pointed out that acoustic comfort reaches the lowest satisfaction score among the different categories. In particular, satisfaction with noise level and speech privacy turned out to be both problematic.

On the whole, the above mentioned situations evidence how acoustic control plays a fundamental role. Solutions for acoustic improvement are particularly important for noise emitted in the low frequency range, i.e. below 1600 Hz (Fig. 2).
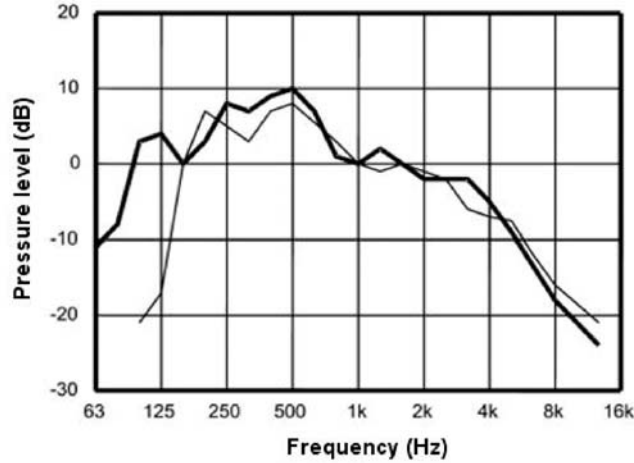
Fig. 1. Average spectra of normal male (thick line) and female (thin line) speech (from [1]).
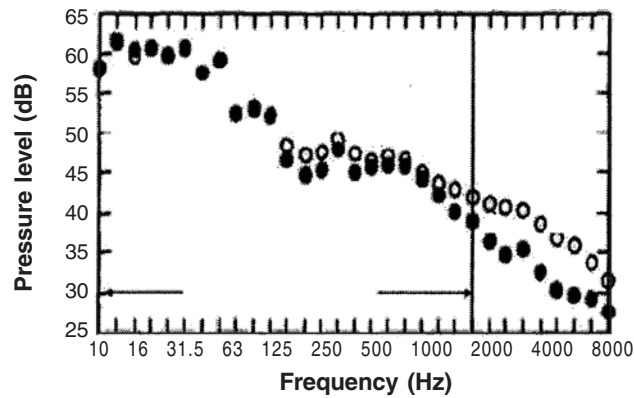
Fig. 2. Example of noise spectra produced in an office with 24 workers: within office hours; _ during lunch time (modified from [1]).

Furthermore, a peculiar phenomenon of enclosed spaces is reverberation, which can be defined as the buildup of sound due to wave reflections on all space surfaces. Reverberation creates a background noise, contributing to increase the overall noise of the room and lowering the speech intelligibility. Usually, this is evaluated by means of the reverberation time RT_{60}, which is the time required for reflections of a direct sound to decay by $_{60}$ dB below its level.

RT_{60} is calculated by means of Equation (1)

$$RT6 = \frac{0161V}{A}$$ (1)

where V is the volume of the room in m^3 and A is the total absorption of the room, in sabines (absorption unit, equivalent to the absorption by a square meter of a surface absorbing all the incident sound).

Ideal RT_{60} depends on the intended purpose of a room and its volume. Higher RT_{60} values are needed in rooms where music is played; on the contrary, lower RT_{60} values are desirable for rooms mainly used for speech. According to equation (1), RT_{60} can be controlled in two main ways: modifying the room size or changing the amount of absorption on its surfaces. The second is particularly suited for large scale buildings.

In fact, when a sound wave strikes a material, a fraction of the sound energy is reflected back while another is absorbed. The absorption coefficient ranges from 0 (no absorption) to 1 (full absorption) and

represents the ratio between the absorbed and the total incident energy. The theoretical limit of the sound absorption coefficient (α) is 1, when all the incident sound is absorbed. Nowadays several efficient methods are used for improving the acoustic features of large scale enclosures [6].

The adopted solutions vary from the design of room shapes, to the control of sound sources and to the use of sound proof materials or sound traps. Among the different approaches, the choice of perforated wood-based panels for exploiting their sound absorption properties is widely diffused.

These panels act both by absorbing the direct sound and by shortening the reverberation time, since they increase component A in equation (1). Beside their absorption behavior in the low frequency range, perforated wood-based panels are appreciated by architects for many other reasons.

In particular they are used for their relative lightness, valuable look, easy lying, sustainability and recyclability. These panels are diffused as ceilings or walls covering (Fig. 3) leaving a space between panels
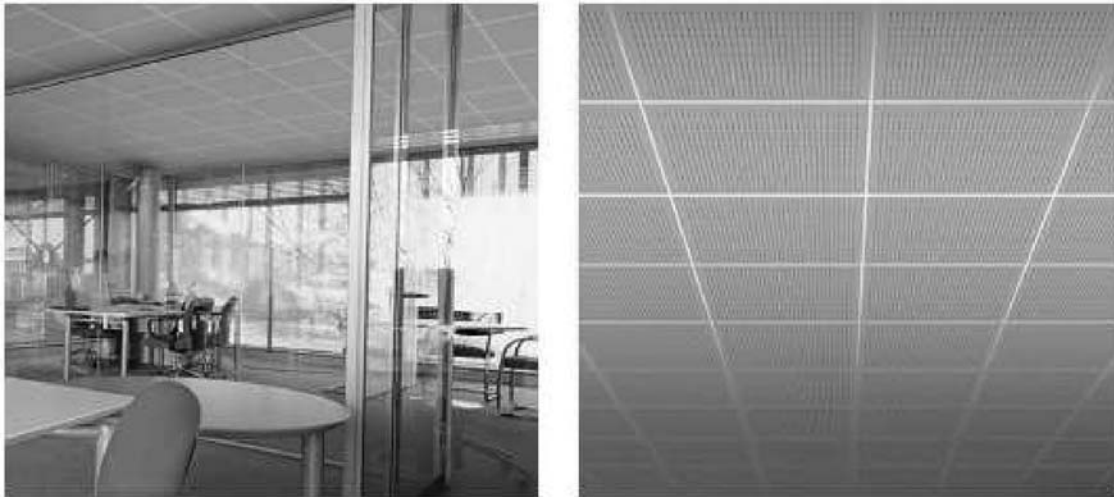
Fig. 3. Application of wood-based perforated panels as a ceiling and wall covering [from 7].

and the wall at the back. This cavity can be empty or further filled with sound absorbing materials.

The combination of perforated panel with an empty space at the back works like a Helmholtz resonator [8,9,10]. This is constituted by two communicating volumes called neck and cavity, which form a mechanical mass-spring system.

When struck by a sound wave, the air contained in the neck (the mass) is pushed into the cavity. As a consequence, the air of the cavity is compressed and reacts (like a spring) expanding and pushing out the incoming air. Hence this air is driven outside and, having a momentum, goes a little beyond the neck. For this reason, the air in the cavity becomes rarefied and recalls inside other air restarting the cycle.

The mass-spring action is able to absorb high amounts of sound energy, which is converted into the air swing. This phenomenon occurs in particular around a specific resonance frequency, at which the maximal sound absorption is provided.

The absorption properties of the system are mainly influenced by the volumes of neck and cavity. Changing in these volumes determines different amounts of absorption and slides the frequency around which absorption is greater.

In particular, the volume V of a Helmholtz cavity having circular or rectangular section can be calculated using Equation (2):

$$V = a \cdot t \tag{2}$$

where a is the area of the section and t is the thickness of the cavity.

Clearly, when the area a is constant, the only way to change the volume V is to modify the thickness t. Other variables, such as shape of the neck or geometry of the cavity, play a minor role in determining the absorption values.

Transferring the Helmholtz principle to the perforated panels, holes in the panel represent the neck, while the empty space between panel and wall constitutes the cavity (Fig. 4).
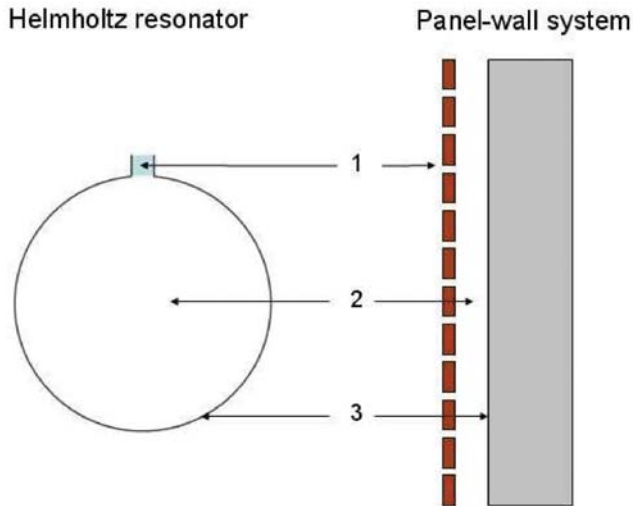
Fig. 4. Longitudinal section of a Helmholtz resonator (left) and a system made of perforated panel and wall (right). 1 is the neck in the resonator, corresponding to the holes in the wood-based panel; 2 is the cavity, corresponding to the empty space between panel and wall; 3 is the cavity surface, which corresponds to the wall.

Figure 5 reports an example of sound absorption values achieved by perforated wood-based panels intended for walls and ceilings covering and currently available on the market. These panels are able to provide high sound absorption in the low frequency range, therefore where is particularly needed for acoustic control in large scale buildings.

Furthermore, the absorption values are higher than 0.8 from about 300 to 1500 Hz. As a consequence, the absorption effect is consistent not only in correspondence of the resonance frequency but also in a wide range around it.

It must be noticed that in figure 5 peak values of α exceed 1. This apparent contradiction with the theory can be attributed to the experimental measurement method. Anyway, in these cases the absorption value can be considered as 1.

Since 1947, several studies have been carried out in order to investigate the sound absorption coefficients of perforated panels. Nevertheless, up to now accurate estimation models are still unavailable and the only means of evaluating the sound absorption behavior of a certain panel is still to perform experimental measurements [11].

Setting up new models with increased accuracy would positively rebound on design and development of fit to purpose perforated panels, in terms of costs and efficiency. In this context, the present work takes into account the influence of cavity size on the sound absorption properties of perforated plywood.

To this purpose, test were performed on specimens with a fixed drilling pattern, while different cavity thickness were arranged behind. Changing the cavity thickness, in fact, represents an easy way for modifying the absorption behaviour of a certain panel.

The results of this preliminary experimentation provide detailed indications, which in literature are still limited, concerning the values of resonance frequency associated to cavity thickness variations.
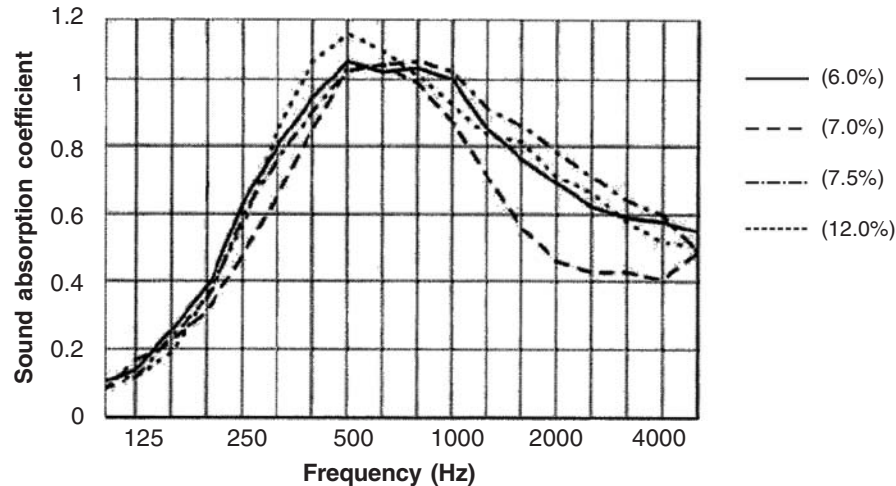
Fig. 5. Sound absorption values of perforated wood-based panels with different passing light percentages: (6.0%); (7.0%); (7.5%); 12.0% [from 7].

2. MATERIALS AND METHODS

For the present work plywood was chosen as a lightweight and nice looking wood-based product adequate for ceilings and walls covering. Nowadays timber is mainly destined for the production of plywood, whose main end-uses are furniture components, interior joinery and interior panelling both in building sector and in marine craft [12].

2.1 The Wood-Based Panel

The plywood used for this work was 4 mm thick with 3-layers composition. The veneers were glued by means of a MUF (melamine-urea-formaldehyde) adhesive system and the panel was complying the class 2 of EN 314-2 for use in humid conditions [13]. The mean density was 460 kg/m^3.

2.2 The Kundt's Tube Test

To measure diffuse sound incidence, the coefficient can be determined through the reverberation room method, in accordance with EN ISO 354 [14]. However, this requires large-sized samples and is not suitable for material at development stages.

An alternative is represented by the impedance tube (Kundt's tube) method, which is limited to normal incidence sound but, requiring smaller samples, is better for research activity. Hence, in this work the normal incidence sound absorption coefficient was determined by the impedance tube method (Fig. 6), according to EN ISO 10534-2 [15].

This method requires placing the specimen at one end of a cylindrical impedance tube. Plane waves are then generated in the tube by a sound source and the relative pressures are measured by two microphones positioned near to the specimen.

The complex acoustic transfer function of the signal is determined and used to compute the normal incidence absorption coefficient.

This is calculated by means of Equation (3)

$$a = 1 - r_2 \qquad\qquad (3)$$

in which the normal incidence reflection factor (r) is estimated for frequencies ranging from 50 to 1.600 Hz according to Equation (4) :
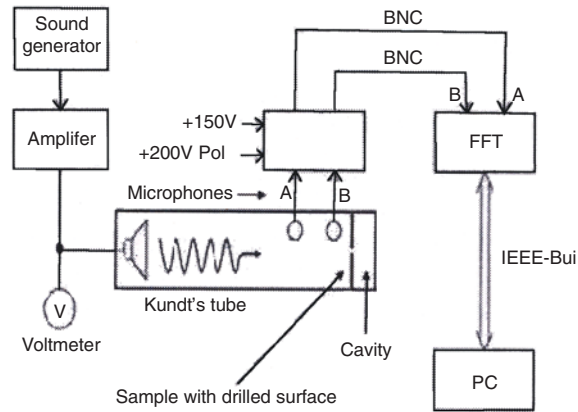
Fig. 6. Outline of the test method device, mainly constituted by a sound generator, the Kundt's tube, two microphones, a FFT analyser and a PC for data processing.

$$r = \frac{H_{12} - H_1}{H_R - H_{12}} e^{2jk_0x_1} \qquad (4)$$

where H_{12} is the transfer function for the total sound field, H_I is the transfer function for the incident wave alone, HR is the transfer function for the reflected wave alone, j $is\sqrt{}^{-1}$, k_0 is the wave number (ratio of angular

2.3 The Specimens

Circular specimens with 99.8 mm diameter were obtained from okoumé plywood. These were cut using a computer numerical control (CNC) milling cutter (Fig. 7), in order to achieve the high dimensional accuracy required by the test (+0.0; -0.1 mm).

Such a precision is necessary for assuring the complete contact between the circular border of the specimen and the inner circumference of the tube. In fact, even small voids would alter the volume of the cavity and consequently influence the test results.

After cutting, specimens were perforated using a hand-drill. Holes diameters were then measured with a digital
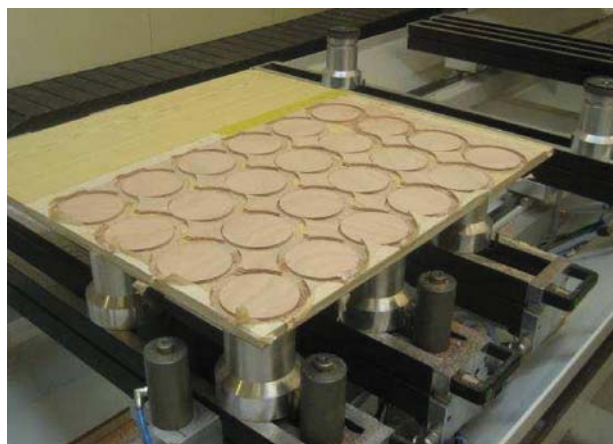
Fig. 7. Cut of 24 circular specimens realized by means of a CNC milling cutter. Specimens were drilled and used for the Kundt's tube test.

calliper in order to check the accuracy of their sizing. The adopted drilling pattern consisted of 9 holes with ray 2 mm, corresponding to 1.5 of drilling percentage (Fig. 8). Holes were symmetrically realized around specimens centre, complying with EN 10534-2.

In this work a single drilling pattern was realized, since the main aim was to evaluate how variations in cavity thickness influence the absorption properties of the system.
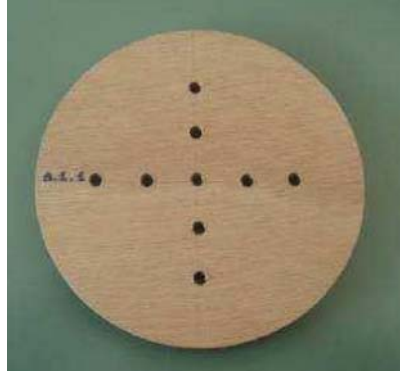
Fig. 8. Tested specimen with diameter 99.8 mm and drilling pattern made of
9 holes of ray 2 mm symmetrically disposed.

Specimens were laid in the Kundt's tube leaving an empty cavity between them and the metallic end of the tube. This setup allowed to simulate the laying conditions of the panels as wall-ceiling covering with an empty space at the back.

The cavity of the impedance tube was set in 7 different thickness, respectively 4.5, 9, 15, 22, 30, 60 and 80 mm. The section area of the cavity was fixed and coincident with the circular perimeter of the tube.

Therefore, changing the thickness was the only way to modify the volume and consequently the sound absorption properties of the tested system, as before mentioned in equation (2). The sound absorption amounts in the low frequency range were measured for each cavity thickness. Following reported data are the average of 3 test repetitions as recommended by EN 10534-2.

While in this testing procedure the only varying parameter was the cavity thickness, in design and production stages the desired sound absorption properties of a certain panel can be obtained by varying holes number, holes diameter or neck thickness.

Aim of the present work was anyway to focus on the influence of cavity thickness. Finally, in order to know the absorption properties of the panel, the above described test was also performed on an undrilled specimen.

3. RESULTS AND DISCUSSION

Before to focus on other results, Figure 9 shows the sound absorption measured in the low frequency range for the undrilled plywood panel.

The above graph clearly indicates that 4 mm plywood is a sound reflecting material. In fact, its sound absorption coefficient varies from 0.02 to 0.04 in the whole low frequency range. This confirms the low values commonly reported regarding the sound absorbing behavior of wood and plywood [16].

Figure 10 illustrates the sound absorption values obtained in the low frequency range for the testing specimens with different thickness of the cavities.

The comparison between figures 9 and 10 underlines how the system made of surface drilling and different cavity volume at the back can considerably improve the sound absorption behaviour.
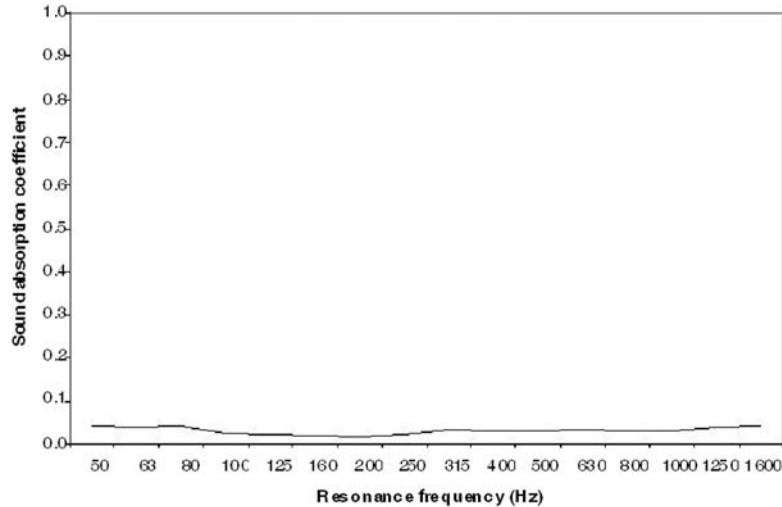
Fig. 9. Sound absorption values measured for the undrilled plywood panel.

Considering that the resonance frequency (ωH) of each curve is the frequency value (in Hz) at which the absorption peak is reached, the figure shows that the different curves are selective around their respective resonance frequency.

In fact, absorption values quickly decrease before and after the peaks. The values of absorption peaks and resonance frequencies depending on cavity thickness are also shown in Table 1.
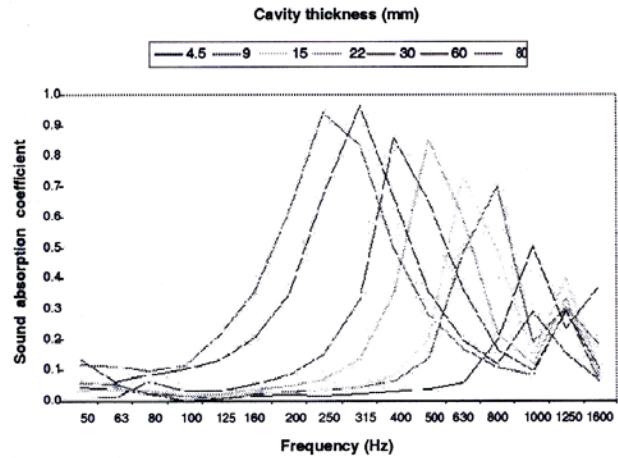
Fig. 10. Sound absorption values measured for different cavity thickness.

Table 1. Cavity thickness of the Helmholtz system with correspondent resonance frequency and averaged absorption peak values

Cavity thickness (mm)	Resonance frequency (Hz)	Average absorption coefficient	std.dev.
4.5	1000	0.50	0.02
9	800	0.70	0.03
15	630	0.77	0.01
22	500	0.85	0.01
30	400	0.86	0.01
60	315	0.96	0.01
80	250	0.94	0.02

These data quantify how changing in cavity thickness determine a slide of peaks towards lower frequencies. This phenomenon goes with a simultaneous increasing of the absorption peaks values, which

grow from 0.50 for the 4.5 mm thick cavity to 0.94 for that of 80 mm. This is due to the increasing of the air volume included into the cavity, which becomes progressively more adequate to perform the spring effect of the Helmholtz system.

Figure 11 takes into account the peak values listed in Table 1. Each peak value is characterized by its specific cavity thickness and resonance frequency. The non-linear regression was performed considering cavity thickness as the independent variable and resonance frequency as the dependent one.
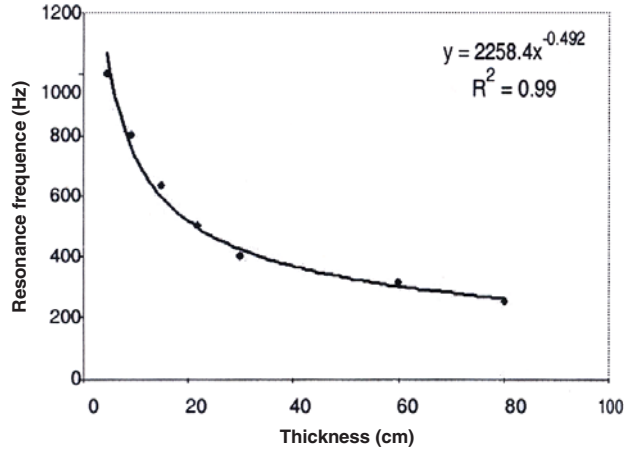
Fig. 11. Cavity thickness vs. resonance frequency of the absorption peaks.

The regression was performed using the power Equation

$$y = ax^b \tag{5}$$

The power form was chosen to attain to the physical law explaining the resonance frequency ωH of an ideal Helmholtz resonator. In fact, ωH is given by the basic Equation (6)

$$\omega H = c_0 \sqrt{\frac{S}{L.V}} \tag{6}$$

where c_0 is the sound speed, S is the hole area, L is the depth of the open hole and V is the volume of the empty cavity [8].

Since the only varying parameter was thickness, the only variable in (6) is the volume V, while S and L can be considered as constants. Therefore the Equation can be rewritten as (7)

$$wH \quad aV^{-0.5} \tag{7}$$

where a is a constant and V is the volume of the cavity.

The coefficients found for Equation 4 regression are given in Equation (8)

$$y = 2258.4\, x^{-0.492} \tag{8}$$

for which R^2 resulted 0.99 (p-value < 0.001). This suggests that the experimental results strictly attain to the physical law of the Helmholtz resonance.

Hence, the coefficients found through this method are reliable and suitable to be used for the development of new estimation models.

Finally, figure 12 shows the correlation between resonance frequency and sound absorption coefficient of the peak values.

The performed correlation assumes the linear form of equation (9)

$$y = -0.0006\,x + 1.1184 \tag{9}$$

for which r resulted -0.98 (p-value < 0.001).

Figure 12 illustrates that for frequencies below 500 Hz the tested system is able to provide sound absorption coefficients higher than 0.80.

On the opposite, increasing in the resonance frequency determines a simultaneous decreasing of the system efficiency. For this reason, perforated wood-based panels are used for acoustic improvement in the low frequency range, while for sound control at medium and high frequency other products are preferred.
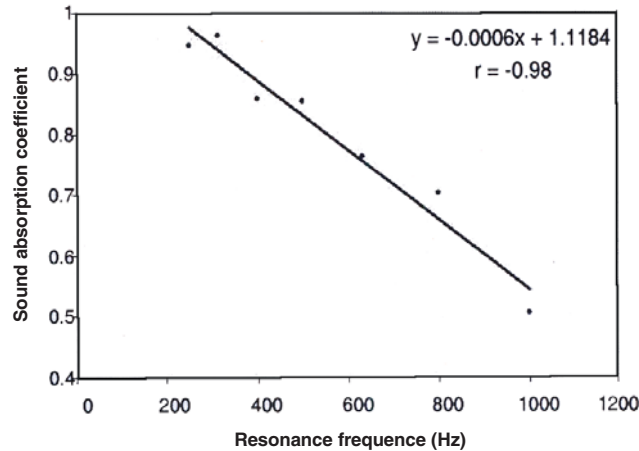
Fig. 12. Negative linear correlation between resonance frequency and sound absorption coefficient achieved by the peaks.

4. CONCLUSIONS

Nowadays many large scale buildings present poor acoustic performance, particularly with respect to the noise emitted in the low frequency range. For sound control in these environments, perforated wood-based panels are widely used as ceilings or walls covering thanks to their sound absorption properties.

Despite the interest in using and producing these panels, to this day accurate estimation models are still unavailable. As a consequence, the only means of evaluating the sound absorption behavior of a certain panel is to perform experimental measurements.

Therefore, the present work analyzed the absorption properties of drilled plywood with empty cavity at the back, in order to simulate the end-use laying conditions. The attention was focused on the influence of cavity thickness, since varying this parameter represents an easy way to modify the sound absorption properties of the panel.

The tested Helmholtz systems turned out able to achieve absorption values higher than 0.90 in the low frequency range. It was also found the regression equation explaining the resonance frequency values depending on cavity thickness.

The coefficients characterizing the regression equation will be further used for R&D activity. In particular, the experimentation will be repeated using different sets of drilling patterns, panel thickness and cavity size, in order to obtain a wider dataset and constitute a large number of regression equations characterizing the different Helmholtz systems.

The aim is to contribute to the elaboration of reliable models explaining the absorption properties of perforated plywood depending on the cavity thickness at their back. Accurate models could enable to fit the absorption properties of a certain panel to the specific needs of the enclosure in which it will be used just by varying the cavity sizing. This represents an easy way to calibrate the acoustic control of an enclosed space and might be particularly relevant in acoustic complex environments such as large scale buildings.

5. ACKNOWLEDGEMENT

6. REFERENCES

[1] S.K. TANG and J.W.C. CHAN, 1996. Some characteristics of noise in air-conditioned landscaped offices. *Appl. Acoust.*, **48** (3), 249-267.

[2] P.H. TROMBETTA ZANNIN and D.P. ZANARDO ZWIRTES, 2009. Evaluation of the acoustic performance of classrooms in public schools. *Appl. Acoust.*, **70** (4), 626-635.

[3] A. WHITE, 1999. The effect of the building environment on occupants: the acoustics of dining spaces. MPhil dissertation, University of Cambridge, UK.

[4] M. PORTO NUNES NAVARRO and R. LEAL PIMENTEL, 2007. Speech interference in food courts of shopping centres. *Appl. Acoust.*, **68** (3), 364-375.

[5] K. JENSEN and E. ARENS, 2005. Acoustic quality in office workstations, as assessed by occupant surveys. Proceedings of Indoor air: 10th International Conference on Indoor Air quality and Climate, Beijing, China, Sept. 4th-9th.

[6] H.V. FUCHS, X. ZHA, X. ZHOU and H. DROTLEFF, 2001. Creating low noise environments in communication rooms. *Appl. Acoust.*, **62** (12), 1375-1396.

[7] A.P. PATT (Ed.), 2010 - Acoustic paneling. Patt Spa, Udine, Italy.

[8] V. FASOLD and E. VERES, 1998. Sound protection and room acoustics in practice: design examples and building solutions (German). Verlag für Bauwesen, Berlin, Germany.

[9] T.D. ROSSING (Ed.), 2007. Springer handbook of acoustics. Springer, Würzburg, Germany.

[10] F.A. EVEREST and K.C. POHLMANN, 2009. Master handbook of acoustics 5th edition. McGraw-Hill, USA.

[11] M.D. LIN, K.T. TSAI AND B.S. SU, 2009. Estimating the sound absorption coefficients of perforated wooden panels by using artificial neural networks. *Appl. Acoust.*, **70** (1), 31-40.

[12] F. BRUNCK, F. GRISON and H.F. MAÎTRE, 1990. L'okoumé Aucoumea klaineana Pierre: monographie. CIRAD-CTFT, Nogent-sur-Marne, France.

[13] EN 314-2:1993. Plywood. Bonding quality. Part 2: requirements.

[14] EN ISO 354:2003. Acoustics. Measurement of sound absorption in a reverberation room.

[15] EN 10534-2:2001. Acoustics. Determination of sound absorption coefficient and impedance in impedance tubes. Part 2: transfer-function method.

[16] V. BUCUR, 1995. Acoustics of wood. CRC Press, Boca Raton, Florida.

1 - 3 Piezocomposite Tonpilztransducer for Underwater Applications

*Regiva Abisekaraj I., Sanjaya Kumar Swain, AVNR Rao, K. Trinath, L.A. Gavane† and C. Durga Prasad†

Naval Science & Technological Laboratory, Visakhapatnam, India
†Naval Materials Research Laboratory, Ambernath, India
e-mail: abisekaraj@gmail.com

ABSTRACT

Underwater tonpilz transducer using 1-3 piezocomposite rings has been designed and the performance of the same for transmitting voltage response (TVR), free field sensitivity (FFS) and bandwidth has been analysed using ATILA, a FEM package. Equivalent material properties in the form of single phase were computed and the same material is used for the purpose of modeling. The modeling is also described in brief. Tonpilz transducers have been fabricated using 1-3 piezocomposite rings. The prototype transducers are evaluated for their TVR and FFS.

1. INTRODUCTION

Certain limitations like high attenuation in water medium precluded the use of electromagnetic (EM) waves for underwater applications, thus leaving this window of opportunities to sound waves which have obvious advantage over EM waves with respect to range in underwater environment. Piezoceramic materials, due to their high electromechanical coupling coefficients, high piezoelectric charge coefficients and low electrical and mechanical losses are widely used as active material in different electro-acoustic transducers for underwater applications. But at the same time they suffer from some inherent limitations like brittleness, high density and high acoustic impedance, difficulty in large area coverage etc to name a few. Hence to overcome these limitations of conventional piezoceramics while retaining their superior properties, there have been attempts for new materials over the past several decades. Piezocomposites, a combination of piezoceramic and polymer emerged as suitable material for acoustic transducer applications [1, 2, 3]. A piezocomposite is a two phase material, wherein arrangement of piezoceramic and polymer within the material or otherwise called connectivity, ten possible connectivity patterns like 0-0, 0-1, 0-2, 0-3, 1-1, 2-1, 2-2, 2-3, 1-3 and 3-3   are possible for a diphasic composite [4,5]. Out of these 1-3 type of piezocomposites consisting of aligned, unidirectional piezoceramic rods within a three dimensional polymer matrix have attracted considerable attention with reference to underwater applications because of their superior piezoelectric properties, flexibility to conform to curved surfaces, ease of fabrication, lower and adjustable acoustic impedance, minimum lateral mode response etc [6,7,8,9].

The most important performance parameters of an electro-acoustic transducer are resonance frequency, bandwidth, transmitted sound pressure level and receiving sensitivity. These parameters in turn depend upon design of transducer, passive and active material used in transducer and nature of application. Considering the above influencing factors, a sandwich like design called Tonpilz transducer is most widely

used for low frequency and high power applications. Tonpilz meaning singing mushroom in German is made up of piezoactive materials sandwiched between head and tail mass, prestressed by a central bolt. As 1-3 piezocomposite has superior properties compared topiezoceramics and other piezocomposite materials, an attempt is made to design and fabricate a tonpilz transducer using 1-3 piezocomposite rings.

The tonpilz transducer using 1-3 piezocomposite rings is designed and simulated using FEM software ATILA(Analysis of Transducer by Integration of LAplace equation). Finally the same is fabricated and tested in an acoustic tank facility for underwater acoustic properties like transmitted voltage response, receiving sensitivity, resonance frequency and bandwidth and the results are reported here.

2. MODELING OF 1 - 3 PIEZOCOMPOSITE RINGS

The most important properties of a 1-3 piezocomposite with reference to underwater electro-acoustic transducer applications are piezoelectric strain coefficients, electromechanical coupling coefficient, stiffness and acoustic impedance. As piezocomposites are the heart of the tonpilz transducer, the output acoustic parameters of the transducer are greatly influenced by the dielectric, piezoelectric and elastic properties of 1-3 piezocomposite. Since 1-3 piezocomposite is a two phase material, its effective properties will be determined by the properties of its constituents i.e., piezoceramic and polymer, their volume fraction within piezocomposite, periodicity and the shape and size of 1-3 piezocomposite [10]. Hence before using 1-3 piezocomposite for tonpilz transducer fabrication, it is utmost important to determine the effective properties of 1-3 piezocomposite with respect to the above factors. A typical 1-3 piezocomposite material is shown in fig. 1. It is very difficult and time consuming to model this configuration. In order to simplify the problem, the 1-3 piezocomposite is simulated with a single phase material with equivalent properties. For this a theoretical model for the calculation of new material parameters of 1-3 composite having fine lateral periodicity developed by Chan and Unsworth [11] is used. Considering the important factors required for an electro-acoustic transducer in our intended application, PZT-5H, a Navy Type VI material and epoxy from Ciba - Geigy are taken as the constituents. PZT-5H is chosen as the active material due to its higher value of piezoelectric strain coefficients (d_{33} & g_{33}), electromechanical coupling coefficient (k_{33}) and dielectric constant [12]. The important properties of PZT 5H and Epoxy are given in the table 1. Rings are chosen as the desired shape in transducer fabrication to reduce mode coupling between vibration modes like thickness mode, radial mode and wall thickness mode [13, 14]. For this the lateral periodicity is chosen as sufficiently fine, so that 1-3 piezocomposite can be regarded as a single homogeneous phase. Then using the above model variation of piezoelectric properties, dielectric properties and elastic properties of 1-3 piezocomposite with volume fraction of PZT 5H are derived. Figures 2, 3 & 4 are showing the variation of key parameters like thickness coupling coefficient(kt) and piezoelectric strain coefficients(d_{33} & g_{33}) with volume fraction of PZT-5H.
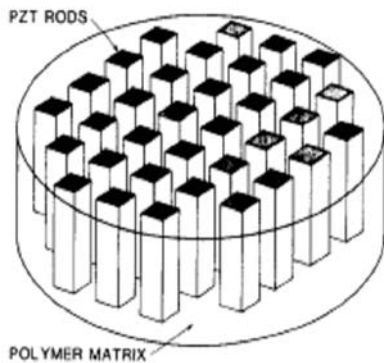

Fig. 1. Typical 1-3 piezocompositestructure showing one-dimensional alignment of PZT rods in a polymer matrix.
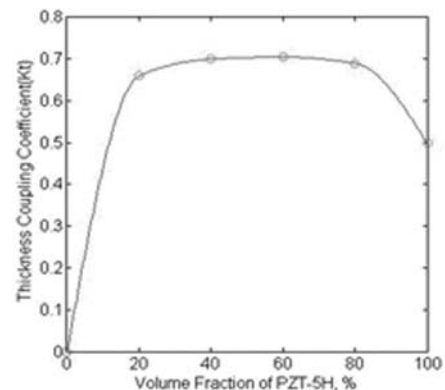
Fig. 2. Variation of electromechanical coupling coefficient of 1-3 piezocomposite material with volume fraction of PZT-5H.
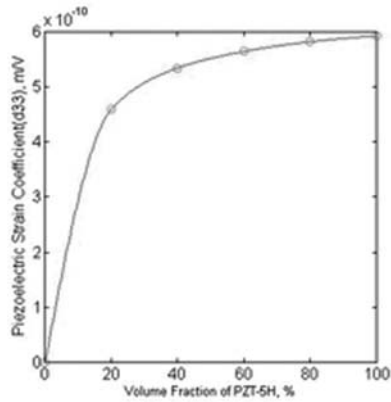
Fig. 3. Variation of d_{33} of 1-3 piezocomposite material with volume fraction of PZT-5H.
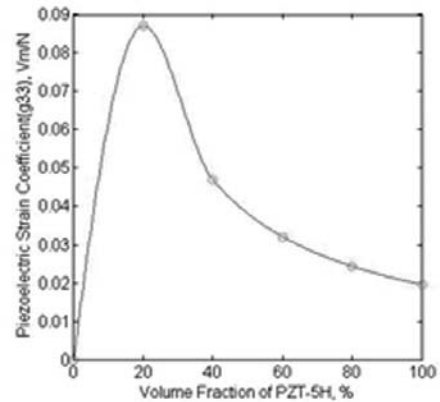
Fig. 4. Variation of g_{33} of 1-3 piezocomposite material with volume fraction of PZT-5H.

Considering the fact that the transducer being designed will be used for both transmission and reception, a number of parameters have to be optimized to achieve the desired characteristics. The piezocomposite with 60 volume percent PZT phase has shown a maximum kt (fig.2) and the d_{33} value is almost near to the maximum (fig.3). Even though the g_{33} coefficient is not high at 60 volume percent PZT phase, a trade off has to be arrived at as the same transducer is used for both transmitting and receiving applications. Then the effective properties of 1-3 piezocomposite at that volume fraction are calculated for tonpilz transducer design and are given in appendix I.

3. FABRICATION OF 1-3 PIEZOCOMPOSITE RINGS

Sintered, poled PZT 5H blocks of dimensions of 50 x 50 x 5 mm thickness were mounted on ahigh speed ceramic cutting machine and deep grooves were made in the plates using a diamond impregnated saw blade. The plates were removed and cleaned ultrasonically and the polymer was poured under vacuum into the grooves and cured at room temperature. After polishing of excess polymer, the plate is remounted on the machine and a series of parallel cuts were made at 90 degrees to that of the first set of cuts to get PZT rods of required cross section. After refilling with polymer as per the procedure mentioned above, the plates were surface ground to 3 mm thickness. Piezocomposite plates of required dimensions have been cut from each block. A centre hole of 6 mm diameter has been drilled and each block has been machined to get a composite ring of 19 mm OD, 6 mm ID and 3 mm thickness. The fabrication of 1-3 piezocomposites has been described in detail elsewhere [16, 17]. The piezocomposite rings so formed were electroded using silver epoxy and repoled by corona poling to retain the piezoelectric activity that might have lost due to the grinding operations adopted in fabricating thepiezocomposites followed by development of composite rings of required dimensions. These rings were used for the development of piezocompositetonpilz transducers. The piezocomposite rings developed for this application are shown in fig.5.

Fig. 5. 1-3 iezocompositerings

4. DESIGN OF TONPILZ TRANSDUCER

In a conventional tonpilz transducer, the radiating head and tail mass are used to reduce the resonance frequency of the piezoactive stack used and bring it close to the operating frequency and thus increase the amplitude of vibration at the operating frequency. Hence the material required for radiating head should have acoustic impedance between the values of water and 1-3 piezocomposite material. Again it should be a low loss material for good transfer of energy. In order to avoid the flexing of transducer to any significant extent, it is desirable to make its flexural resonance above two times the operating frequency. Hence a material having high value of mechanical conductance is suitable for this purpose. Considering all these factors aluminium is considered for head mass as it has better corrosion resistance properties and moderate acoustic impedance (13.8 MRayl), high mechanical quality factor ($\geq 50,000$) and high mechanical conductance (2.5×10^2 m/s). The tail mass is typically 3 to 5 times more massive than the radiating head mass in order to minimize the acoustic radiation from the back of the transducer. The role of the tail mass is to limit backward acoustic radiation and to tune the resonance frequency. To be effective, it must be made of a dense enough material (e.g. brass, steel). Brass is selected as tail mass based on corrosion resistance properties and impedance considerations. As 1-3 piezocomposites are stronger in compression than in tension, there is a need to apply a static compressive force in order to prevent dynamic tensile forces in the ceramic. For this a stress bolt is used to pre-compress the piezocomposite material by passing it through the center of the piezo composite stack. The steady compressive force applied by the bolt should be greater than the peak alternating force in the stack. It is advisable to allow a factor of safety by making this compressive force at least four times the peak value of the alternating force in the piezocomposite. The bolt must be strong enough to safely apply the required compressive force. Since the stresses in a transducer are dynamic, the requirement for a center bolt is a material that has a high fatigue limit and tensile strength. Beryllium copper (Be-Cu) is selected as stress bolt because of its high tensile strength (1470×10^6 N/m^2) and high fatigue strength (290×10^6 N/m^2). Beryllium copper is less susceptible to the effects of stress concentrations and this results in a bolt design with rather better safety factors. The mechanical properties of Aluminium, Brass and Beryllium copper are given in the table.2.

In general, tonpilz transducers are designed with radiating head dimension corresponding to $\lambda/2$, where λ is the wavelength of sound in water medium. The dimensions of active and passive materials used in the transducer as mentioned above are calculated based on the operational frequency requirement and other factors like power handling capacity, transmitting sound pressure level , receiving sensitivity and pressure withstanding capacity[18,19,20].

To optimize the dimensions and the design of the transducer for desired output, finite element modeling (FEM) method is used. Finite element modeling (FEM) is a convenient and powerful method of estimating the properties of 1-3 piezocompositetonpilz transducers like resonance frequency, transmitted sound pressure level, receiving sensitivity and 3-dB bandwidth with great accuracy[21,22,23]. So the designed 1-3

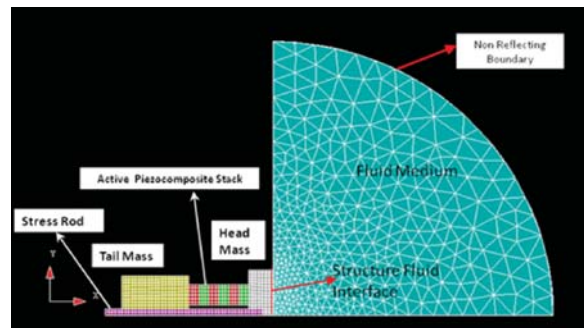Fig. 6. A designed and developed prototype 1-3 iezocompositetonpilztransducer.

Fig.7. 2D Axis-symmetric model of tonpilz withfluid.

piezocompositetonpilz transducer is simulated with finite element method software ATILA [24]. ATILA is capable of handling piezoelectric structures in a fluid domain incorporating fluid-structure interactions. A 2D axis-symmetric model is constructed using the equivalent single phase material and the radiating fluid. The model is then converted into FE model by meshing. The FE model is explained in fig. 7. The properties of piezocomposite rings developed for this application are considered for analysis. The active piezocomposite rings in the stacks are connected electrically in parallel and mechanically in series. The infinite boundary of fluid is achieved by putting the non-reflecting elements. The model is solved for the transmitting voltage response, receiving sensitivity etc. The modeling results are reported elsewhere [25].

5. PROTOTYPE FABRICATION

After modeling and simulation four number of prototype 1-3 piezocompositetonpilz transducers (E1, E_2, E3 & E4) are fabricated using the above active and passive materials, and one of the prototypes is shown in fig.6. Six number of 1-3 piezocomposite rings are stacked together by using an adhesive specially developed and well proven for this purpose. These multi-layer stacks have advantages over a single-layer transducer of equivalent thickness. If there are N layers in a stack, then the electric field in the stack is N times as that of a single layer of equivalent thickness and so is the output pressure amplitude. The fabrication of multilayer 1-3 piezocomposite stack is tricky as misalignment of pillars could severely affect the performance of the transducer [26] and poor adhesion of various layers would result in weak structural integrity of the stacks, which in turn leads to spurious resonances. The 1-3 piezocomposite rings in the stack are in mechanically series configuration and electrically connected in parallel configuration to reduce the overall electrical impedance of the transducer.

6. RESULTS AND DISCUSSION

All the transducers are encapsulated using an acoustically transparent material. The transmitting and receiving performances of these 1-3 piezocompositetonpilz transducers are measured using tone-burst method [27] under free-field conditions over a desired frequency range. Comparison calibration method with Bruel&Kjaer Hydrophone Calibration System 9718 is used to determine the transmitting and receiver properties of the transducers. Hydrophones of type 8104 (Bruel & Kjaer, Denmark) are used as the standards. The measured Transmitting Voltage Response (TVR) and the Free Field Sensitivity (FFS) response as a function of frequency are shown in fig. 8 and 9.
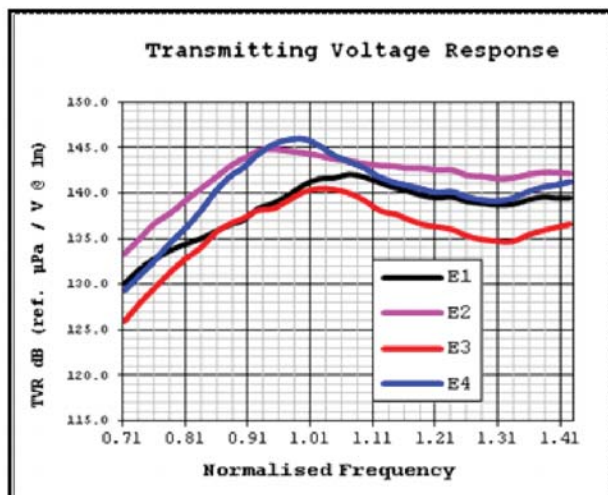

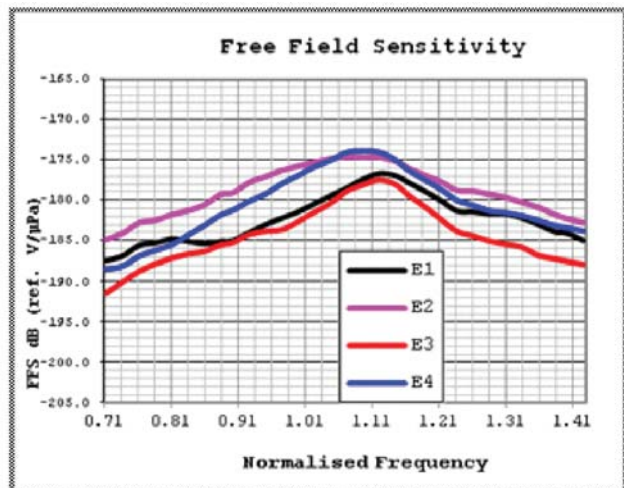Fig. 8. TVR of prototype transducers tested in acoustic tank.

Fig. 9. FFS of prototype transducers tested in acoustic tank

TVR, FFS and bandwidth are the most desired parameters of an electro-acoustic transducer required for underwater weapon systems to achieve higher source level and hence the range, higher data transfer rate and more options for operating band . Higher and higher values of these parameters are always desirable. But at the same time it is not possible to get higher values of all these at a particular resonance frequency. Hence there is always a trade-off between these parameters. The results of the measurement shows the 3 dB bandwidth of 9 kHz with a peak TVR of 144.9 dB ref. µPa/V @ 1m. Similarly, the best FFS 3 dB bandwidth is 6 kHz with a peak FFS of   -174.5 dB ref. V/µPa. The values of TVR and bandwidth obtained are better than a conventional tonpilz transducer using piezoceramic rings as active elements and FFS is comparable for same frequency of operation. But the 1-3 piezocompositetonpilz transducers are less in weight and length for the same frequency and band of operation which is an added advantage for underwater weapon systems like torpedo where space and weight are critical and stringent.

The variations in the TVR and FFS among the transducers are due to the misalignment of the piezoceramic pillars in the piezocomposite ring stack which is a very critical factor regarding the output parameters of transducer. These variations can be minimized and the performance of the transducers can be improved by ensuring proper alignment of piezoceramic pillars of all the rings.

7. CONCLUSION

Tonpilz transducer to be used in active mode for underwater applications is designed using 1-3 piezocomposite ring with optimum volume fraction of PZT-5H. The same is simulated by ATILA for underwater elctro-acoustic properties like TVR, FFS and bandwidth. Four numbers of prototype 1-3 piezocompositetonpilz transducers are fabricated and tested in an acoustic tank for the above acoustic properties over a desired frequency range. There is a scope to improve the performance in terms of amplitude and bandwidth by ensuring the proper alignment of active PZT rods in all the six rings in each stack.

8. ACKNOWLEDGEMENT

REFERENCES

[1]   R.E. NEWNHAM, L.J. BOWEN, K.A. KLICKER and L.E. CROSS, Composite piezoelectric transducers, *Mater. Eng*. **2**, 93–106.

[2]   W.A. SMITH, A.A. SHAULOV and B.M. SINGER, 1984. Properties of Composite Piezoelectric Materials For Ultrasonic Transducers, Ultrasonics Symposium , *IEEE* 539-544.

[3]   A. SAFARI, 1994. Development of piezoelectric composites for transducers, *J. Phys. III* **4**, 1129-1149.

[4]   R.E. NEWNHAM, D.P. SKINNER and L.E. CROSS, 1978. Connectivity and Piezoelectric-Pyroelectric Composites,*Mat. Res. Bull.* **13**, 525-536.

[5]   W.A. SMITH, 1993. Modeling 1–3 composite piezoelectrics: hydrostatic response, *IEEE Trans.* Ultrason. Ferroelec. Freq. Control **40**, 41–48.

[6]   T.R. GURURAJA, W.A. SCHULZE, L.E. CROSS, R.E. NEWNHAM, B.A. AULD, and Y.J. WANG, 1985. Piezoelectric composite materials for ultrasonic transducer applications: Part I: Resonant modes of vibration of PZT rod–polymer composites, *IEEE Trans*. Sonics Ultrason. SU32, No. **4**, 481-498.

[7]   W.A. SMITH and B.A. AULD, 1990. Modelling 1–3 composite piezoelectrics: thickness-mode oscillations, *IEEE Trans.* Ultrason. Ferroelec. Freq. Control **38** 40–47.

[8].   G. HAYWARD, J. BENNETTE and R. HAMILTON, 1995. A theoretical study on the influence of some constituent material properties on the behaviour of 1–3 connectivity composite transducers, *J. Acoust. Soc. Am*. **98**, 2187–2196.

[9].   1989. Simple Model for Piezoelectric Ceramic / Polymer 1-3 Composites Used in Ultrasonic Transducer Applications – Helen Lai Wah Chan and JosephUnsworth, *IEEE UFFC*, **36**, 434-441.

[10] C P Chong, H L W Chan, M H Chan and P C K Liu,2005, Resonances in 1-3 Piezocomposite Rings, *Applied Physics* A **80**, 1793 – 1799.

[11] C. DURGA PRASAD, L.A. GAVANE, S.C. SHARMA and RAMJILAL, 1998. PZT-polymer composite hydrophones for underwater applications, *Proceedings of UDT* Pacific 98 Conference and Exhibition, Sydney, Australia, 356 – 361.

[12] D. STANSFIELD, 2003. Underwater Electroacoustic Transducers, *Peninsula Publishing*.

[13] Oscar Bryan Wilson, Introduction to Theory and Design of Sonar Transducers, *Peninsula Publishing*, 1988.

[14] H. CHARLES SHERMAN and L. JOHN BUTLER, 2007. Transducers and Arrays for Underwater Sound, *Springer Science + Business Media, LLC*.

[15] DA LIE PEI AND YONGRAEROH, 2008. Design of an Underwater Tonpilz Transducer with 1-3 Piezocomposite Materials, *Japanese Journal of Applied Physics*, **47**, 4003–4006.

[16] ATILA Finite element modelling software for elastic, piezoelectric, magnetostrictive and electrostrictive structures radiating in a fluid, *ISEN Recherche*, Lille, France, 2003.

[17] R.J. BOBBER, 1970. Underwater Electroacoustic Measurements, *Naval Research Laboratory, Washington*, USA.

Detached Eddy Simulation of Propeller Noise

S. Rama Krishna[1], S. Subhas[2], A. Rama Krishna and K. Ramji[3]
*[1]Department of Mechanical Engineering, G.V.P. College of Engineering (A),
Visakhapatnam 530041, Andhra Pradesh, India*
*[2]Department of Mechanical Engineering, VITAM, Visakhapatnam 530048,
Andhra Pradesh. India*
*[3]Department of Mechanical Engineering, Andhra University College of engineering (A),
Visakhapatnam 530003, Andhra Pradesh. India*
e-mail: shinagamsai@gmail.com

ABSTRACT

Noise reduction and control is an important problem in the performance of underwater acoustic systems. Sound generated by a propeller is critical in underwater detection and it is often related to the survivability of the vessel especially for military purpose. Detached eddy simulation (DES) is a suitable method for the simulation of the sound radiation of turbulent flows, providing access to resolve turbulent scales at minimal computational cost. Experiments are very expensive and time consuming, so the present paper deals with a complete computational solution for the flow using Fluent 6.3 software. This paper presents a numerical investigation of unsteady non-cavitating turbulent flow around a full scale INSEAN E779a propeller consists of four blades of diameter 227 mm with the eddy viscosity model of Spalart and Allmaras and the DES approach. Through this study, the dominant noise source of the underwater propeller is analyzed, which will provide a basis for proper noise control strategies.

Spalart and Allmaras eddyviscosity model is able to give an excellent description of the flow, in terms of both velocity prediction and force coefficients. DES modeling can track the vorticity field of unsteady fluctuation of the flow for a longer distance and successfully predicts the onset of instabilities in the wake to predict the noise, with excellent agreement with experiments. To generate the structural grid with hexahedral cells commercially available grid generation code ICEM CFD was used. The noise is predicted in the time domain and the flow noise is transformed to the frequency spectrum using Fast Fourier transform. The flow field is analyzed with DES method and then the time-dependent pressures are used as the input for Ffowcs Williams-Hawkings formulation to predict the far-field acoustics. Noise characteristics are presented according to noise sources and conditions. The receiver position is 1m in downstream of propeller aligned to the propeller shaft. From noise results it is observed that maximum sound pressure level is at inlet of the propeller is 107.3 dB. Peak sound pressure level values are observed at first blade passing frequency and its harmonics. The unsteady loading noise is known to be dipole in nature, with a strong radiation tendency toward the observer on the hub axis. The unsteady loading noise is mainly governed by irregularities of the fluctuation of surface pressure on propeller blades. Through this study, the dominant noise source of the underwater propeller is analyzed, which will provide a basis for proper noise control strategies.

1. INTRODUCTION

Sound generated by a propeller is critical in underwater detection, and it is often related to the survivability of the vessels especially for military purposes. The propeller generally operates in a non-uniform wake field behind the vessel. As the propeller rotates, it is subjected to unsteady force, which leads to discrete tonal noise, and cavitation. Therefore, underwater propeller noise can be classified into cavitating and non-cavitating noise. Cavitation of the underwater propeller is the most prevalent source of underwater sound in the ocean and it is often the dominant noise source of a marine vehicle. Submarines and torpedoes are usually operated under the deep sea enough to avoid cavitation. The non-cavitation noise of underwater propeller is numerically investigated in this study. Numerical investigation of unsteady non-cavitating turbulent flow around a full scale marine propeller is carried out with the eddy viscosity model of Spalart and Allmaras and the detached eddy simulation (DES) approach.

Steady and even unsteady Reynolds-averaged Navier-Stokes (SRANS and URANS, respectively) simulations cannot reproduce with sufficient accuracy the wake structures of wide-ranging spatial and time scales, whereas direct numerical simulations (DNS) of this type of flow are not feasible before due to the huge computational costs required. An essential problem in the use of LES is again the high computational cost required to sufficiently resolve the near-wall region, especially in high-Reynolds number cases. A possible alternative to LES is the detached-eddy simulation (DES), which is one of the hybrid methods that combine URANS and LES to obtain realistic solutions of practical high- Reynolds number cases flows at acceptable computational costs.

2. LITERATURE REVIEW

Seol et al. [1] analyzed noise prediction using time-domain acoustic analogy and boundary element method. The flow fieeld is analyzed with potential-based panel method, and then the time-dependent pressure data are used as the input for Ffowcs Williams Hawkings formulation to predict the farfield acoustics. Seola et al. [2] presents a numerical study on the non-cavitating and blade sheet cavitation noises of the underwater propeller. The noise is predicted using time-domain acoustic analogy. The flow field is analyzed with potential-based panel method, and then the time-dependent pressure and sheet cavity volume data are used as the input for Ffowcs Williams-Hawkings formulation to predict the far-field acoustics. Yu-cun Pan et al. [3] source-to-far-field computation procedure aiming at predicting the noise generated by the underwater propeller was presented. Detached eddy simulation (DES) was used to resolve the unsteady flow field, which was taken as input data as noise propagation. Far-field sound radiation was performed by means of Ffowcs Williams-Hawkings (FW-H) equation. The computation procedure was finally applied to a typical marine propeller, David Taylor Model Basin (DTMB) 4118. The sound pressure and directivity patterns of this propeller were discussed. Muscari et al. [4] presents the capabilities of numerical simulations with different turbulence models (RANSE and DES) to predict the complex flow past an isolated propeller have been assessed.

Pan [5] numerical study is on the acoustic radiation of a propeller interacting with non-uniform inflow has been conducted. Real geometry of a marine propeller DTMB 4118 is used in the calculation, and sliding mesh technique is adopted to deal with the rotational motion of the propeller. The performance of the DES (Detached Eddy Simulation) approach at capturing the unsteady forces and moments on the propeller is compared with experiment. Far-field sound radiation is predicted by the formation developed by Farassat, an integral solution of FW-H (Ffowcs Williams-Hawkings) equation in time domain. Jin-Ming [6] presents the blade frequency noise of a cavitating propeller in a uniform flow is analyzed in the time domain. The unsteady loading (of a dipole source) and the sheet cavity volume (of a monopole source) on the propeller surface are calculated by a potential-based surface panel method. Then the time-dependent pressure and the cavity volume data are used as the input for the Fowcs Williams-Hawkings formulation to predict the acoustics pressure.

3. NUMERICAL MODELS

The numerical methods used for simulation of flow field and acoustic prediction are as follows.

3.1 Flow solver

The Navier-Stokes Equations do not only describe turbulent flows but also their sound radiation. A direct numerical simulation (DNS) of the sound radiation is not possible with available computer resources for the Reynolds numbers of technical interest. The far-field radiation is then computed by solving integrals over a control surface based on acoustic analogies. To reduce the computational effort in the source region, the precise DNS is substituted by less expensive methods such as Large Eddy Simulation (LES) or Detached Eddy simulation (DES). Both methods rely on modelling the smaller scales while the larger scales are resolved in space and time. The difference between LES and DES lies in the treatment of the turbulent boundary layers. The resolution requirements of LES in the near wall region lead to unfeasibly fine grids for higher Reynolds number flows. DES is a hybrid RANS-LES method that applies RANS to the near-wall region and LES to separated flow regions, and is aimed at bridging the gap that exists between conventional Remolds averaged nervier stokes (RANS) and LES methods in terms of computational expense and predictive accuracy.

The Spalart-Almaras model in the RANS and the DES approach is used to model the unsteady fluctuation of the turbulent flow around a full scale marine propeller. The turbulent flow within the blade is formulated in a rotating reference frame, the Shear Stress Transport (SST) turbulent model is adopted in this paper. To predict the flow noise, the pressure and the geometry information of the propeller should be known. Here, the boundary pressure of the propeller at each time step, the area, and the normal vector are exported from CFD. Finally, the sound pressure is predicted in the time domain and the flow noise is transformed to the frequency spectrum using FFT.

Spalart and Allmaras eddy-viscosity model was able to give an excellent description of the flow, in terms of both velocity prediction and force coefficients. A further aspect that triggered the interest for the present analysis is the possibility to perform noise predictions based, for instance, on the Ffocws-William Hawking formulation where the hydrodynamic data are to be used as input for the noise computations. Unfortunately, a wall-resolved LES seems unpractical owing to the discretization requirements in the boundary layer region. Consequently, the only feasible approach to this problem seems to be the DES, where any attempt to directly capture the unsteady dynamics of the flow close to rigid walls is replaced by Remolds averaged nervier stokes modeling, while the direct description of the flow in the wake (the detached vortices) is retained.

The RANS models employed span a wide scale of mathematical complexity, beginning with the one equation Spalart-Allmaras (S-A) model with Edwards correction. Two-equation models are represented by the Wilcox k-ω model and linear local realisable k-ω model. The main feature of the DES performed in this study is that a single turbulence model (a slightly modified version of the S-A model) serves as a statistical model (i.e., URANS mode) in near-wall regions, and also serves as a subgrid-scale model (i.e., LES mode) in far-wall regions. Specifically, the nearest-wall-distance 'n' that governs the eddy viscosity in the original S-A model is replaced in the DES by a new length scale n □ defined as

$$n \,\square = \min\,[n, 0.65\Delta\_max]\;\Delta_{max}= \max\,[\Delta x, \Delta y, \Delta z]$$

where Δx, Δy and Δz denote the size of a control volume (or the grid spacing) in each direction. This simple formulation of the DES, however, raises an issue concerning the physical interpretation of the 'grey area' (n≈0.65Δ_max), where the operation mode is switched between URANS and LES, and the justification of this switch solely relies on the disparity in the scales between the attached- and detached-eddies.

3.2 Acoustic prediction

Lighthill proposed the acoustic analogy in the 1950s. Ffowcs Williams-Hawkings (FW-H) generalized the Lighthill acoustic analogy and included the effects of the general surfaces in the arbitrary motion in 1969. The FW-H equation is an appropriate tool for predicting the noise generated by the complex motion of the

solid bodies. Today, almost all deterministic rotor noise predictions are based on the FW-H equation. In recent years, various solutions were derived or the FW-H equation either in the frequency domain or in the time domain. In the early 1970s, most noise prediction methods were in the frequency domain because the time-domain methods generally require powerful computers.

The analytic solutions were obtained for some significant problems using the frequency domain analysis with some approximation. In the frequency domain analysis, the blade loading is often distributed on the ideal surface without thickness instead of the true blade boundary surface, and some approximation is also made for the distance between the noise source and the observer. Farassat developed several formulations for the solution of the FW-H equation in the time domain. In particular, the formulation is provides a solution for the monopole and dipole tonal sources for a given geometry, displacement and aerodynamic loading of the moving bodies. The implementation of this formulation is quite straight forward because the contributions from each propeller surfaces with different retarded times can be added to form an acoustic wave. The solutions need an estimation for the retarded times and an accurate representation for the blade loading.

4. NUMERICAL SETUP

Modelling of the propeller is done using CATIA V5R20. In order to model the blade, it is necessary to have sections of the propeller at various radii. These sections are drawn and rotated through their respective pitch angles. Then all rotated sections are projected onto right circular cylinders of respective radii as shown in Fig. 1. Now by using multi section surface option, the blade is modelled. After enclosing the entire surfaces solid is created as shown in Fig. 2. To generate the structural grid with hexahedral cells commercially available grid generation code ICEM CFD was used. Fig. 3 shows the computational domain used in the present noise
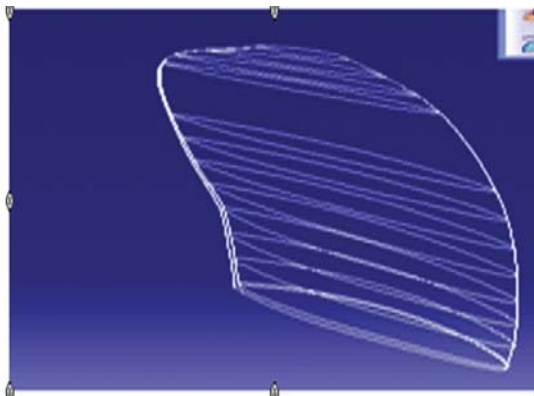

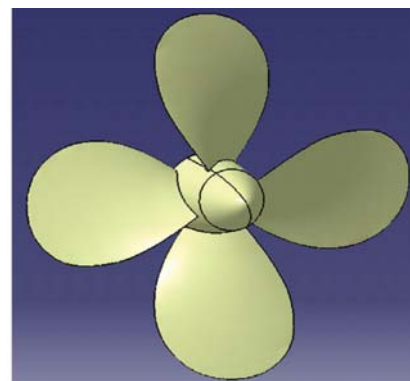Fig. 1. Profile of the propeller blade
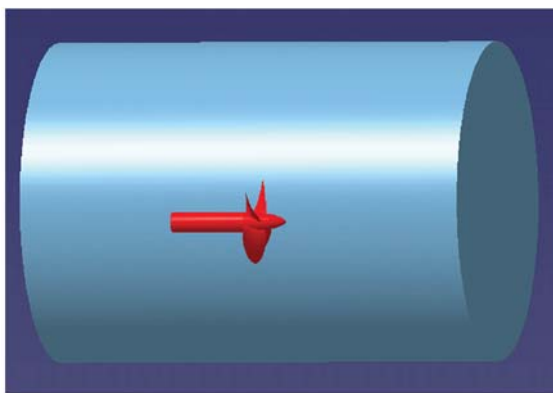

Fig. 2. Solid model of the propeller

Fig. 3. Complete domain of the propeller

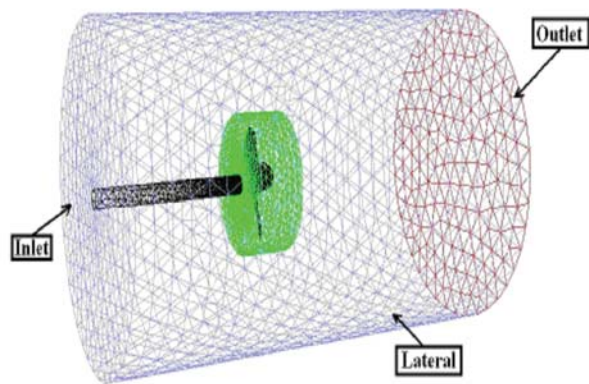

Fig. 4. Grid over the entire domain

simulations. The inlet was considered at a distance of 3D (where D is diameter of the propeller is 0.227 m) from mid of the chord of the root section. Outlet is considered at a distance of 4D from same point at downstream. In radial direction domain was considered up to a distance of 4D from the axis of the hub. This peripheral plane is called far-field boundary. The mesh was generated in such a way that cell sizes near the blade wall were small and increased towards outer boundary.

The numerical simulations have been carried out with a finite volume code method using FLUENT. The computation being performed in the rotating non-inertial frame of reference, a steady solution was obtained for the RANSE simulation; for the DES simulation, the solution was computed by including the physical time derivatives, and the chosen time step was always corresponding to a rotation of one degree for the propeller for the finer grid. After convergence there are 335454 and 750467 tetrahedral elements are in the inner volume (propeller volume) and outer volume (far field volume) respectively. The inlet and outlet are defined as "velocity inlet (6.22m/sec)" and "outflow". Fluid zone in the inner volume is defined as "moving mesh" and 1800 rpm in x-direction. However, fluid in the outer volume is defined as "velocity inlet (6.22m/sec)". Fig. 4 shows the grid and boundary conditions applied over the entire domain of the propeller. The reference pressure used for present simulations is 1?Pa and the frequency range is 0 to 800 Hz. The meshes of the propeller are physically rotated, and the time step is 0.0002s with a total simulation time of 10s.

5. RESULTS AND DISCUSSION

As to the question regarding the need of a (very CPU expensive) DES simulation with respect to a much faster RANSE approach. The results from the unsteady DES computation are presented to the field obtained by averaging 3600 instantaneous fields (i.e. 10 revolutions). In the unsteady force on the propeller surfaces are discretized by a number of tetrahedral elements. The strength of the noise source on each propeller surfaces is assumed to be constant. The contributions from each propeller surface with different retarded time can be added to form an acoustic wave. The acoustic pressure history in the observer's time is then formed. The time history of the acoustic pressure is transformed into the noise spectrum in the frequency domain through Fourier transformation. The receiver position is 1 m in downstream of propeller aligned to the propeller shaft. From these results it is observed that maximum sound pressure level is at inlet of the propeller is 107.3 dB. Fig. 5 shows the noise prediction graphs at inlet. Fig. 5 clearly shows that peak sound pressure level values are observed at rotational frequency (30 Hz), first blade passing frequency (120 Hz) and at the second order harmonic and these are predominated at low frequency only. The unsteady loading noise is known to be dipole in nature, with a strong radiation tendency toward the observer on the hub axis. The unsteady loading noise is mainly governed by irregularities of the fluctuation of surface pressure on propeller blades. Through this study, the dominant noise source of the underwater propeller is analysed, which will provide a basis for proper noise control strategies.
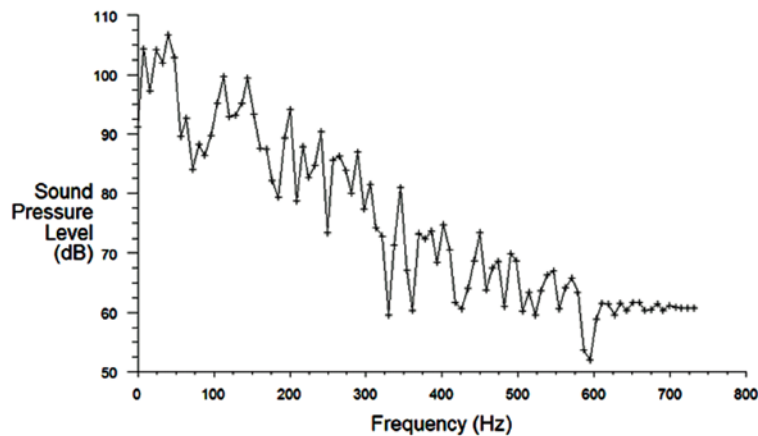
Fig. 5. Noise prediction graph at inlet of propeller

6. CONCLUSION

The non-cavitating noise generated by underwater propeller is analyzed numerically in this study. The non-cavitating turbulent flow around a full scale marine propeller is simulated with the Spalart and Allmaras and the DES (Detached Eddy Simulation) approach. For non-cavitation noise prediction, Ffowcs Williams-Hawkings equation is adopted in the form proposed by Farassat. This DES method is suitable for modelling of the vorticity field of unsteady fluctuation of the flow for a longer distance. The DES method allows to capture the tip vortices evolution as long as the mesh is reasonably refined with a good qualitative and quantitative agreement with experiments.

7. REFERENCES

[1] H. SEOL, B. JUNG, J.-C. SUH and S. LEE, 2002. Prediction of Non-Cavitating Underwater Propeller Noise, *Journal of Sound and Vibration*, **257** (1), 131-156.

[2] HANSHIN SEOLA, JUNG-CHUN SUHB and SOOGAB LEE, 2005. Development of hybrid method for the prediction of underwater propeller noise, *Journal of Sound and Vibration*, **288**, 345-360.

[3] YU-CUN PAN and HUAI-XIN ZHANG, 2010. Numerical hydro-acoustic prediction of marine propeller noise, *Journal of Shanghai Jiaotong University* (*Science*), **15** (6), 707-712.

[4] ROBERTO MUSCARI, ANDREA DI MASCIO and ROBERTO VERZICCO, 2013. Modeling of vortex dynamics in the wake of a marine propeller, *Computers & Fluids*, **73**, 65-79.

[5] YU-CUN PAN and HUAI-XIN ZHANG, 2013. Numerical prediction of marine propeller noise in non-uniform inflow, *China Ocean Engineering*, **27** (1), 33-42.

[6] YE JIN-MING, XIONG YING, LI FANG and WANG ZHAN-ZHI, 2012. Numerical Prediction of Blade Frequency Noise of Cavitating Propeller, *Journal of Hydrodynamics*, *Ser*. *B*, **24** (3), 371-377.

A Study of Intonation Patterns in Echolalic Responses of Autistic Children

Gish Chacko[1], T. A. Subbarao[2] and Venkat Raman Prusty[3]

[1]*Audiologist & Speech Pathologistat Sweekaar Academy of rehabilitation Sciences, Hyderabad*
[2]*Principal, DR. M.V Shetty College of Sp& Hg, Mangalore*
[3]*Audiologist & Speech Pathologistat MediCiti Institute of Medical Sciences,Ghanpur, AP*
e-mail: gishchacko@gmail.com

ABSTRACT

Intonationrefers to distinctive patterns of vocal melody. Supra-segmental aspect of speech is multifaceted and has many features like pitch, loudness, duration and pauses and components like intonation, tempo, stress and rhythm. The melodies of speech are related to virtually all levels of verbal communication, including emotional expression, pragmatics, and syntactic structure. On the acoustic level, melody patterns result from linguistically significant changes in the fundamental frequency (f_0) of the voice. Intonation providesinformation regarding discourse; attitudes, intentions and speech register. These can be distinguished based on some typical pitchcharacteristics such as rise or fall of FO, terminal FO counter and overall contour. It is well evidenced that many individuals with communicationimpartment due to hearing and neurological disorders and autism have difficulty inproducing the intonation pattern. Intonation patterns have been considered as an important area of research in children with autism. The present study was attempted to compare the imitated utterance in response to clinician and caretaker. A total of 30 children with Autism (verbal type), aged 4-9 years, served as participants. Children with any identified genetic disorder, sensory deficit, severe motor deficit, associated mental retardation (IQ <70), were excluded. A list of five spontaneous daily utterances (Good morning, Good afternoon, Thank You, Bye bye, Goodnight) was presented to elicit responseafter the clinician as well as caretaker utterances. All the utterances were recorded with PRAAT (version 5.3.30) software through a computer. The utterance samples were grouped as after clinician, after caretaker, and then analyzed acoustically using PRAAT. The factors analyzed were Mean pitch, Median, Minimum pitch, Maximum Pitch. Further, the intonation pattern for each utterance was also noted for rising, falling, fall rising and rise falling pattern.In these autistic children undergoing speech language therapy and home training, the generalacoustical parameters of the echolalic of the everyday utterance did not differ significantlybetween the clinician and parental presentation. However the pitch range exceeded mean 100Hzfor all utterances, similar is the study in agreement with some of the recent studies studying theimitation of prosodic patterns. The intonation contours were predominately rising pattern and to alesser extent rise falling. The present study indicates that the intonation contours mentionedabove are significantly different for clinician and caretaker presentation. It is possible that the autistic children may experience poor sensoryexpressive particularly auditory and this may affect the development of intonation.

---

1. INTRODUCTION

Intonationrefers to distinctive patterns of vocal melody(Crystal,1991). Suprasegmental otherwise termed prosody of speech is multifaceted. It is not a single homogenous entity, but has many features like pitch, loudness, duration and pauses and components like intonation, tempo, stress and rhythm (Crystal, 1981).The melodies of speech are related to virtually all levels of verbal communication, including emotional expression, pragmatics, and syntactic structure.

On the acoustic level, melody patterns result from linguistically significant changes in the fundamental frequency (f_0) of the voice.

Many studies have indicated that intonation providesinformation regarding discourse; attitudes, intentions and speech register(Crystal, 1982). These can be distinguished based on some typical pitchcharacteristics such as rise or fall of FO, terminal FO counter and overall contour (Hargrove, 1994).

It is well evidenced that many individuals with communicationimpartment due to hearing and neurological disorders and autism have difficulty inproducing the intonation pattern.Diehl and Paul (2012) have listed some studies which have acoustically analyzedecoholalic, imitation and spontaneous speech in conversation and narratives inchildren, adolescent and adults with ASD. Important prosodic difference was foundin the variance of fundamental frequency (f_0), duration of syllables and prosodiccontours. A good co-relation between acoustic features and perception have beenreported, such differences may signal detection and diagnosis of ASD (Oller et.al, 2010).Shardaet, al (2010) have studied the intonation patterns of children with ASDand found developmental difference.

Intonation patterns have been considered as an important area of research in children with autism. The present study was attempted to compare the imitated utterance inresponse to clinician and caretaker.

2. METHODOLOGY

A total of 30 children with Autism in the age range of 4-9 years were recruited from schools for autism (NGOs) of Hyderabad and Secunderabad cities. All the children with Autism were verbal and had been diagnosed as per Clinical diagnosiscriteria provided in Diagnostic and Statistical Manual of Mental Disorders-Fourth Edition- Text Revision (DSM-IV-TR; American Psychiatric Association). Children with any identified genetic disorder, sensory deficit, severe motor deficit, associated mental retardation i.e. (IQ <70), were excluded.

The assessment tool used in the present study was a list offive spontaneous daily utterances.

Good morning, Goodafternoon, Thank You, Bye bye, Goodnight

Each child was asked to repeat after the clinician as well as caretaker utterances. All the utterances were recorded with PRAAT (version 5.3.30) software through a computer. The utterance samples were grouped as after clinician, after caretaker, and then analyzed using PRAAT. The factors analyzed were Mean pitch, Median, Minimum pitch, Maximum Pitch. Further, the intonation pattern for each utterance was also noted for "rising, falling, fall rising and rise falling" pattern.

3. RESULTS & DISCUSSION

3.1 Acoustical parameters

The responses to the clinician response were compared with response to the caretaker response. All the pitch parameter were similar in both response and statistically was not significant.Overall it can be seen that the pitch values did not differ in the echolalic/repetitive response ,when imitating clinician or caretaker .So this generally points to the fact that autistic children echolalic utterance are independent of the presenters.This is generally in agreement with previous assumptions that autistic children expressions are monotonous and lack the emotional context.

Table 1. Pitch parameters for the stimulus "goodmorning.

GROUP	N	Mean	Std. Deviation	t-values	
Median	clinician	30	281.0408	70.42516	-1.4930
	care taker	30	307.9569	69.24271	
Mean	clinician	30	291.43223	77.388840	-.895
	care taker	30	308.24760	67.909016	
Max	clinician	30	368.13183	99.579098	-.895
	care taker	30	391.01250	98.380135	
Min	Clinician	30	238.70503	59.292753	-.155
	care taker	30	240.97640	54.252571	

Table 2. Pitch parameters for the stimulus "good-afternoon".

GROUP	N	Mean	Std. Deviation	t-value	
Median	clinician	30	301.9624	58.54602	.652
	care taker	30	291.9301	60.56168	
Mean	clinician	30	311.36923	54.566436	.726
	care taker	30	300.49237	61.224791	
Max	clinician	30	407.63730	68.809072	-.017
	care taker	30	407.92943	66.374210	
Min	clinician	30	257.36343	60.006788	.888
	care taker	30	242.47353	69.497376	

Table 3. Pitch parameters for the stimulus "thank you".

GROUP	N	Mean	Std. Deviation	t-value	
Median	clinician	30	297.45377	62.703667	-1.442
	care taker	30	321.84393	68.211151	
Mean	clinician	30	299.59043	55.039773	-1.457
	care taker	30	321.67487	62.142376	
Max	clinician	30	401.69793	71.403866	.055
	care taker	30	400.69793	69.667574	
Min	clinician	30	232.21947	56.793336	-1.387
	care taker	30	252.47405	56.309733	

3.2 Intonation patterns

It was observed frommajority of the intonation contours are rising pattern in both stimulus presentation so it can be concluded that rising intonation contours is the most frequently used. It is generally seen that rising intonation contours is associated with question intonations.

The present study was attempted to look at the echolalic responses of the autistic children. In agroup of Indian children undergoing speech language therapy and home training the generalacoustical parameters of the echolalic of the everyday utterance did not differ significantlybetween the clinician and parental presentation. However the pitch range exceeded mean 100Hzfor all utterances, similar is the study in agreement with some of the recent studies studying theimitation of prosodic patterns for e.g. Diehl and paul

Table 4. Pitch parameters for the stimulus "bye bye ".

GROUP		N	Mean	Std. Deviation	t-value
Median	clinician	30	283.7885	67.23822	-.612
	care taker	30	296.7796	94.82599	
Mean	clinician	30	294.90917	66.699075	-.508
	care taker	30	304.57233	79.993890	
Maximum	clinician	30	367.70097	91.779725	-1.709
	care taker	30	409.96470	99.576139	
Minimum	Clinician	30	238.6240	56.56708	-1.801
	care taker	30	208.7385	71.17043	

Table 5. Pitch parameters for the stimulus "good night ".

GROUP		N	Mean	Std. Deviation	t-value
Median	clinician	30	285.759067	52.87941847	0.675
	care taker	30	275.044533	69.32855535	
Mean	clinician	30	294.015367	54.01115337	0.537
	care taker	30	285.7158	65.01827807	
Max	clinician	30	397.540533	76.91288464	-0.278
	care taker	30	403.1955	79.59542026	
Min	clinician	30	210.6111	68.94781484	0.176
	care taker	30	207.480067	68.22812399	

Table 6. Group performance on the intonation contours for stimulus "good afternoon".

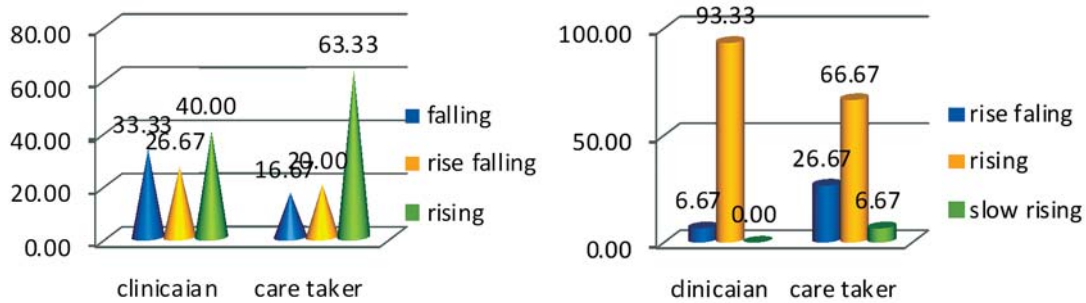|			good afternoon intonation		Total	
			fall rise	falling	rising	
GROUP	Clinician	Count	2	2	26	30
		% within GROUP	6.7%	6.7%	86.7%	100.0%
	care taker	Count	2	2	26	30
		% within GROUP	6.7%	6.7%	86.7%	100.0%
Total		Count	4	4	52	60
		% within GROUP	6.7%	6.7%	86.7%	100.0%

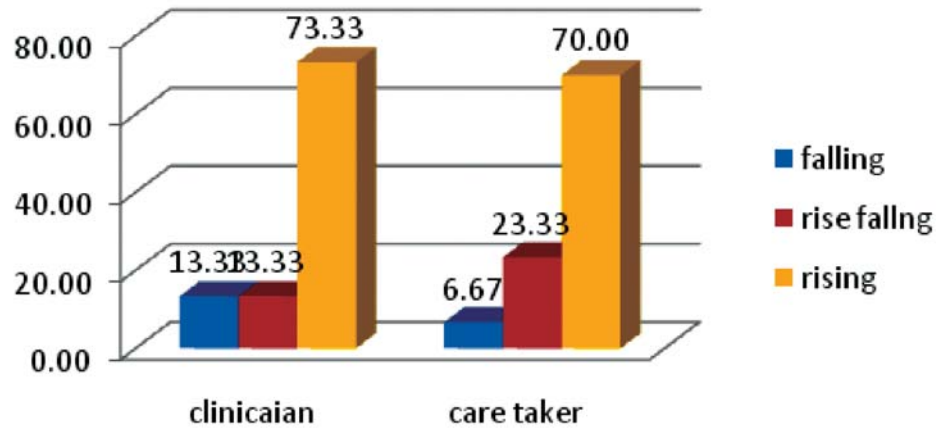Fig. 1 & 2. Intonation patterns for good afternoon; thank you.

Fig. 3. Intonation patterns for bye-bye.

(2012), found that the ability of children andadolescent with ASD to imitate prosodic patterns were significantly poor when compared with agroup learning disability and typically developing group. The intonation contours were predominately rising pattern and to alesser extent rise falling. The present study indicates that the intonation contours mentionedabove are significantly different for clinician and caretaker presentation. Although there are nostudies using similar method some support can be found in the Sharada(2010) study in which thedevelopment of pitch patterns of speech in autism was studied, this study did point to a distinctpattern of the pitch contours in the speech of autistic children Snow and Ertmer (2011) whilestudying development of intonation in cochlear implant have reported that the intonationdevelopment of children with CI is markedly different compared to normal hearing children.They reported that it is possible some intonation patterns can be acquired even with robustauditory experience .it is possible that the autistic children may experience poor sensoryexpressive particularly auditory and this may affect the development of intonation.

4. REFERENCES

[1]   American Psychiatric Association. *Diagnostic and statistical manual of mental disorders, text revision*. 4th ed. Washington, D.C.

[2]   D.A. CRYSTAL, 1991. dictionary of linguistics and phonetics. 3rd edition Blackwell; Oxford: Developmental Disorders, **9**, 11-29.

[3]   J.J. DIEHL and R. PAUL, 2012. Acoustic and perceptual measurements of prosody production on the PEPS-C by children with autism spectrum disorders. *Applied Psycholinguistics*.

[4]   D. SNOW and D. ERTMER, 2009. The development of intonation in young children with cochlear implants: A preliminary study of the influence of age at implantation and length of implant experience.*Clinical Linguistics and Phonetics*, **23** (9), 665-679.

[5]   P. HARGROVE, 1994. Prosodic aspects of language impairment in children.*Topics in Language Disorders*. **17**, 76-83.

[6]   P. HARGROVE, 1997. Prosodic aspects of language impairment in children.*Topics in Language Disorders*, **17** (4), 76-83.

[7]   D.K. OLLER, P. NIYOGI, S. GRAY, J.A. RICHARDS, J. GILKERSON, D. XU, U. YAPANEL and S.F. WARREN, 2010.Automated vocal analysis of naturalistic recordings from children with autism, language delay, and typical development. PNAS, **107**, 13354-13359.

[8]   M. SHARADA, 2010. Sounds of melody-Pitch patterns of speech in autism. *Neuroscience Letters*, **478**, 42-45.

A Fast Method For an Anisotropic Eiknoal Equation with Application to Sonic Boom Propagation in Atmosphere

D. Dahiya and S. Baskar

Department of Mathematics, Indian Institute of Technology Bombay,
Powai, Mumbai - 400 076, India
e-mail: baskar@math.iitb.ac.in

ABSTRACT

The first arrival time of a monotonically propagating front (wave front or shock front) in an inhomogeneous medium at rest satisfies the well-known eikonal equation. Geometrical acoustics theory based on ray tracing method is the classical way to obtain the solution of the eikonal equation. This is basically a characteristic method, where the front folds and develops cusp type of singularities. In many practical situations, this solution is not physically realistic and therefore motivates the need of interpreting the solution in the weak sense, called the *viscosity solution*. As there is no exact method for obtaining viscosity solution to the eikonal equation, numerous numerical methods have been developed. Among these methods, the fast marching method is the most efficient method with respect to the computational time, and also stable for isotropic problems, where the characteristic direction coincides with the normal direction of the front. Thus, the fast marching method is not suitable for studying front propagation in a medium filled with moving fluids, for instance sonic boom propagation in the windy atmosphere. In such applications, the governing equation involves a convective term incorporating the ambient flow effect on the propagating front, which results in an anisotropic eikonal equation. The fast marching method needs to be appropriately modified for the anisotropic eikonal equation in order to obtain accurate numerical results. Recently, we have developed a characteristic based fast marching method for the anisotropic eikonal equation in moving medium, called the *Characteristic Fast Marching Method*. In the present work, we briefly demonstrate the algorithm of our method. We show numerically that our method captures the viscosity solution of the anisotropic eikonal equation by comparing the numerical results of the method with the approximate solution obtained using ray tracing method. We finally consider an idealistic situation, where we apply our method to study the first arrival time of the leading shock front generated by a supersonic aircraft moving with a constant speed over a horizontal flight path.

1. INTRODUCTION

The *anisotropic eikonal equation* (*also called the generalized eikonal equation*) governing the first arrival time $T = T(x)$ of a front (wavefront or a shock front) is given by

$$|\nabla T|^2 = \frac{1}{c^2}(1 - v.\nabla T)^2,$$ (1)

where $c = c(\mathbf{x})$ is the ambient sound speed, $\mathbf{v} = \mathbf{v}(\mathbf{x})$ is the ambient flow velocity, and $\mathbf{x} = (x_1, x_2)$ denotes a two dimensional vector. The term $(\mathbf{v}.\nabla T)$ represents the effect of the ambient flow in the equation. When the ambient medium is at rest, we have $\mathbf{v} = \mathbf{0}$ and the above equation reduces to the well-known (isotropic) eikonal equation. The wave propagation in moving media was earlier studied by Blokhintzev [1], where a derivation for Eq. (1) is presented. The derivation of Eq. (1) was also given by Pierce [2], where the author obtained a concise form of the linear wave equation in moving media. Heller [3] derived Eq. (1) when the propagating front is a shock front. For an extensive review of the literature on wave propagation in moving media, we refer to Ostashev [4].

A classical method for solving Eq. (1) is the well-known ray tracing method (see Pierce [5]), where the solution of Eq. (1) is obtained by tracing ray trajectory of each point on the front $T(x) = t$ (t = constant) using the *Hamiltonian system* (characteristic system of ordinary differential equations)

$$\frac{d\mathbf{x}}{dt} = \frac{c^2 \mathbf{s}}{1 - \mathbf{v} \cdot \mathbf{s}} + \mathbf{v},$$
$$\frac{ds_i}{dt} = -\left(\frac{1 - \mathbf{v} \cdot \mathbf{s}}{c} \frac{\partial c}{\partial x_i} + \sum_{j=1}^{2} s_j \frac{\partial v_j}{\partial x_i} \right), \quad i = 1, 2, \tag{2}$$

where $\mathbf{s} = \nabla T$. Exact global smooth solution of the system of Eqs. (2) can be obtained in some special cases (for instance, see Kornhauser [6]). However, in certain ambient media, the rays may converge and form a caustic region beyond which the propagating front folds and develops singularities. Therefore we cannot expect, in general, a smooth solution of Eq. (1). In such circumstances, we need to interpret the solution of Eq. (1) in a weak sense called *viscosity solution* as suggested by Crandall and Lions [7]. Viscosity solution of Eq. (1) cannot be computed explicitly and we need to look for a numerical method to obtain an approximation to this solution. Sethian [8] developed an efficient method called the *fast marching method* for the isotropic eikonal equation. This method becomes unstable when directly used for Eq. (1) without any change. This is because, the method intrinsically assumes that the characteristic direction coincides with the normal direction, which is not the case for Eq. (1). Sethian and Vladimirsky [9] developed an ordered upwind method for a general anisotropic Hamilton-Jacobi type equations in which Eq. (1) is a particular case. But their method is more complicated to implement for Eq. (1) and also the scheme may become unstable in certain situations. Recently, Dahiya *et. al.* [10] showed that the fast marching method becomes unstable in computing numerical solution of Eq. (1) when the ambient velocity v is sufficiently strong. They also showed that the ordered upwind algorithm cannot not be used directly for Eq. (1), which clearly shows the need for a suitable modification in the method. They developed a characteristic based fast marching method, called by them as the *Characteristic Fast Marching Method* (*CFMM*), where the upwind direction is obtained by locally obtaining the characteristic direction using the ray tracing system Eq. (2).

Geometrical acoustic theory with Whitham's theory of shock dynamics is widely used in the study of sonic boom propagation (see the recent work by Berci and Vigevano [11] and the references therein). Baskar and Prasad [12] developed a new method based on shock ray theory, where they developed a one-parameter family of Cauchy problems to obtain the structure of the sonic boom emerging from an accelerating supersonic aircraft flying in a homogeneous quiescent medium over a curved path. In the present article, we are interested in applying the CFMM for Eq. (1) to study the first arrival time of the leading front created by a supersonic aircraft moving in the atmosphere.

In Section 2, we briefly present the narrow band algorithm for the CFMM. To validate the method, we give an example in Section 3, where the external velocity v is not axis-aligned and the initial front is taken to be planar parallel to the y-axis. We compare the numerical results obtained using the characteristic fast marching method with the numerical solution of the ray tracing system (Eq. (2)). In Section 4, we apply our method to study the first arrival time of the leading shock front generated by a supersonic aircraft moving with constant speed over a horizontal flight path. Here, we study the propagation of the shock front in an idealistic situation where the near field medium is assumed to be homogeneous and quiescent, and after a sufficiently large distance, we take the medium to be inhomogeneous and moving with constant external velocity.

2. NARROW BAND ALGORITHM FOR THE CFMM

Let us take the computational domain to be a rectangle, which is uniformly discretized with grid size Δx and Δy in the x-coordinate and the y-coordinate, respectively. We denote each grid point as (x_i, y_j) and use the notation T_{ij} to denote an approximate value of the solution of Eq. (1) at this grid point. Using first order finite difference approximations to the partial derivatives in Eq. (1), we arrive at the quadratic equation

$$PT_{i,j}^2 + QT_{i,j} + R = 0, \text{ where } \left. \begin{array}{l} P = \alpha^2(c^2 - v_1^2) + \eta^2(c^2 - v_2^2) - 2\alpha\eta v_1 v_2 \\ Q = 2\alpha\beta(c^2 - v_1^2) + 2\eta\mu(c^2 - v_2^2) - 2(\alpha\mu + \beta\eta)v_1 v_2 + 2\alpha v_1 + 2\eta v_2 \\ R = \beta^2(c^2 - v_1^2) + \mu^2(c^2 - v_2^2) - 2\beta\mu v_1 v_2 + 2\beta v_1 + 2\mu v_2 - 1 \end{array} \right\}, \tag{3}$$

where c and $\mathrm{v} = (v_1, v_2)$ are evaluated at the grid point (x_i, y_j), and the first order finite difference approximation with respect to x-variable is given by

$$\frac{\partial T}{\partial x}(x_i, y_j) \approx \alpha T_{i,j} + \beta, \text{ where } \alpha = \begin{cases} \dfrac{1}{\Delta x}, & \text{for backward difference,} \\ \dfrac{-1}{\Delta x}, & \text{for forward difference,} \end{cases} \quad \beta = \begin{cases} \dfrac{-T_{i-1,j}}{\Delta x}, & \text{for backward difference,} \\ \dfrac{T_{i+1,j}}{\Delta x}, & \text{for forward difference.} \end{cases}$$

Similarly, $(\partial T / \partial y)(x_i, y_j) = \eta T_{i,j} + \mu$, where η are μ defined in a similar way as above, but now with respect to the y-variable. To get a genuinely upwind scheme for Eq. (1), we need to choose the right finite difference operator (forward or backward) for the partial derivatives of T at each grid point (x_i, y_j). This choice depends on the characteristic direction $\phi_{i,j}$ at the point (x_i, y_j) whose formula up to first order finite difference approximation can be obtained from the first equation of the system Eq. (2) and is given by

$$\varphi_{i,j} \approx \tan^{-1}\left(\frac{c_{i,j}^2(\eta T_{i,j} + \mu) + (v_2)_{i,j} G_{i,j}}{c_{i,j}^2(\alpha T_{i,j} + \beta) + (v_1)_{i,j} G_{i,j}} \right),$$

where

$$c_{i,j} = c(x_i, y_j), \ (v_1)_{i,j} = v_1(x_i, y_j), \ (v_2)_{i,j} = v_2(x_i, y_j), \text{ and } G_{i,j} = (1 - (v_1)_{i,j}(\alpha T_{i,j} + \beta) - (v_2)_{i,j}(\eta T_{i,j} + \mu)).$$

For instance, if $\phi_{i,j}$ points from the third quadrant (ie., $0 \le \varphi_{i,j} \le \pi/2$) , then we have to use backward difference approximation for $(\partial T / \partial x)$ and backward difference approximation for $(\partial T / \partial y)$.

We use the narrow band algorithm to implement the above numerical scheme. We brief the algorithm and refer to Dahiya *et. al.* [9] for more details. We divide the set of grid points in the computational domain into three parts, namely, (i) *alive points*, which are the points that are already crossed by the wavefront, (ii) *far away points*, which are the points that are not yet touched by the wavefront and are not immediate neighboring points of any of the alive points, and (iii) *narrow band points*, which are neighboring points of both far away and alive points. We assume that the value of T is known at all alive points and therefore any further computation will not be carried over at these points. Narrow band points carry approximate values of T, which are initialized at the beginning of the algorithm. Values of T at far away points are initialized as infinity (or a sufficiently large number). The narrow band algorithm involves the following steps:

1. Find the minimum value of T among all the narrow band points (using heap sort algorithm). Let this point be denoted by **X**. Mark this point as an alive point.

2. Take all the four neighboring points of **X** and compute the solution using the scheme Eq. (3) at each of the neighboring points that are not alive points.

3. If any of these four points is a far away point, then after computation, remove this point from far away category and mark it as narrow band point.

4. Go to step 1.

Repeat these steps until all the grid points in the computational domain are marked alive points. Here, to ensure the stability of the scheme, we need to force the choice of the right finite difference operator purely depending on the characteristic direction, which is achieved by introducing a new parameter called the *quadrant indicator map*. For the definition and the usage of this map in the scheme, we refer to Dahiya *et. al*. [9].

3. PROPAGATION OF A NORMAL FRONT: COMPARISON RESULTS

In this section, we show numerically that the CFMM briefed in Section 2 is accurate in capturing the viscosity solution of Eq. (1). We show this using an example, where a planar front parallel to the y-axis touches the computational domain at $x=0$ and propagates in a planar and layered anisotropic medium with a periodic external velocity **v**. We take the sound speed (Figure 1(a)) as

$$c(y,) = \begin{cases} 2 - \dfrac{1}{2}\cos^2\left(\pi\left[y - \dfrac{1}{2}\right]\right), & \text{if } 0 \le y \le 1, \\ 2, & \text{other wise} \end{cases}$$
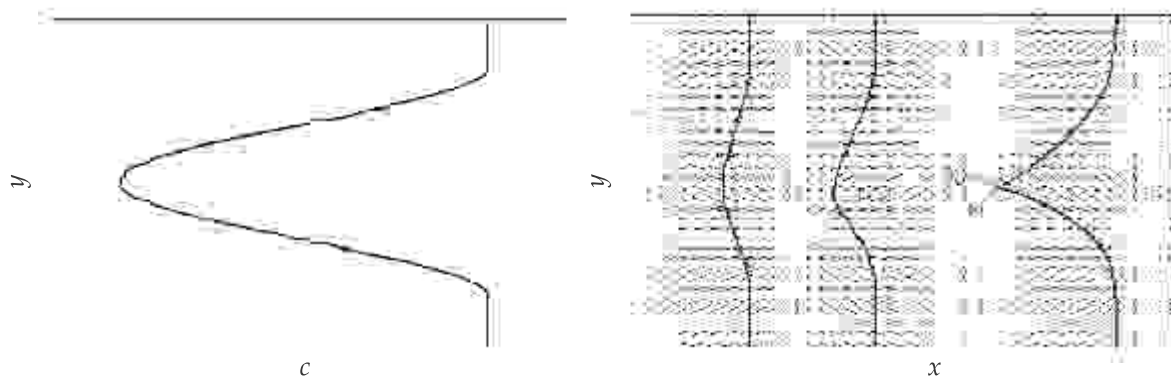

Fig. 1. (a) depicts the speed function c. (b) depicts the propagation of a initially planar wavefront at $T(x, y) = 0.15$, $T(x, y) = 0.35$, and $T(x, y) = 0.7$ (from left to right). Background represents the vector field of **v** given by Eq. (4).

where the x-variable is taken in the longitudinal direction, which is the direction of propagation of the front and the y-variable is taken in the vertical direction. The external velocity is taken as

$$v = \left(\frac{1}{2}\sin(2\pi x), \frac{1}{4}\cos(2\pi y)\right).$$

(4)

We compare the numerical solution obtained using CFMM with the numerical solution of the ray tracing system given by Eq. (2), which is solved using the 4th order Runge-Kutta method. Figure 1(b) depicts the front propagation. The blue solid line represents the first arrival time of the front computed using CFMM and the red dashed line represents the front computed using the ray tracing method. We can clearly observe that the front obtained using ray tracing method folds and becomes multi-valued after a finite time. On the other hand the CFMM captures the viscosity solution, which is precisely the same as the folded front, but without the folded part. This comparison result provide numerical evidence that the CFMM is more accurate in computing the viscosity solution of Eq. (1) even when the external velocity is not axis-aligned.

One limitation of the CFMM is that the method works only when $c - |v| >> 0$. In other words, the external flow in the medium is 'sufficiently' subsonic. When the external flow is supersonic or transonic or 'sufficiently' close to transonic but subsonic, the method ceases to give solution because the quadratic equation Eq. (3) in such cases fails to have real roots. In the case of ambient subsonic flow, we can always choose the discretization parameters Δx and Δy suitably (depending on c and **v**) such that Eq. (3) has real roots. However, the question

of how to choose these discretization parameters remains open. In the transonic or supersonic cases, CFMM does not work and a suitable modification of the method in such cases remains open.

4. OBLIQUE FRONT PROPAGATION

In this section, we consider an aircraft moving with a constant supersonic speed over a horizontal path. We assume an idealistic situation, where the leading shock front emerging from the aircraft propagating through a homogeneous quiescent medium encounters an inhomogeneous moving medium as shown in Figure 2.

We consider an inhomogeneous anisotropic medium where there is a cavity (with lesser sound speed) in the sound speed. This situation can occur in the present application, where the shock front propagates in the cloudy atmosphere. In this example we apply the CFMM to Eq. (1) with sound speed having an elliptic cavity given by

$$c(x,y) = 2.5 - 0.4y - 0.8\exp\left(-10(y-0.9)^2\right)\exp\left(-20(x-0.55)^2\right)$$

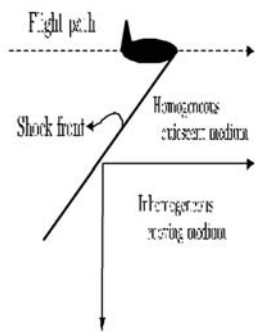and the ambient fluid velocity is taken to be **v** = (-0.2,-0.2).
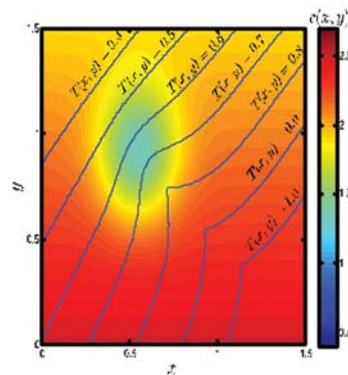

Fig. 2. Schematic diagram of the physical problem.

Fig. 3. First arrival time of the oblique shock front computed using CFMM. The ackground color epresents the sound peed.

An oblique front touches the computational domain [-0.5,2]×[-0.5,1.5] at the point (-0.5, 1.5) making an angle of 45° to the x-axis. The first arrival time is computed using the CFMM, which are depicted in blue solid line in Figure 3. The computation is performed with $(\Delta x\ \Delta y)$ = (0.0025,0.002), that is, with 1001 grid points both in the x- and the y-coordinates. As the planar front propagates through the elliptic cavity, where the sound speed is low, it bends and eventually focuses. The rays intersect and form a caustic region. Equivalently, the front obtained using ray tracing method folds and becomes multi-valued (not shown in the figure). Since, the CFMM captures the viscosity solution, this multi-valued part is not appearing in the computational result, but we can observe a point singularity on the front.

5. CONCLUSION

An accurate and robust numerical method based on the characteristic direction of the anisotropic eikonal Eq. (1) has been deviced to compute the first arrival time of a front propagating in an inhomogeneous moving fluid. A comparison study shows that the method captures the viscosity solution of Eq. (1). This method has been used to find the first arrival time of the leading shock front emerging from a supersonic aircraft moving with a constant speed over a horizontal path.

6. REFERENCES

[1]   D. BLOKHINTSEV, 1946. The propagation of sound in an inhomogeneous and moving medium *I. J. Acoust. Soc. Am.* **18**, 322-328.

[2]   A.D. PIERCE, 1990. Wave equation for sound in fluids with unsteady inhomogeneous flow, *J. Acoust. Soc. Am.*, **87**, 2292-2299.

[3]   G. S. Heller, 1953. Propagation of acoustic discontinuities in an inhomogeneous moving liquid medium, *J. Acoust. Soc. Am.*, **25**, 950-951.

[4]   V. E. OSTASHEV, 1997. *Acoustics in Moving Inhomogeneous Media*, E&FN Spon.

[5]   A. D. PIERCE, 1989. *Acoustics: An Introduction to its Physical Principles and Applications*, Acoustical Society of America.

[6]   E.T. KORNHAUSER, 1953. Ray theory for moving fluids, *J. Acoust. Soc. Am.*, **25**, 945-949.

[7]   M.G. CRANDALL and P.L. LIONS, 1983. Viscosity solutions of Hamilton-Jacobi equations, *Trans. Amer. Math. Soc.*, **277**, 1-42.

[8]   J.A. SETHIAN, 1996. A fast marching level set method for monotonically advancing fronts, *Proc. Natl. Acad. Sci. USA*, **93**, 1591-1595.

[9]   J.A. SETHIAN and A. VLADIMIRSKY, 2003. Ordered upwind methods for static Hamilton-Jacobi equations: Theory and algorithm, *SIAM J. Numer. Anal.* **41**, 325-363.

[10]   D. DAHIYA, S. BASKAR and F. COULOUVRAT, 2013. Characteristic fast marching method for monotonically propa-gating fronts in a moving medium, *SIAM J. Sci. Comput.* **35**, A1880-A1902.

[11]   M. BERCI and L. VIGEVANO, 2012. Sonic boom propagation revisited: A nonlinear geometrical acoustic model, *Aero. Sci. & Tech.*, **23**, 280-295.

[12]   S. BASKAR and P. PRASAD, 2006. Formulation of the problem of sonic boom by a maneuvering aerofoil as a one-parameter family of Cauchy problems, *Proc. Indian Acad. of Sci. - Math. Sci.*, **116**, 97-119.

Acoustical Society of India
(Regn. No. 65-1971)

Executive Council (2010 - 2014)

President : **Dr V Rajendran**

[KRSCT, Tiruchengode; veerajendran@gmail.com; +91-99 94 13 03 03]

Vice President : **NS Naidu**

[NSTL, Vizag; nsnaidu04@yahoo.com; +91-94 90 75 05 82]

General Secretary : **PVS Ganesh Kumar**

[NSTL, Vizag; gkpakki@rediffmail.com; +91-98 66 40 08 94]

Jt. Secretary : **Dr K. Trinadh**

[NSTL, Vizag; hello_trinath@yahoo.co.in;; +91-97 04 71 95 00]

Treasurer : **Prof AV Sharma**

[AU, Vizag; sarmavakella@yahoo.co.in; +91-94 90 43 17 17 26]

Chief Editor : **Dr Mahavir Singh**

[CSIR-NPL, New Delhi; mahavir@nplindia.org; +91-98 71 69 33 46]

Council Members : **Dr SV Ranga Nayakulu**

[VITAE, Hyderabad; nayakulu@rediffmail.com; +91-98 66 53 26 13]

Dr I Johnson

[SJ College, Trichy; jnaadarsh@hotmail.com; +91-94 12 97 28 90]

Dr Rajiv K Upadhayay

[Govt PG College, Rishikesh; rku8@rediffmail.com; +91-94 12 97 28 90]

Dr S Shekhar

[Oxford College, Trichy; acousticssekar@yahoo.co.in; +91-99 94 92 00 30]

Dr V Bhujanga Rao

[Past President; NSTL, Vizag; vepcrew1@rediffmail.com; +91-98 66 44 10 74]

Co-opted Members : **Rajshekhar Uchil**

[Josts, Bangalore; ruchil@josts.in; +91-98 80 17 08 95]

Dr NK Narayanan

[CIT, Kozhikode; csirc@rediffmail.com; +91-94 46 95 58 30]

INFORMATION FOR AUTHORS

ARTICLES

The Journal of Acoustical Society of India (JASI) is a refereed publication published quarterly by the Acoustical Society of India (ASI). JASI includes refereed articles, technical notes, letters-to-the-editor, book review and announcements of general interest to readers.

Articles may be theoretical or experimental in nature. But those which combine theoretical and experimental approaches to solve acoustics problems are particularly welcome. Technical notes, letters-to-the-editor and announcements may also be submitted. Articles must not have been published previously in other engineering or scientific journals. Articles in the following are particularly encouraged: applied acoustics, acoustical materials, active noise & vibration control, bioacoustics, communication acoustics including speech, computational acoustics, electro-acoustics and audio engineering, environmental acoustics, musical acoustics, non-linear acoustics, noise, physical acoustics, physiological and psychological acoustics, quieter technologies, room and building acoustics, structural acoustics and vibration, ultrasonics, underwater acoustics.

Authors whose articles are accepted for publication must transfer copyright of their articles to the ASI. This transfer involves publication only and does not in any way alter the author's traditional right regarding his/her articles.

PREPARATION OF MANUSCRIPTS

All manuscripts are refereed by at least two referees and are reviewed by the Publication Committee (all editors) before acceptance. Manuscripts of articles and technical notes should be submitted for review electronically to the Chief Editor by e-mail or by express mail on a disc. JASI maintains a high standard in the reviewing process and only accept papers of high quality. On acceptance, revised articles of all authors should be submitted to the Chief Editor by e-mail or by express mail.

Text of the manuscript should be double-spaced on A4 size paper, subdivided by main headings-typed in upper and lower case flush centre, with one line of space above and below and sub-headings within a section-typed in upper and lower case understood, flush left, followed by a period. Sub-sub headings should be italic. Articles should be written so that readers in different fields of acoustics can understand them easily. Manuscripts are only published if not normally exceeding twenty double-spaced text pages. If figures and illustrations are included then normally they should be restricted to no more than twelve-fifteen.

The first page of manuscripts should include on separate lines, the title of article, the names, of authors, affiliations and mailing addresses of authors in upper and lowers case. Do not include the author's title, position or degrees. Give an adequate post office address including pin or other postal code and the name of the city. An abstract of not more than 200 words should be included with each article. References should be numbered consecutively throughout the article with the number appearing as a superscript at the end of the sentence unless such placement causes ambiguity. The references should be grouped together, double spaced at the end of the article on a separate page. Footnotes are discouraged. Abbreviations and special terms must be defined if used.

EQUATIONS

Mathematical expressions should be typewritten as completely as possible. Equation should be numbered consecutively throughout the body of the article at the right hand margin in parentheses. Use letters and numbers for any equations in an appendix: Appendix A: (A1, (A2), etc. Equation numbers in the running text should be enclosed in parentheses, i.e., Eq. (1), Eqs. (1a) and (2a). Figures should be referred to as Fig. 1, Fig. 2, etc. Reference to table is in full: Table 1, Table 2, etc. Metric units should be used: the preferred from of metric unit is the System International (SI).

REFERENCES

The order and style of information differs slightly between periodical and book references and between published and unpublished references, depending on the available publication entries. A few examples are shown below.

Periodicals:
[1]   S.R. Pride and M.W. Haartsen, 1996. Electroseismic wave properties, *J. Acoust. Soc. Am.*, 100 (3), 1301-1315.
[2]   S.-H. Kim and I. Lee, 1996. Aeroelastic analysis of a flexible airfoil with free play non-linearity, *J. Sound Vib.*, 193 (4), 823-846.

Books:
[1]   E.S. Skudzryk, 1968. *Simple and Comlex Vibratory Systems*, the Pennsylvania State University Press, London.
[2]   E.H. Dowell, 1975. *Aeroelasticity of plates and shells*, Nordhoff, Leyden.

Others:
[1]   J.N. Yang and A. Akbarpour, 1987. Technical Report NCEER-87-0007, Instantaneous Optimal Control Law For Tall Buildings Under Seismic Excitations.

SUMISSIONS

All materials from authors should be submitted in electronic form to the JASI Chief Editor: Dr Mahavir Singh, Acoustics, Ultrasonics & Vibration Section, CSIR-National Physical Laboratory, Dr. K. S. Krishnan Road, New Delhi-110 012 (email: mahavir@nplindia.org Tel: +91-11-4560.8317, Fax: +91-11-4560.9310). For the item to be published in a given issue of a journal, the manuscript must reach the Chief Editor at least twelve week before the publication date.

SUMISSION OF ACCEPTED MANUSCRIPT

On acceptance, revised articles should be submitted in electronic form to the JASI Chief Editor (mahavir@nplindia.org)

JOURNAL OF ACOUSTICAL SOCIETY OF INDIA

Volume 41   Number 2   April 2014

A Quarterly Publication of the JASI
http://www.acousticsindia.org

Journal of Acoustical Society of India

The Journal of Acoustical Society of India is a refereed journal of the Acoustical Society of India (ASI). The ASI is a non-profit national society founded in 31st July, 1971. The primary objective of the society is to advance the science of acoustics by creating an organization that is responsive to the needs of scientists and engineers concerned with acoustics problems all around the world.

Manuscripts of articles, technical notes and letter to the editor should be submitted to the Chief Editor. Copies of articles on specific topics listed above should also be submitted to the respective Associate Scientific Editor. Manuscripts are refereed by at least two referees and are reviewed by Publication Committee (all editors) before acceptance. On acceptance, revised articles with the text and figures scanned as separate files on a diskette should be submitted to the Editor by express mail. Manuscripts of articles must be prepared in strict accordance with the author instructions.

All information concerning subscription, new books, journals, conferences, etc. should be submitted to Chief Editor:

Acoustics, Ultrasonics & Vibration Section, CSIR-National Physical Laboratory, Dr. KS Krishnan Road, New Delhi 110 012, Tel: +91.11.4560.8317, Fax: +91.11.4560.9310, e-mail: mahavir@nplindia.org

Annual subscription price including mail postage is Rs. 2000/= for institutions, companies and libraries and Rs. 2000/= for individuals who are not ASI members. The Journal of Acoustical Society of India will be sent to ASI members free of any extra charge. Requests for specimen copies and claims for missing issues as well as address changes should be sent to the Editorial Office:

Acoustics, Ultrasonics & Vibration Section, CSIR-National Physical Laboratory, Dr. KS Krishnan Road, New Delhi 110 012, Tel: +91.11.4560.8317, Fax: +91.11.4560.9310, e-mail: mahavir@nplindia.org

Journal of Acoustical Society of India (JASI)

JASI

A quarterly publication of the Acoustical Society of India

Volume 41, Number 2, April 2014

Acoustic Absorption Characteristics of Fibrous Materials

The aim of this article was to explore and analyze the effect of different factors on the absorption of coir fiber. The experimental results were compared by the analytical techniques employing Johnson-Allard rigid frame model. It was found that the analytical method can provide a well consistent agreement with the experimental results. Factors that may have positive or negative effect are elaborated in this study. It describes how the physical elements of coir fiber absorber panel can change the absorption behavior. Results obtained show that layer thickness and fiber diameter have a significant effect on the absorption, whereas bulk density does not have any considerable effect. In addition, an example is presented in order to show the approaches of enhancing the absorption utilizing the advantage of modification in the physical elements. It exhibits that properly chosen fibers along with suitable amount of bulk density can increase the absorption for the same layer thickness. It indicates that these analyses can be powerfully exploited to improve the absorption of coir fiber and at the same time maintain a reasonable thickness which would be very efficient for limited space structure. Moreover, these results can serve as a guideline for the future implementation of acoustic absorber using naturally collected coir fiber.

In practical application, most of the sound absorbing products used in the building construction industry consist of synthetic materials. Because of the dominance of these materials in the commercial market, the study of alternative materials has been limited. The study of the acoustical performance of natural substance coir fiber material is important to use it efficiently in applications such as transportation sector, buildings, automotive interior noise, wall lining, room interior surface, muffling system etc. Market demands increases for porous absorbers with the aspirations like lower frequency absorption ability, wide band frequency absorption capacity, thin structure for limited space absorber, specific acoustic absorption spectrum and low cost materials. To achieve these divergent targets and make an optimized absorber using a porous material, it is important to truly understand the relationship between the chemistry, structure, morphology and physical properties of an individual technology concerns to porous material. Therefore, modeling the coir fiber and exploring the effect of different physical and non physical elements on the absorption coefficient is vital and inevitable, since acoustic absorption characteristics have to be enhanced and optimized for commercial use. The main objective of this study is to analyze the effect of different factors on the absorption of coir fiber using the Johnson-Allard rigid frame model.

Mahavir Singh

Effective Thickness and Eigenmodes of a Plate with Blind Holes

Dubois Jérôme and IngRosKiri

Instrumentation&Signal Processing(ISP) Section, ESPCI ParisTech,
CNRS UMR 7587, 1 Rue Jus-sieu, 75005 Paris, France
e-mail: jerome.dubois@espci.fr

ABSTRACT

In order to focus ultrasound in air, generally, a focused transducer or a transducers array with beamforming are used. We have recently shown that it is possible to focus acoustic waves in air with a thin square plate using time reversal process. This device allows focusing the acoustic waves with a small number of transducers. The contrast of focusing is enhanced proportionally to the square root of the number of modes of the plates. This can be made, for example, by drilling an array of resonant blind holes in the plate. Near the first frequency resonance of the blind holes, the dispersion relation of a phononic crystal composed of a plate with blind holes has flat bands along all the principal directions of the Bloch wavenumber. This means that there are localized modes inside the blind holes, so we can expect a local augmentation of the eigenmodes of this plate near these flat bands. The question is: can we determine the increase of modes of a plate with blind holes? In order to do that, we have studied the cumulative eigenmodes as a function of the frequency of simple plates and plates with blinds holes using ComsolMultiphysics. The cumulative eigenmodes of a simple plate increase linearly with the frequency and analytical formula of this increase can be found in the literature. For the plate with blind holes, there is local augmentation of the cumulative eigenmodes around the resonances of the blind holes. However, they increase linearly between these resonances with the same slope which is greater than the case of the simple plate with same thickness. This means that this plate behaves like an effective plate with a lower flexural rigidity. Considering that the plates are made with a unique material (because the blind holes are drilled into the plate), the Young's modulus, the Poisson's ratio and the mass density of the effective plate are identical to the ones of the initial plate. So the only property remaining is the effective thickness.This effective thickness has been deduced numerically by minimizing the error between the analytical curve of the cumulative eigenmodes and the one obtained with ComsolMultiphysics. It appears that the effective thickness is defined by the average of the mean thickness of the plate and the thickness defined by the mean flexural rigidity. On all our simulations this effective thickness differs from the one obtained numerically by less than 3%. Moreover, the local augmentation of the eigenmodes around the resonances of the blind holes has been calculated and is roughly equal to the number of blind holes. With these results we are able to predict the augmentation of the cumulative eigenmodes as a function of the frequency for a plate of any shape with a regular or random array of blind holes.

1. INTRODUCTION

Acoustic focusing is widely used in medical imaging or non-destructive evaluation. In order to focus

ultrasound in air, generally, a focused transducer or a transducers array with beamforming are used. We have recently shown that it is possible to focus acoustic waves in air with a thin square plate using time reversal process [1].With this device,it is possible to focus acoustic waves with a small number of transducers but with a non optimal contrast level.

The contrast of focusing is enhanced proportionally to the square root of the number of modes of the plates [2]. So the contrast of focusing can be improved by drilling an array of resonant blind holes in a plate for example. Indeed, the dispersion relation of a phononic crystal composed of a plate with resonant blind holes has flat bands nearthe first frequency resonance of the blind holes,along all the principal directions of the Bloch wavenumber.This means that there are localized modes inside the blind holes, so we can expect a local augmentation of the eigenmodes of this plate near these flat bands. Moreover the flexural rigidity of the phononic crystal seems to be lower than the one of a simple plate [1].

The goal of this paper is to predict the augmentation of eigenmodes of a plate with blind holes compared to a regular thin plate. In order to do that, we first study the cumulative eigenmodes of different regular and drilled plates. It appears that the cumulative eigenmodes of plates with blind holes increase linearly with the frequency such as for the regular plates, expect in the vicinity of the resonances of the blind holes. Then we extract an empirical expression of the effective thickness of an equivalent plate which has the same cumulative eigenmodes behaviour. Moreover we determine the local augmentation of the eigenmodes due to the resonances of the blind holes.

2. NUMBER OF EIGEN MODES IN A PLATE

In this section, we present the evolution of the cumulative eigenmodes in a plate for different geometries, areas and types of plates. The two geometries consider here are square plates and chaotic cavities which consist in a disk with one segment cut off (Fig. 1). These plates can be regular (plate with the same thickness everywhere) or with blind holes drilled into them. In a first part, we present an analytical expression of the cumulative eigenmodes in a regular rectangular plate. Then we compare this formula with the cumulative eigenmodes obtained by numerical simulations made with COMSOL. After, we look at the evolution of the cumulative eigenmodes for plate with a periodic or random array of blind holes.

2.1 Regular plates

2.1.1 Theory

We consider here the flexural vibrations of a plate using the Kirchhoff theory. The flexural wave equation of motion of a plate of thickness h_0 is given by:

$$D\Delta^2 w(\mathbf{r},t) + \rho h_0 \frac{\partial^2 w(\mathbf{r},t)}{\partial t^2} = 0, \tag{1}$$

where $w(r, t)$ is the vertical displacement of a point at the position $\mathbf{r}$ and time t and Δ is the Laplacian operator. $D\Delta^2 w(\mathbf{r},t) + \rho h_0 \frac{\partial^2 w(\mathbf{r},t)}{\partial t^2} = 0,$ is the flexural rigidity of the plate,E, ν and ρ are the Young's modulus, the Poisson's ratio and the mass density of the plate respectively. The equation (1) leads to the dispersion relation:

$$k^4 = \frac{\rho h_0 \omega^2}{D}, \tag{2}$$

where ω is the angular frequency. In this case, Xieet $al.$ [3] have shown that the cumulative eigen-modes $N(k)$ of a rectangular plate of length L and width l, with free boundary conditions, is given by:

$$N(k) = \frac{k^2 Ll}{4\pi} + \frac{k}{\pi}(L+l) - \delta, \tag{3}$$

whereδ is a corrective constant.

2.1.2 Numerical results

Numerically, the cumulative eigenmodes are obtained using the Mindlinplate's model of the software COMSOL. The two geometries studied here are presented in the figure 1. We consider a Duralumin plate of thickness h_0=1 mm with a Young's modulus, a Poisson's ratio and a mass density equal to 74 GPa, 0.33 and 2790 kg.m^{-3} respectively. We have determined the cumulative eigen-modes of these plates for three different areas: A_1=0.01 m^2, A_2=2.25 A_1 and A_3=4 A_1 . These areas correspond to L_1=100 mm, L_2=150 mm and L_3=200 mm respectively for the square plate and R_1=62.9 mm, R_2=94.35 mm and R_1=125.8 mm respectively for the chaotic cavity.
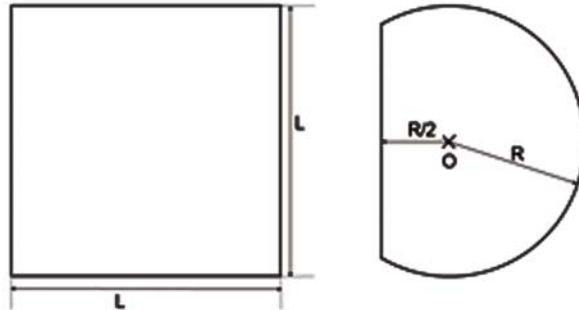
Fig. 1. Geometry of the plates: the square plate (left) and the chaotic cavity (right).
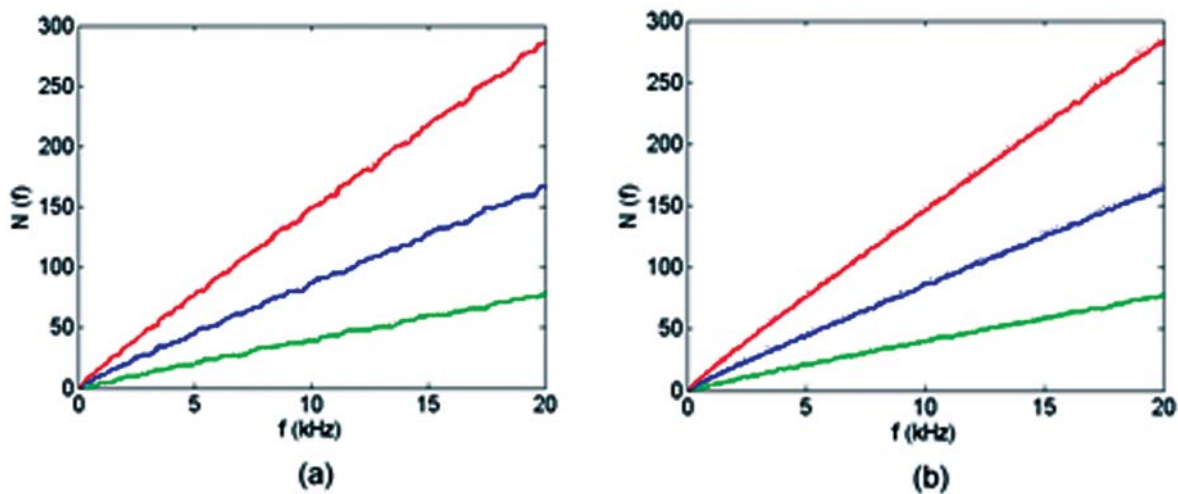
Fig. 2. Cumulative eigenmodes of the plates of area A_1 (green), A_2 (blue) and A_3 (red), a: obtained numerically (solid lines) and analytically (dotted lines);b: obtained numerically for the square plates (solid lines) and for chaotic cavities (dotted lines).

The cumulative eigenmodes obtained with COMSOL and with Eq. (3) are reported on Fig. 2.a, they increase linearly with the frequency. The value of ? is found to be roughly equal to four by minimizing the square relative error between Eq. (3) and the numerical results, without taking into account the static eigenmodes of the plates. The analytical formula fits very well with the numerical curves, the relative error is less than 5% (except at very low frequency). We can notice that both the analytical formula and the numerical results count two eigenmodes when there are degenerative modes.

The cumulative eigenmodes of the square plates and the chaotic cavities are represented on Fig. 2.b. It seems that the evolution of the cumulative eigenmodes of regular plate does not depend on the shape of the

plate but only on the surface and boundary conditions when the degenerative modes are count. So we can predict the cumulative eigenmodes of a chaotic cavity with the Eq. (3) considering $L = l = \sqrt{A}$.

2.2   Plates with blind holes

We now study the evolution of the cumulative eigenmodes of plates in which there are n blind holes of radius a=5.5 mm and thickness h_1=0.1 mm arranged periodically or randomly (Fig. 3). There are n_1=25, n_2=49 and n_3=100 holes in the plate of area A_1, A_2 and A_3 respectively. This kind of blind holeshas a monopolar resonance at f=8.2 kHz and a dipolar resonance at f =16.4 kHz [1].

It has been shown that the dispersion curve of a phononic crystal composed of a square array of blind holes presents flat bands at the first frequency resonance of the blind holes, which means that there are localized modes in the holes at this frequency [2]. This is confirmed with the cumulative eigenmodes of our plates because the curves have a jump in the vicinity of the monopolar and dipolar resonances (Fig. 3). One can notice that the jump is more important at the dipolar than at the monopolar resonance.

Except in the vicinity of the resonances, the cumulitive eigenmodes increase linearly with the frequency and with the same slop everywhere. Moreover this slop is more important than the one of a regular plate with the same area (figure 3.a), this means that the flexural rigidity of the plate with holes is lower than the one of the simple plate. So, at low frequency, it should be possible to determine an equivalent plate which has the same cumulative eigenmodes than a plate with scatterers (except for the jumps at the frequency resonances).

The cumulative eigenmodes do not depend on the arrangement of the holes (Fig. 3.b), but the mode density of the random arrangement is smoother than the one of the periodic array. Moreover the degeneration of the eigenmodes is broken by the random arrangement of the blind holes. We do not show it here, but we have the same results for chaotic cavities.
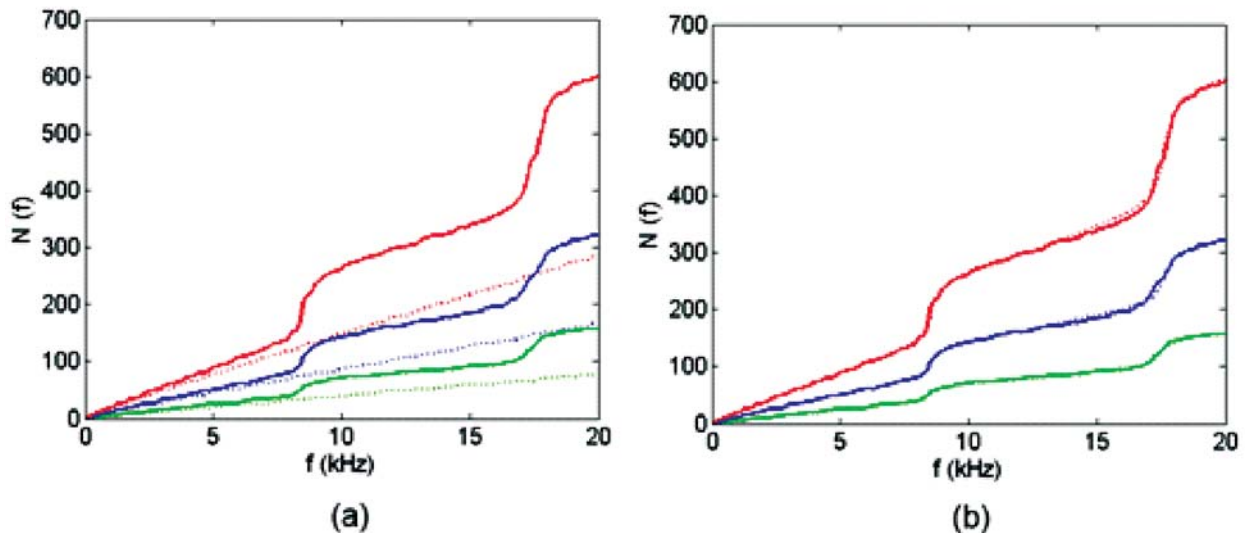
Fig. 3. Numerical cumulative eigenmodes of the platesof area A1 (green), A2 (blue) and A3 (red), a:
regular plates (dotted lines) and plates with a periodic array of blind holes (solid lines);
b: plates with a periodic (solid lines) or random (dotted lines) array of blind holes.

3.   PREDICTION OF THE CUMULATIVE EIGENMODES

3.1 Effective thickness

As we have seen in the previous section, the flexural rigidity of the plate with blind holes seems to be lower than the one of the simple plate. The question is: is it possible to determine the effective properties of the

plate with scatterers? Considering that the plates are made with a unique material (because the scatterers are drilled into the plate), the Young's modulus, the Poisson's ratio and the mass density of the equivalent plate are identical to the ones of the initial plate. So the only property remaining is the effective thickness. In order to determine this thickness, we have counted the eigenmodes of different plates with different numbers and geometries of blind holes. A priori, the effective thickness can be the mean thickness of the plate:

$$h_{\text{eff}}^{\text{mt}} = h_0 (1-\phi) + h_1 \phi, \tag{4}$$

orit can be the thickness which defines the mean flexural rigidity of the plate:

$$h_{\text{eff}}^{\text{mfr}} = \sqrt[3]{h_0^3 (1-\phi) + h_1^3 \phi}, \tag{5}$$

or even the one which defines the mean wavenumber in the plate:

$$h_{\text{eff}}^{\text{mw}} = \sqrt{\frac{h_0^2 h_1^2}{h_1^2 (1-\phi) + h_0^2 \phi}}. \tag{6}$$

Empirically we have found that the effective thickness is the mean of mean thickness and the thickness which defines the mean flexural thickness: $h_{\text{eff}} = \left(h_{\text{eff}}^{\text{mt}} + h_{\text{eff}}^{\text{mfr}} \right)/2$. The comparison between this expression and the effective thickness obtained numerically by minimizing the square relative error between Eq. (3) (we minimize the quadratic error by tuning the value of h in Eq. (3)) and the numerical cumulative eigenmodes is presented in Fig. 4 for various concentrations while kipping h_0=1 mm and h_1= 0.1 mm. This process is made on the first linear part of the cumulative eigen-modes, before the first jump of the curves. Our expression of the effective thickness is accurate (the relative error is less than 3%) except at very high concentration.
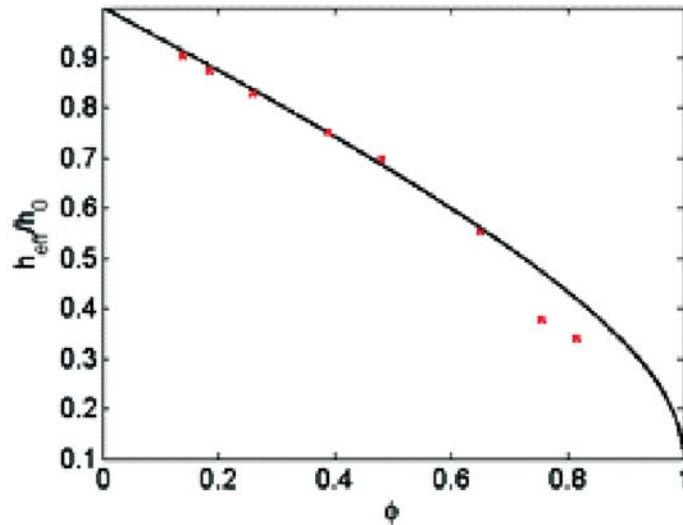
Fig. 4. Effective thickness versus concentration, comparison between
$h_{\text{eff}} = \left(h_{\text{eff}}^{\text{mt}} + h_{\text{eff}}^{\text{mfr}} \right)/2$ (black line) and numerical results (red crosses).

3.2 Increase of the eigenmodes in the vicinity of the holes resonances

We have seen in Section 2 that the slop of the cumulative eigenmodes of a plate with blind holes is the same everywhere except in the vicinity of the resonancesof the holes. Moreover, numerically or analytically we can determine the effective thickness of the plate. So before the monopolar resonance, the cumulative eigenmodes can be expressed by Eq. (3) and between the monopolar and the dipolar resonance they can be expressed by Eq. (3) plus a constant (considering $h=h_{\text{eff}}$ in Eq. (3)). This constant is equal to the increase of the

eigenmodes due to the holes monopolar resonance. The same process can be applied after the dipolar resonance in order to determine the increase of the eigenmodes due to the dipolar resonance. By doing this for different number of blind holes in a plate with constant area, we access to the increase of the eigenmodes as a function of the number of holes as we can see in Fig. 5.a for a plate of area A3 with different number of blind holes of radius a=2.5 mm and thickness h_1=0.1 mm. The increase of eigenmodes can be expressed as a linear function of the number of holes n: $N(n) = Y_{1n}+Y_2$ where the increase factor Y_1 is close to 1 (for the monopolar resonance) or 2 (for the over resonances) and Y_2 is a small corrective constant.

By determining the increase factor for different types of blind holes, it appears that this factor decreases with the ratio h_1/h_0 (Fig. 5.b):

$$Y_1 \approx -11{,}73\left(\frac{h_1}{h_0}\right)^2 +0.65\frac{h_1}{h_0}+0.99, \tag{7}$$

for the first resonance. This is probably due to the fact than the more the ratio   increases, the more the resonance is flat. So there is maybe a coupling of the resonances of different holes.
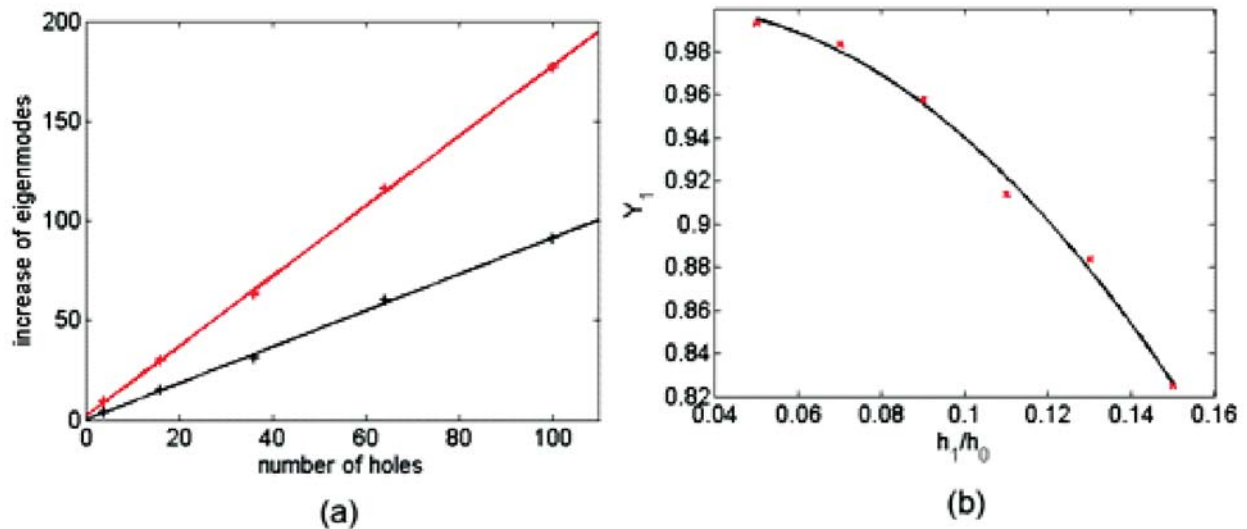
Fig. 5. a: increase of eigenmodes due to the monopolar (black) and dipolar (red) resonances, numerical simulation (cross) and linear interpolation (solid line); b: increase factor Y_1 versus h_1/h_0, numerical simulation (red cross) and quadratic interpolation (black line).

4. CONCLUSION

The increase of cumulative eigenmodes of different types of thin plates has been investigated: regular plates and plates with a periodic or random array of blind holes. It appears that the cumulative eigenmodes do not depend on the shape of the plate and on the arrangement of the blind holes. Moreover, for regular plate, the cumulative eigenmodes are well defined by the formula given by Xi*eet al*. [1] and they increase linearly with the frequency.

When there is an array of blind holes, there is local augmentation of the cumulative eigen-modes in the vicinity of the resonances of the holes. Except in these frequency bandwidths the cumulative eigenmodes still increase linearly with the frequency with a greater slop than in the case of regular plate. This means that this kind of plate can be described by an equivalent plate which has the same mechanical properties but with a weaker effective thickness.

This effective thickness is determined numerically by minimizing the square error between the formula of Xie*et al*. [1] and the numerical cumulative eigenmodes. It appears, empirically, that this effective thickness is given by the average between the mean thickness of the plate and the thickness defined by the mean flexural rigidity of the plate.

The local augmentation of the cumulative eigenmodes is also determined. It appears to be roughly equal to the number of blind holes in the plate for the monopolar resonance and twice this number for the other resonances.

5. REFERENCES

[1]   N. ETAIX, J. DUBOIS, M. FINK and R.-K.ING, 2013. Increasing the modal density in plates for mono-element focusing in air, *Journal of the Acoustical Society of America*,**134** (2), 1049-1054.

[2]   A. DERODE, A. TOURIN and M. FINK, 2001. Random multiple scattering of ultrasound. II. Is time reversal a self-averaging process?, *Physical Review E*, **64** (3), 036606.

[3]   G. XIE, D. J. THOMPSON and C. J. C. JONES, 2004. Mode count and modal density of structural systems: relationships with boundary conditions,*Journal of sound and vibration*, **274**, 621-651.

High Resolution Ultrasonic Tomography System

Vladimir Petrov, Nikolay Kositsyn and Sergey Lapin
Saratov State University, 410012, Astrakhanskaya St.,Saratov City, Russia
SpectrAcoustics Co. B.Kazach'ya St, 113, 410012, Saratov, Russia
e-mail: petrovvv@info.sgu.ru

ABSTRACT

The investigation results of new developed high resolution ultrasonic tomography system (Acoustical Tomography device (AT)) are discussed in present paper. The developed system represents the mobile and compact device aimed for nondestructive testing of surfaces and inner structures of metal objects. The system allows creating the A, B, and C - scans of investigating objects by means of mechanical scanning on X and Y coordinates, when Z coordinate is directed in parallel to the ultrasound velocity vector. The space resolution of designed system is 10 micrometers with working frequency 100 MHz.

1. INTRODUCTION

There are sufficient amount of scientific and technical tasks that require the necessity of inner structure and surfaces of objects investigation. The ultrasonic methods are very promising and widely used for such application. Most attractive in between of known methods is that, that allows building of three-dimensional (3D) images of investigating objects. In our recent publications [1-5] we have discussed the possibility of 3D holographic images recreation by means of application of complicated acoustical field created by multielement array of piezoelectric transducers. In paper [6] we also declared about creation of new high resolution system for 3D image capturing and reconstruction. In present paper we want to discuss more in detailed about this system..

2. TOMOGRAPHY SYSTEM DESIGN

The ultrasonic tomography system consists of three main blocs (see Fig. 1): the measuring block; the electronic block, and the personal computer. The system allows creating the A, B, and C - scans of investigating objects by means of mechanical scanning on X and Y coordinates, when Z coordinate is directed in parallel to the ultrasound velocity vector. Short electrical pulse generated by electronic block is directed to electro - acoustical transducer of acoustical objective in which the electrical signal transforms to acoustical short pulse. The acoustical objective is designed in such a way that the acoustical pulse propagates in sound conductor (produced on a fused quarts) the certain time, that provides the necessary time - delay. That time delay is necessary to obtain the time interval that is free of passive signals reflected from surfaces of acoustical lens. The acoustical lens is calculated tacking into account required deepness of acoustical testing of investigating object so that the caustic's zone of ultrasonic beam is covered the investigating area. The multilayer electro - acoustical transducer is calculated and design in such a way so that to provide it's electrical matching to the electro - magnetic tract which leads the electrical signal to the transducer. From the other hand the multilayer transducer provides the acoustical matching of piezo - electric and sound - conducting materials so that to minimize the acoustical reflection from bands of multilayer system of transducer. 10 micrometer space resolution is obtained by such acoustical objective working of central frequency 100 MHz.

Fig. 1. General view of ultrasonic tomography system

The mechanical scanning system of AT is based on micro step motors that are controlled by special developed program that synchronized to the system of pulse signal generation and reception. Analog - Digital device allows representing the whole processing information to 4 - dimensional data matrix. That 4 - dimensional data base is then saved and can be used for building necessary 2- dimensional cut images of investigating object, created with chosen deepness and angle of inclination. Besides this data base allows as well building the 3- dimensional images of object surfaces (bough - the nearest surface and further surface) as well as the chosen 3D area inside the investigating object. Specially developed program allows creating the 2D and 3D images of all required areas of objects as well as obtaining the metrological information about the geometrical features of defect or interested object peculiarity.

The developed device provided also with original designed system of immersion liquid delivering to the place of acoustical testing. The immersion liquid (water) is saved in special changeable container that places into the handle of measuring block (see Fig 2.)

Fig. 2. Measuring block with changeable water container

Original developed software allows easily communicating with developed AT, operating through the computer interface with all necessary abilities of designed system.

3. RESULTS OF OBJECTS INVESTIGATION

The design system allows obtaining the information about whole volume of investigating area of object with further recreation of 2 D or 3D image. The developed computer software contains two programs. First program

named «Scanning» allows collecting the 4-dimensional information data about investigating object, when second program named «Processing» allows building desirable images of investigating area of object: two - or three dimensional images of surfaces or desirable «cuts» inclined under any angle.

On Fig. 3 the reconstructed image of sign «2013» etched on the surface of aluminum object is presented.
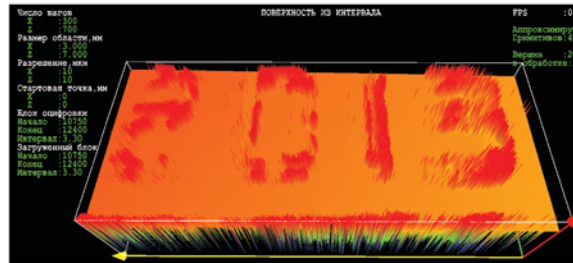
Fig. 3. The reconstructed 3D image of etched relief with deepness of 10 micrometers

The deepness of etched figures is 10 micrometers.
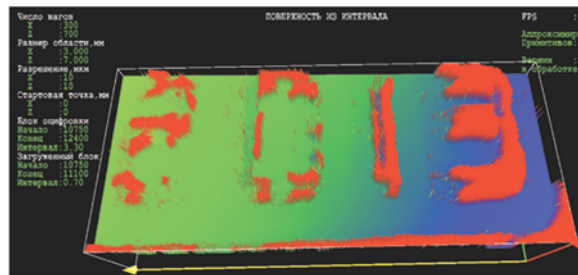
Fig. 4. Reconstructed 3D image after computer filtration

On Fig. 4 the same image is represented after computer filtration process. There are several possible filtering algorithms contained the developed program including Fourier, Wavelet, Mean-type and others.

Next experiment was devoted to the study of inner structure of complicated shape object. The general view of this object is presented on Fig.5 a). As it can be seen from the picture on the side surface of the object there is a crack coming from central part of the object (showed by arrow). For studying the inner condition
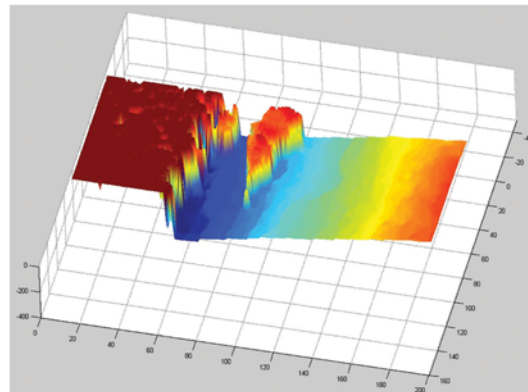
(a) (b)

Fig. 5. The investigated object (a) and 3D reconstructed image of inner structure (the crack)

of the object the ultrasonic beam was directed from the upper surface, approximately across the investigating crack. After raster scanning and processing of obtained data, the three dimensional image of the crack was obtained.

On Fig. 5 (b) the 3D image of investigated crack is presented. As it is seen from the picture on the surface of the crack there is an island the existence of which can not be predicted.

4. CONCLUSION

In present paper we have described the design peculiarities and have discussed the results of experimental investigation of surface and inner parts of metal samples.

One more peculiarity of developed AT is the possibility to be fixed on the surface of investigated object that is very important when operating in special requirements.

The developed system can be successfully applied for solving special tasks for example, inside of space satellite modulus or in other special conditions.

5. REFERENCES

[1] VLADIMIR PETROV, 2002. Holographic Video. *Acoustooptical Approach* (GosUNZ - Publishing House), 77.

[2] V.V. PETROV. 2004. Modern Application of high Frequency Acoustooptics, *Optica Applicata*, **4**, 597-606.

[3] V.V. PETROV, 1996. Setup for Electronic Forming of Three Dimensional Holographic Image, *Patent of Russian Federation* 2117975, Priority 31.11.

[4] V.V. PETROV, 2006. *Digital Holography for bulk Image Acoustooptical Reconstruction. Digital Holograph and Three-Dimensional Display* Ting-Chung Poon - ed., (Springer)

[5] V.V.PETROV,2005. 3D Image Reconstruction based on Acoustically Create Hologram. , Proc SPIE **5821**, 60-75.

[6] N.V. KOSITSYN, S.A. LAPIN and V.V. PETROV, 2013. High Resolution System for 3D Image Capturing and Reconstruction, *CC2DMR*, June 24-28, Jeju, South Korea, 633-634.

Planar Synthetic Aperture for the Imaging of Buried objects. Sea Experiment

Manell E. Zakharia* and Afif Belkacem**
*Currently at French Embassy in India, Service for Science & Technology, New Delhi India
**Salman Bin Abdjlaziz University, College of Sciences, Saudi Arabia
e-mail: braczac@gmail.com

ABSTRACT

Synthetic aperture sonar technique has become a mature discipline mainly applied to sidescan sonar (linear movement of the sonar platform). Recently, we have extended the technique to bottom and sub-bottom imaging using a planar movement of the sonar platform and an optimized 2D focussing algorithm. The extension of the synthetic aperture processing to a 2D scanning (X and Y) -leading to 3D grids- is called Planar Synthetic Aperture -PSAS- processing. First validated by simulation and by tank experiments, PSAS has been applied to real situations at sea. In Particular, a dump site with a great amount of UXO (unexploded ordinances) fully or partially buried in the mud has been studied. Sea experiment will be briefly described. Off-the shelf equipment were used: commercial parametric sonar (TOPAS 120) mounted on a ROV (Remote Operated Vehicle) navigating at approximately 10 meters above the bottom. ROV position was monitored by a conventional long baseline system. The experiment took place at a dumpsite in the Baltic in water depth of about 70 meters. The site is well documented and regularly surveyed over years with conventional tools (sonar, video, direct observations). Ground truth was extracted from these surveys. Raw data were recorded and stored for offline processing. The adaptation of the algorithm to real data (unevenly spaces on a grid) will be discussed. The solution proposed has allowed the processing of the sea data with a minimum processing complexity. Processed signal were then post-processed (bottom tracking) and echoes after the bottom one were exploited for sub-bottom volumetric imaging. For every ping, a set of positions of consecutive echoes were extracted. Both bottom structure and sub-bottom features were then investigated. Raw and processed sonar images (3D reconstructions) of buried objects have been reconstructed and compared to video images (captured before full burial). Results show the great potential of PSAS for buried man-made objects reconstruction and recognition.

1. INTRODUCTION

Widely used in radar, synthetic aperture has been introduced in sonar by Cutrona [1] in 1975. It has become a well recognized and validated technique for underwater imaging [7]. It was mainly applied to the Side-Scan Sonar with a linear scanning (1D) either in low frequency (a few kHz) for bottom imaging [2], [3] and for the detection of buried mines [9],[10], or in high frequency (few tens of kHz to a couple hundreds) for proud mine hunting applications [7], [8]. Recent works has been investigating the extension of this technique to two other scanning geometries such as circular [12] or planar [4-5].

Planar Synthetic Aperture -PSAS- consists in extending the conventional synthetic aperture processing to a 2D scanning (X and Y) driving to 3D data structure (longitude, latitude and depth).

Planar Synthetic Aperture Sonar (PSAS) technique has been first validated on both simulated and tank data (scaled experiment) [4-5]. It has been applied to imaging both bottom and sub-bottom imaging as well as buried objects and has proved to be an efficient tool that provides significant resolution improvement of volume imaging: improving the resolution of images in all directions.

The defocusing effect due to the presence of different sound speed in the sediment and in the water column has been shown to be a second order effect that could be neglected for burial depth of less than a meter in unconsolidated sediments.

In this paper we present its application to real data acquired during sea experiments on a dump site in the Baltic Sea. Data were acquired during a European project "SITAR" (Seafloor Imaging and Toxicity: Assessment of Risks caused by buried waste) [6].

2. SEA EXPERIMENT

Raw data were acquired thanks to the use of sonar mounted on a ROV (Remote Operated Vehicle) navigating at approximately 10 meters above the bottom. The experiment took place at a dumpsite of the Baltic Sea, in water depth of about 70 meters.

Prior to the experiment, the site was regularly surveyed by conventional tools: sidesan sonar, multibeam sonar, video cameras, direct observations… Together with survey data, available historical data were used to select the studied areas.

The transmitter was a Parametric Sonar (TOPAS120: primary frequency 100 kHz, main aperture 6°) fixed on a ROV which position was monitored by long baseline system. Two secondary frequency ranges were investigated centred around 10 kHz and 20 kHz.

Figure 1 shows the sonar mounted on the ROV.

Fig. 1. Experimental set up using the ROV of FOI, PLUMS (Platform for Underwater
Measurement Systems) where TOPAS 120 parametric sonar was installed.
ROV navigation was monitored by a long baseline.

Raw data were monitored on board for quality check and then digitized and stored on a hard disk for future processing.

3. PRE-PROCESSING

Initially PSAS algorithm was designed for data obtained on a regular (ideal) planar grid. In order to use it at

sea with realistic navigation conditions, significant modifications had to be implemented: an ideal plane over-sampled regular grid (eight of a wavelength) was first constructed. The associated focussing laws were pre-computed (echo migration compensation in the time domain).

A "rearrangement" algorithm was then developed for projecting actual data on this grid after navigation correction. The method was first tested validated on tank data prior to application to sea data. Processing could be viewed, in a sense, as optimal interpolation between real pings.

Rearrangement algorithm consists in the redistribution of data positions to a new oversampled regular grid. Real pings are distributed on this new regular grid with a $\lambda/8$ meshing. Grid positions where no corresponding real pings were found were associated to zeros signal. Conventional PSAS was then applied to re-arranged data.

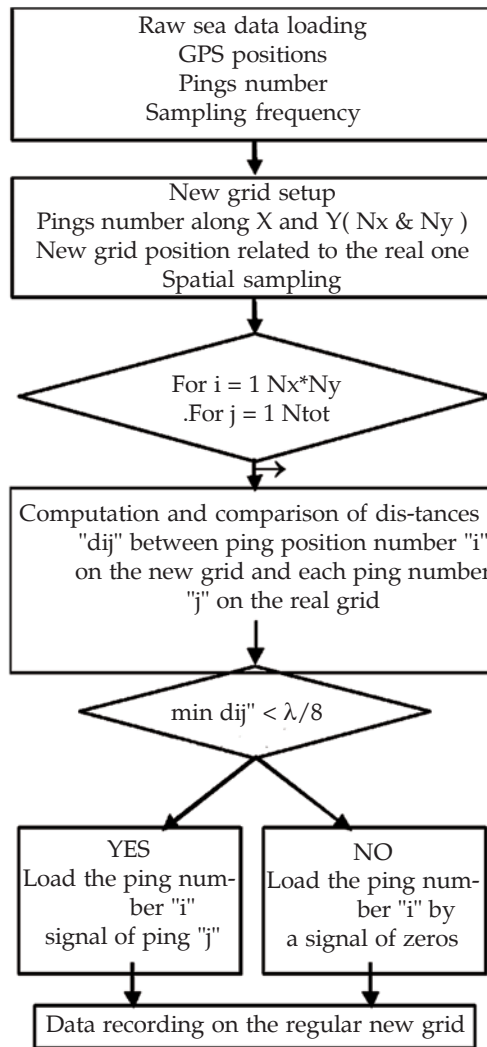The preprocessing algorithm is presented in figure 2:

Fig. 2. Pre-processing algorithm

4. PROCESSING AND POST-PROCESSING

PSAS processing algorithm and its simplification are described in details in reference [5].

In this paper we only show the geometry of the problem (figure 3a) and illustrate the 2D focusing (figure 3b). Figure 3b shows how PSAS aims at re-concentrating the volume dispersion of the energy backscattered by a point reflector in a focusing point corresponding to its position.

a: PSAS Geometry echoes   b: PSAS back migration of
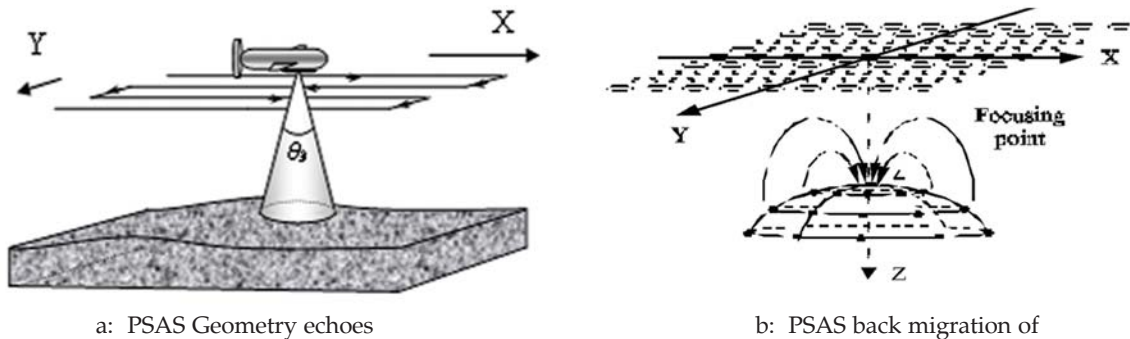
Fig. 4. Principle of planar SAS approach

For every ping, processed focused data were then post-processed with an algorithm inspired from bottom echo tracking. Knowing the rough bottom position, bottom echo is isolated (taking into account the axial resolution) and its energy is computed. Then the second echo is isolated and its energy computed…. The synthetic ping is thus transformed in a set of depth positions and corresponding energy.

5. RESULTS

The sea data shown in this paper were acquired in the following experimental conditions:

- Water depth	about 73 m	- Array aperture (2θ3)	6°
- Sound velocity	1439 m/s	- Sampling frequency	200 kHz.
- Scanned area	4 m x 8 m		

The dump site is well know and documented (historical data) and has been surveyed routinely over the years.

5.1 Raw data

Raw data are represented in figures 4 for 2 tracks at different secondary frequencies.

The depth scale shows that the bottom is rather flat and slightly sloping from bottom-left to top-right (less tan 3%). The figures also show the actual tracks of the ROV. These tracks will first be corrected by navigation data before as part of a complementary pre-processing.

5.2 Processed data

The volumetric representation of sediment generates a large quantity of information. If we consider an area of 10 m x 10 m, a depth range of interest of 4 m and an elementary volume of 1 cm3, we will end up with about 4 G samples. The optimisation of access to data was an essential task for allowing processing the sea data on a conventional desktop machine.

The display of such an amount of data is also a rather complex task. In addition, it has to display reflected energy as a function of 3 parameters (longitude-x, latitude-y, and depth-z). It has to show, at the same time, bottom structure and sub-bottom features. This can be achieved using slices representation several energy maps (x,y) for every depth layer (z) compatible with the axial resolution [4]. This is a very efficient way to represent all the available information as shown in figure 5. It clearly displays the volumes backscattering high energy. Nevertheless it is les convenient for identifying objects shape.
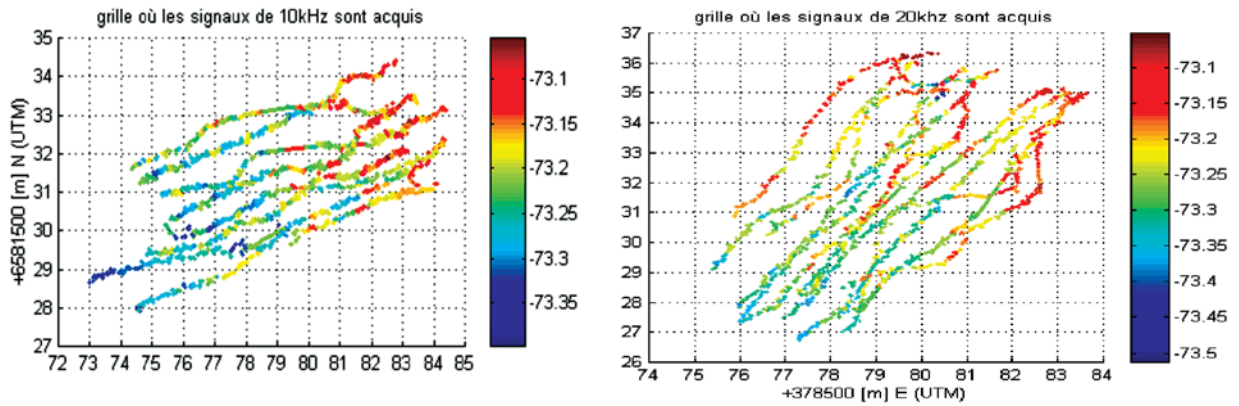
Fig. 4. raw data representation, horizontal and vertical scales are in meters. Colours represent the position of the first (bottom echo). Left tracks at 10 kHz - Right track at 20 kHz

Fig. 5. Strata representation of the 20 kHz scan (fig 4b) after preprocessing and PSAS. Strata of 5 cm/stratum, 2dB /grey level.

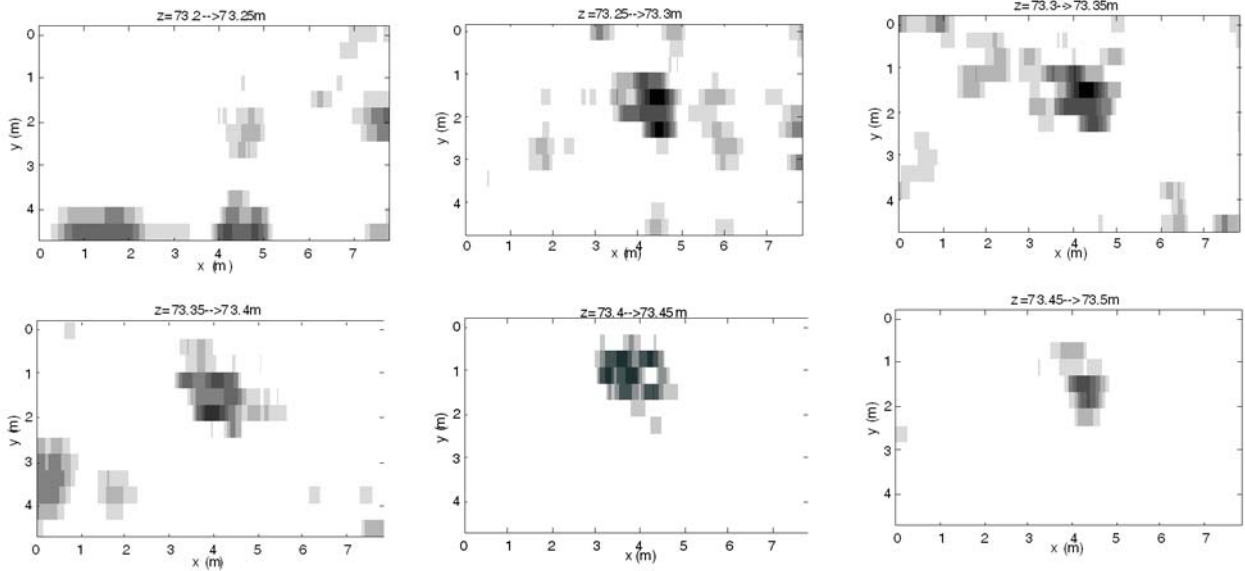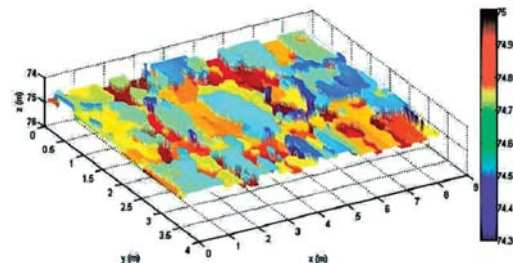a- video image of a dump site   b- 3D representation of processed data

Fig. 6. Processed data (of raw data presented in figure 4b)

In complement to the previous display mode an in order to identify the shape objects, the following procedure was adopted: identifying bottom echo (interface) for every ping, detecting the first echo after interface echo and computing the range of this echo and display it in a 3D conventional display.

The result is shown in figure 6b. Colour scale corresponds to depth (74.3 to 75 m). Although the information is less comprehensive (energy information has been removed), the data interpretation is easier. In the centre of the display (fig. 5b) one can see a rectangular spot of turquoise colour. This feature has been highlighted by dotted lines. It represents a flat surface about a meter below the surface of approximate size 1m x 2 m. Such characteristics correspond to boxes of ammunitions as shown in figure 6a. The picture has been taken well before the sonar survey where the box was only partially buried.

6. CONCLUSION

After being validated on simulation and the on tank data, PSAS has been proved to be an efficient tool for volumetric imaging of bottom and sub-bottom features. The initial processing algorithm was successfully modified in order to handle real un-evenly space sampling of the planar trajectory using an adapted pre-processing scheme. Processing was applied to data obtained at sea on a well known and documented dump site used a test bed.

Considering the large amount of data to display, two display modes were used: the first one enabled the detection of areas of interest while the second one allowed shape identification.

Despite sit apparent complexity (complex acquisition scheme, large amount of data to acquire process and display), PSAS has been showed to be an efficient tool for the reconstruction and the identification of dumped UXO (unexploded ordinances) covered with sediment. The techniques could be extended to other areas of application such as non-destructive testing.

7. ACKNOWLEDGEMENTS

8. REFERENCES

[1]   L. CUTRONA, 1975. Comparison of sonar system performance achievable using synthetic aperture techniques with the performance achievable by more convention al means. *J. Acoust. Soc. Am.*, **58** (2), 336-348.

[2]   J. CHÂTILLON, A. ADAMS, M. LAWLOR and M. ZAKHARIA, 1999. "SAMI: A low frequency prototype for mapping and imaging of the seabed by means of synthetic aperture", *IEEE J. on Ocean. Eng.*, **24** (1), 4-15.

[3]   M.E. ZAKHARIA and J. CHÂTILLON, 2002. "Chapter 4: Synthetic aperture mapping and imaging "; In "Underwater acoustic digital signal processing and communication systems"; R.S.H. Istepanian and M. Stojanovic (eds.), *Kluwer Academic Publishers*, 37-88.

[4]   K. BELKACEM, J. BESBES, M.E. CHÂTILLON and ZAKHARIA, 2006. "Planar SAS for sea Bottom and Sub-bottom Imaging. Concept validation in tank". *IEEE Journal of Oceanic Engineering*. **31** (3), 614-627.

[5]   E. AFIF BELKACEM, MANELL, ZAKHARIA and KAMEL BESBES, 2006. "A fast algorithm for 3D planar synthetic aperture imaging" *acta acustica United with acustica*, **92**, 493-496.

[6]   PH. BLONDEL and A. CAITI, 2007. Buried waste in the seabed, Acoustic imaging and bio-toxicity, Results from the European SI-TAR project. *Springer-Praxis*.

[7]   P. MICHAEL, HAYES and T. PETER, GOUGH, 2009, "Synthetic Aperture Sonar: A Review of Current Status" *IEEE J. on Ocean. Eng.*, **34** (3), 207-209.

[8]   R.E. HANSEN, T.O. SÆBØ, K. GADE and S. CHAPMAN, 2003. "Signal processing for AUV based inter-ferometric synthetic aperture sonar," in Proc. *MTS/IEEE OCEANS* Conf., San Diego, CA, **5**, 2438-2444.

[9]   D. KEVIN, LEPAGE and HENRIK SCHMIDT, 2002. " Bistatic Synthetic Aperture Imaging of Proud and Buried Targets From an AUV ", *IEEE J. on Ocean. Eng.*, **27** (3).

[10] M.A. PINTO, A. BELLETTINI, R. HOLLETT and A. TESEI, 2002. "Real- and synthetic-array signal processing of buried targets," *IEEE J. Ocean. Eng.*, **27** (3), 484-494.

[11] S.K. MITCHELL, K.N. SCARBROUGH, S.P. PITT and T.L. KOOIJ, 2006. High Resolution Circular SAS with Con-trolled Focus, In *The International Conference on Synthetic Aperture Sonar and Synthetic Aperture Radar*, Lerici, Italy, 11-12 September.

Use of the Acoustic Remote Sensing for the Mixing Layer Height Determination

Lokoshchenko M.A.

Department of Meteorology and Climatology, Faculty of Geography,
Lomonosov Moscow State University. 119991, Lengory, Moscow, Russia
e-mail: loko@geogr.msu.su

ABSTRACT

The problem of the mixing layer height (MLH) determination with the use of the sodar data is discussed. Unlike the most of other methods a new suggestion is to determine separately two different mixing layer heights: "upper" or "stable" MLH which indicates a top of an inversion inside wind shear layer (in which dynamical turbulence exists and creates echo-signal) and "lower" or "unstable" MLH which indicates as a rule unstable or weak-stable stratification below the elevated inversion bottom. Some experimental data confirm that two different MLH sometimes, usually in the morning, exist simultaneously one above another. According to this idea the diurnal courses of mixing layer heights - both "upper", and "lower" - have been calculated on a base of long-term sodar sounding at Moscow State University (MSU) during 15 years. Dynamics of both heights at various seasons is discussed.

1. INTRODUCTION

The mixing layer height (MLH) is an important parameter of the lower troposphere which allows determining of the maximal possible range of the air pollution dispersion. The MLH was suggested for the first time by Holzworth in 1962 and initially it was measured on a base only of direct measurements (using radiosonde and the ground meteorological data). Accordingly to classical method, this parameter is equal to the first intersection of the diurnal thermal profile and dry-adiabatic line (which means the value of $\gamma = -\partial T/\partial z = 0.98$ °C/100 m) from the ground point of the maximal daily temperature. It should be noted that, instead of its clear physical meaning, in itself the MLH demonstrates often poor statistical relations with real levels of the air pollution (Aron, 1983). Indeed, it is only one of important atmospheric parameters which must be accounted together with MLH. Later, in addition to MLH, one more parameter - the 'mixing volume' - was used as well. It is product of MLH and average wind velocity V below this height so that the 'mixing volume' may be presented geometrically as a cube which vertical size is equal to MLH and which horizontal size along one axis is equal to the mean V. However, it should be noted as well that both MLH and 'mixing volume' represent not real range of the air pollution dispersion but the potential, i.e. the highest possible one. It may be real in case if air pollutants have sufficient time to reach it. In other words, both parameters indicate potential limit of dispersion in stationary conditions.

The acoustic remote sensing since the pioneer work (McAllister, 1969) discovered new possibilities for more accurate determination of MLH. Now sodars are well-known everywhere all over the world mostly as a tool for wind profiling. However, it is not the only application of the sodar data. Besides Doppler wind measurements, classic so-called 'sodar record' of old non-Doppler sodars (i.e. an echo-signal intensity in

---

time-height coordinates) allows indicating of the thermal stratification type, including inversion layers which prevents to upward dispersion of the air pollutants (Krasnenko, 1986; Lokoshchenko, 1996 and others). Fine spatial resolution of sodars (as a rule, 10-20 m) represents the main advantage of the acoustic remote sensing of the atmosphere due to comparatively low sound velocity (331 m/s in normal conditions). As a result sodars is an almost ideal tool for studying of the atmospheric boundary layer fine-structure. Among others, sodars allows indicating of low level jets in wind profiles as well as thin elevated inversions on sodar records.

The long-term rows of sodar data about thermal stratification were received only in New Delhi in India (Singal et al., 1984), in Krakow in Poland and in Moscow in USSR and Russia (Lokosh-chenko, 2006 and 2007). It should be noted that works of famous Indian school of the acoustic remote sensing are well-known everywhere. The sodar sounding is carried out at Moscow University since 1988, i.e. during last quarter a century. The observation site is situated at the South-Western periphery of Moscow city on 7 km from the city centre. It represents quite flat and open locality. Two sodars have been used there: vertical sodar "ECHO-1" by GDR production since 1988 and Doppler sodar "MODOS" by production of METEK firm (Germany) since 2004. However, only classic data about the thermal stratification which were received at MSU by the use of the "ECHO-1" sodar will be discussed below. Its vertical range is from 25 to 800 m, the operation frequency is 1666.6 Hz, the spatial resolution of the data is equal to 12.5 m.

2. MIXING LAYER HEIGHT BY THE SODAR DATA

As it is said above a sodar record, besides determination of a thermal stratification type, is a useful tool for the MLH estimation as well. The initial determination of the MLH following the Holz-worth's idea was limited only by the unstable stratification, although he wrote by himself later that nocturnal mixing in conditions of the stable stratification due to wind shear "in some cases… may be important". When sodar records began to be used a lot of works were devoted to determination of the MLH by the sodar data including the stable stratification (Kallistratova et al., 1991; Kras-nenko and Fursov, 1992; Maughan et al., 1982; Singal et al., 1984, etc.). It should be noted that comparatively small range of the sodar data - as a rule, from 500 to 1000 m - doesn't allow measuring diurnal mixing height in the afternoon directly - unlike, e.g., some lidar systems (Emeis et al., Münkel, 2009). A top of vertical turbulent structures on sodar records ("plumes", "roots", "grass", "stalagmite", "prongs of a comb", etc.) which are connected with separate convective cells is usually significantly less than their real upper height. Sometimes, however, the MLH in the afternoon is considered to be equal to the average top of convective "plumes" on sodar records (e.g., Krasnenko and Fursov, 1992). Another way is to suppose formally that the diurnal MLH is equal to the height range of a sodar if any elevated inversions are absent above convective structures on a record (Maughan et al., 1982). But the best possible way with the use of a sodar is to receive indirect estimations of this parameter by comparisons between a top of vertical turbulent structures on sodar records and real diurnal mixing height. As it is shown in (Lokoshchenko, 2002) with the use of radiosonde data the ratio between these parameters is close to 1:4 for conditions of Moscow. It is important to note that this estimation was received by the data of the same sodar "ECHO-1" and that its gain factor didn't be changed during a long time. It should be noted as well that in conditions of India this ratio was nearly the same (Singal et al., 1984). One of well-known summary methodic of the MLH determination with the use of sodar records was suggested by (Kallistratova et al., 1991). It should be noted that, in spite of great variety of different turbulent structures on sodar records, it is quite simple for everybody to discern four general types: layers of strong echo-signal intensity connected with inversions, intermitted patchy structures of weak echo-signal intensity connected as a rule with weak-stable stratification (close to isothermal when $\partial T/\partial z = 0$), vertical "plumes" connected with the unstable stratification and totally blank record in time of indifferent stratification. At the latter case a record can't give any information about real MLH but, fortunately, absolutely blank records which mean exactly adiabatic vertical profile of T (when $\partial \Theta/\partial z = 0$) can be seen extremely rarely. So, following (Kallistratova et al., 1991), the MLH is supposed to be equal either to a top of the surface inversion, or to a top of an air layer with weak-stable stratification, or to a bottom of the elevated inversion (if the surface one is absent below), or to a quadruple height of the average top of convective structures, so-called 'plumes' (if this value is less than a bottom of elevated inversion above).

Author used this scheme during a long time. Additionally, author suggested using the instability energy for calculations of the MLH when the data of radiosonde profiling of T are available (Lo-koshchenko, 2002). As for the sodar data of the MLH, the results of measurements on a base of hourly coding of sodar records at Moscow University were published by (Kallistratova and Lokosh-chenko, 1998) for period 1988-1991 and later by (Lokoshchenko, 2002) for longer period 1988-1998. In fact, an average MLH calculation accordingly to (Kallistratova et al., 1991) represents generally quite logical results in common features - both at the annual course (with maximum in the warm period) and at the diurnal one (with a strong maximum in the afternoon, especially in summer). However, a joining of different stratification types at the same parameter sometimes leads to illogical and paradoxical dynamics of the MLH. For example, after sunrise when the surface inversion begins to lift above the ground the MLH value accordingly to (Kallistratova et al., 1991) is sharply changed from a top of the surface inversion to its bottom (when it lifts already) - see Fig.1. At the diurnal course this change may be seen as a sudden fall of the MLH in the early morning like a jump although it is evident mixture of two principally different physical processes. Evidently it is a disadvantage of methodic which was suggested by (Kallistratova et al., 1991).

For more correct studying of the MLH at its dynamic a new approach is to analyze separately two mixing heights: "stable" or "upper" and "unstable" or "lower" (see Fig.1 and 2). This idea was published briefly for the first time in (Lokoshchenko, 2010). Accordingly to it, the "stable" MLH is equal either to a top of any inversion (i.e. a height of an upper margin of turbulent structure connected with an inversion layer on a sodar record), or to a top of an air layer with weak-stable stratification. The "unstable" MLH means either a top of a layer with weak-stable stratification as well or a quadruple average height of convective structures ("plumes") when elevated inversion is absenta-bove. If the unstable stratification exists in a layer below the elevated inversion the "unstable" MLH is equal either to a bottom of the inversion if it is less than a quadruple height of plumes or to a quadruple height of plumes otherwise. Thus, when weak-stable stratification takes place at any layer a top of this layer represents both "upper" and "lower" heights because this type is intermediate and frontier between stable and unstable stratification.

In conditions of unstable stratification the "upper (stable)" MLH is absent. From the other hand, in time of the surface inversion the "lower (unstable)" MLH is considered to be equal to zero.

As one can see in Fig.1 sudden fall of MLH is absent accordingly to new suggestion. In fact the stable MLH which indicated a top of former surface inversion during night really exists even later - in morning when the same inversion became elevated already. At the same time new unstable MLH appears
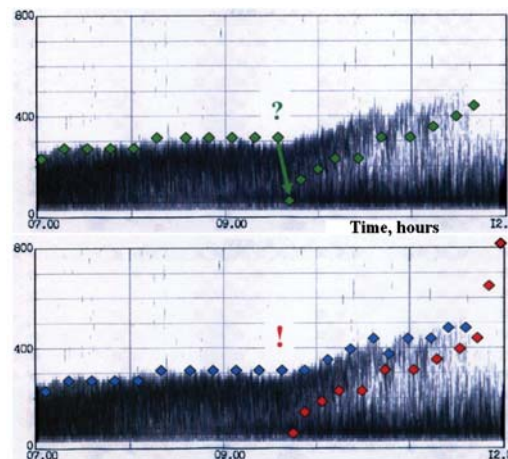

Fig. 1. Dynamics of MLH in morning time in conditions of elevated inversion: traditional methodic (paradoxical fall) - upper part; new suggestion at the same sodar record - lower part. Green rhombuses - traditional MLH; blue rhombuses - upper MLH (new suggestion); red rhombuses - lower MLH (new suggestion).

(a) Surface inversion.   (b) Elevated inversion;

(c) Unstable stratification   (d) Weak-stable stratification
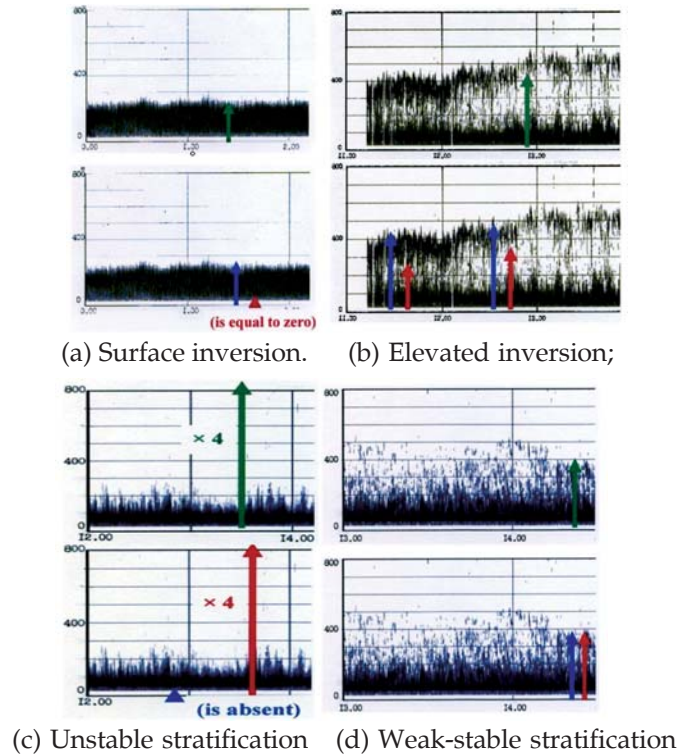
Fig. 2. Mixing layer heights by the sodar data. Green lines indicate the traditional MLH; blue lines - "stable" MLH (new suggestion); red lines - "unstable" MLH (new suggestion).

simultaneously below the stable one. Thus, new method of two different MLH represents successful solution of this paradoxical dynamics.

3. EXPERIMENTAL CONFIRMATION

Indeed, experimental data often demonstrate two different MLH simultaneously - especially, in morning time. One of confirmations is given by lidar data (e.g., Emeis S., K.Schäfer, C.Münkel, 2009). In Fig.3 the diurnal course of the lidar backscatter density is presented for Hamburg city. As one can see in color scale of this parameter, three air layers with different background levels existed simultaneously in time from 05 to 11 a.m.: the highest values - in the ground air layer, the middle ones - in the upper part of the ABL above and, finally, the lowest values (blue color) - in free troposphere since 1.8-2.3 km. Correspondingly, two MLH existed simultaneously between these three layers.

One more experimental confirmation was received by author in time of special experiment when sodar and tethered balloon operated simultaneously (Lokoshchenko and Shifrin, 2009; Lokosh-chenko, 2010). The tethered balloon was supplied, among others, by electrochemical ozonosonde. The experimental ozone profiling with fine resolution in the lower atmosphere demonstrated as well that two different MLH sometimes exist in the morning simultaneously one above another - both below the elevated inversion and above it.

4. CLIMATOLOGY OF MIXING LAYER HEIGHTS

The daily courses of both mixing layer heights at different seasons are presented on Figure 4. They were calculated on a base of hourly coding of sodar records which were received at Moscow University in period from 1988 to 2003 (totally - almost of 35.000 hours of records were analyzed by author). As it is seen the "upper" MLH (blue rhombs) in winter doesn't demonstrate any significant changes during a day. However,
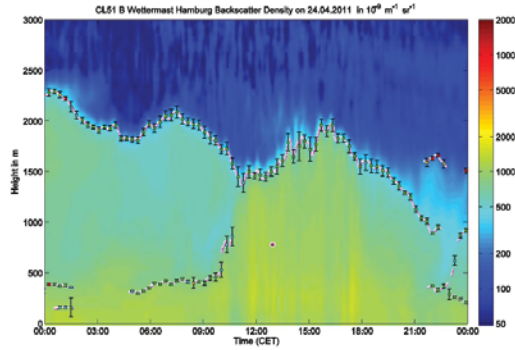
Fig. 3. The diurnal course of the lidar backscatter density in Hamburg accordingly to (Emeis et al., 2009)

(a) Winter

(b) Spring

(c) Summer

(d) Autumn
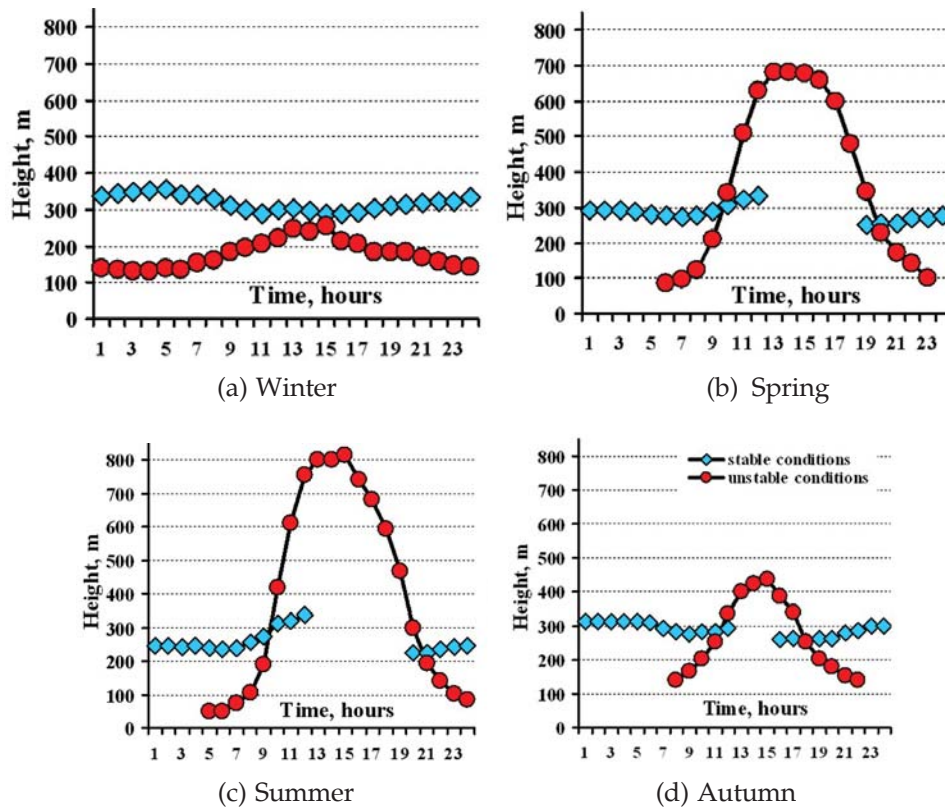
Fig. 4. The diurnal course of both mixing layer heights at various seasons by
the sodar data for the period 1988-2003. Moscow.

it is slightly higher at night and a bit lower in the afternoon. In spring and in summer the "upper" MLH which is connected with stable conditions increases in the morning that is a result of lifting of the morning elevated inversion (which is as a rule former surface inversion) top. Except morning time, the "upper" stable MLH is nearly the same from one hour to another during all the rest of a day. The average value of the "upper" MLH is close to 300 m and varies in limits from 250 to 350 m. It is highest in winter due to more thickness of surface inversions and lowest in summer. In the middle of a day in spring, in summer and in autumn the stable stratification exists extremely rarely so that calculation of the average "upper" MLH in these conditions is not supported by sufficient statistical sampling. Vice versa, the "lower" MLH that is

either unstable or weak-stable stratification (red circles) may be observed very rarely after midnight. Only in winter the diurnal course of the "lower" MLH is full due to comparatively often cases of weak-stable stratification at night - both in presence and in absence of elevated inversions above it [12].

Unlike the "upper" MLH the "lower" one connected mostly with unstable conditions has a clear diurnal course with maximum in the afternoon which is especially strong in spring and in summer. The maximal average values of the "lower" MLH in the middle of a day consist up to 700 m in spring and up to 800 m in summer. In fact, the diurnal convective mixing layer in mid-latitudes may be really equal to 800 m in summer as it was demonstrated by lidar in [1]. However, usually it seems to be more and convective turbulent structures on sodar records in summer are often higher than 200 m as well. The average values of the "lower" MLH on Fig.4 indicate total calculation including cases of elevated inversions which sometimes exist at low levels. Due to them the average "lower" MLH is not so large. It should be noted that the diurnal course of this parameter is quite similar in spring and in summer whereas in autumn the daily maximum of the "lower" MLH is very weak already. Thus, there is an evident asymmetry of mixing conditions at transitional seasons.

5. CONCLUSIONS

1. The acoustic remote sensing is a useful tool for determination of the mixing layer height, especially at nocturnal and morning time. If inversion layers exist in the lower atmosphere real mixing height as a rule is close to their margins which may be detected on a sodar record. As regard as diurnal convective mixing layer, only indirect estimations of the MLH are possible by the use of a sodar.

2. Different physical processes of mixing can operate at the same time at various levels of the atmosphere. Among others, sometimes in the morning two mixing heights exist simultaneously below and above elevated inversion.

3. It seems to be useful to analyze separately two different mixing heights one of which is connected as a rule with a top of an inversion and another one - mainly with a bottom of an inversion or with a top of convective cells. The weak-stable stratification has an intermediate position between these processes. This approach of two kinds allows understanding and studying the dynamics of the MLH more correctly.

4. Accordingly to long-term sodar observations at Moscow University the "upper" MLH connected with stable conditions consists in average nearly of 300 m (from 200 to 400 m). It is the largest in winter and the smallest in summer.

5. The "lower" MLH connected mostly with unstable conditions is the largest in summer and in spring (up to 700-800 m in average in the afternoon) and the smallest in winter. There is clear asymmetry between conditions of mixing in spring and in autumn.

6. REFERENCES

[1]   R. ARON, 1983. Mixing height – an inconsistent indicator of potential air pollution concentrations. *Atmospheric Environment*, **17** (11), 2193-2197.

[2]   S. AUTUMN EMEIS, K. SCHÄFER and C. MÜNKEL, 2009. Observation of the structure of the urban boundary layer with different ceilometers and validation by RASS data. *Meteorologische Zeitschrift*, **18** (2), 149-154.

[3]   G.C. HOLZWORTH , 1962. A study of air pollution potential for the western United States. *J. of Applied Meteorology*, **1**, 366-382.

[4]   M.A. KALLISTRATOVA *et al.*, 1991. Method of remote measurement of mixing layer parameters by Doppler sodar. *Preprint of IAP*, Moscow, (in Russian) **1**, 77-94.

[5]   M.A. KALLISTRATOVA and M.A. LOKOSHCHENKO, 1998. Studying of mixing layer height by radiosonde and sodar observations. *In: Proceedings of the 9th ISARS*, Vienna, Austria, 285-288.

[6]   N.P. KRASNENKO, 1986. The Acoustic Remote Sensing of Atmosphere – a monograph (in Russian). Novosibirsk: Nauka, Siberian division, 168.

[7] N.P. KRASNENKO and M.G. FURSOV, 1992. The remote acoustic monitoring of meteorological parameters in atmospheric boundary layer. *Atmospheric and Oceanic Optics*, Tomsk, **5** (6), 652-654.

[8] M.A. LOKOSHCHENKO, 1996. Use of vertical sodars in meteorology (review), *Atmospheric and Oceanic Optics*, Tomsk, **9** (7), 616-628.

[9] M.A. LOKOSHCHENKO, 2002. Long-term sodar observations in Moscow and a new approach of the potential mixing determination by radiosonde data, *Journal of Atmospheric & Oceanic Technology*, **19,** 1151-1162.

[10] M.A. LOKOSHCHENKO, 2006. Thermal Stratification and Weather Phenomena on Sodar Records. In: *Proceedings of the 13th ISARS*, Garmisch-Partenkirchen, Germany, 131-136.

[11] M.A. LOKOSHCHENKO, 2007. Temperature stratification of the lower atmosphere over Moscow, *Russian Meteorology and Hydrology*, **32** (1), 35-42.

[12] M.A. LOKOSHCHENKO, 2010. Climatology of the mixing layer height by long-term sodar data. *In: Proceedings of the 15th ISARS,* Paris, France.

[13] M.A. LOKOSHCHENKO and D.M. SHIFRIN, 2009. Temperature stratification and altitude ozone variability in the low troposphere from acoustic and balloon sounding, *Russian Meteorology and Hydrology,* **34** (2), 72-82.

[14] R.A. MAUGHAN, A.M. SPANTON and M.L. WILLIAMS, 1982. An analysis of the frequency distribution of sodar derived mixing heights classified by atmospheric stability. *Atmospheric Environment*, **16** (5), 1209-1218.

[15] L.G. MCALLISTER *et al.* 1969. A new approach to the study of atmospheric structure. In: *Proc. of the IEEE*, **57** (4), 579-587.

[16] S.P.SINGAL, B.S. GERA and S.K. AGGARWAL, 1984. Nowcasting by aoustic remote sensing: experiences with the systems established at the National Physical Laboratory, New Delhi. *J. of Scientific & Industrial Research*, **43**, 469-488.

Acoustics Requirements in Human Spaceflight Mission

G Venkata Narayana, P Sunil, S Mohanakumar and S Unnikrishnan Nair

Human Spaceflight Project, Vikram Sarabhai Space Centre, ISRO,
Trivandrum - 695 022

ABSTRACT

More and more countries are showing interest in undertaking human spaceflight missions. The crew members will be confined to the limited volume of crew module during launch, on-orbit and reentry phases of mission with the total mission duration lasting from few days to weeks / months. Noise control is an important subject matter in human spaceflight. In order to maintain the health, hearing, communication and habitability requirements, the acoustic environment in the crew cabin shall be within acceptable limits during all phases of mission, more importantly during the long orbital phase where the crew members will be demanded to do many assigned tasks and have enough relaxation and sleep. Noise effects physiological behaviour, performance level and causes annoyance to the crew members depending upon the state of crew, type of work, duration and frequency content of noise. There is no evidence that human auditory functioning change in space under microgravity conditions. However, the noise loss factors will differ from one atmospheric pressure conditions on earth to no-atmospheric pressure in outer space. The primary concern in human spaceflight is of sound that arrives at the crew member's ear through an airborne path. Audible noise with constant sound levels of 85 dBA or greater is hazardous regardless of the duration of exposure. Hearing protection devices must be provided for noise levels of 85 dBA or greater. Crew members should not be exposed to noise levels which exceed 120 dBA in any frequency band and 135 dBA of overall noise level under any circumstances. The crew module / cabin architecture in human spaceflight shall establish a satisfactory noise environment relative to the human response - to prevent hearing loss, to minimise disruption of speech communications and to minimise noise induced annoyance / stress factors. This objective is achieved through proper selection and placement of equipments without compromising the acoustic quality. This paper provides acoustic design limits for general design goals, and noise exposure limits for working and living areas of crew cabin. Also, suggestion for appropriate noise limits for manned spacecraft, techniques to minimise the noise and methods for protecting the humans during spaceflight are included.

1. INTRODUCTION

In human spaceflight, crew members will be subjected[1,2] to many physiological and psychological stresses during launch, on-orbit and re-entry phases. Noise control is an important subject matter in crew health and performance during human spaceflight mission. The acoustic environment in the crew cabin shall be within acceptable limits during all phases of mission, more importantly during the long orbital phase where the crew members will be demanded to do many assigned tasks. Also, they should have adequate relaxation and sleep. Noise affects physiological / psychological behaviour, performance level and causes annoyance to the crew members depending upon the state of crew, type of work, duration and frequency content of

noise. Noise travels in different paths to reach the human ear. The primary concern in human spaceflight is sound that arrives at the crew member's ear through an airborne path. This paper provides acoustic design limits for general design goals, and noise exposure limits for working and living areas of crew cabin. Also, suggestion for appropriate noise limits for manned spacecraft, techniques to minimise the noise and methods for protecting the crew from high acoustic levels during spaceflight are included.

2. EFFECT OF ACOUSTICS ON HUMANS

Noise effects on humans also must be considered while designing the crew module / cabin. The degree of exposure to noise that will result in damage depends on intensity and individual susceptibility. Even low levels of noise can interfere with communication. Reduced cabin pressure causes a reduction in sound transmission. This means that crew members have to talk louder to be heard which can potentially lead to[1,3] huskiness on the part of some crew members. The problem becomes more noticeable as the distance between individuals increases.

2.1 Performance effects

Noise can adversely affect performance, with the effects being greater for more complex tasks. Intermittent noise has more adverse effects[1] than steady-state noise. Masking of speech occurs when the presence of one sound, inhibits the perception of another sound. Hence, a given frequency will mask signals at neighboring frequencies rendering them completely inaudible. Crew member's efficiency is impaired when noise interferes with voice communications. When this occurs, the penalty is an increase in time required to accomplish communication through slower, more deliberate verbal exchanges. This results in increased possibilities of human error due to misunderstandings. Crew member's communication limitations must be considered as an integral part of the system in which they perform. Table 1 provide performance effects of noise on humans with duration of exposure. The following performance related effects can be caused by noise.

    a.   Irregular and regular periodic noise reduces performance on a complex visual tracking task.

    b.   Increased alertness due to high noise intensity result in improved performance up to a point. But, beyond certain level of intensity, over attentiveness will degrade the performance.

    c.   Psychological effects of noise can include anxiety, helplessness, degraded task performance and narrowed attention.

2.2 Physiological effects

Exposure to intense sound may result in temporary or permanent hearing loss. The severity of the loss depend upon the duration of exposure, the physical characteristics of the sound (intensity, frequency, pure or wide-band), and the nature of the exposure (continuous or intermittent). Table 2 furnish the physiological effects of noise for various conditions of exposure. Physicians and psychologists are of the view that[1,2] continued exposure to noise level above 80 to 100 dBA is unsafe. The observed health hazards of noise

Table 1. Performance effects of noise.[1,4-7]

SPL, dBA	Duration	Performance effects
75	10 - 30 days	Degraded performance
85	24 h	Fatigue, Nausea, Headache
90	12–24 h	Degradation of multiple-choice
		Vigilance decrement
		Altered thought processes
		Interference with mental work
105	8–12 h	Reduced visual acuity
		Stereoscopic acuity
110	8 h	Chronic fatigue

Table 2. Physiological effects of noise.[1,4-6]

SPL, dBA	Physiological effects
100	Tense feeling Grim-facing
	Covering the ears
	Urge to avoid / escape
120	Discomfort in the ears
135	Pain in the ears
150	Reduced visual acuity
	Chest wall vibrations
	Choke / Strangle sensations
	Respiratory rhythm changes
155	Eardrum membrane rupture

include: (i) Increased concentration of corticosteroids in the blood as well as brain and affects the size of the adrenal cortex, (ii) Continued noise exposure change the functioning of liver and kidneys and cause gastrointestinal ulcers, (iii) Vasoconstriction in the extremities, with simultaneous changes in blood pressure, (iv) Noise pollution causes increase in the rate of heart-beat, increased cholesterol level and constriction of blood vessels which leads to blood pressure that result[1,2] in heart attack, and (v) Noise can wake people from their sleep with a jerk and keep them awake or disturb their sleep pattern. This could make people irritable and tired the next day.

2.3 Annoyance effects

The term annoyance refers[1,2] to the degree of noise that is perceived to be unwanted, objectionable, or unacceptable. High noise levels can interfere with rest and hearing of wanted sounds. Sensitivity to annoyance by noise varies greatly from person to person. It is difficult to define a noise level below which people will not be annoyed by noise. People are more sensitive to unpredictable noise and noise they feel is unnecessary. People who are most sensitive to noise become increasingly disturbed as the noise persists, whereas the annoyance level of less sensitive individuals remains constant over time.

3. ACOUSTIC ENVIRONMENTS IN HUMAN SPACEFLIGHT

Spacecraft crew members should be provided with an acoustic environment that will not cause[1] injury or hearing loss, interfere with voice or any other communications, cause fatigue, or in any other way degrade overall man / machine system effectiveness.

3.1 Launch and abort phases

A high noise level environment typically occurs during the launch (rocket motor propulsion aided ascent) and abort (if any) phases. The primary concern[1] is crew member exposure that will cause hearing loss or interfere with intercom and radio voice transmission. The noise environment within the spacecraft during the launch phase is, initially, the result of high level jet noise of the booster rockets impinging on the outer surface of the module and being transmitted to the spacecraft interior. Typical maximum crew module external noise level at lift-off will be 142 dBA. This noise level shall be brought down to the acceptable limit (? 120 dBA) with suitable acoustic protection system in the crew module architecture and helmet equipped with communication-type ear muffs. As the spacecraft accelerates from its launch pad, noise reduces due to loss of ground reflection, and jet noise diminishes as velocity increases. With increasing velocity, however, the crew module fairing (crew module resides inside the fairing) receives aerodynamic noise generated by boundary layer turbulence along the outer surface of the fairing. This boundary layer noise reaches its maximum level as the spacecraft passes through the range of maximum dynamic pressure and decreases progressively thereafter. Aerodynamic noise becomes insignificant approximately two minutes after lift-off (above 100 km altitude) due to space vacuum.

3.2 On-orbit phase

The on-orbit phase of spacecraft missions is of relatively long duration. During work periods, the summation of the individual sound pressure levels from all operating systems and subsystems should not exceed exposure limits that will cause hearing loss or interfere with voice communication. Sleep and rest period noise levels should not exceed noise levels that interfere with sleep or comfort and the hearing of wanted sounds. There is no evidence[1] that human auditory functioning changes in space under microgravity conditions. However, the noise loss factors will differ[1] from one atmospheric pressure conditions on earth to no-atmospheric pressure in outer space. The effect of small and low-frequency noise in a crew module is especially significant, because propagation of low-frequency noise through the crew cabin pressure hull into the vacuum of outer space cannot occur. The on-orbit acoustic environment within the spacecraft is composed[1] of (i) Continuous noise sources - environmental control equipments (motors, fans, pumps) and avionics equipments (transformers, oscillators), and (ii) Intermittent noise sources - waste control system (pumps, fans, valves), personal hygiene station (pumps, fans, valves), pressure regulators and thrusters firing

3.3 Re-entry phase

The high noise levels that occur during re-entry phase are similar to the launch phase. Unlike in the launch phase, the crew module is directly exposed to the atmosphere (in the absence of fairing) during re-entry phase. Hearing loss and interference with intercom and radio voice transmission are of primary concern during re-entry. The noise environment within the spacecraft in the re-entry phase is dominated by boundary-layer turbulence containing broadband noise of high intensity. The sound pressure levels during atmospheric re-entry are comparable with those produced during the maximum dynamic pressure of launch phase. Though the sound levels are comparable, exposure durations are longer during re-entry phase.

4. ACOUSTIC SPECIFICATIONS FOR CREW CABIN

The maximum allowable on orbit continuous broadband sound pressure exposure limits produced by the summation of all individual sound pressures from all sources, operating systems, subsystems and payloads, considered over a 24 h period are defined.[6] The following general guidelines are presumed for crew cabin design.

a. All noisy equipments shall be located such a way, to reduce noise in crew member stations.
b. System designs shall include noise control provisions.
c. Means shall be provided onboard to facilitate measurement of acoustic noise levels to verify that exposure levels within the design limits.

Spacecraft crew member noise exposure design limits shall be satisfied depending on crew member tasks and acceleration regimes. Noise design limits are established by the following three criteria; (i) Hearing conservation, (ii) Communication requirements and (iii) Annoyance considerations.

4.1 Hearing conservation

Hearing conservation criteria are based[1] on comprehensive statements of the relation between various descriptive parameters of the noise exposure, such as sound pressure level, exposure time, and the probability of temporary or permanent hearing loss. The allowable crew noise exposure limits are given in Table 3.

Table 3. Crew noise exposure limits.[1]

Duration / Level	SPL, dBA
Continuous (Unlimited)	50
24 h limit	75
8 h limit	? 85
Hazard level	? 85
Max. exposure (2 minutes in 24 h period)	? 120
Unacceptable level	> 120 (any frequency), 135 (OASPL)@

@ Overall Sound Pressure Level

4.2 Communication requirements

In the presence of background noise direct (face-to-face) communication provides visual cues that enhance voice communication intelligibility. Intelligibility is the degree to which meaningful words, phrases and sentences can be understood over face-to-face or over communication systems. Intelligibility is affected by spoken clarity, explicitness and precision. The distance from speaker to listener, background noise level, voice level, ambient air pressure and gaseous composition of the air are important considerations, because they affect voice efficiency and frequency content. Table 4 lists the influence of background noise on face-to-face communication. The ratio of speech level to background noise level affects intelligibility. For satisfactory communication of most voice messages in noise, 75 % intelligibility is required. Sound pressure levels permissible for different states inside crew cabin are shown in Figure 1. Noise in the work areas shall not exceed the Noise Criteria (NC)-50 contour, as shown in the figure, unless otherwise specified.

Table 4. Influence of background noise on face-to-face communication.[1,9]

Back ground noise level, dBA	Face-to-face communication
30 - 40	Satisfactory in normal voice up to 4 m
40 - 50	Satisfactory in normal voice up to 1 to 2 m Satisfactory in raised voice up to 2 to 4 m
50 - 60	Satisfactory in normal voice up to 0.3 to 0.6 m Satisfactory in raised voice up to 1 to 2 m Telephone use – Slightly difficult
60 - 70	Satisfactory in raised voice up to 0.3 to 0.6 m Slightly difficult in raised voice up to 1 to 2 m Telephone use – Difficult
70 - 80	Slightly difficult in raised voice up to 0.3 to 0.6 m Slightly difficult with shouting up to 1 to 2 m Telephone use – Very difficult
80 - 85	Slightly difficult in shouting up to 0.3 to 0.6 m Telephone use – Unsatisfactory

Another important crew cabin noise design consideration is control of reverberation time (time for sound decay). Rooms used for speech / communication typically need[8] a shorter reverberation time, so that speech can be understood more clearly. The reverberation time of a spacecraft compartment shall be adjusted according to habitable volume and the criterion for conversational speech. In areas where crew members are assigned with a task to observe the display parameters as well as to communicate by voice among themselves and/or to the ground stations, a room reverberation time of approximately 0.5 s is to be provided.[1]

4.3 Annoyance considerations

Maximum continuous noise level: Problems of annoyance and task disruption will be minimal[1] if acoustic requirements for acceptable speech communication, sleep, and rest are met. The maximum allowable continuous broad band sound pressure levels produced by the summation of all the individual sound pressure levels from all operating systems and subsystems considered at a given time shall not exceed the NC-50 curve for work periods (Figure 1).
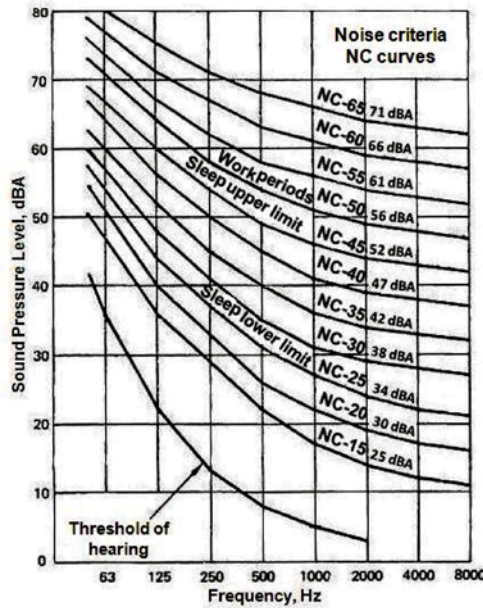

Fig. 1. Crew cabin noise criteria.[1,10]

Sleep compartment noise level: In sleep areas, the noise level shall not exceed the NC-45 curve and need not be less than NC-25 curve (Figure 1). Hearing protection devices may be made available in sleep areas to provide acoustic isolation as needed. Anticipated impulse or transient noises shall not exceed background noise by more than 10 dBA during sleep / rest periods.

5. NOISE MITIGATION TECHNIQUES

The amount of noise reaching the receiver is dependent on the source level and the degree to which the transmission paths reduce the disturbances due to various attenuation factors encountered along the way. Noise control is based on what we know about how sound behaves. In planning[1,3,4] for effective noise control, consider all opportunities that may exist in the following three interdependent stages. (i) Control at the source, (ii) Control in transmission path, and (iii) Personal hearing protection.

5.1 Control at the source

Noise control at the source typically involves[1,3,4] avoiding generation of excess noise through selection of inherently quieter equipment, regular maintenance and sensible operation. Source control may also involve preventing noise from escaping from the source by adding appropriate control devices such as mufflers, fairings and water injection on to the booster rocket jet at lift of on launch pad. Identify source using instruments and senses (look, listen, touch). The sources of equipment / system noise are vibration, impact, friction and fluid flow turbulence. Table 5 list typical methods to control noise at the source.

Table 5. Typical noise sources and corrective actions.[1]

Vibration	Impact	Friction	Turbulence
Avoid resonance	Eliminate impact	Lubricate	Reduce velocities
Stiffen	Reduce clearances	Avoid frictional contact	Streamline flow
Secure tightly	Reduce impact area	Use rolling contact	Use mufflers
Isolate from drive	Isolate impact areas	Anti-friction bearings	Line air ducts
Reduce speed	Enclose impact area	Precision gears	Use quiet fans
Surface damping	Reduce impact speed	Optimum loadings	

5.2 Control in transmission path

Once noise has been created and has escaped from the source, there are various ways to prevent it from reaching noise sensitive areas. Airborne noise can be reduced[1,3,4] by (a) Enclosure and barriers between noise source and crew members, (b) Sound absorption linings, and (c) Sealing of enclosure and perimeter wall penetrations. Another proven method is employment of a noise barrier. An effective noise barrier must meet[4] the following three requirements:

a. It must be tall enough and long enough to clearly block the line of sight from the noise receiver to the noise source zone,

b. It must be dense (heavy) enough and be free from gaps and cracks so that there is no significant transmission of sound through it, and

c. It must be continuous throughout the noise source zone.

The effectiveness of sound absorbing materials depends on its thickness, amount of airspace and density. All materials intended to use inside the crew cabin shall be bio and vacuum compatible in nature. Mass law states that for each doubling of the frequency (Hz) there will be about 6 dBA less transmitted sound. For each doubling of the distance there will be about 3 dBA reduction[1,3,4] in sound. In the crew module design, acoustic protection material location is conceived in the annular place of double walled module. Example: In space shuttle orbiter Inertial Multiple Unit (IMU), 22 dBA reduction in 2000 Hz was accomplished[1] by introducing a straight-through, foam-lined, dissipative muffler.

5.3 Hearing protection

Noise that has not been sufficiently reduced requires the use of hearing protection devices. These devices consist of ear-plugs, ear muffs, noise-attenuating helmets, or combinations of these. Example: A NASA helmet equipped with communication-type ear muffs will provide[1] 17 dBA attenuation over the range of frequencies from 63 to 8,000 Hz, reducing launch noise at the crew member's ear to about 93 dBA from 110 dBA.

6. CONCLUSION

Acoustic performance of crew cabin is a prime design goal in human spaceflight missions. Human tolerance to various noise levels depend on many physiological and psychological factors. Spacecraft crew member noise exposure limits are established by hearing conservation, communication requirements and annoyance considerations. The amount of noise reaching the crew is dependent on the source level and the degree to which the transmission paths reduce the disturbances due to various attenuation factors encountered along the way. Audible noise with constant sound levels of 85 dBA or greater is hazardous regardless of the duration of exposure. Hearing protection devices must be provided for noise levels of 85 dBA or greater. Crew members should not be exposed to noise levels which exceed 120 dBA in any frequency or overall sound pressure level of 135 dBA under any circumstances. Techniques to minimise the noise and methods for protecting the crew in spacecrafts are suggested.

7. REFERENCES

[1] *Man Systems Integration Standards*, 1995. NASA-STD-3000, V-I, Revision-B.

[2] M.L. DAVIS and S.J. MASTEN, 2008. Ed., *Principles of Environmental Engineering and Science*, 2nd Edition, McGraw-Hill.

[3] E.B. MAGRAB, 1975. *Environmental Noise Control*, Wiley (New York).

[4] *Human Factors Engineering*, 1972. Department of the Air Force, HQ A/F Systems Command, AFSC-DH 1-3.

[5] E.M. ROTH. ED., 1968. *Compendium of Human Responses to the Aerospace Environment*: V-II, Lovelace Foundation for Med. Ed & Research, NASA-CR-1205(II).

[6] *Human Factors Engineering Design for Army Material*, 1981. U.S. Army Human Engineering Lab, DOD, MIL-HDBK-759A.

[7] J.F. PARKER and V.R. WEXT. *Bioastronautics Data Book*, Biotechnology, Inc., Office of Naval Research/ NASA. NASA-SP-3006.

[8] MICHAEL VALENTE, HOLLY HOSFORD-DUNN and J. ROSS ROESER, 2008. Ed., *Audiology: Treatment*, 2nd Edition, Thieme, New York.

[9] L.E. HUMES, D.D. DIRKS, T.S. BELL, CHRISTOPHER AHLSTROM and G.E. KINCAID, 1986. Application of the Articulation Index and the Speech Transmission Index to the Recognition of Speech by Normal Hearing and Hearing Impaired Listeners, *Journal of Speech and Hearing Research*, **29**, 447-462.

[10] R.J. FARRELL and J.M. BOOTH, 1984. *Design Handbook for Imagery Interpretation Equipment*, Boeing aerospace Co., D180-19063-1.

Sensor Networks for Condition Monitoring of Rotating Machinery

T. Venkata Ratnam[1], PVS Ganesh Kumar[2], P. Seetharamaiah[3] and L. Bhupathi Rao[4]
[1]Technical Officer 'D', Naval Science and Technological Laboratory, Visakhapatnam, India
[2]Scientist 'G', Naval Science and Technological Laboratory, Visakhapatnam, India
[3]Professor Emeritus, Andhra University College of Engineering (A), Visakhapatnam, India
[4]Asst. Professor, Vignan Institute of Engineering for Woman, Visakhapatnam, India
e-mail: ratnamtv2k6@gmail.com

ABSTRACT

A sensor network is a collection of sensors that are distributed over an area, to collect the physical phenomenon such as temperature, vibration, pressure etc. Sensor networks are mainly used in monitoring applications. These are Area Monitoring, Temperature Monitoring, Machine condition Monitoring etc. This paper implements the software for condition monitoring by using sensor networks to know the condition of the rotating machinery. Condition monitoring of rotating machinery is the measurement of various parameters related to the mechanical condition of the machinery which makes it possible to determine whether the machinery is in good or bad mechanical condition.

This paper aims at development of sensor network that comprises three vibration sensors placed over the rotating machinery for condition monitoring. The network consists of sensors mounted on the machine which acquires vibration parameters and a data acquisition system (DAQ) to convert the data from analog to digital form. A LAN interface Module is used for acquiring the data from DAQ to the computer. A frame work is developed to perform the simulations on acquired data. A rule based expert system is included in the framework to help the machine operator for identifying machinery faults.

The framework is implemented using MATLAB software tools with input as vibration parameters. It automatically detects the possible cause for the fault in a machine and suggests suitable remedies. A demonstrative example is used for bringing out the utility of the methodology.

1. INTRODUCTION

A sensor network is a collection of sensors that are distributed over an area, to collect the physical phenomenon such as temperature, vibration, pressure etc. Sensor networks are used in many applications such as military surveillance, human health monitoring, industrial applications, environmental monitoring etc [1]. Condition monitoring of rotating machinery is one of the application of sensor networks. Condition monitoring is the measurement of various parameters related to the mechanical condition of the machinery (such as vibration, bearing temperature, oil pressure, oil debris, and performance), which makes it possible to determine whether the machinery is in good or bad mechanical condition. If the mechanical condition is bad, then condition monitoring makes it possible to determine the cause of the problem. Most of the defects encountered in the

rotating machinery give rise to a distinct vibration pattern (vibration signature) and hence mostly faults can be identified using vibration parameter. The objective of condition monitoring of a machine using sensor networks is to predict the machinery fault well in advance of its occurrence. Each machine fault produces a unique set of vibration components that can be used for identification. Some of the common machinery faults which occur in rotating machinery [2] are depicted in Fig. 1.
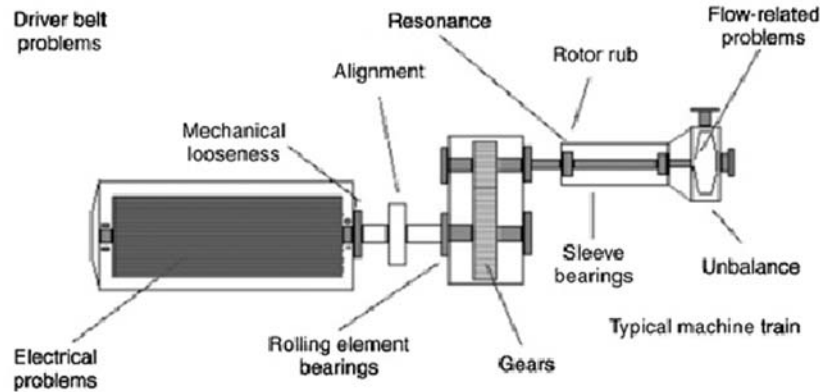

Fig. 1. Most common faults occurs in rotating machines.

In this paper, application of sensor networks to machine condition monitoring has been demonstrated. The network consists of sensors mounted on the machine which acquires vibration parameters and a data acquisition system (DAQ) to convert the data from analog to digital form. The digitized data is transferred to software in a computer for further analysis processing to know the status of the rotating machine. Fig. 2 shows the sensor networks applied on rotating machinery.
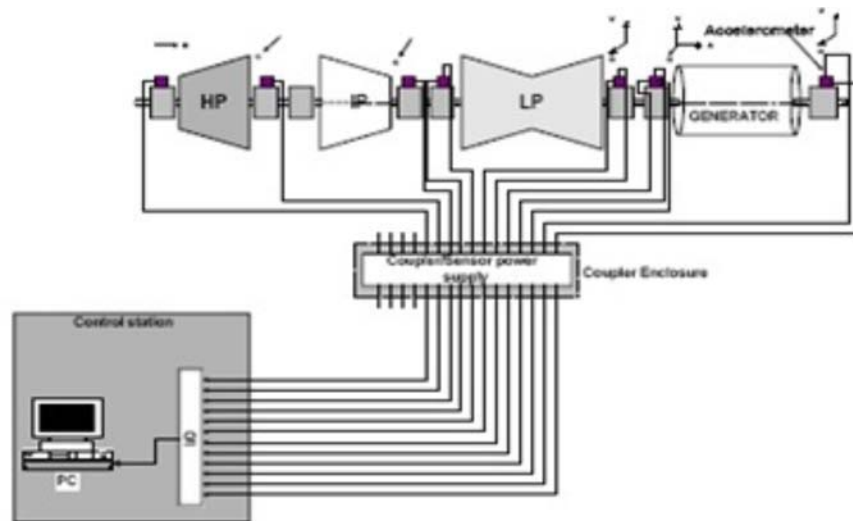

Fig. 2. Sensor Networks applied on rotating machinery.

2. TYPES OF CONDITION MONITORING

There are two types of techniques that are available for condition monitoring of rotating machinery namely off-line and on-line condition Monitoring. In off-line monitoring, sensors are mounted on machinery at selected location and vibration is measured (or recorded and later analyzed) at selected time intervals in the

field; then an analysis is made either in the field or in the laboratory. Advanced analysis techniques usually are required for fault diagnosis and trend analysis. Trend monitoring provides information at a very early stage about incipient failure and usually is used where (i) very early warning of faults is required, (ii) advanced diagnostics are required, (iii) measurements must be made at many locations on a machine, and (iv) machines are complex [3]. Fig. 3 shows typical setup for offline condition monitoring.
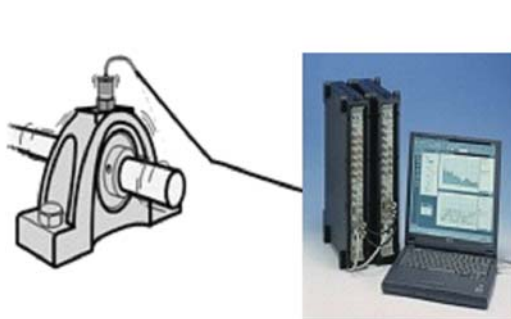

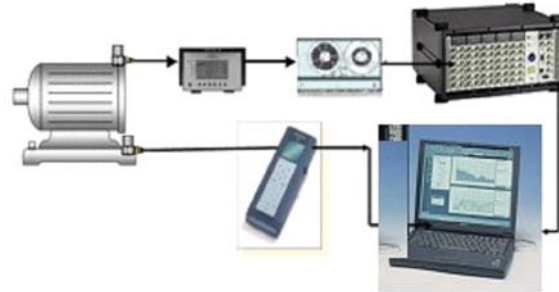Fig. 3. Off Line Condition Monitoring.   Fig. 4. On Line Condition Monitoring.

In on-line monitoring, sensors are mounted on machinery and vibration is measured continuously at selected locations of the machine and is constantly compared with acceptable levels of vibration. The principal function of an online condition monitoring system is to protect one or more machines by providing a warning that the machine is operating improperly and/or to shut the machine down when a preset safety limit is exceeded, thereby avoiding catastrophic failure and destruction. In on-line monitoring system, sensors are mounted permanently at each selected measurement location. For this reason, such a system can be very costly, so it is usually used only in critical applications. Fig. 4 shows typical setup for online condition Monitoring.

3. METHODOLOGY PROPOSED

The work presented in this paper is based on the online condition monitoring approach. In online condition monitoring data is acquired continuously from various places. Thus, system needs a number of sensors to read vibration data from different locations and these data are transferred into computer for further analysis to exhibit the present condition of the machine. Hence sensor networks are used to continuously measure the data from different locations to perform the online condition monitoring of rotating machinery. Fig. 5 shows the model diagram of sensor networks for condition monitoring. Various sensors are connected at data acquisition system to computer through LAN cable. TCP/IP communication protocol is used to make communication between PC and DAQ.
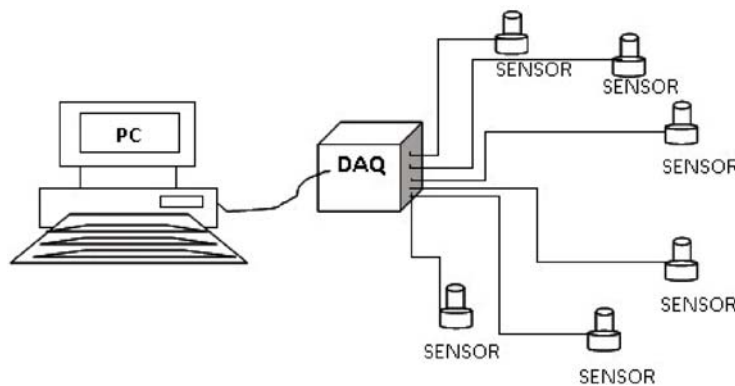

Fig. 5. Model Diagram for sensor networks for Condition Monitoring.

Data Acquisition System consists of a Filter to control the noise and A to D converter to convert the analog data into digital form. Data acquisition system is acquired the sensor data and transfer the data to PC through LAN Cable. The TCP/IP protocol is used to make the communication between Computer and Data Acquisition System. Fig. 6 shows the Block diagram of the sensor networks for condition monitoring of rotating machinery.
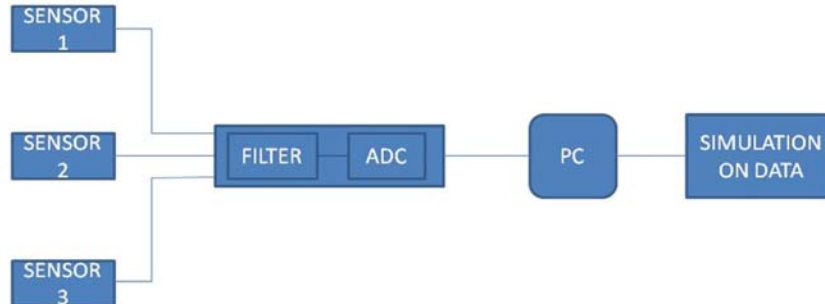

Fig. 6. Block diagram for Sensor Networks with three sensors.

The DAQ Front-end communicates with the PC using an Ethernet connection. The communication protocol used is the same as that used to connect your PC to a network. Before the PC can communicate with the DAQ, the PC that the system is to be connected must know what IP address that the Front-end (DAQ) is using [4]. Typical Front-end setup is shown in Fig. 7. After the setup is configured, the system will be ready for measurements.
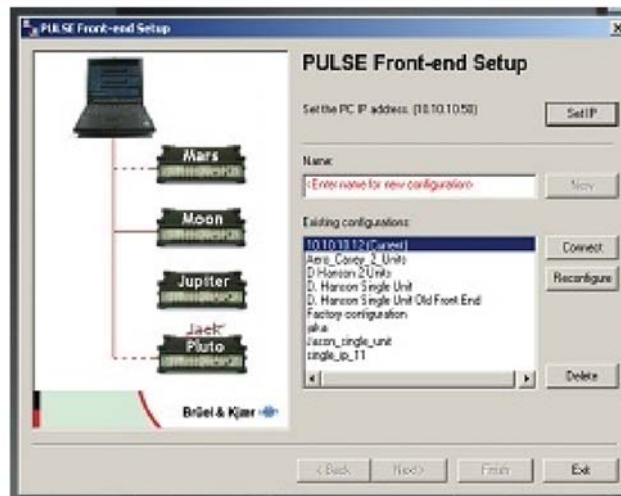
Fig. 7. Front-end Setup

4. IMPLEMENTATION OF SOFTWARE

A GUI based Software has been implemented to post process the data measured through sensor network. A screen shot of the software is shown in Fig. 8.

Various modules are briefly explained below:

CMSMAIN: Various functions are performed by this module. It indicates the user various options available with the software and   prompts him to select the option according to his requirements. It enquires
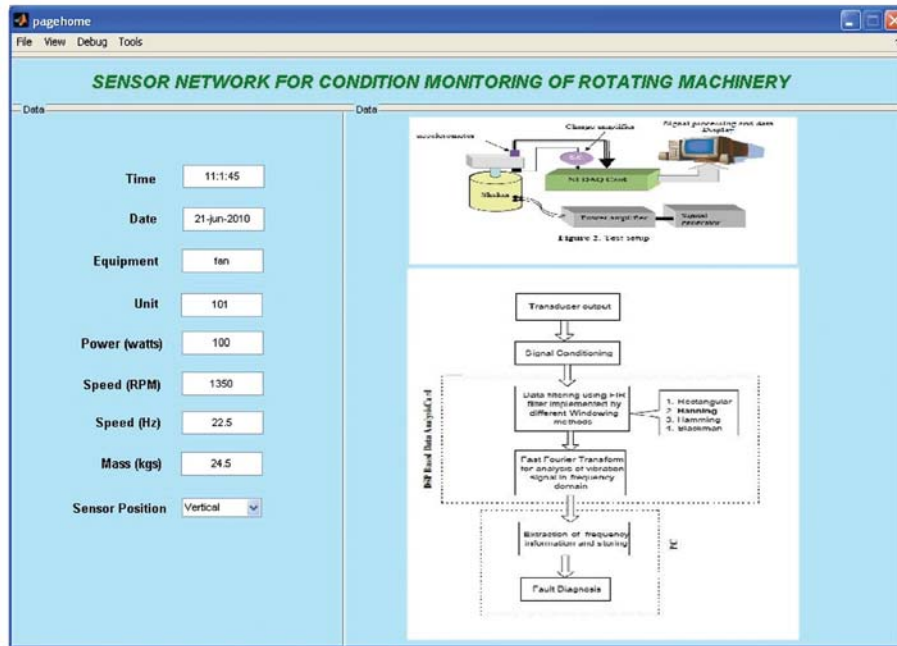
Fig. 8. GUI Screen sho.

for input data and receives it. It reads the file, calls the subroutines as and when required, at various stages of program. In general, the program being user friendly and very interactive, guides the user throughout running of the program via this interface.

Time Domain: The function of this module is to display the data in time Vs amplitude Graph.

FFT: The function of this module is to read the number of samples from time domain data, required frequency range from the user and uses FFT algorithm for converting Time Domain Spectrum to FFT spectrum. Finally, it displays the Frequency Vs Amplitude Graph.

Trending: The function of this module is to obtain the previous data from data base and plot the Graph of Frequency Vs Amplitude for comparing previously measured and present data. Display the data of frequency Vs Amplitude for previous and present data.

Fault Diagnosis: Various possible faults along with symptoms are implemented as rule based expert system. The function of this module is to apply the rule base on FFT spectrum to determine the possible faults and to display the corrective action.

Report Generation: The function of this module is to generate the total report for present condition of Machine.

5. CASE STUDY

A typical case study is presented here for the demonstration of condition monitoring of Rotating Machinery Using Sensor Networks. An industrial fan was considered for demonstration of methodology. Vibration data was acquired using an instrumentation setup as shown in Fig. 9 (a). The set up consists of three vibration accelerometers (Bruel & kjaer Type 4382) and Data acquisition system (Bruel & Kjaer Pulse Controller Type 7536).

Measurements were carried out on the fan with three sensors simultaneously first without any fault and then with a simulated fault of unbalance. For simulation of unbalance, a mass was attached to one of the fan blades as shown in Fig. 9 (b).

<table>
<tr><td>Fig. 9(a). Hardware setup with on fan.</td><td>Fig. 9(b). with unbalance mass.</td></tr>
</table>

Typical vibration acceleration spectra thus acquired are shown in Fig. 10 (a) and Fig. 10 (b) respectively for the cases of fan without unbalance and fan with unbalance. It can be clearly seen from spectra that there is an increase in amplitude at fundamental frequency (1 X RPM) due to unbalance. For unbalance, the FFT spectrum will show a predominant 1x rpm frequency of vibration as is well known. Vibration amplitude at the 1x rpm frequency will vary proportional to the square of the rotational speed. The acquired data was fed to developed software. The software output indicated unbalance using the three sensor network data thus vindicating that the methodology is useful for condition monitoring using sensor network.

(a)   (b)
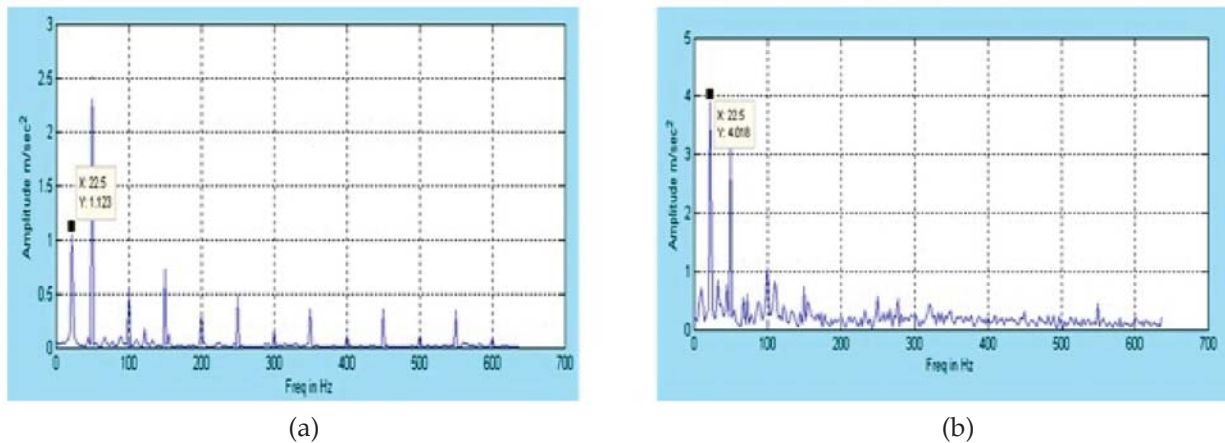
Fig. 10. Vibration spectrum with fan running (a) without unbalance (b) with unbalance

6. CONCLUSIONS AND DISCUSSION

i.   Sensor network was successfully designed by positioning the vibration sensors on rotating machinery and connecting these sensors to data acquisition system and to computer using LAN interface cable. The LAN interface module was used to acquire the vibration data from data acquisition system to computer. A TCP/IP communication protocol was used to make the communication between computer and data acquisition system.

ii. A MATLAB software tool was used to implement the condition monitoring software. Software modules were implemented to read the vibration data and exhibit the time domain analysis, frequency

analysis, trend analysis and fault detection. The software was successfully demonstrated for industrial fan.

iii. Wired sensor networks are in vogue in most applications today. With the advent of wireless technology, wireless sensor networks are being slowly adopted for the condition monitoring of rotating machinery. Future direction for condition monitoring appears to be remote and wireless monitoring.

7. ACKNOWLEDGEMENTS

8. REFERENCES

[1]   I.F. AKYILDIZ, W. SU, Y. SANKARASUBRAMANIAM and E. CAYIRCI, 2002. "Wireless sensor networks: a survay. Computer Networks", **38** (4), 393-422.

[2]   PARESH GIRDHAR *et al.*, 2004. "Practical Machinery Vibration Analysis and Predictive Maintenance", Newnes An imprint of Elsevier,

[3]   Webresource:*www.cursos.itcg.edu.mx.libres.*

[4]   Web resource: *www.varg.unsw.edu.au.*

Study of Coded Ultrasound Imaging using FIELD II

Harish Guggilla[1], Narendra.D.Londhe[2] and Dilip Kumar Sethi[3]
Department of Electrical Engineering,
National Institute of Technology Raipur, Raipur,Chattisgarh.
e-mail: harishnit22@gmail.com

ABSTRACT

The ultrasound is the most popular and cost effective real time imaging technique, but it suffers from problem of poor resolution as compare to other existing imaging modalities. So, in this paper the effect of using the coded excitation i.e. frequency modulated chirp is analysed in view to explore the further possibilities to enhance the resolution of an ultrasound image. This paper basically deals with the application of coded excitation for simulating of cyst phantom image using FIELD-II. For this, the state of art linear propagation method based on spatial impulse response, FIELD-II is used. The received echoes in the simulation are gathered for image formation, using the Time-Delay estimation method, from user selected target region. The linear frequency modulated (chirp) pulse produced by two most promising window techniques are discussed and compared with response of conventional ultrasound pulse. For the simulations, a 3.5 MHz, 16x12 element, rectangular phased array transducer is used.

1. INTRODUCTION

The tissue inhomogenity causes wavefront distortion and the quality of image is degraded in ultrasound imaging. This leads to poor signal to noise ratio (SNR) and penetration depth. Due to low SNR and penetration depth, coded excitation can be used in ultrasound imaging to improve SNR and penetration depth maintaining its high axial and lateral resolutions. Coded excitation is widely used in the radar systems. Their application to medical ultrasound was observed in 1970s when they were first used to improve the performance of flow estimation by Ohtsuki et al. [1] and in ultrasound imaging by Takeuchi et al.[2, 3] Therefore here we use delay and sum beamformer with coded excitation to compensate to some extent for the distortion. The use of coded excitation in ultrasound has been mentioned in previous works [4, 7].

Other applications of coded excitation include
A. Increasing the frame rate and improving resolution [8],
B. Enhancing the detection of contrast agent [9],
C. Increasing the depth of field [10],
D. Improving the SNR in finite amplitude distortion based harmonic imaging [11],
E. Enhancing the generation of harmonics by contrast agent micro-bubbles [12, 13] and
F. Suppressing selected harmonic components in nonlinear imaging [14].

The main idea behind coded excitation is to increase emitted energy by elongating the transmitted waveform (without increasing peak level) while still preserving resolution by the time compression processing. The beam formation as per Hyugen's principle is a prime function to be focused on.

The functions of a beamformer include the following:

A. Generate transmit timing and possible apodization (the term apodization will be used as a synonym for weighting. tapering, and shading) during transmit.

B. Supply the time delays and signal processing during receive.

C. Supply apodization and summing of delayed echoes.

D. Possible additional signal processing related activities.

The goal of all of these functions is to create a narrow and uniform beam with as low sidelobes over as long a depth as possible. During both transmit and receive operations, appropriate delays will be supplied to accomplish the focusing and steering needed. Most adaptive imaging techniques used in medical ultrasound operate by correcting phase and amplitude aberration errors to improve image contrast and resolution [12, 13].

2. FIELD II

The most widely used linear model for ultrasound wave propagation has been developed by Jensen et al. who have named their program as FILED. The FIELD [15] is based on Tulphome-Stepanishen approach of calculating the spatial impulse responses. It is very efficient and accurate approach to calculate all types of fields like emitted, received, pulsed, CW with all possible transducer geometries. It is based on the inhomogeneous wave equation derived for describing scattering and propagation in an inhomogeneous medium [16]. The model can be implemented with any kind of transducer geometry and excitation [17].

The FIELD-II program written in Matlab, is the modified version of original FIELD program. The modified version facilitates time varying focusing and apodization which yields in simulation of imaging of tissues and blood flow estimation. Some standard simulation phantoms are used for designing and evaluating ultrasound transducers, beam formers and systems. The phantoms investigated provide indication of sidelobe levels, focusing abilities and imaging contrast ability to detect low contrast objects for real imaging [18].

3. DELAY AND SUM BEAMFORMER

Delay-and-sum (DAS) beamforming is the standard technique in medical ultrasound imaging. An image is formed by transmitting a narrow beam in a number of angles and dynamically delaying and summing the received signals from all channels. The side-lobe level of the DAS beamformer can be controlled using aperture shading, resulting in increased contrast at the expense of resolution. In contrast to the predetermined shading in DAS, adaptive beamformers use the recorded wave-field to compute the aperture weights. By suppressing interfering signals from off-axis directions and allowing large side-lobes in directions in which there is no received energy, the adaptive beamformers can increase resolution [19].

4. LINEAR FREQUENCY MODULATED WAVE

Convectional ultrasound pulses are used in imaging soft tissues in the previous days. But with the improvement of technology and with the problems associated with convectional ultrasound imaging such as more band width and greater axial level the focus was moved on to linear frequency modulated wave in which the ultrasound pulse is modulated using a linear frequency wave. This is a method of coded excitation technique.

The general linear FM (or *chirp*) signal can be expressed in complex notation as:

$$\psi(t) = a(t).\exp[j2\pi(f_0 t + \frac{B}{2T}t^2)], -\frac{T}{2} \le t \le \frac{T}{2}$$

where f_0 is the center frequency, T is the signal duration and B is the total bandwidth that is swept.

As we know that the time derivative of the phase is the instantaneous frequency, it is given by:

$$f_i = \frac{d(f_0 t + \frac{B}{2T}t^2)}{dt} = f_0 + \frac{B}{2T}t.$$

In practical terms Fi indicates the spectral band in which the signal energy is concentrated at the time instant t. The parameter $B=T$ is often denoted as μ, and referred to as the *FM slope* or the *rate* of FM sweep.

The signal sweeps linearly the frequencies in the interval $[f_0 - \frac{B}{2}, f_0 + \frac{B}{2}]$.

The linear FM pulse is shown in Figure 1 has been used in the simulations. Its frequency spectrum and time autocorrelation are also shown in Figure 1.
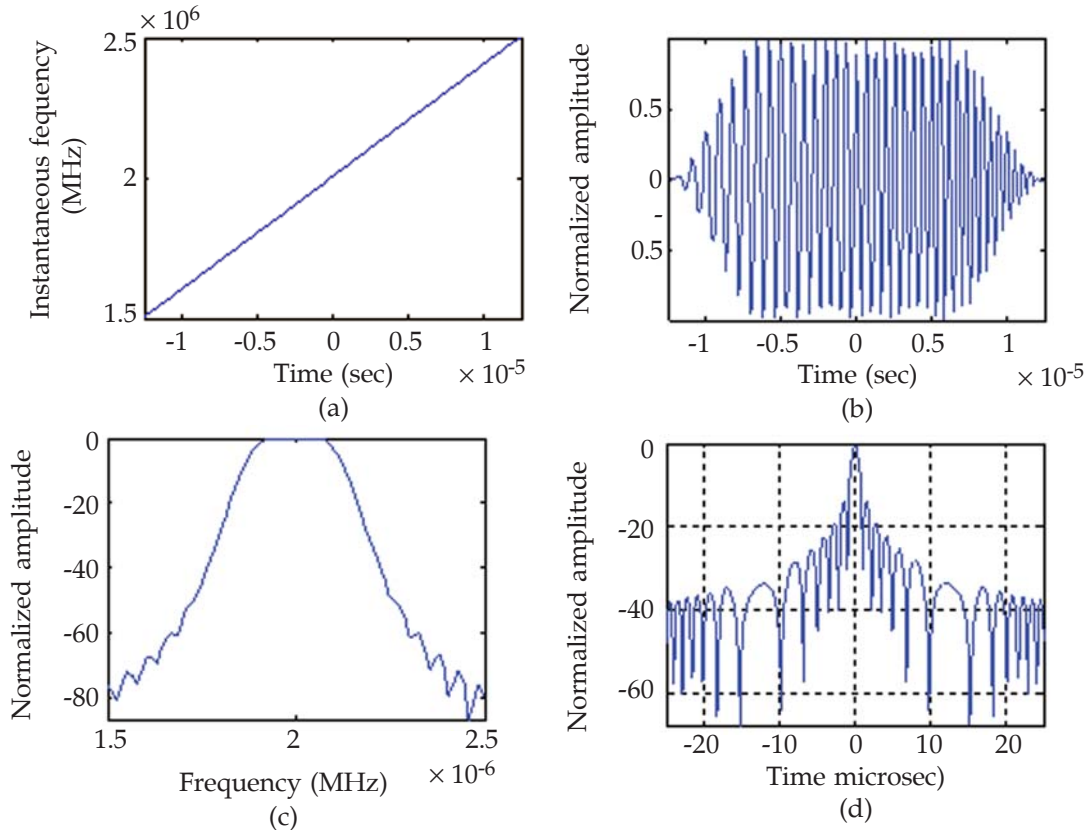

Fig. 1 (a) Instantaneous frequency vs time, (b) LFM chirp waveform, (b) its frequency spectrum, (d) time autocorrelation function, obtained with center frequency 2MHz, bandwidth 1MHz and pulse duration of 25μs.

5. RESULTS

Delay and sum beamformer is studied with coded excitation on cyst phantom. The cyst phantom consists of a collection of point targets, five cyst regions, and five highly scattering regions. This can be used for characterizing the contrast-lesion detection capabilities of an imaging system. The scatterers in the phantom are generated by finding their random position within a 60 x 40 x 15 mm cube, and then assign Gaussian distributed amplitude to each scatterer. If the scatterer resides within a cyst region, the amplitude is set to zero. Within the highly scattering region the amplitude is multiplied by 10. The point targets have fixed amplitude of 100, compared to the standard deviation of the Gaussian distributions of 1.

A linear scan of the phantom is done with a phased array transducer of 3.5 MHz center frequency with following excitation parameters:

No of elements   = 192

No of active elements   = 64

Element height   = 5 mm,

Width   = Wavelength

Kerf   = 0.05 mm

Apodization   Hanning

The pulses used are linear frequency modulated pulses. A single transmit focus was placed at 60 mm, and receive focusing was done at 20 mm intervals from 30 mm from the transducer surface. The resulting image for 100,000 scatterers has been observed in this work.

The two most promising window techniques used for generating linear frequency modulated are shown below along with the generated chirp signals in Figure 2.
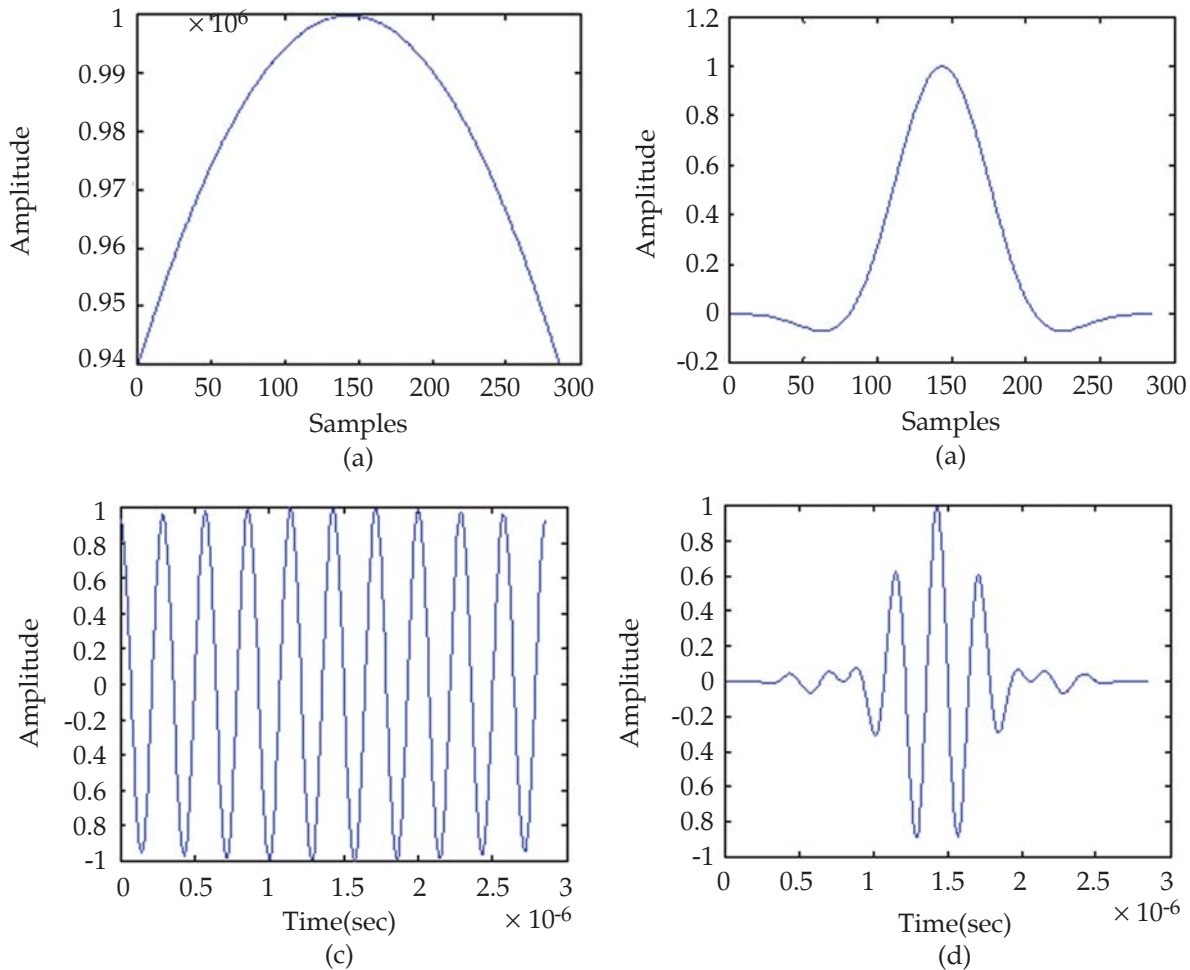
Fig. 2. Window techniques and generated linear frequency modulated pulses (a) Kiaser window. (b) Flattopwin window, and their respective LFM pulses of center frequency 3.5 MHz
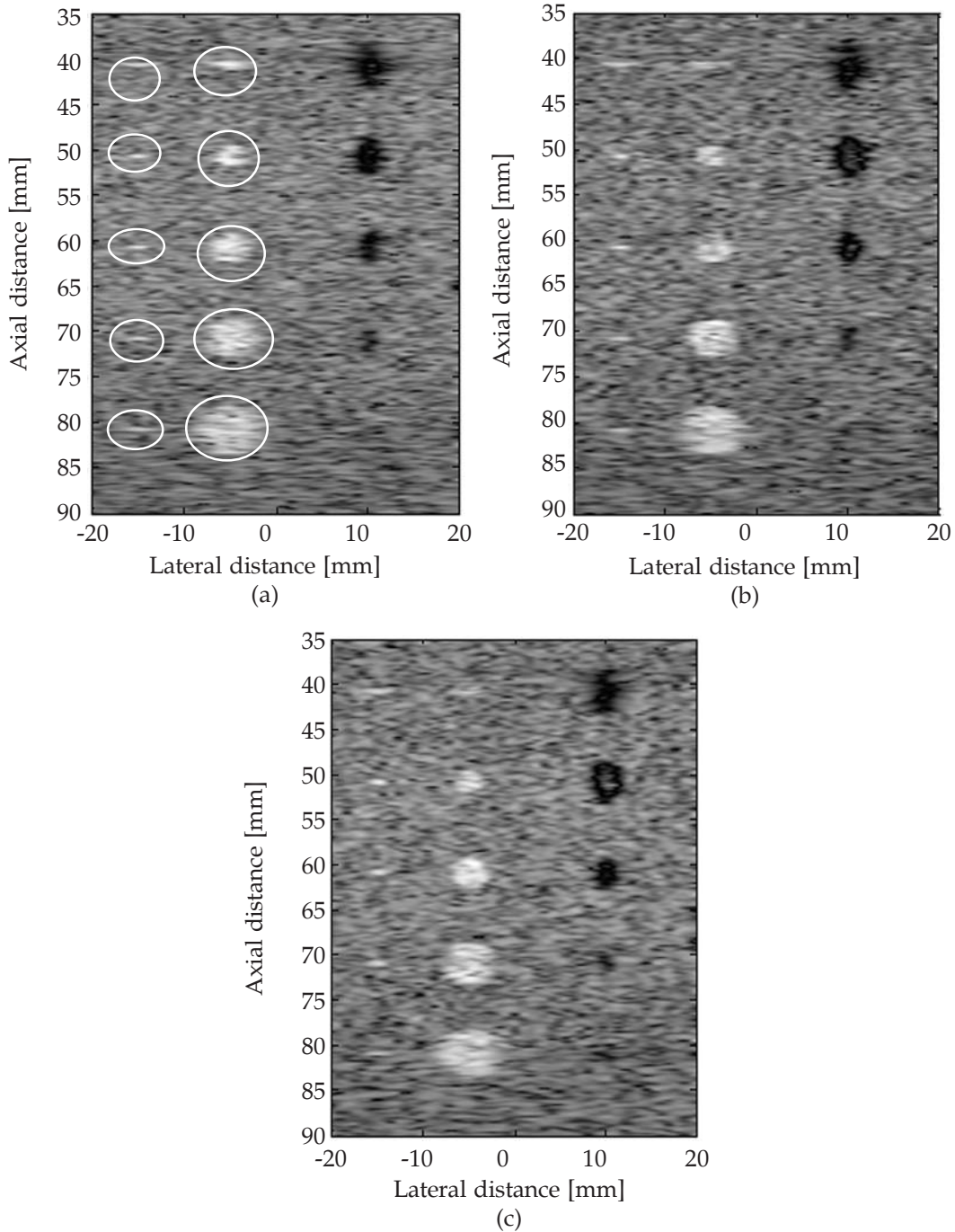
Fig. 3. Cyst phantom image produced using (a) LFM pulse with flattopwin window,
(b) LFM pulse with Kaiser window and (c) conventional ultrasound pulse.

The above FM pulse is transmitted and received by a phased array transducer of above mentioned configuration. According to the delay and sum beamformation, received responses are gathered to form an image of artificial phantom as shown in Figure 3.

In Figure 3(a), the highly scattering regions are shown using the white circles and the remaining black circular shapes on right are the cysts to be imaged. The cysts are clearer and sharp in images formed using

linear FM pulses. The second cyst from top in Figure 3(c) is showing scattering of ultrasound at the centre. Similarly, the shapes and boundaries of others cysts in figure 3(c) are unclear and not that sharp. There is very small difference in quality of images formed using linear FM pulses with flattopwin window and Kaiser, but still visually image with Kaiser window looks more satisfactory. The third cyst from top exactly at focal depth is the best place to compare three images. By observing the Figure 3, it can easily be mentioned that the use of coded excitations can further enhance the image quality.

6. CONCLUSIONS

As per the above study, it is very clear that using the coded excitation methods the imaging ability of the ultrasound can be further enhanced. The intelligent selection of coded excitation combined with beamformation algorithm can lead to further improvement of both lateral and axial resolutions. The linear FM pulse with appropriate window technique can generate the ultrasound field suitable for imaging various organs. The correct combination of them will of course affect the quality of an image. This will surely help physicians to diagnose the smaller and distant objects in the human anatomy with sharper images. The ultrasound imaging can be further investigated with optimized LFM pulses and may be with other coding techniques. The beaforming algorithm suitable for the selected coding technique and their correlation can also be studied.

7. REFERENCES

[1]   S. OHUTSUKI and M. OKUJIMA, 1973. Ultrasonic Doppler velocity meter by M-sequence modulation methods. *J. Acoust. Soc. Japan*, **29**, 347-355.

[2]   Y. TAKEUCHI, 1979. An investigation of a spread energy method for medical ultrasound systems Part one: theory and investigation. *Ultrasonics*, **17**, 175-182.

[3]   Y. TAKEUCHI, 1979. An investigation of a spread energy method for medical ultrasound systems. Part two: proposed system and possible problem. *Ultrasonics*, **17**, 219-224.

[4]   M. O'DONNELL, 1992. Coded excitation system for improving the penetration of real-time phased-array imaging systems. *IEEE Trans. Ultrason. Ferroelect. Freq. Contr.*, **39**, 341-351.

[5]   M.A. AVERKIOU, Y. S. LEE and M.F. HAMILTON, 1992. Self-demodulation of amplitude- and frequency-modulated pulses in a thermoviscous fluid. *J. Acoust. Soc. Am.*, **94** (5), 2876-2883.

[6]   Y.R. CHIAO and L.J. THOMAS, 2000. Synthetic transmit aperture imaging using orthogonal golay coded excitation. In: Proc. *IEEE Ultrasonics Symp.*, 1677-1680.

[7]   T. MISARIDIS , and J. A. JENSEN, 2005. Use of modulated excitation signals in medical ultrasound. Part I: Basic concepts and expected benefits. IEEE Trans. *Ultrason. Ferroelectr. Freq. Control*, **52**, 177-191.

[8]   J. SHEN and E. S. EBBINI,1996. "A new coded-excitation ultrasound imaging system-Part I: Basic principles," *IEEE Trans. Ultrason., Ferroelect., Freq. Contr.,* **43** (1), 131-140.

[9]   C.C. SHEN and P.C. LI, 2003. "Pulse-inversion-based fundamental imaging for contrast detection," IEEE Trans. *Ultrason., Ferroelect., Freq. Contr.,* **50** (9), 1124-1133.

[10] S. ZHOU and J. A. HOSSACK, 2003. "Dynamic-transmit focusing using timedependent focal zone and center frequency," IEEE Trans. *Ultrason., Ferroelect., Freq. Contr.,* **50** (2), 142-152.

[11] P.C. LI, 1999. "Pulse compression for finite amplitude distortion based harmonic imaging using coded waveforms," *Ultrason. Imag.,* **21** (1), 1-16.

[12] Y. TAKEUCHI, 1996. "Coded excitation for harmonics imaging," in Proc. *IEEE Ultrason. Symp.,* 1433-1436.

[13] J. BORSBOOM, C.T. CHIN and N. DE JONG, 1988 "Experimental valida J. F. Fuller, E. F. Fuchs, and K. J. Roesler, "Influence of harmonics onpower distribution system protection," *IEEE Trans. Power Delivery,* **3**, 549-557.

[14] E.H. MILLER, 1996b. "A note on reflector arrays," *IEEE Trans*. Antennas Propagat., to be published.

[15] Jensen JA. FIELD-A program for simulating ultrasound systems, Med Biol Eng Comp, 10th Nordic-Baltic Conference on Biomedical Imaging 4351-353.

[16] J.A. JENSEN, 1991a. A model for the propagation and scattering of ultrasound in tissue, *J Acoust Soc Am,* **89**, 182-191.

[17] J.A. Jensen and P. Munk, 1997. Computer phantoms for simulating ultrasound B-mode and CFM images, Acoustical Imaging Symposium, Boston, Massachusetts, USA, April 13-16.

[18] J.A. Jensen, 2004. Simulation of advanced ultrasound systems using FIELD-II, IEEE Ultrason Symposium.

[19] J.F. Synnevag, A.Austeng and S. Holm, 2007 "Adaptive beamforming applied to medical ultrasound imaging," *IEEE Trans. Ultrason, Ferroelect. Freq. Contr.* (Special issue on high resolution ultrasonic imaging), **54**(8), 1606-1613.

Piezocomposites for Acoustic Transducers

C. Durga Prasad, L.A. Gavane, N.M. Gokhale and R.S. Hastak
Naval Materials Research Laboratory, Ambernath, Maharashtra-421506, India
e-mail: harishnit22@gmail.com

ABSTRACT

1-3 piezocomposite materials are gaining prominence in recent years for the development of large area hydrophone arrays, as transducers for high frequency imaging arrays for sonars and so on because of their light weight and superior electromechanical properties. The work carried out in the development of piezocomposite elements for the above applications has been discussed.

1. INTRODUCTION

Transducers in the general sense are devices for converting energy from one form to the other. In electroacoustic transducers we are concerned with the conversion of electrical energy into acoustic energy or vice-versa. Transducers used in sonar, under-water communication, under-water imaging and non-destructive testing applications generally employ piezoelectric materials such as lead zirconate titanate (PZT), as active components, because of their high electromechanical coupling coefficient and low electrical and mechanical losses. However, their higher specific acoustic impedance, higher weight factor and poor mechanical properties are undesirable in certain applications. On the other hand, the piezoelectric polymers like polyvinylidene fluoride (PVDF) have very low specific acoustic impedance offering excellent impedance matching with water/human tissues. The serious drawbacks of these materials are very low values of electromechanical coupling coefficient and dielectric constant. Recently, piezocomposite materials have been developed by combining active piezoelectric materials with passive polymers, thereby taking advantages of the desirable features of both the constituent materials. Some of the advantages of the piezocomposites are higher electromechanical coupling coefficients, low specific acoustic impedance, a wide range of dielectric constant, low dielectric and mechanical losses, variable sound velocity, low mode-coupling, ease of subdividing into acoustically isolated array elements and formability into complex curved shapes etc. Piezocomposite transducers with predetermined properties can be tailor-made for a specific application by optimizing the type and proportion of ceramic and polymer components and their relative arrangements in the composite structure. A pattern in which the piezoceramic and polymer materials of a composite are physically connected in three dimensions in a systematic arrangement is called connectivity. Each phase in a composite is continuous in zero, one, two or three dimensions in a systematic arrangement is called connectivity. Each phase in a composite is continuous in zero, one, two or three dimensions. For a composite with two material phases, there are 10 possible connectivity patterns viz., 0-0, 0-1,0-2,0-3,1-1,1-2,1-3,2-2,2-3 and 3-3. The first number refers to the ceramic phase and the second number to the polymer phase. For example, in 1-3 connectivity, the ceramic material is self connected in only one direction and the polymer material is self-connected in all the three directions corresponding to the coordinate axes [1]. Among the various types of piezocomposites, the one with 1-3 connectivity is widely used because of its relative ease of fabrication and flexibility of design variables [2-4]. In 1-3 piezocomposites, the active ceramic rods are embedded in a polymer matrix. The lateral spacing of the rods in the periodic array plays an important role

---

in deciding the microstructure of the composite plate. The piezocomposite plate is fully electrode on the top and bottom surfaces, poled and operated in the thickness-mode of vibration. In this configuration, the individual ceramic pillars are considered to be axially polarized thin rods and vibrate in the longitudinal (33) mode. The compliant polymer matrix provides flexibility to the composites enabling them to be light-weight and have better acoustic impedance matching. In this paper, the studies carried out for the development of piezocomposite elements for various high frequency transducers and large hydrophone arrays have been discussed.

2. EXPERIMENTAL WORK

NMRL has developed a dice- and- fill technique for the fabrication of 1-3 piezocomposites of larger sizes with reproducible end properties [5]. In this method, parallel cuts are made on a piezoceramic plate in two perpendicular directions parallel to the plane of the plate. At the bottom of the plate, a small portion is left uncut which acts as a base to hold the ceramic pillars. The gaps in the array of rod are later filled with a polymer. Once the polymer is cured, the composite is separated from the ceramic base, polished, electroded and poled. The various critical process variables such as PZT rod size , rod spacing, polymer phase, volume fraction of each phase, electrode material etc have all been optimized for achieving the required performance. However, it is very difficult to fabricate a composite with very fine rod size using this technique. The minimum rod size achievable is limited by the accuracy of the dicing saw and the ability of the ceramic to survive the cutting process.
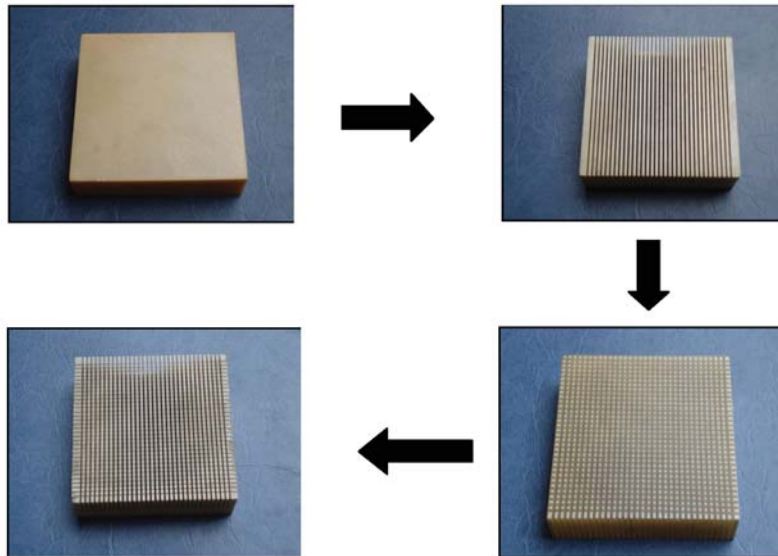

Fig. 1. Fabrication process for a 1-3 Piezocomposite.

3. APPLICATIONS

Improved transducer characteristics of piezocomposites compared to the conventional PZT materials make them very attractive for many underwater applications. The most important property is that the transducer properties can be tailor-made for a particular application, by suitably controlling the ceramic volume fraction in the composite [6-7]. Some of the important applications of 1-3 piezocomposites are listed in the following sections.

3.1 Wide-band transducer

Piezocomposite transducers are lossy in nature and this lead to wide band acoustic response. The active element is normally in a planar shape with thickness much larger than the lateral dimensions. Hence, it is

operated at the thickness-mode resonance. In order to reduce the operating frequency band to sonar frequency ranges, a few layers of composite plates are stacked together to from a multi-layer configuration. In this design, the individual layers are mechanically connected in series and electrically connected in parallel. The resonance frequency of the stack is determined by the overall thickness of the stack [8].
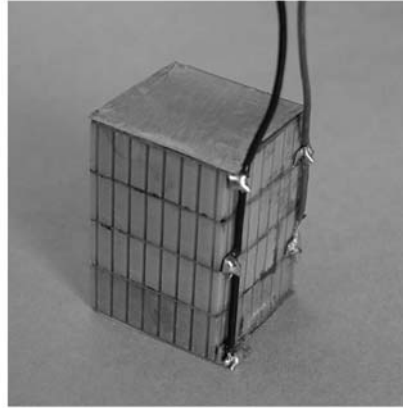
Fig. 2. 1-3 piezocomposite transducer stack.

It is made water-worthy by encapsulating in polyurethane. The photograph of a piezocomposite stack used as a wide band transducer is shown below. A typical Transmitting Voltage Response (TVR) and Receiving sensitivity of such a piezocomposite transducer are also shown below. It can be seen from the figure that this transducer shows a broad band response. These types of transducers enable the sonar operator to choose any operating frequency in this band, depending upon the on-field operational requirements.

Fig. 3. Transmitting and Receiving Voltage response of a 1-3 piezocomposite transducer stack.

3.2 Large-area hydrophone array
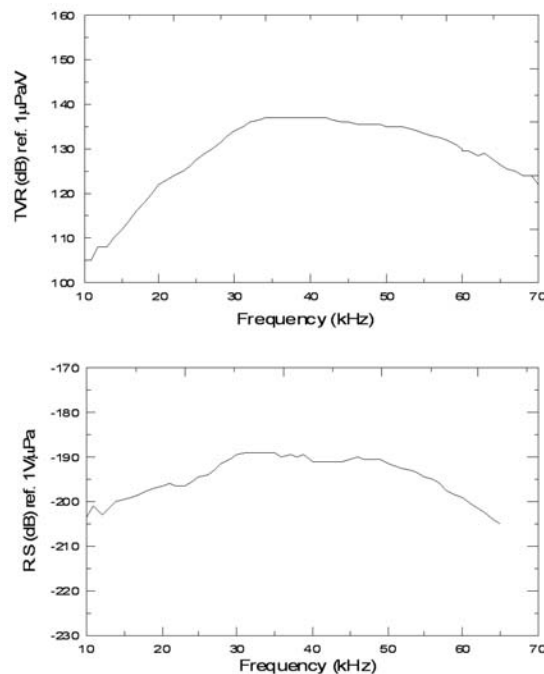
Large-area hydrophones have high Signal-to-Noise Ratio (SNR), which makes them very attractive for passive sonar applications in which the signal strength is very low at large ranges. Large-area hydrophone arrays can be easily fabricated using 1-3 piezocomposites by arranging smaller piezocomposite slabs into a large 2-dimensional array. The array is encapsulated in rubber or polyurethane and fixed on the outer hull of the submarine.
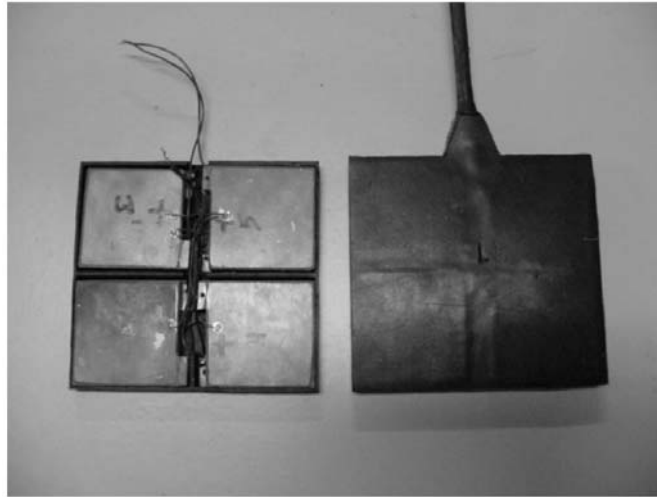

Fig. 4. Prototype of a large area piezocomposite hydrophone array.

Piezocomposites are more suitable for this application, because they have higher receiving sensitivity and figure-of-merit than the PZT hydrophones of the same size and similar design. It is possible to fabricate conformal arrays, which are large-area hydrophone arrays conforming to the hydrodynamic shape of the ship or submarine. Another important feature associated with the piezocomposite hydrophones is that the receiving sensitivity is less-dependent on the hydrostatic pressure acting on the arrays at greater depths of operation, making them more useful for submarine- based sonar application.

The main requirements for a high frequency operation are the high spatial and bearing resolutions at relatively closer ranges to detect obstacles in the path of the ship. This is achieved by operating the sonar at high frequencies.

A known volume of water in front of the ship is insonified using a transmitter and the echo is received by an array of hydrophones and processed to obtain an underwater acoustic image of the scanned volume. The important criteria of the transducer array used for this application is that it should be able to transmit shorter pulses with very little or no ringing. In addition, this application requires arrays with large number of transducer elements individually driven to meet specific beam width requirements. The high frequency of operation poses a challenge in assembling smaller transducer elements into an array form using PZT ceramics. All these problems can be avoided if one uses a piezocomposite as active element. 1-3 piezocomposite transducers have very less ringing and are most suitable for high resolution applications [9-12]. Transducer arrays with large number of elements can be fabricated from a monolithic 1-3 piezocomposite panel on which the required electrode pattern can be applied to define the individual transducer elements. This avoids the complications in assembling an array out of individual elements that are too small to handle. The most important advantage of a piezocomposite array is that the inter-element coupling is very low, of the order of about -30 dB and hence, the individual elements can be safely driven with different voltages, although the array is made up of a single large block of piezocomposite. This is impossible to achieve using the conventional PZT-based transducer arrays.
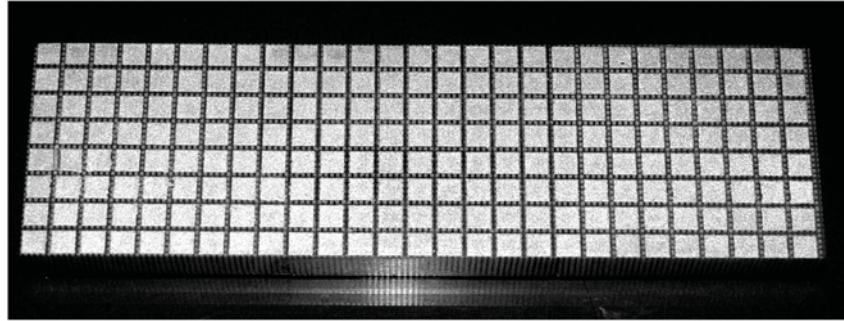
Fig. 5. A typical piezocomposite array with patterned electroding.

3.4 Underwater imaging sonar array

1-3 Piezocomposite transducers are high-resolution broad-band transducers. Hence, they are widely used in underwater imaging applications such a side-scan sonar that maps the sea floor. A transducer line-array towed from a ship scans the sea bottom with narrow beams on either sides of the ship's trajectory. The movement of the ship along a linear path helps to scan an area of the sea floor with successive beams. Any buried objects viz, ship wreck, can be easily located.

The important property of the transducer array for high frequency application is the ease with which the beam pattern can be controlled precisely. The side-lobes, that deteriorate the image quality, can be greatly controlled using patterned electrodes that are easily applied on piezocomposites. This helps in enhancing the image contrast. The inter-element cross-talk is very less in 1-3 piezocomposites due to the presence of compliant polymer matrix, which provides structural isolation and reduces the lateral coupling between adjacent elements.

3.5 Transducer array for torpedoes

Because of the smaller size of the platform and short range detection requirements, the torpedo sonar systems are operated at fairly higher frequencies. Further, they are disposable and are operated at relatively lower power levels. Considering the higher speed of the platform and the shorter ranges of operation, the transducer array must be capable of transmitting shorter pulses without ringing and has to be light- weight. 1-3 piezocomposite transducers satisfy these criteria and are found to be the most suitable active material for this application.

3.6 Constant beam-width transducer

The beam-width of a transducer generally decreases with increase in frequency. Hence, the spectral content of the transmitted or received signal varies with relative position of the target in the beam and the fidelity of an underwater acoustic system depends on the orientation of the transducer with respect to the target. It leads to design complications in certain applications where a transducer is expected to operate over a wide frequency range. In such cases, it is highly desirable to use a Constant Beam-width Transducer (CBT).

The concept of CBT relies on an axisymmetric velocity distribution acting over a spherically curved surface. The velocity distribution follows a Legendre shading function realised by dividing the surface electrodes into discrete concentric rings as shown in the figure and applying a weighted potential to the individual electrodes.

This is easily achieved by using 1-3 piezocomposites, which can be formed into the shape of a spherical shell and it is feasible to apply shaded electrodes on the spherical surfaces. The 1-3 piezocomposite slab with thermoplastic matrix, can be formed into a spherical shape and applied with patterned electrode. The PZT pillars lying under each electrode segment constitute one element and all such elements formed into concentric circles are driven with weighted voltages to achieve constant beam-widths over a band. Although the

electrodes are applied on the same monolithic spherical shell of piezocomposite, the excitation of one segment does not affect the adjacent segment due to the excellent structural de-coupling properties of 1-3 piezocomposite, which make them superior to other piezoelectric materials for this application.

4. CONCLUSION

Piezocomposite materials especially with 1-3 connectivity are emerging as suitable candidates for the design and development of acoustic transducers for high frequency imaging applications owing to their unbeatable characteristics. The material characteristics can be tuned to suit a specific system application which is an added advantage.

5. REFERENCES

[1] R.E. NEWNHAM, L.J. BOWEN, K.A. KLICKER and L.E. CROSS, 1980. Composite Piezoelectric Transducers, *Mater. Eng.* **2**, 93-106.

[2] W.A. SMITH, A.A. SHAULOV and B.M. SINGER, 1984. Properties of Composite Piezoelectric Materials for Ultrasonic Transducers, Ultrasonics Symposium, *IEEE*, 539- 544.

[3] A. SAFARI, 1994. Development of Piezoelectric Composites for Transducers, *J. Phys. III* **4**, 1129-1149.

[4] T.R. GURURAJA, W. A. SCHULZE, L.E. CROSS, R.E. NEWNHAM, B.A. AULD and Y.J. WANG, 1985. Piezoelectric Composite Materials for Ultrasonic Transducer Applications: Part I: Resonant Modes of Vibration of PZT Rod-Polymer Composites, IEEE Trans. Sonics Ultrason. **32** (4), 481-498.

[5] C. DURGA PRASAD, L.A. GAVANE, S.C. SHARMA and RAMJI LAL, 1998. PZT-polymer Composite Hydrophones for Underwater Applications, *Proceedings of UDT Pacific* 98 Conference and Exhibition, Sydney, Australia, 356-361

[6] G. HAYWARD, J. BENNETTE and R. HAMILTON, 1995. A Theoretical study on the influence of some constituent material properties on the behaviour of 1-3 connectivity composite transducers

[7] D. STANSFIELD, 2003. Underwater Electroacoustic Transducers, *Penninsula Publishing*.

[8] R. RAMESH, C. DURGA PRASAD, T.K. VINOD KUMAR, L.A. GAVANE and R.M.R. VISHNUBHATLA, 2006. Experimental and Finite Element Modeling Studies on Single Layer and Multi-layer 1-3 Piezocomposite Transducers, *Ultrasonics*, **44**, 341-349.

[9] G. SURESH, V. NATARAJAN and C. DURGA PRASAD, 2012. Design, Fabrication and Evaluation of an Underwater Acoustic Imaging Sensor Array, *Proceedings of XIX National Symposium on Ultrasonics*, NPL, New Delhi, 30-31.

[10] G. SURESH, V. NATARAJAN, R. RAJESHWARI and C. DURGA PRASAD, 2013. February NPOL, Kochi, Design, Fabrication and Evaluation of Underwater Acoustic Imaging Sensor arrays, *Proceedings ASCENT-II* Advances in Sonar Concepts, Engineering and Technologies, 27-28.

Vocal Tract Resonance and Speech Intelligibility in Combined Maxillectomy and Mandibulectomy

Subbarao Bachalli, Premalatha, Deepa Dominic and Sujatha S

Department of Speech Language Studies, Dr.S.R.Chandrasekhar Institute of Speech and Hearing, Lingarjapuram, Bangalore, Karnataka, India.
e-mail: drbspremalatha@gmail.com

ABSTRACT

Resonances characteristics are related to changes of cavity in size and configuration, Quality of oral resonance is often directly related to the opening of the mouth, achieved by mandible posturing and the relative height of the placement of the tongue within the oral cavity. Oral resonances can be perceived as the formant frequencies which are observed best during the production of vowels. Following the maxillectomy and mandibulectomy surgery for cancerous lesion, there is an observable change in size and configurations of the vocal tract resulting to changes in the resonances thus affecting the formant frequencies. Need for the study: Though there are literatures available on the speech characteristics namely articulation, resonance and speech intelligibility of maxillectomy and / or mandibulectomy patients, there is limited information documented regarding the resonance characteristics and its impact on speech intelligibility of patients who have undergone both maxillectomy and mandibulectomy with reconstruction of the mandibular defect and use of palatal prosthesis for closure of the maxillectomy defect. Aim: The present study was aimed to determine the vocal tract resonance characteristics and usefulness of palatal prosthesis in improving the resonance and speech intelligibility in subjects of combined maxillectomy and mandibulectomy. Method and Materials: Two male subjects, who had undergone maxillectomy and mandibulectomy for extensive lesion of buccal mucosa, were recruited for the study. They had undergone maxillectomy of variant type and mandibulectomy with reconstruction of the primary defect. Subject A had also received post operative radio therapy and chemotherapy for the same. The defect of the mandible was reconstructed by pectoralis major myocutaneous muscle flap. Subject B had received pre operative radiotherapy and reconstruction of the defect by radial forearm flap on right cheek and buccal fad pad on left cheek. Following maxillectomy surgery, both of the subjects been using palatal prosthesis. Objective evaluation of speech was carried out using CSL 4400 instrument to evaluate acoustic parameters of resonance such as formant frequencies of vowels and 2nd formant transition. Formant frequencies of vowels were considered for the study as they represent the resonance of the vocal tract. Since the vowels are produced orally with open vocal tract, for effective production of vowels the resonance would take place only in the oral cavity. Formant frequencies were measured with and without the prosthesis and the 2nd formant transition were also measured to evaluate objectively the placement and the movement of the tongue within the oral cavity. Analysis of formant frequencies of vowels /a/, /i/ and /u/ in isolation and in words such as /a/ in /a: ne/, /i/ in /illi/ and /u/ in /u: ta: /, which had embedded vowels was examined spectrographically. The mouth to microphone distance was maintained at 6cms. The acoustic signals were digitized at 44100 Hz per channel with 32 bit resolution to a computer. Results and Discussion: The study revealed that both the subjects, subsequent to excision of lesion showed a varied picture of affected resonance and speech intelligibility. Oral Peripheral Mechanism Examination revealed deviated

lip to left side in subject A and to right side in subject B, missing teeth on top row, with intact tongue and its movement. Velar elevation was restricted. Intra oral pressure could not be built by the subjects due to inadequate lip seal. Vocal tract resonance was observed to be altered in both subjects after surgery due to ablation of the palate, leading to impaired connection between the oral and nasal cavity. Spectrographic analysis without the palatal prosthesis revealed all formant frequencies (F1, F2 and F3) to be deviated from normal due to the presence of anti resonances due to the presence of hypernasality. Formants were not clearly visible without the prosthesis. It was noted that dampening of the energy was more without the prosthesis than with prosthesis, thus attributing to the perception of hypernasality. Assessment of second formant transition and duration of transition did not differ significantly with and without palatal prosthesis indicating that speech intelligibility is predominantly affected by the nasal air emission and rate of speech rather than imprecise placement of tongue following the surgery. Speech intelligibility was found to be better with prosthesis.

1. INTRODUCTION

Head and neck cancer particularly oral cancer are one of the major health hazards faced in India. The treatment options for oral cancers are usually multi modality based. Cancer outcomes are measured in terms of overall disease free survival, and prognosis (including quality of life). Oral cancers are usually treated by combined modality such as surgery followed by radiotherapy. Maxillectomy and / or mandibulectomy surgical procedure involves removal of the part(s) affected by cancerous lesion. Resection may be partial or total. Total resection involves complete removal of the structure whereas partial resection involves either only segmental or hemi - resection which includes excision of half of the entire structure (either maxilla or mandible). Resection of the maxilla causes problems in fundamental activities such as speech, swallowing and mastication, because of the loss of an anatomical separation between the nasal and oral cavities. Coupling of the oral and nasal cavities increases nasal resonance, resulting in hypernasality.

The mandible also plays a very important role in mastication and / or speech production by modifying the resonant characteristics of the vocal tract. Segmental resection of the mandible leads to significant patient morbidity than marginal mandibulectomy with no loss of local control (Randall,, and Walsh - Waring, 1987). Loss of mandibular support to the teeth, tongue and lip causes dysfunctional mastication, swallowing, speech, airway protection and oral competence. Although jaw movement is very slight during normal speech production, inadequate, inappropriate or sluggish movement may contribute to articulatory deficits. Patients also suffer disfigurement following segmental mandibulectomy because the mandible is an important aesthetic landmark. The degrees to which dysfunction and disfigurement occur depend both on the location of the mandibular segment removed and the amount of surrounding soft tissue excised. Therefore preservation of the mandible and maxilla is key to good functional and cosmetic results after surgical excision in oral cavity. Patients who have undergone both maxillectomy and mandibulectomy, which is a rare condition, usually exhibit combined effects of truisms, cosmetic deformity and functional disability such as speech impairment and swallowing disability. Speech impairment in terms of production of imprecise articulation, varied resonance characteristics and reduced overall speech intelligibility are commonly seen. Thus the combined effect is more severe than that experienced after surgeries of only maxilla or mandibular lesions. The defects created by maxillectomy can be managed by prosthetic obturator or reconstruction using free and microsurgical transplants, grafts and distant or regional flaps. However, the prosthetic management would be preferred due to its rapid accomplishments, low cost and the possibility of modification according to the patient needs.

Resonances characteristics are related to changes of cavity in size and configuration, Quality of oral resonance is often directly related to the opening of the mouth, achieved by mandible posturing and the relative height of the placement of the tongue within the oral cavity. Oral resonances can be perceived as the

formant frequencies which are observed best during the production of vowels. Following the maxillectomy and mandibulectomy surgery for cancerous lesion, there is an observable change in size and configurations of the vocal tract resulting to changes in the resonances thus affecting the formant frequencies.

2. NEED FOR THE STUDY

Though there are literatures available on the speech characteristics namely articulation, resonance and speech intelligibility of maxillectomy and / or mandibulectomy patients, there is limited information documented regarding the resonance characteristics and its impact on speech intelligibility of patients who have undergone both maxillectomy and mandibulectomy which is a rare condition, a with reconstruction of the mandibular defect and use of palatal prosthesis for closure of the maxillectomy defect.

2.1 Aim

The present study was aimed to determine the vocal tract resonance characteristics and usefulness of palatal prosthesis in improving the resonance and speech intelligibility in subjects of combined maxillectomy and mandibulectomy.

2.2 Method and Materials

Two male subjects (A and B) aged 48 years and 61 years respectively had undergone maxillectomy and mandibulectomy for extensive lesion of buccal mucosa, were reported to the department of speech language studies of Dr.S.R.Chandrasekhar institute of speech and hearing, Bangalore, with the complaint of reduced clarity of speech and swallowing difficulty were recruited for the study. Their surgical details revealed at the time of the study, subject A had undergone partial left maxillectomy and hemi mandibulectomy with temporary tracheostomy. He had also received post operative radio therapy and chemo therapy for the same. The defect of the mandible was reconstructed by PMMC flap 1 year back. Subject B had undergone mandibulectomy and segmental maxillectomy and temporary tracheotomy for recurrence of squamous cell carcinoma on the right infra temporal fossa and posterior maxilla for past history of oral sub mucosa fibrosis excision. Subject B had received pre operative radiotherapy and reconstruction of the defect by radial forearm flap on right cheek and buccal fad pad on left cheek. Mandibular defect was reconstructed by free fibula flap. The left part of the lower lip is stretched to complete the construction. Due to this lower lip was deviated to the left side. Following maxillectomy surgery, both of the subjects been using palatal prosthesis. They were subjected to perceptual and Objective evaluation that included

1. Examination of oral structural and function
2. Resonatory assessment and
3. Assessment of speech intelligibility.

Objective analysis of speech was carried out using CSL 4400 instrument to evaluate acoustic parameters of resonance such as formant frequencies of vowels and 2nd formant transition. Formant frequencies of vowels were considered for the study as they represent the resonance of the vocal tract. Since the vowels are produced orally with open vocal tract, for effective production of vowels the resonance would take place only in the oral cavity. Formant frequencies were measured with and without the prosthesis and the 2nd formant transition were also measured to evaluate objectively the placement and the movement of the tongue within the oral cavity. Analysis of formant frequencies of vowels /a/, /i/ and /u/ in isolation and in words such as /a/ in /a: ne/, /i/ in /illi/ and /u/ in /u: ta: /, which had embedded vowels was examined spectrographically. The mouth to microphone distance was maintained at 6cms. The acoustic signals were digitized at 44100 Hz per channel with 32 bit resolution to a computer. The recording was carried out for both the subjects with and without palatal prosthesis. Speech intelligibility for both the subjects' recording was assessed by 3 speech language pathologist with minimum 5 years of experience using 3 point rating scale. All speech recordings were carried out in a silent room. Speech intelligibility was

3. RESULTS AND DISCUSSION

The study revealed that both the subjects, subsequent to excision of lesion showed a varied picture of affected resonance and speech intelligibility. Oral Peripheral Mechanism Examination revealed deviated lip to left side in subject A and to right side in subject B, missing teeth on top row, with intact tongue and its movement. Velar elevation was restricted. Intra oral pressure could not be built by the subjects due to inadequate lip seal. Vocal tract resonance was observed to be altered in both subjects after surgery due to ablation of the palate, leading to impaired connection between the oral and nasal cavity. Spectrographic analysis without the palatal prosthesis revealed all formant frequencies (F1, F2 and F3) to be deviated from normal due to the presence of anti resonances due to the presence of hyper nasality. Formants were not clearly visible because of open vocal tract that is recorded without prosthesis (fig1). There was also no noted change in the intensity indicating that the distance between the microphone and the subject's mouth was kept constant. Therefore, this dampening of the energy was more without the prosthesis than with prosthesis, thus attributing to the perception of hypernasality (fig 1). From figure 2, the formant frequencies can be viewed more clearly and hence the resonance characteristics improved with the prosthesis. Therefore, acoustic analysis of speech sounds indicated improvement in resonance and speech intelligibility in subjects with palatal prosthesis, as opposed to condition without palatal prosthesis. This also correlated in the results of the perceptual evaluation of speech intelligibility of words to be better with prosthesis. Study done by Teles, Krook&Lauris, (2006), suggested the use of obturator to obliterate the undesired communication between the oral and nasal cavities as a result of maxillectomy, and to improve speech intelligibility. Of the 23 patients who had undergone infra medial- structural maxillectomy, 16 patients exhibited a significant hyper nasality reduction with the obturator in place. Hagino, et al (2008) studied the speech intelligibility(SI),of eleven patients who underwent mandibulectomy without glossectomy, with and without prosthesis to evaluate their speech ability and the
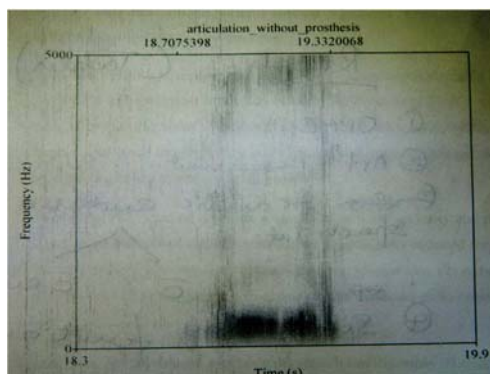

Fig. 1. Formant frequency of Vowel /a/ without palatal prosthesis of subject A
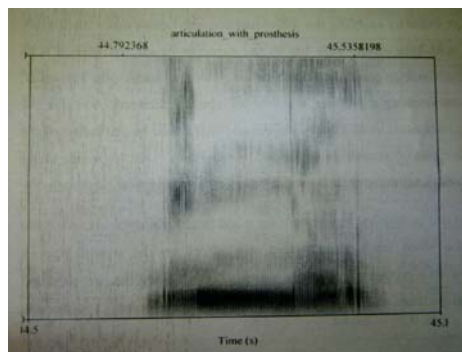

Fig. 2. Presence of formant frequency of vowel /a/ with   palatal prosthesis of subject B

acoustic features such as Formant 1 (F1) and Formant 2 (F2) range to evaluate objectively the limitation of tongue movement. Their study indicated that the three variables such as ease of tongue movement, mandibular bone contribution and soft tissue grafting, contributed to the recovery of speech ability with prosthodontic treatment. Acoustic analysis of the five vowels in maxillectomy patients was reported that lower F2 for all vowels and higher F1 for /i/ and also reported that F2 range decreased indicating the difficulty to maintain F2 properly (Sumita, Ozawa, and Mukohyama, 2002). Assessment of second formant transition and duration of transition did not differ significantly with and without palatal prosthesis indicating that speech intelligibility is predominantly affected by the nasal air emission and rate of speech rather than imprecise placement of tongue following the surgery. Speech intelligibility was found to be better with prosthesis. Our study is in correlation with the study done by Emily, Tobey and Lincks (1989) who evaluated the acoustic speech changes after maxillectomy and prosthetic management. They have also reported that prosthodontic restoration significantly reduced the nasal resonance leading to overall improvement in speech. They suggested that Acoustic speech changes after maxillectomy and prosthetic management showed significantly reduced nasal resonance in all patients either: (1) completely eliminating the resonances, (2) reducing the amplitudes of the resonances and (3) changing the frequency of the resonances to more nearby regions of the vowels. Assessment of Speech intelligibility revealed a significant improvement with the palatal prosthesis. Subjects experienced greater escape of air without the palatal prosthesis leading to reduced rate of speech, thus affecting speech intelligibility. However, when palatal prosthesis was used, amount of nasal air emission reduced, thereby enabling the subjects not only to speak more intelligibly but also with less effort. Both the subject's speech was perceived to be unintelligible and given a score of 0 for subject A and score of 1 for Subject B without the palatal prosthesis whereas improved score of 2 on the rating scale with prosthesis indicated the improved speech intelligibility. Our study is in accordance with the study done by Teles, Krook & Lauris, (2006),

4. CONCLUSION

Disabilities resulting from maxilla and mandibular resection include impaired speech articulation and speech intelligibility, difficulty swallowing and deviation of the mandible during functional movements, poor control of saliva secretions and cosmetic disfigurement was manifested following maxillectomy and mandibulectomy. The present study highlights the importance of the use of palatal prosthesis for the maxillary defect and the surgical reconstruction for the mandibular defect would help in better speech intelligibility in terms of reduced nasal air emission, better articulatory precision and also to reduce the effort of speaker. The surgical reconstruction for mandibular defect would contribute to improve the vocal tract resonance characteristics and speech intelligibility resulting in satisfactory verbal communication and there by quality of life.

5. REFERENCES

[1] C.J. RANDALL and G.P. WALSH – WARING, 'et al. 1987. Marginal Mandibulectomy for Malignant disease: Indications, Rationale and Results, *Journal of Laryngoscope and Otology;* **101**, 676–684.

[2] V.D.C. TELES, M.I.P. KROOK and J. R.P. LAURIS, 2006. Speech evaluation with and without palatal prosthesis obturator in patients submitted to maxillectomy, *Journal of applications of oral sciences*, **14** (6), 421–426

[3] A. HAGINO, K. INOHARA, Y. I SUMITA and H. TANIGUCHI, 2008. Investigation of the factors influencing the outcome of prostheses on speech rehabilitation of mandibulectomy patients. *Nihon GakkaiZasshi.;* **52** (4), 543-549**.**

[4] Y.I. SUMITA, S. OZAWA and H.T. MUKOHYAMA, 2002. Digital acoustic analysis of five vowels in maxillectomy patients. *Journal of Oral Rehabilitation,* **29** (7), 649–656.

[5] A. EMILY TOBEY and JACK LINCKS, 1989. Acoustic analyses of speech changes after maxillectomy and prosthodontic management. *The Journal of Prosthetic Dentistry.* **62** (4), 449–455.

Acoustical Society of India
(Regn. No. 65-1971)

Executive Council (2010 - 2014)

President	:	**Dr V Rajendran**
		[KRSCT, Tiruchengode; veerajendran@gmail.com; +91-99 94 13 03 03]
Vice President	:	**NS Naidu**
		[NSTL, Vizag; nsnaidu04@yahoo.com; +91-94 90 75 05 82]
General Secretary	:	**PVS Ganesh Kumar**
		[NSTL, Vizag; gkpakki@rediffmail.com; +91-98 66 40 08 94]
Jt. Secretary	:	**Dr K. Trinadh**
		[NSTL, Vizag; hello_trinath@yahoo.co.in;; +91-97 04 71 95 00]
Treasurer	:	**Prof AV Sharma**
		[AU, Vizag; sarmavakella@yahoo.co.in; +91-94 90 43 17 17 26]
Chief Editor	:	**Dr Mahavir Singh**
		[CSIR-NPL, New Delhi; mahavir@nplindia.org; +91-98 71 69 33 46]
Council Members	:	**Dr SV Ranga Nayakulu**
		[VITAE, Hyderabad; nayakulu@rediffmail.com; +91-98 66 53 26 13]
		Dr I Johnson
		[SJ College, Trichy; jnaadarsh@hotmail.com; +91-94 12 97 28 90]
		Dr Rajiv K Upadhayay
		[Govt PG College, Rishikesh; rku8@rediffmail.com; +91-94 12 97 28 90]
		Dr S Shekhar
		[Oxford College, Trichy; acousticssekar@yahoo.co.in; +91-99 94 92 00 30]
		Dr V Bhujanga Rao
		[Past President; NSTL, Vizag; vepcrew1@rediffmail.com; +91-98 66 44 10 74]
Co-opted Members	:	**Rajshekhar Uchil**
		[Josts, Bangalore; ruchil@josts.in; +91-98 80 17 08 95]
		Dr NK Narayanan
		[CIT, Kozhikode; csirc@rediffmail.com; +91-94 46 95 58 30]

INFORMATION FOR AUTHORS

ARTICLES

The Journal of Acoustical Society of India (JASI) is a refereed publication published quarterly by the Acoustical Society of India (ASI). JASI includes refereed articles, technical notes, letters-to-the-editor, book review and announcements of general interest to readers.

Articles may be theoretical or experimental in nature. But those which combine theoretical and experimental approaches to solve acoustics problems are particularly welcome. Technical notes, letters-to-the-editor and announcements may also be submitted. Articles must not have been published previously in other engineering or scientific journals. Articles in the following are particularly encouraged: applied acoustics, acoustical materials, active noise & vibration control, bioacoustics, communication acoustics including speech, computational acoustics, electro-acoustics and audio engineering, environmental acoustics, musical acoustics, non-linear acoustics, noise, physical acoustics, physiological and psychological acoustics, quieter technologies, room and building acoustics, structural acoustics and vibration, ultrasonics, underwater acoustics.

Authors whose articles are accepted for publication must transfer copyright of their articles to the ASI. This transfer involves publication only and does not in any way alter the author's traditional right regarding his/her articles.

PREPARATION OF MANUSCRIPTS

All manuscripts are refereed by at least two referees and are reviewed by the Publication Committee (all editors) before acceptance. Manuscripts of articles and technical notes should be submitted for review electronically to the Chief Editor by e-mail or by express mail on a disc. JASI maintains a high standard in the reviewing process and only accept papers of high quality. On acceptance, revised articles of all authors should be submitted to the Chief Editor by e-mail or by express mail.

Text of the manuscript should be double-spaced on A4 size paper, subdivided by main headings-typed in upper and lower case flush centre, with one line of space above and below and sub-headings within a section-typed in upper and lower case understood, flush left, followed by a period. Sub-sub headings should be italic. Articles should be written so that readers in different fields of acoustics can understand them easily. Manuscripts are only published if not normally exceeding twenty double-spaced text pages. If figures and illustrations are included then normally they should be restricted to no more than twelve-fifteen.

The first page of manuscripts should include on separate lines, the title of article, the names, of authors, affiliations and mailing addresses of authors in upper and lowers case. Do not include the author's title, position or degrees. Give an adequate post office address including pin or other postal code and the name of the city. An abstract of not more than 200 words should be included with each article. References should be numbered consecutively throughout the article with the number appearing as a superscript at the end of the sentence unless such placement causes ambiguity. The references should be grouped together, double spaced at the end of the article on a separate page. Footnotes are discouraged. Abbreviations and special terms must be defined if used.

EQUATIONS

Mathematical expressions should be typewritten as completely as possible. Equation should be numbered consecutively throughout the body of the article at the right hand margin in parentheses. Use letters and numbers for any equations in an appendix: Appendix A: (A1, (A2), etc. Equation numbers in the running text should be enclosed in parentheses, i.e., Eq. (1), Eqs. (1a) and (2a). Figures should be referred to as Fig. 1, Fig. 2, etc. Reference to table is in full: Table 1, Table 2, etc. Metric units should be used: the preferred from of metric unit is the System International (SI).

REFERENCES

The order and style of information differs slightly between periodical and book references and between published and unpublished references, depending on the available publication entries. A few examples are shown below.

Periodicals:
[1]   S.R. Pride and M.W. Haartsen, 1996. Electroseismic wave properties, *J. Acoust. Soc. Am.*, 100 (3), 1301-1315.
[2]   S.-H. Kim and I. Lee, 1996. Aeroelastic analysis of a flexible airfoil with free play non-linearity, *J. Sound Vib.*, 193 (4), 823-846.

Books:
[1]   E.S. Skudzryk, 1968. *Simple and Comlex Vibratory Systems*, the Pennsylvania State University Press, London.
[2]   E.H. Dowell, 1975. *Aeroelasticity of plates and shells*, Nordhoff, Leyden.

Others:
[1]   J.N. Yang and A. Akbarpour, 1987. Technical Report NCEER-87-0007, Instantaneous Optimal Control Law For Tall Buildings Under Seismic Excitations.

SUMISSIONS

All materials from authors should be submitted in electronic form to the JASI Chief Editor: Dr Mahavir Singh, Acoustics, Ultrasonics & Vibration Section, CSIR-National Physical Laboratory, Dr. K. S. Krishnan Road, New Delhi-110 012 (email: mahavir@nplindia.org Tel: +91-11-4560.8317, Fax: +91-11-4560.9310). For the item to be published in a given issue of a journal, the manuscript must reach the Chief Editor at least twelve week before the publication date.

SUMISSION OF ACCEPTED MANUSCRIPT

On acceptance, revised articles should be submitted in electronic form to the JASI Chief Editor (mahavir@nplindia.org)

JOURNAL OF ACOUSTICAL SOCIETY OF INDIA

A Quarterly Publication of the JASI
http://www.acousticsindia.org

Journal of Acoustical Society of India

CHIEF EDITOR:
Mahavir Singh
Acoustics, Ultrasonics & Vibration Section
CSIR-National Physical Laboratory
Dr. KS Krishnan Road
New Delhi 110 012
Tel: +91.11.4560.8317
Fax: +91.11.4560.9310
E-mail: mahavir@nplindia.org

ASSOCIATE SCIENTIFIC EDITOR:
Applied Acoustics

Trinath Kart
Control Component India Pvt. Ltd
6th Floor, Warp Tower
Plot # 13, 14, &15
SJR i-Park, EPIP Zone, Phase 1
Whitefield Road, Bangalore 560066

Editorial Office:
MANAGING EDITOR
Omkar Sharma

ASSISTANT EDITORS
Yudhisther Kumar
Anil Kumar Nain
Kirti Soni
Acoustics, Ultrasonics & Vibration Section
CSIR-National Physical Laboratory
Dr. KS Krishnan Road
New Delhi 110 012
Tel: +91.11. 4560.8317
Fax: +91.11.4560.9310
E-mail: mahavir@nplindia.org

The Journal of Acoustical Society of India is a refereed journal of the Acoustical Society of India (ASI). The ASI is a non-profit national society founded in 31st July, 1971. The primary objective of the society is to advance the science of acoustics by creating an organization that is responsive to the needs of scientists and engineers concerned with acoustics problems all around the world.

Manuscripts of articles, technical notes and letter to the editor should be submitted to the Chief Editor. Copies of articles on specific topics listed above should also be submitted to the respective Associate Scientific Editor. Manuscripts are refereed by at least two referees and are reviewed by Publication Committee (all editors) before acceptance. On acceptance, revised articles with the text and figures scanned as separate files on a diskette should be submitted to the Editor by express mail. Manuscripts of articles must be prepared in strict accordance with the author instructions.

All information concerning subscription, new books, journals, conferences, etc. should be submitted to Chief Editor:

Acoustics, Ultrasonics & Vibration Section, CSIR-National Physical Laboratory, Dr. KS Krishnan Road, New Delhi 110 012, Tel: +91.11.4560.8317, Fax: +91.11.4560.9310, e-mail: mahavir@nplindia.org

Annual subscription price including mail postage is Rs. 2000/= for institutions, companies and libraries and Rs. 2000/= for individuals who are not ASI members. The Journal of Acoustical Society of India will be sent to ASI members free of any extra charge. Requests for specimen copies and claims for missing issues as well as address changes should be sent to the Editorial Office:

Acoustics, Ultrasonics & Vibration Section, CSIR-National Physical Laboratory, Dr. KS Krishnan Road, New Delhi 110 012, Tel: +91.11.4560.8317, Fax: +91.11.4560.9310, e-mail: mahavir@nplindia.org

Journal of Acoustical Society of India (JASI)

A quarterly publication of the Acoustical Society of India

Volume 41, Number 3, July 2014

EDITORIAL

ARTICLES

INFORMATION

How do you compare an NRC rating with an STC rating?

The Noise Reduction Coefficient (NRC) is a scalar representation of the amount of sound energy absorbed upon striking a particular surface. An NRC of 0 indicates perfect reflection; an NRC of 1 indicates perfect absorption. In particular, it is the average of four sound absorption coefficients of the particular surface at frequencies of 250 Hz, 500 Hz, 1000 Hz, and 2000 Hz. These frequencies encompass the fundamental frequencies and first few overtones of typical human speech, and, therefore, the NRC provides a decent and simple quantification of how well the particular surface will absorb the human voice. A more broad frequency range should be considered for applications such as music or controlling mechanical noise. Specifications for materials used in sound absorption commonly include an NRC for simplicity, in addition to more detailed frequency vs amplitude charts. Acoustical materials manufacturers often report NRC values higher than 1.0 due to the way the number is calculated in a laboratory. A test material's area does not include the sides of the panel (which are exposed to the test chamber) which vary due to its thickness. A certain percentage of the sound will be absorbed by the side of the panel due to diffraction effects.

Sound Transmission Class (STC) is an integer rating of how well a building partition attenuates airborne sound. In the USA, it is widely used to rate interior partitions, ceilings/floors, doors, windows and exterior wall configurations (see ASTM International Classification E413 and E90). Outside the USA, the Sound Reduction Index (SRI) ISO standard is used. The ASTM test methods have changed every few years and over many years have been changed significantly. Thus, STC results posted before 1999 may not produce the same results today, and this difference becomes wider as one goes back in time (that is the differences in test method from the 1970's to today are vast). The STC number is derived from sound attenuation values tested at sixteen standard frequencies from 125 Hz to 4000 Hz. These transmission-loss values are then plotted on a sound pressure level graph and the resulting curve is compared to a standard reference contour. Acoustical engineers fit these values to the appropriate TL Curve (or Transmission Loss) to determine an STC rating. The measurement is accurate for speech sounds but less so for amplified music, mechanical equipment noise, transportation noise or any sound with substantial low-frequency energy below 125 Hz. Sometimes, acoustical labs will measure TL at frequencies below the normal STC boundary of 125 Hz, possibly down to 50 Hz or lower, thus giving additional valuable data to evaluate transmission loss at very low frequencies, such as a subwoofer-rich home theater system would produce. Alternatively, Outdoor-Indoor Transmission Class (OITC) is a standard used for indicating the rate of transmission of sound between outdoor and indoor spaces in a structure that considers frequencies down to 80 Hz (Aircraft/Rail/Truck traffic) and is weighted more to lower frequencies.

Mahavir Singh

Oil Filled Free Flooded Segmented Ring Transducer for Deep Sea Applications

M. R. Subash Chandrabose and D. D. Ebenezer

Naval Physical and Oceanographic Laboratory, DRDO, Kochi 682021, India
e-mail: subashbos@gmail.com

ABSTRACT

Free-flooded segmented ring transducers are widely used for deep sea applications. The material used for encapsulating the transducer has considerable effect on the transducer performance. Moulding directly over the segmented ceramic ring with polyurethane or rubber can affect the transducer performance. Compared to a directly potted transducer an oil filled segmented ring transducer enhances the bandwidth and efficiency by close coupling the cavity and hoop mode resonances. In the present study, the performance of a moulded transducer and a free-flooded segmented ring transducer in an oil-filled rubber boot are compared. The effect of different types of fill fluids, wedge material, ceramic wall thickness and oil column thickness, between the ceramic outer diameter and boot inner diameter, on the Transmitting Voltage Response and Receiving Sensitivity are also studied. ATILA - a software package for the analysis of sonar transducers - is used to model the transducers.

1. INTRODUCTION

Free-flooded segmented ring transducers are ideal for deep sea applications and preferred over a one piece radially expanding ceramic ring because they have higher electromechanical coupling, power output, and efficiency. Segmented ring transducers can be manufactured by gluing together ceramic wedges or stacks of inexpensive ceramic slabs and metallic or non metallic wedges [1] as shown in Fig.1. Pre-stress can be provided by metallic straps, fibre winding over the assembled segments or using wedges [2] [3] A segmented ring with wedge shaped ceramics and pre-stressed with fibre winding is shown in Fig. 2. The coupling coefficient of segmented ring is approximately double that of single piece ceramic ring because of the 33 mode operation of ceramic slabs of segmented ring compared to the 31 mode of ceramic ring. The resonance frequency of the segmented ring transducer can be lowered by using non metallic wedges like Lucite or perforated metallic wedges [5] [6] [7] . The material used for encapsulating the transducer has considerable effect on the transducer performance. Potting directly over the segmented ceramic ring transducer with polyurethane or rubber can affect the resonance frequency, receiving and transmission sensitivities and reduction in source level [8] [9] . Renna [10] in his US patent has reported oil filled, fibre glass wound segmented ring transducer that enhances the bandwidth and efficiency by close coupling the cavity and hoop mode resonances. The boot couples the transducer to the fluid in which it is immersed. The cavity at the centre of the transducer is free flooded. Lipper and Borden [8] have reported output power reduction upto 8 dB in the frequency band of 7-15 kHz for a poly-urethane potted transducer compared to oil filled transducer and such reduction will have serious consequences for deep submergence operations. The authors have not provided any dimensional details or oil column thickness over the ceramic diameter of the transducer.

2. OBJECT OF THE STUDY

In the present study, the performance of a potted transducer with polyurethane and rubber are compared with a free-flooded segmented ring transducer in an oil-filled boot. The effects of different fill fluids, oil column thickness between the ceramic outside diameter (OD) and boot inside diameter (ID), wedge material, and ceramic ring wall thickness on the Transmitting Voltage Response and Receiving Sensitivity are also studied.
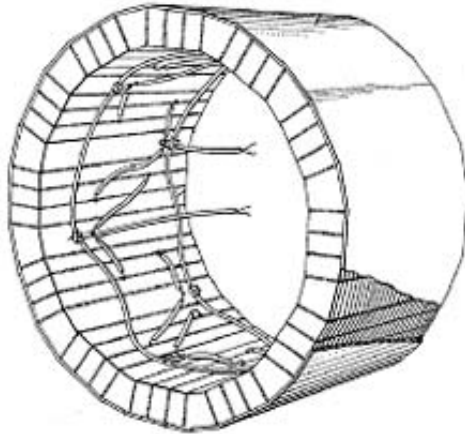

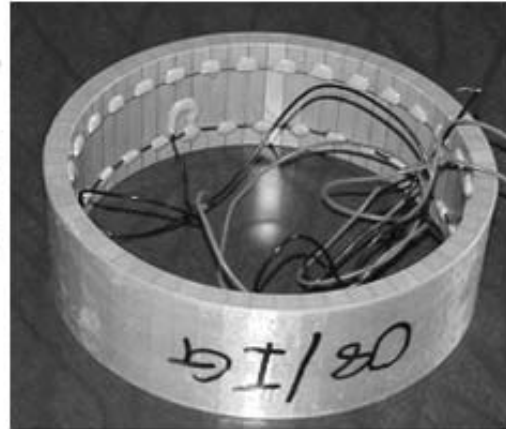Fig. 1. Segmented ring with wedges and slabs.

Fig. 2. All ceramic segmented ring with wedge shaped ceramic and fibre winding

3. DESCRIPTION OF THE TRANSDUCERS STUDIED AND THE MODEL

The active material of the transducer studied is piezoceramic slabs of PZT4 with 10 mm thickness. The transducer base model has an outside diameter of 150 mm and inside diameter of 130 mm. First the transducer is studied for direct moulding over ceramic ring with an encapsulation thickness of 5 mm all around. In the next case, the transducer is positioned in a rubber casing in which the cavity around the ceramic is filled with a fill fluid. In order to study the effect of different type of fill fluids on transducer, widely used fill fluids like Silicone oil, Castor oil and Isopar L are considered [11] . To study the effect of oil column thickness between the outside diameter of the ceramic and inside diameter of the boot, keeping ceramic OD same the boot ID is changed. The effect of wedge material used for the transducer on transducer performance is studied by changing the wedge material like Brass, Aluminium, Tungsten and PVC. Effect of ceramic wall thickness on transducer characteristics is studied by varying the inner diameter of the transducer by keeping the outer diameter same. ATILA - a software package for the analysis of sonar transducers - is used to model the transducers. Because of the symmetry only $1/4^{th}$ of the transducer is modelled. Eight noded quadrilateral elements are used to model the piezoelectric, elastic, fill fluid, and water surrounding the transducer. Schematic and 2D model of the transducer are shown in Figs.3 and 4.

4. RESULTS AND DISCUSSIONS

The basic model of the transducer considered is with Brass wedges and PZT4 ceramic slabs. The direct rubber and polyurethane moulded transducers are compared with a Silicone oil filled rubber booted transducer. The transmitting voltage response (TVR) and receiving sensitivity (RS) for the transducers are shown in Figs. 5 and 6, respectively. The Silicone oil filled transducer has about 3.5 dB more TVR at resonance compared to the rubber and PU moulded transducers. The response of the rubber and PU moulded transducers follow similar pattern. However the resonance frequency of the oil filled transducer is about 500 Hz higher. The effect of different type of fill fluids on transducer performance is studied by using Silicone oil, Castor Oil and Isopar L. The results are shown in Figs. 7 and 8. The results shows that Castor Oil filled
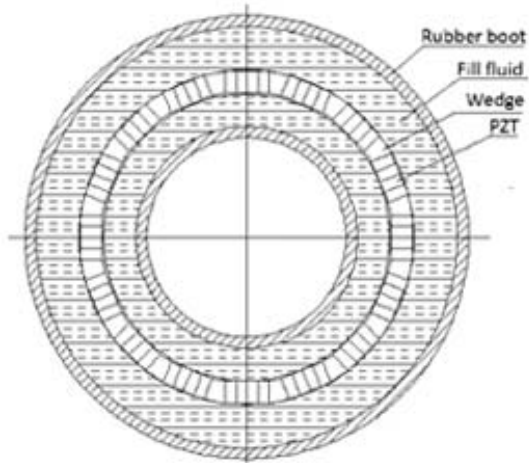
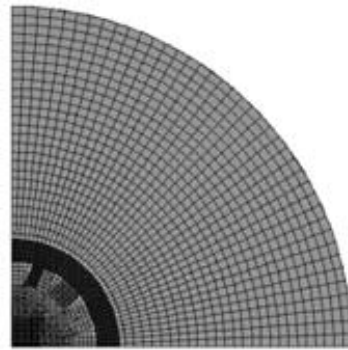Fig. 3. Schematic of the fluid filled transducer.

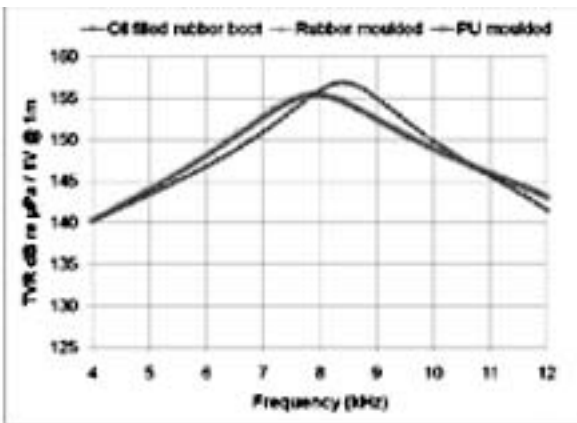Fig. 4. FE Model of transducer.

Fig. 5. Effect of encapsulation on TV.
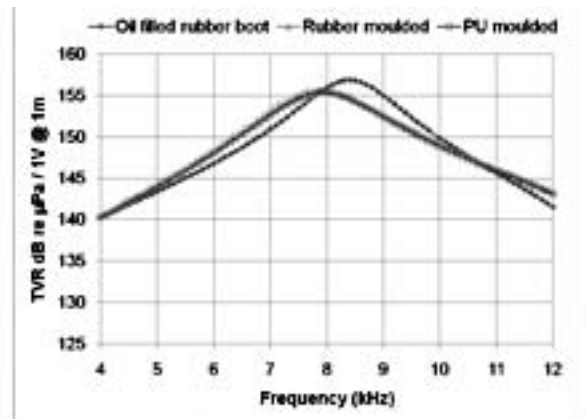
Fig. 6. Effect of encapsulation on RS.
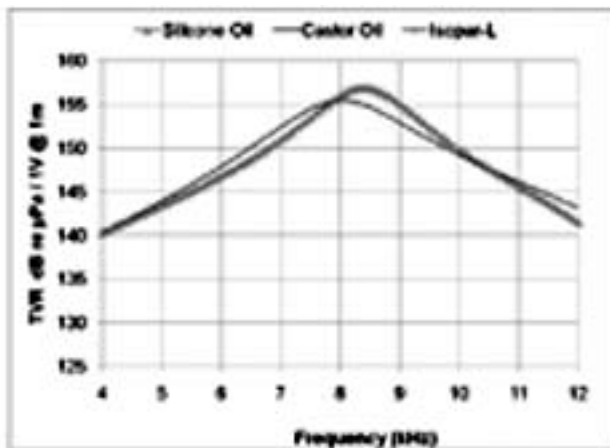
Fig. 7. Effect of Fill fluid on TVR.
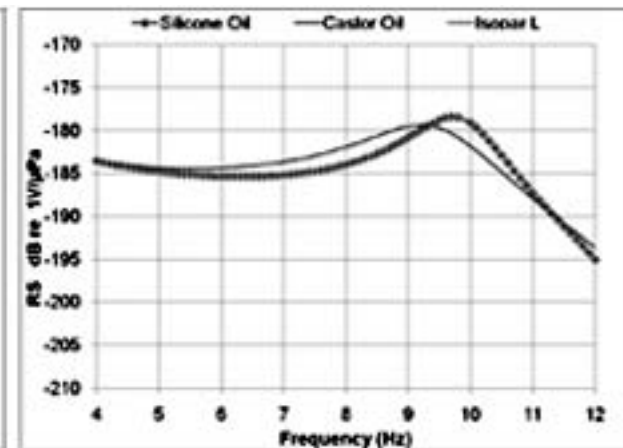
Fig. 8. Effect of fill fluid on RS.

transducer has about 500 Hz lower resonance frequency and a broader bandwidth than Silicone oil and Isopar-L filled transducers but a lower TVR at resonance.

The effect of oil column thickness over the outside diameter of the ceramic is studied for different thicknesses like 10, 20, and 30mm between inner diameter of the rubber boot and the ceramic OD. The results are shown in Figs. 9 and 10. The results indicate that the TVR at resonance increases with increase in oil column thickness but the bandwidth reduces. However the TVR and RS of the transducer with 10 mm thickness are higher at frequencies away from resonance.
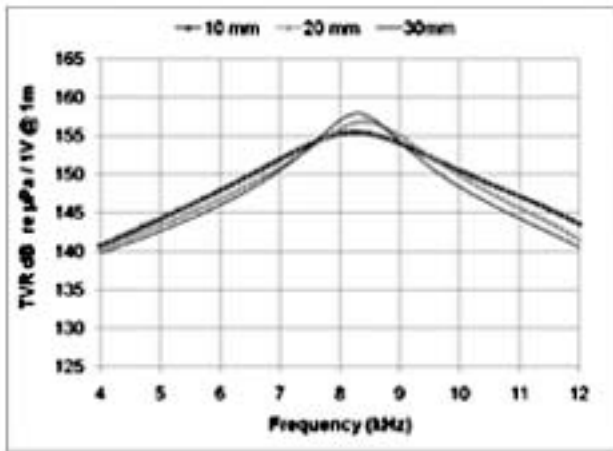
Fig. 9. Effect of fluid column thickness on TVR.　　Fig. 10. Effect of fluid column thickness on RS.
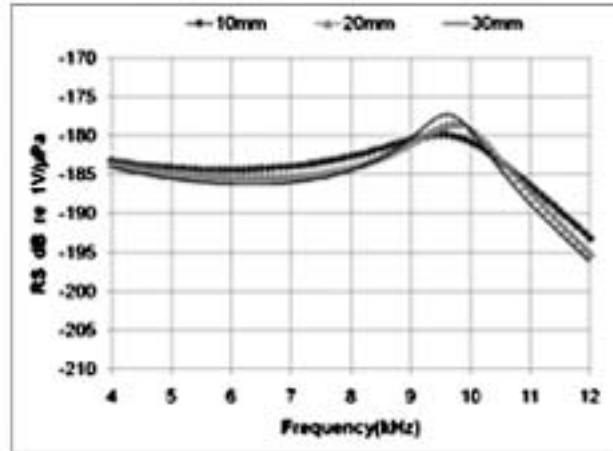
The effect of wedge material on transducer performance is studied by using Brass, Aluminium, Tungsten, and PVC. The results are shown in Figs. 11 and 12. It can be seen that by changing the wedge material to a soft material like PVC the resonance frequency can be shifted to lower side but with a large reduction in TVR and RS. When a dense metal like Tungsten is used as wedge material it reduces the resonance frequency by about 400 Hz without any reduction in peak TVR. However the cost and machining aspects of Tungsten needs to be considered before using it as wedge material.

Effect of ceramic wall thickness on transducer characteristics is studied by varying the inner diameter of the transducer but keeping the outside diameter constant. Modelling is carried out with wall thicknesses of
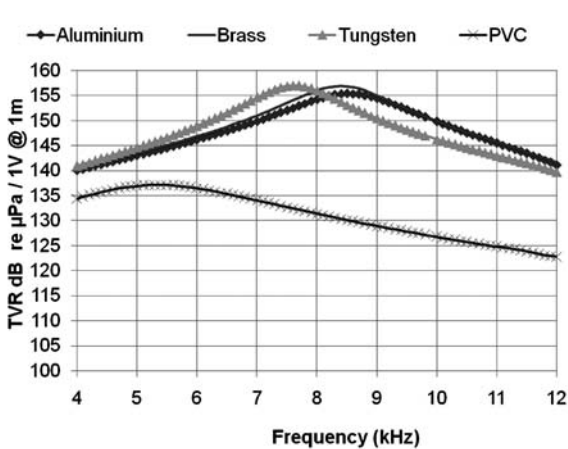
Fig. 11. Effect of wedge material on TVR.　　　Fig. 12. Effect of wedge material on RS.
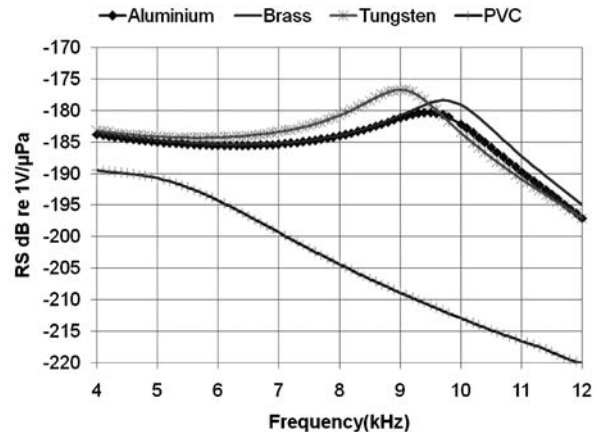
5, 10, and 15 mm. Increasing the wall thickness of the ceramic results in an increase in the TVR and resonance frequency while the bandwidth is reduced. However, if the wall thickness is increased considerably it may become difficult to pre-stress.
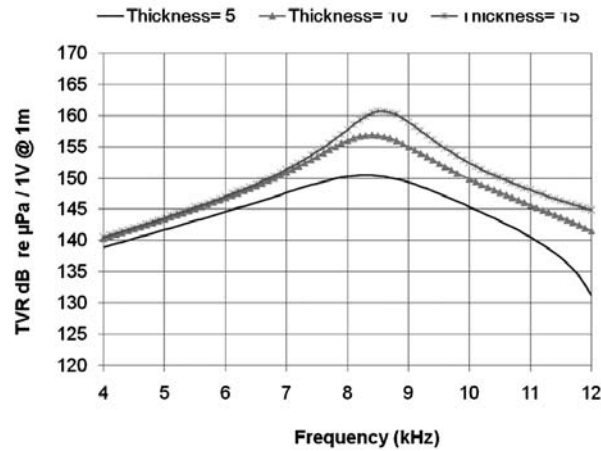
Fig. 13. Effect of ceramic wall thickness on TVR.
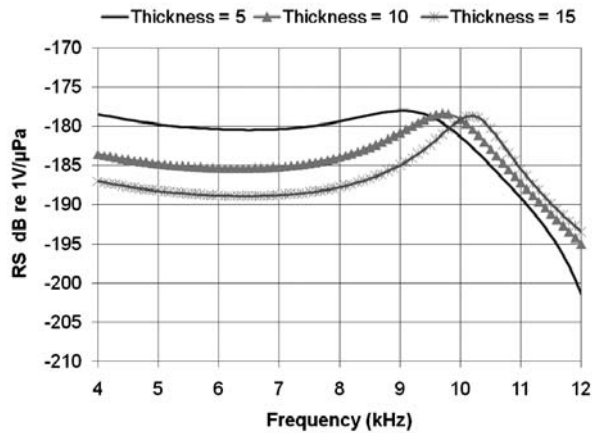
Fig. 14. Effect of ceramic wall thickness on RS.

5. CONCLUSIONS

Fluid filled free-flooded segmented ring transducer performance is compared with a directly moulded transducer. Moulding directly over the segmented ceramic ring transducer with polyure-thane or rubber reduces the transducer performance. Effect of type of fill fluid, fluid column thickness between the ceramic OD and boot ID, effect of wedge material and ceramic wall thickness on the Transmitting Voltage Response and Receiving Sensitivity are also studied.

6. ACKNOWLEDGMENT

7. REFERENCES

[1]   C.E. GREEN, 1965. Mosaic construction for electro-acoustical cylindrical transducers, US Patent No. 3177382,

[2]   W.L. CLEARWATERS, 1962. Electrostrictive transducer. US Patent 3043967.

[3]   D.E. PARKER, 1966. Reinforced Ceramic Cylinder Transducer, US Patent No.3230505.

[4]   M. EDOUARD *et al.*, 2000. Pre-stressed annular Acoustic transducer, US Patent Number: **6**,065,349.

[5]   W.T. HARRIS, 1964. Ring shaped transducers, US Patent 3142035

[6]   J.L. BUTLER, 1976. Model for a ring transducer, *J. Acoustical Society America* **59**(2), 480-481.

[7]   Xin-ran XU1, 2012. Theoretical and experimental study on a new structure free-flooded ring transducer, *Proceedings of the IEEE Symposium on Piezoelectricity, Acoustic Waves and Device Applications* (SPAWDA), 81-84.

[8]   A. LIPPER and J. BORDEN, 2012. Urethane Transducer Encapsulation versus Oil Filled Boot Encapsulation of Transducers, *Proceedings of IEEE Oceans*, 1-4

[9]   A. LIPPER and J. BORDEN, 2013, Comparing encapsulation methods of piezoelectric transducers, *Sea Technology*, 31-34.

[10] N. RENNA, Jr. 1972. Underwater acoustic projector. US Patent 3706967.

[11] T. H. MEHNERT, 1972. Handbook of fluid filled depth/pressure compensated systems for deep ocean applications. Naval Ship Research and Development Centre, Annapolis Laboratory, Maryland, USA.

Characteristics of Acoustic Emissions Originated from Snow During Mechanical Deformation

Prem Datt[1], J C Kapil1, Ashavani Kumar[2],
Karamjeet Singh[1] and Vinod Kumar[1]
[1]Snow and Avalanche Study Establishment (SASE), Manali (HP), India
[2]National Institute of Technology (NIT), Kurukshetra (HR), India
e-mail: datt_prem@rediffmail.com

ABSTRACT

When a material is loaded with some external force, the material can undergo deformation and microscopic failure processes within it. During these processes the stored energy releases rapidly and forms stress waves, these waves are named as acoustic emissions. Snow is a porous sintered material consisting of ice skeleton, air and in moist conditions water vapor and thin layer of liquid water also. Snow exists very close to its phase change temperature; this makes snow a thermally very active and structurally dynamic material. Thus, snow is in the constant state of evolution micro-structurally, consequently, its physical and mechanical properties also keep on changing with time which can lead to the stable or unstable snowpack. Snow avalanches occur due to the breaking of inter-granular bonds which leads to cata-strophic failure of a snowpack on a mountain slope. Monitoring of acoustic emissions from snow can be used for evaluation of snowpack stability nondestructively. In snow, acoustic emissions are emanated during the constant deformation and failure of grains itself or bonds between grains or both. Detection and characterization of acoustic signatures from snow are important for evaluation of snowpack state and finding of appropriate precursors for ava-lanche. In this paper we report some of the characteristics of acoustic emissions originated from deforming snow subjected to mechanical loading in cold laboratory located at SASE, Manali, H.P., India. Cylindrical snow samples of different grain size range, <0.5 mm, 0.5 - 0.7 mm and 0.7 - 1.0 mm, were prepared by sieving the snow stored in a cold chamber at -20 °C. The sieved snow samples were allowed to sinter at -20 °C for approximately seventy two hours in sample storage cold chamber. Snow samples were then subjected to uni-axial compression in a universal testing machine (UTM) at different deformation rates 1 mm/min, 5 mm/min and 10 mm/min. Acoustic emissions were recorded for different deformation rates using an experimental setup consisting different AE sensors and data acquisition system. The acoustic sensors were coupled with snow sample through an aluminum plate. Experimental data was analyzed to find out the distribution of various parameters like hits/events, counts, amplitude frequency etc. for different deformation rates and grain sizes. The mean and peak amplitude of acoustic emissions increases with the deformation rates.

1. INTRODUCTION

Snow is a porous sintered material consisting of ice skeleton, air and in moist conditions water vapor and thin layer of liquid water also. At homologues temperature scale snow is considered as a hot material, since

Prem Datt*1, J C Kapil, Ashavani Kumar, Karamjeet Singh1 and Vinod Kumar

it exists very close to its phase change temperature. This makes snow a thermally very active and structurally dynamic material. Snow is in the constant state of evolution micro-structurally, consequently, its physical and mechanically properties also keep on changing with time under the influence of environmental conditions. These metamorphic changes can lead the snowpack either stable or unstable condition. Existence of buried weak layer is most often responsible for the failure of mountain snowpack and formation of most devastating slab avalanches. Assessment of stability of a snowpack is vital information for an avalanche forecaster but at the same time it is very difficult and hazardous to get this information from real avalanche slopes. Change in mechanical strength due to continuous evolution of snowpack under different temperature regimes, new snowfall or any man made activity (trekker, skier etc) can create excessive stress and which can lead to the failure of buried weak layer. At microscopic level failure is caused by breaking of bonds between snow grains and the released elastic energy travels as stress wave in the material and can be picked up by piezoelectric acoustic sensors (McClung D and Schaerer P, 1999). These stress waves are termed as acoustic emissions (AE). St. Lawrence and others (1973) were the pioneers for detecting acoustic emissions in the lab from deforming snow. They recorded acoustic emissions for three different deformation rates form the snow samples subjected to uniaxial mechanical loading. The emissions were attributed to the intra-crystal failure for low deformations and inter-crystal failure for high deformations. Lawrence et al, 1980 further developed a constitutive relation between acoustic emissions response of snow to the applied stress and strain. Scapozza et al (2004) also carried out compression tests on snow specimen in laboratory conditions for different strain rates. They also confirmed the transition snow behavior from ductile to brittle at strain rates more than $\sim 10^{-3}$ s^{-1}. Most of the researchers have focused on the acoustic emission rates with snow samples subjected to different deformation and detailed description of other parameters related to AE measurements are lacking. In this paper we have reported the analysis of distribution of hits, amplitude and frequency of acoustic waves generated for different stress rates and grain sizes.

2. EXPERIMENTAL PROCEDURES

2.1 AE equipment

An acoustic emission (AE) measurement system (PAC) was used to record the emissions generated during the mechanical loading of snow samples. The AE setup consists of a high speed data acquisition system with 16 input channels having bandwidth of 400 KHz and simultaneous software selectable sampling rate up to 1MSPS for each channel. Piezoelectric based acoustic sensors with different frequency range and sensitivities were placed in the bottom plate on which snow specimen was mounted. (Figure 1a &1b). It was very difficult to couple the AE sensors to the snow specimen directly because of its porous and fragile nature. Therefore, sensors were mounted in a metal plate using silicon jell as a coupling agent. The sensors were calibrated by pencil lead breaking test on a metal plate (Pollock, 1995). Before starting the actual experiment, the noise characterization of environment, wind draft of chamber, compressor noise etc was carried out. The threshold of the transient acoustic signals is very critical because it affects various other parameters used for hit based analysis like, total number of hits, total number of counts, and duration of AE etc. The threshold level was decided by allowing the acoustic sensors to record all environmental noise and gradually the threshold level was increased. It was found that the amplitude of environmental noise was below 40/45 dB. Sensors details used during the experiments is given in table 1.

2.2 Snow specimen preparation

Snow samples were prepared by using stored snow brought from Patsio, a field observatory located in Great Himalaya range and was stored at -20 ^{0}C in a storage cold chamber. Snow samples were prepared for different grain size range by sieving the snow in a sieve shaker and gradually allow it to fill metallic cylindrical sampler of ~65 mm diameter and ~150 mm length. These samples were allowed to sinter for 72 hours at -20 ^{0}C before they were subjected to the mechanical loading. Snow samples from metallic sampler were removed carefully and placed on circular metallic plate already mounted on universal testing machine with AE sensors. During the ageing process the snow inside the sampler settled and after removing from the sampler both the end of the sample were smoothened to make the proper contact with plunger and base metal disc.

Fig. 1. Experimental setup for AE measurements:
(a) Acoustic emission monitoring system; (b) Snow sample under testing.

Table 1. Details of snow samples and acoustic emission sensors

Deformation rate	Grain size (mm)	Sample height (mm)	Snow density (gm/cm3)	AE sensor	Frequency range (kHz)
1 mm/min	0.7-1.0	136	0.4	AE1	1-30 (4.5*) kHz
	0.5-0.7	138	0.4	AE2	5-20 (15*) kHz
	<0.5	135	0.4	AE3	10-70 (30*) kHz
5 mm/min	0.7-1.0	137	0.37	AE4	40-100 (60*) kHz
	0.5-0.7	140	0.41	AE5	50-200 (150*) kHz
	<0.5	139	0.36	AE6	125-450 (300*) kHz
10 mm/min	0.7-1.0	140	0.37	AE7	25-530 (29*) kHz
	0.5-0.7	141	0.38		*Values in parenthesis show reso
	<0.5	141	0.41		nant frequencies in kHz

Experiments were conducted for different deformation rates varying from 1 mm/min to 10 mm/min keeping the snow specimen temperature at -10 0C. Three snow specimens corresponding to grain sizes <0.5 mm, 0.5-0.7 mm and 0.7-1.0 mm were tested for each deformation rate.

3. RESULTS & DISCUSSION

In this section, we present and discuss the AE amplitudes and their distribution, dominant frequency and released AE energy for different deformation rates.

3.1 AE amplitude

AE amplitude is an important parameter because it determines the detectability of any acoustic signal emitted from the source. Figure 2 shows the AE hit amplitude distribution for various sensors ranging from AE1 to AE7. Panel A, Panel B and Panel C represent the box plots of AE amplitudes corresponding to the 1 mm/min, 5 mm/min and 10 mm/min respectively. It was observed that the low amplitude from 45 to 55 dB hits were recorded during the 1mm/min deformation rate. The AE amplitude increases with the increase in the deformation rate and it reached up to 75 dB and 99 dB for deformation rate 5 mm/min and 10 mm/min respectively. The scatter of the AE amplitude also increases with increasing the load applied on the snow

Prem Datt*1, J C Kapil, Ashavani Kumar, Karamjeet Singh1 and Vinod Kumar

specimen. It was also observed that sensor 4 (40 kHz-100 kHz; resonant 60 kHz) received the maximum amplitude in all the cases. The extreme events have amplitude up to 80 dB for 1 mm/min and 5 mm/min deformation rate, however, for 10 mm/min deformation rate, events having maximum amplitude close to 100 dB were also recorded. Snow specimen subjected to lower deformation rates did not fail and no visible fractures were observed on the samples. The low amplitude acoustic events generate during the deformation process without catastrophic failure are mainly originated from the breaking of the bonds between the grains (St Lawrence & Bradely, 1980) within the volume of snow specimen. Snow samples subjected the higher deformation of rate of 10 mm/min show increased AE activity with relatively very high amplitude of AE events (Panel C) and multiple fractures were also observed on sample's surface. The increased AE amplitude with deformation rate was registered by all the sensors. Cumulative AE hits from 40-100 dB for different deformation rate and grain size range are shown in figure 3. It is clear from the figure that the number of AE hits increased significantly with increasing deformation rate from 1 mm/min to 10 mm/min. The effect of grin size could not be established from this preliminary analysis.
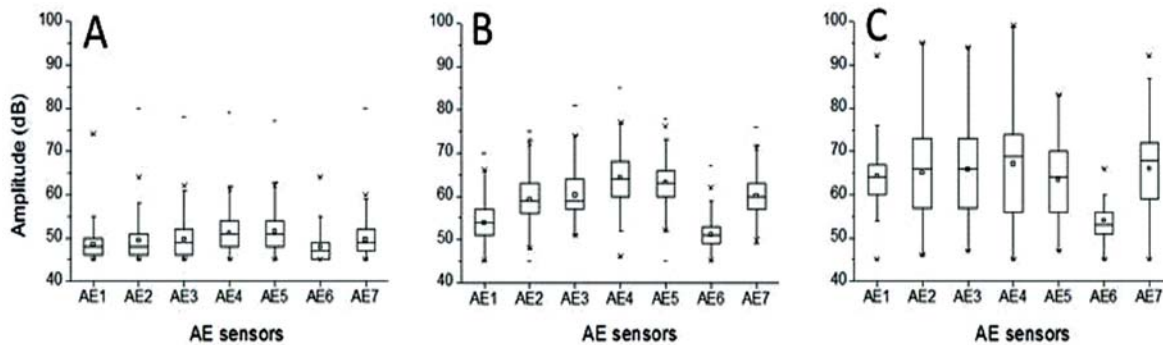
Fig. 2. Acoustic emission amplitude distribution response of various AE sensors (AE1-AE7):
(i) Panel (A); AE amplitude with deformation rates 1 mm/min (ii) Panel (B));
AE amplitude with deformation rates 5 mm/min (iii) Panel (C));
AE amplitude with deformation rates 10 mm/min for grain size <0.5 mm.

Table 2. Summary of AE amplitudes and hit rates corresponding to different deformation rates

	1 mm/min	5 mm/min	10 mm/min
Mean amplitude (dB)	50	59	64
Median amplitude (dB)	49	59	64
Maximum amplitude (dB)	76	76	93
Hit rate (hits/sec)	2	52	93

3.2 AE frequency

Frequency corresponding to each hit was extracted by performing real time FFT on the received AE waveforms by using built in feature of AEWin software. Figure 4 depicts the graphical representation of the frequency distribution for all the sensors (AE1-AE7). It was observed that the mean frequency of AE waves varied between 32- 66 kHz for all three deformation rates.

4. CONCLUSIONS

Experimental work carried out in a cold laboratory to study the acoustic emission characteristics emanated from snow samples at different deformation rates are presented. Multiple AE sensors were used to record the emission through a metallic disc as a waveguide. It was observed that the amplitudes and hit rates of the acoustic emission increases significantly with increasing the mechanical deformation rate. The mean AE
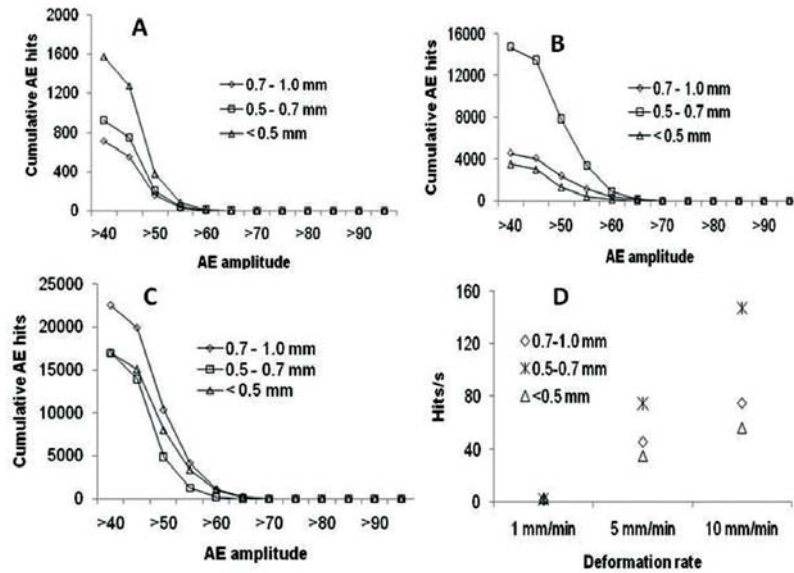
Fig. 3. Panel (A): Cumulative AE hits with AE amplitude for 1 mm/min; Panel (B):
Cumulative AE hits with AE amplitude for 5 mm/min; Panel (C): Cumulative AE hits with
AE amplitude for 10 mm/min; panel (D): AE hit rate with deformation rate.
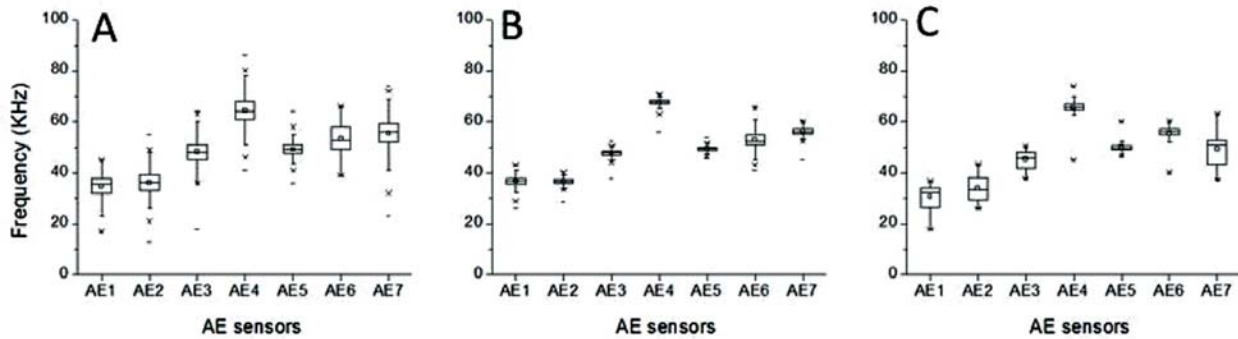
Fig. 4. Acoustic emission frequency response of various AE sensors (AE1-AE7): (i) Panel (A);
AE frequency for 1 mm/min (ii) Panel (B)); AE frequency with deformation rates 5 mm/min
(iii) Panel (C)); AE frequency with deformation rates 10 mm/min.
All the three samples were <0.5 mm grain size.

amplitude increases from 50 dB to 64 dB for deformation rate from 1 mm/min to 10 mm/min. The emission corresponding to deformation rates 1 mm/min and 5 mm/min are mainly attributed to the microscopic deformation of ice matrix for the snow grain re-arrangements under the external mechanical load. However, the snow sample subjected to higher deformation rate emitted both low level emissions and the high amplitude AE emissions corresponding to the fracture. We observed the frequency of AE signals in the range of 32-66 kHz. Further we are analyzing the other parameters of acoustic emission to correlate with snow deformation.

5. ACKNOWLEDGEMENTS

Prem Datt*1, J C Kapil, Ashavani Kumar, Karamjeet Singh1 and Vinod Kumar

6. REFERENCES

[1]   D. MCCLUNG and P. SCHAERER, 1999. *The Avalanche Handbook,* Published by The Mountaineers.

[2]   C. SCAPOZZA, F. BUCHER, P. AMANN, W.J. AMANN, and P. BARTELET, 2004. The temperature and density dependent acoustic emission response of snow in monoaxial compression tests, *Annals of Glaciology*, **38**, 291-298.

[3]   R. A. SOMMERFELD, and H. GUBLER. 1983. Snow avalanches and acoustic emissions. *Annals of Glaciology*, **4**, 271–276.

[4]   W.F. ST. LAWRENCE, T.E. LANG, R.L. BROWN, and C.C. BRADELY, 1973. Acoustic Emissions in snow at constant rates of deformation. *Journal of Glaciology*, **12**(64), 144-146.

[5]   W.F. ST. LAWRENCE, 1980. The acoustic emission response of snow. *Journal of Glaciology*, **26**(94), 209-216.

[6]   J.C. KAPIL, P. DATT, A. KUMAR, K. SINGH, V. KUMAR, and P.K. SATYAWALI, 2012. Deformation Induced acoustic emissions from snow under uni-axial loading and controlled temperature environment. *Proceeding of International symposium in Cryospheric Climates Change* (ISCCC- 2012), SASE Manali, India

[7]   A.A. POLLOCK, 1995. Inspecting bridges with continuous emission – inspection details about in-service steel bridges and monitoring weld operations: application guidelines. Princeton Junc tion, New Jersey: *Physical Acoustics Corporation.*

Improved Speech Recognition by Controlling Perplexity

Chitralekha Bhat, Imran Ahmed, Vikram Saxena and Sunil Kumar Kopparapu

TCS Innovation Labs - Mumbai, Tata Consultancy Services, Yantra Park,
Pokhran Road No 2, Thane(W), Mumbai - 400601
e-mail: SunilKumar.Kopparapu}@TCS.Com

ABSTRACT

The penetration of mobile phones into rural India, has made it possible for them to access relevant and current information remotely. Unlike in urban areas, limited English literacy and the lack of penetration of internet in the rural area makes information about daily train services or information about personal banking, out of reach of this population. An ideal solution is a speech based mobile application which can be queried in native natural language to seek information. The user experience of such a speech based application would largely depend on the speed of response, the accuracy and concurrency of the information. The recognition accuracy of an Automatic Speech Recognizer (ASR) is mainly dependent on factors like acoustic modeling (AM) and statistical language models (SLM). For resource deficient languages, generating acoustic models is a challenge. Although building a speech application for a specific domain significantly simplifies the language model, for a natural language interface, this is still a challenge. Given a speech recognition engine, controlling the perplexity of the language model can significantly benefit the overall recognition accuracy of the speech solution. In this paper, we verify this and show how the perplexity can be controlled for a specific example, the railway enquiry, by making use of several attributes with the sole aim of improving the speech recognition accuracies.

1. INTRODUCTION

A survey on automation preferences by Harris Interactive [1] suggests that speech based applications, especially applications with natural language interfaces are more appealing when it comes to information enquiry. Assuming such a study is applicable to Indian scenario, with its own unique challenges [2], such as linguistic diversity, background noise, technology adaptation by rural population, speech enabled-automated information dissemination mode becomes inevitable. Although spoken dialog based IVR systems have been tried out for Indian languages, a lot desires to be be improved in terms of speech recognition, noise handling, channel variations for actual commercial implementation to see the light of the day. A speech based mobile application that accepts queries in the form of natural spoken speech in Indian language emerges as the most desired solution. Given that the recognition accuracies of state of the art ASR's for Indian languages are low on account of being resource deficient in terms of training data, building a native mobile application is all the more challenging. Moreover, enabling a full fledged ASR with elaborate language models on a mobile phone with its limitations on processing power and memory places constraints on the speed and accuracy of response, thereby impacting the user experience. In our current work, using a limited deployed speech based railway enquiry system, we first explore the impact of perplexity on recognition accuracies

and then describe a methodology which can be used to decrease the perplexity and thereby improve recognizer accuracy by bringing an element of adaptiveness using meta information that is available. The rest of the paper is organized as follows, in Section II, a review of the work done on adaptive Language Models and its impact on perplexity is presented. In Section III, a case study on Rail Jankari, the specific application under consideration, Section IV presents the experimental setup and results. Conclusion is presented in Section V.

2. ADAPTIVE LANGUAGE MODELS AND PERPLEXITY

Statistical language model is intended to capture the regularities of natural language, an estimate of probability distribution of linguistic units like words, word sequences or sentences. Perplexity when considered as a function of language, estimates the entropy or complexity of the language corpus. A reduction of 5% in perplexity is generally not significant practically; a 10%-20% reduction usually leads to some improvement in the application performance and a reduction of 30% or more provides significant improvement [3].

Language model adaptation harnesses the available a priori information regarding the recognition task. While maintaining a sufficient representation of the domain, it would also need to cater to potential variations. The three major philosophies based on which adaptation is carried out are (i) model interpolation (ii) constraint specification or (iii) meta-information extraction [4]. Several methods have been proposed for adaptation of SLM over the past three decades. Cache based-cross domain adaptation was first introduced by Ronald Kuhn [5]. In some of their work [6,7], Ronald Kuhn et. al. did report reduction in perplexity. In [8] cache-trigram-language-model (CTLM) applied on dictation application, exploits the information in the partially dictated document to adapt the language model, reporting a reduction in perplexity by 23%. Dimensionality reduction using technique of latent semantic analysis in order to capture the most salient correlations between specific combinations of words on one hand and clusters of documents on the other, when combined with n-gram a perplexity reduction of 30% was reported by [9]. In [10], LM adaption was done using Topical Mixture Models (TMM) that dynamically explore the long-span latent topical information. Contemporary newswire texts and in-domain automatic transcripts were used to build the adaptive LM for Mandarin news broadcast recognition, claiming promising results in perplexity and character error rate reductions. Interpolation of a baseline LM (ILM) using small human generated literal and/or machine generated semi-literal such as "um", "ah" so as to be applied on quasispontaneous speech during medical dictations, showed improvement in perplexity and recognition results when compared to the baseline LM [11]. Ikbal et. al.[12] propose exploiting the relationship that exist mostly in spoken dialog based applications, between named entities spoken across dialog states which is in a manner of speaking adaptation of the language model at each node. Another novel method proposed for Chinese speech recognition used data from web search as adaptation data and used latent semantic analysis (LSA) to extract the knowledge from the web to adapt into a well trained model [13], perplexity reduction by 13% was achieved by this method.

In this paper, we describe a specific recognition task in hand namely that of enquiring information related to trains in India. We first describe the perplexity of the speech recognition task and show how the perplexity can be reduced by exploiting the domain information. We later show that this results in an increased recognition accuracy.

3. RAIL JANKARI - A CASE STUDY

Rail Sampark [14] is a service run by the Indian Railways [15] for railway enquiry. The 24 x 7 service is powered by call centre agent support in eleven Indian languages. According to Indian Railways, the Rail Sampark service recorded 292 million calls in the year 2012 which translates to about 0.8 million calls every day [16]. The SMS based enquiry services introduced recently, failed to make a significant dent in the calls to the call center due to low English literacy levels in rural India as well as due to the strict SMS format of the query leaving several queries unanswered.

This calls for a speech enabled railway enquiry system for practical use by Indian population, given the diversity in language, expected call volume and the need. With this scenario in view, a mobile application that allows the user to query, in speech, in a language of his preference in the natural form is ideal. However,

given the constraints of a mobile phone, a native, natural language based railway enquiry application may not provide acceptable accuracies. Even for querying the Arrival or Departure of a train at a particular station, there are more than ten different ways of enquiring in Hindi language. Considering the long distance trains plying through the city and suburbs of Mumbai, around 400 trains with a total of roughly 1200 stations on their route, the size of the text corpus to generate the language model is huge enough to pose serious processing challenges on a mobile phone environment. Our experiments were directed towards understanding the behaviour of the recognizer with reduction in perplexity and the methods that could be used to achieve reduced perplexity in order to enhance the recognition accuracies in terms of word error rates (WER). As a specific case study, information regarding the Arrival (or Departure) of a train at a particular station as well as seat availability on a particular train between any two stations is being considered. Here, we define perplexity as the number of train names along with its variations, which are eligible for for recognition. Availability of the below information would enable reducing the perplexity of the trains and hence assist in building the language model dynamically.

1. Global Positioning system (GPS) - gives the exact location of the mobile phone user. Language model can be built only for those trains passing through stations within a selected distance from the user location. Selection of stations would also be based on the number of trains passing through the station, bigger the number, more important the station and hence should be in the language model.

2. Time/Day of enquiry - further, based on the time of enquiry, for Arrival (or Departure), trains arriving (or departing) from the selected stations (from Step 1) within a fixed time duration on a that particular day of the week, will only be included in the LM.

3. Train frequency - more weightage could be given to daily trains in comparison to non-daily trains.

4. Information from Web - information regarding popularity of trains can be garnered by analysing data from publicly available forums, blogs and seat availability on a particular at a given point in time.

The main focus of the paper is in using points 1 and 2 to arrive at a reduced perplexity of the trains that need to be recognized and using this information to dynamically build language model.

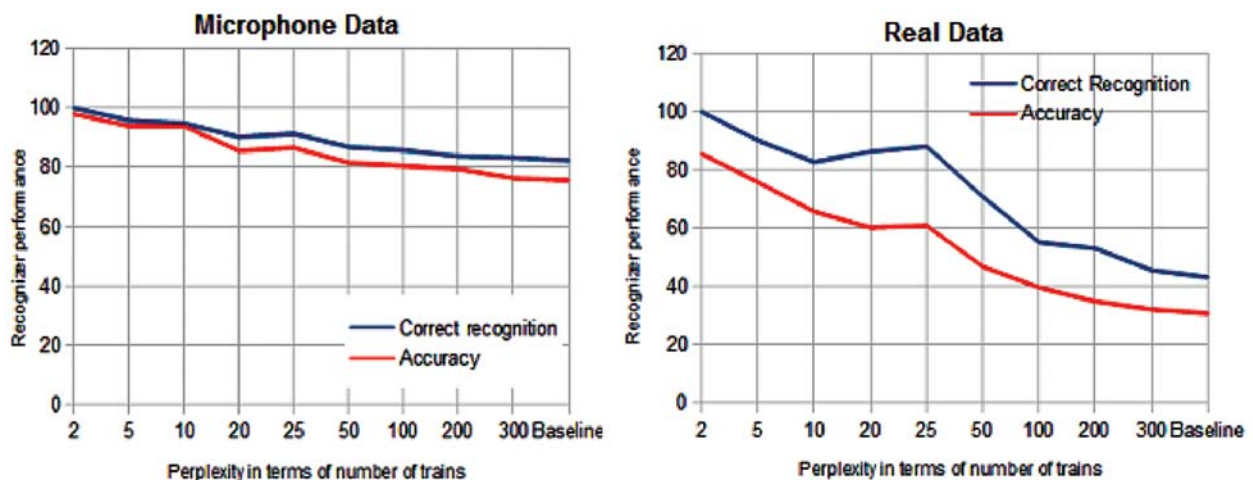Fig. 1. Perplexity in terms of train numbers for microphone data and real data.

4. EXPERIMENTAL SETUP AND RESULTS

Initial set of experiments were conducted to determine the ideal pruning in terms of number of trains to be included in the LM to achieve good recognition. Experiments were conducted with both data collected using (a) a microphone (16 kHz, 16 bit) under clean conditions, wherein ten speakers uttered the names of

ten different trains and (b) real telephonic data (8 kHz, 8 bit) from users of the limited deployed system in our laboratory. Step wise perplexity pruning was done on a baseline LM of four hundred trains. Figure 1 depicts the ASR recognition for different perplexity (x-axis) for the two sets of spoken data. The correct recognition and accuracy is computed as follows. Let

X → Total number of utterances evaluated

x → Number of utterances correctly recognized

y → Number of utterances not recognized user is asked to repeat

z → Number of utterances wrongly recognized

Correct Recognition   = $x/(x+z)$.

Accuracy   = x/X.

Note that $x + y + z = X$, and correct recognition is always greater that or equal to the accuracy. It can be seen that a perplexity of twenty five or fewer trains gives acceptable recognition accuracies. Note that with some amount of post processing, the recognition results can be further improved. Further, our endeavors are towards scientifically reducing the perplexity of the baseline LM (400 trains) to a number of 25 or less trains.

As a case study, assume a person is using the railway enquiry system application from Dombivali, a suburb of Mumbai, with geo-locational coordinates 19.21683,73.088086. Figure 2 shows the five long-distance train stations namely - Kalyan Junction, Thane Junction, Panvel Junction, Bhiwandi Road and Diva Junction that are closest to this location in terms of distance.
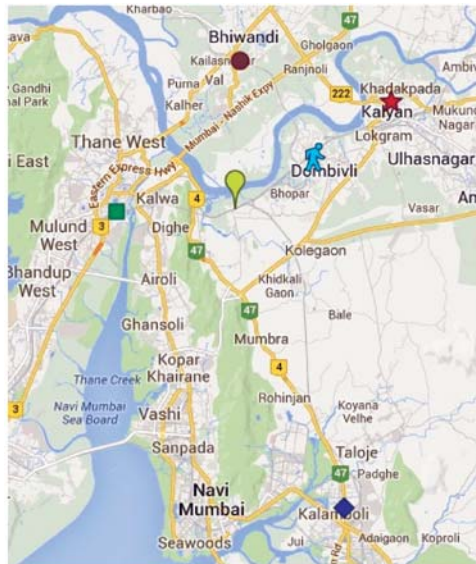
Fig. 2. A map of the user geo-location and nearest five stations.

The total number of trains passing through these stations, which are in the vicinity of the user location is 252; Clearly this is significantly less than the total number of trains (400) passing through the entire Mumbai railway network. The reduced perplexity of the trains enhances the recognition accuracy of the ASR. However, this alone is not sufficient as seen earlier, a perplexity of 25 or less trains results in the desired level of recognition accuracy (90+). In addition to the number of trains passing through the stations within a certain distance from the location of the person querying, we also consider the time of the day of the query to further prune the LM. Table 1 gives the number of trains that pass through the stations near the user in a set period of time. For example, in a twenty four hour span all the 252 trains pass through these stations.

However if one considers only a time duration of 12 hours, then the number of trains is either 110 or 142 depending on the time. Clearly if the user queried between midnight and 12 noon (0000-1159) then one needs to consider only 110 trains to be the list of trains from which to recognize. Table 1 shows that if we consider only the trains which are likely to pass through the stations in a period of 2 hours around the time of the query then the number of trains that need to be considered for recognition are close to the desired perplexity of 25.

Table 1. Time slot wise breakdown in perplexity in terms of number of trains.

0000-2359 252 trains											
0000-1159 110 trains						1200-2359 142 trains					
0000-0559 67 trains			6000-1159 43 trains			1200-1759 57 trains			1800-359 85 trains		
0000-0259 25 trains		0300-0559 42 trains	0600-0859 26 trains		0900-1159 17 trains	1200-1459 35 trains		1500-1759 22 trains	1800-2059 33 trains		2100-2359 52 trains
0000-0159	0200-0359	0400-0559	0600-0759	0800-0959	1000-1159	1200-1359	1400-1559	1600-1759	1800-1959	2000-2159	2200-2359
20	13	34	16	14	13	28	14	15	22	37	26

Note that the desired perplexity in terms of the trains is achieved by considering a time window of about two hours from the actual time of query of the user. So by looking for only trains which pass through the stations that are close to the geo-location of the user, one can be assured of high speech recognition accuracies.

5. CONCLUSION

A speech based mobile application for day to day transactions such as railway information, emerges as an inevitable solution for the Indian scenario because of mobile technology penetration and adoption, linguistic diversity, noisy background and technology challenges. The recognition accuracy of an ASR is mainly dependent on acoustic models and statistical language models. For resource deficient languages, generating acoustic models is a challenge. Improving recognition through a reduction in perplexity for our specific task of railway enquiry by using meta-information such as the geo-locational coordinates of the user and day and time of the enquiry has been explored.

6. REFERENCES

[1]   NUANCE. [Online]. Available: http://www.nuance.com

[2]   C. JADHAV, I. AHMED, M. PANDHARIPANDE, T. VENKATAKRISHNA, B. S. MITHUN, V. KULKARNI, C. BHAT, A. PANDE and S. KOPPARAPU, 2012. Challenges in enabling speech as a service channel for Indian scenario, in Regional International Telecommunications Society India Conference, New Delhi.

[3]   R. ROSENFELD, 2000. Two decades of statistical language modeling: where do we go from here?, Proceedings of the *IEEE*, **88** (8), 1270,1278.

[4]   JEROME R BELLEGARDA, Statistical language model adaptation: review and perspectives, *Speech Communication*, **42** (93), 0167-6393.

[5] ROLAND KUHN, 1988. Speech recognition and the frequency of recently used words: A modified markov model for natural language. In *12th International Conference on Computational Linguistics*, 348–350, Budapest.

[6] ROLAND KUHN and RENATO DE MORI, 1990. A cache-based natural language model for speech reproduction. *IEEE Transactions on Pattern Analysis and Machine Intelligence*, **12**(6), 570–583.

[7] ROLAND KUHN and RENATO DE MORI,1992. Correction to: A cache-based natural language model for speech reproduction. *IEEE Transactions on Pattern Analysis and Machine Intelligence*, **14**(6), 691–692.

[8] F. JELINEK, B. MERIALDO, S. ROUKOS and M. STRAUSS, 1991. A dynamic language model for speech recognition. In Proceedings of the workshop on Speech and Natural Language (HLT '91). Association for Computational Linguistics, *Stroudsburg*, PA, USA, 293-295.

[9] J.R. BELLEGARDA, 2005. Latent semantic mapping: dimensionality reduction via globally optimal continuous parameter modeling, Automatic Speech Recognition and Understanding, *IEEE Workshop*, **127** (132), 27-27.

[10] B. CHEN, 2005. Dynamic language model adaptation using latent topical information and automatic transcripts, Multimedia and Expo, 2005. ICME 2005. *IEEE International Conference*, **4**, 6-8.

[11] SAVOVA, GUERGANA, SCHONWETTER, MICHAEL, PAKHOMOV and SERGEY, 2000. Improving language model perplexity and recognition accuracy for medical dictations via within-domain interpolation with literal and semi-literal corpora, In *ICSLP*, **1**, 206-209.

[12] S. IKBAL, O.D. DESHMUKH, K. VISWESWARIAH and A. VERMA, 2010. Utilizing relationships between named entities to improve speech recognition in dialog systems, Spoken Language Technology Workshop (SLT), *IEEE*, **55** (60), 12-15.

[13] T QIN GAO, XIAOJUN LIN, and XIHONG WU, 2006. Just-in-time Latent semantic adaptation on language model for chinese speech recognition using web data, Spoken language technology workshop, *IEEE*, **50** (53), 10-13

[14] 139 - rail sampark. [Online]. Available: http://pib.nic.in/newsite/erelease.aspx?relid=49211

[15] Indian railway. [Online]. Available: http://www.indianrailway.Com/

[16] Calls on railways IVRS. [Online].Available: http://zeenews.india.com/news/nation/railways-enquiry-no-139-got-record-19-20-cr-calls 845173.html.

Development of Sonar Device for Fuel Subassembly Vibration Measurement in PFBR

P. Anup Kumar, R. Vidhyalakshmi, M. Thirumalai,
S. Chandramouli and V. Prakash

Fast Reactor Technology Group, Indira Gandhi Centre for Atomic Research,
Kalpakkam - 603102, INDIA
e-mail: panup@igcar.gov.in

ABSTRACT

The core of Prototype Fast Breeder Reactor (PFBR) consists of 1758 subassemblies supported at the bottom on the grid plate sleeves. There are 181 fuel subassemblies in the core and coolant flow through the maximum rated subassembly is 36 kg/s. Due to better thermal and neutronic properties, sodium is chosen as the coolant for FBRs, and it flows axially from the bottom of the subassembly to top and it is in highly turbulent regime. This turbulent flow can excite flow-induced vibration of fuel subassembly which can cause failure of the fuel pin clad tubes from fatigue, wear and vibration induced fretting. Excessive vibration of fuel sub-assembly can also results in reactivity noise, fatigue or rattling. To understand the vibration characteristics of fuel subassembly and fuel pins, studies were conducted on full scale experimental fuel subassembly in water test rig, and the design of PFBR subassembly was qualified. However it is planned to measure the amplitude and frequency of vibration during commissioning of PFBR.

Since measurement has to be carried out in high temperature sodium environment, conventional contact type sensors such as accelerometers, strain gages etc cannot be employed for vibration measurement. Non-contact measurement technique using ultrasound waves was planned to be developed for vibration measurement. Extensive experiments were carried out in various test facilities and ultrasonic vibration measurement technique was established and demonstrated. Ultrasonic transducer transmits sound waves at ultrasound frequencies and pulses reflected by the target are detected as echoes. The time delay between each transmitted and echo pulse is used to accurately determine the sensor-to-target distance. Movement of subassembly causes a variation in the time delay and thus the time delay between the transmitted pulse and received echo will be a representation of the subassembly movement or vibration. The crown region of fuel subassembly acts as the orthogonal target to the ultrasound waves and extraction of vibration data is carried out using algorithm developed in LabVIEW platform.

A device named, SONAR which works on ultrasonic technique was designed and a prototype device is manufactured. The device comprises of ultrasonic sensors of 5 MHz frequency, its electronics and a drive mechanism for positioning the sensors. The device was tested for its performance in water and sodium and based on the experimental results, SONAR device for PFBR is manufactured. In PFBR, the device will be located in the central canal of control plug and the entire core region can be accessed by suitable rotation of plugs. This paper discusses the details of the ultrasonic technique, SONAR device and experiments carried out in water and in sodium with prototype device and its results and conclusion.

P. Anup Kumar, R. Vidhyalakshmi, M. Thirumalai, S. Chandramouli and V. Prakash

1. INTRODUCTION

PFBR core consists of 1758 subassemblies vertically supported on the grid plate including 181 fuel subassemblies [1]. Coolant sodium flows axially from the bottom of the subassembly to top and is in turbulent regime, in order to increase the heat transfer performance. Fuel subassembly is prone to flow-induced vibrations (FIV), which can result in the failure of the fuel clad tubes from fatigue, wear and vibration induced fretting [2]. Excessive vibration of fuel subassemblies may also lead to reactivity fluctuations. It is planned to measure the subassembly vibrations in PFBR during commissioning. It is very difficult to carry out such measurement under sodium at high temperature, using conventional contact type vibration sensors such as accelerometers, strain gages etc.

By using high temperature non-contact type ultrasonic (US) sensor, it is planned to measure the subassembly vibration under sodium. As the ultrasonic sensor transmits and receives sound waves in order to detect the vibration of fuel subassemblies, it is analogous to the SONAR (SOund Navigation And Ranging) used for detecting the target under water, hence it is named as SONAR device. Measurements are planned in PFBR during the isothermal run at 2000C with dummy fuel subassemblies loaded in the core [3].

Extensive experiments were carried out in various test facilities in Fast Reactor Technology Group of Indira Gandhi Centre for Atomic Research for establishing the technique. Based on the experimental results, conceptual design of SONAR device (Fig.1) for PFBR was arrived at and a prototype device was designed and fabricated. The prototype SONAR device was tested in water and in sodium for assessing its performance and manufacturing of PFBR SONAR device is in progress. This paper discusses the details of the device, test procedure, results and discussion and conclusion.

2. ULTRASONIC TECHNIQUE AND SENSOR

Ultrasonic sensors in pulse echo mode is used for the detection of subassembly movement. The time of flight technique is used to detect the position of the subassembly at an instant of time. The device focuses the sensors at the target and measures the time delay between each emitted and echo pulse to accurately determine the sensor-to-target distance. So continuous triggering of the sensor yields the time of flight corresponding to the subassembly movement. The movement of the subassembly will cause a variation in the time delay and thus the time delay between the transmitted pulse and received echo will be a representation of the subassembly position with respect to the sensor. By suitably extracting the time of flight data, it is possible to measure the subassembly movement/vibration [3].

Fig. 1. SONAR Device.

Table 1. Ultrasonic sensor details

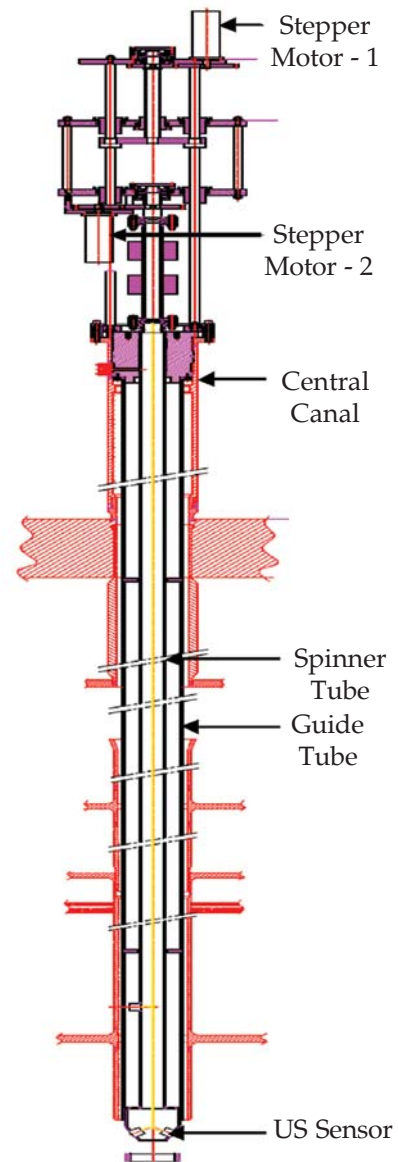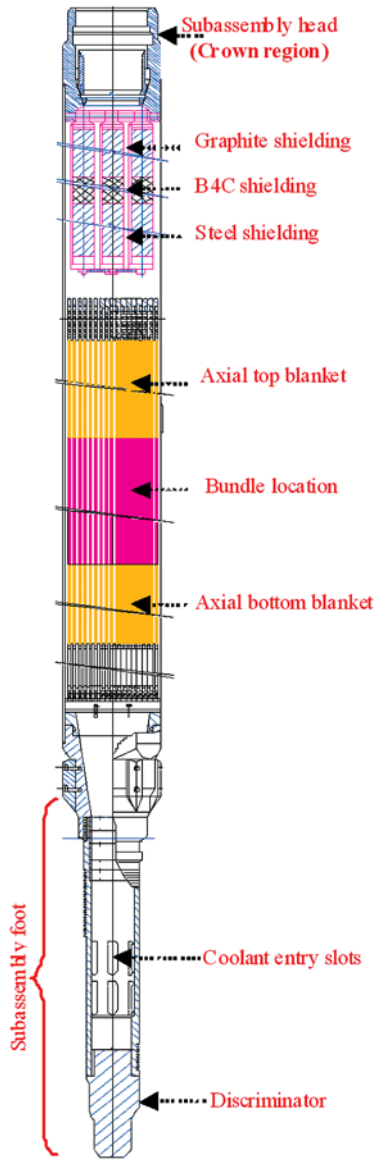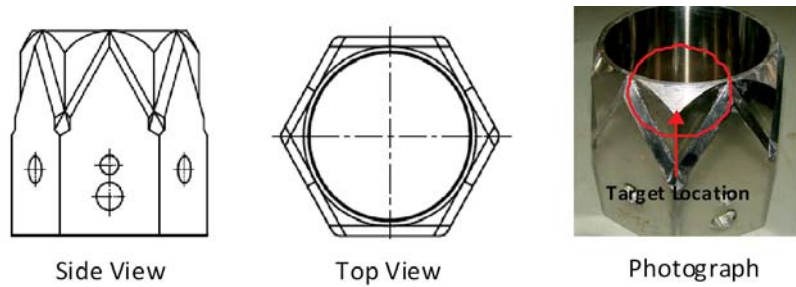| SN.	Description	Parameter
1.	Sensor Material	PZT
2.	Frequency	5 MHz
3.	Diameter	30 mm
4.	Casing Material	Nickel
5.	Operating temperature	2200 C
6.	Operation mode	Pulse echo

Fig. 2a. PFBR Subassembly
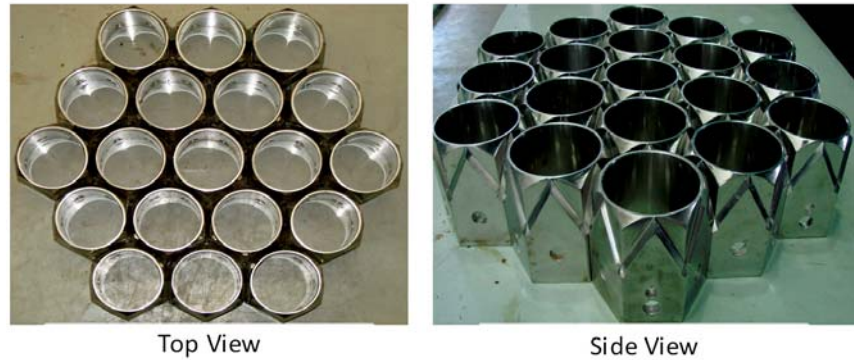

Figure 2b. PFBR Subassembly crown region.

Figure 3. Cluster of PFBR Subassembly crowns.

Ultrasonic sensor used in SONAR device houses a piezoelectric transducer made up of PZT (Lead Zirconate Titanate) crystal that vibrates at ultrasonic frequency of 5 MHz. The high temperature ultrasonic transducer for SONAR device was developed at IGCAR and Table 1 depicts the transducer details. The ultrasound waves emitted by the sensor are reflected by the target which is the subassembly crown region. Figure 2a shows the schematic of PFBR fuel subassembly and Fig.2b shows the crown region. Figure 3 shows a cluster of PFBR subassembly top crown. Ultrasonic trans-receiver is used to excite the ultrasonic transducer, which in turn transmits ultrasound waves towards the target. The received echo is amplified and filtered and recorded using high frequency data acquisition system. The recorded signal is analyzed and processed to extract the vibration signal using algorithm developed in LabVIEW platform.

3. DESCRIPTION OF SONAR DEVICE

SONAR device comprises of a mechanical arrangement to mount ultrasonic sensor over the sub-assembly focussing the crown region, Data Acquisition System (DAS) and a motion controller consisting of stepper motors and its electronics to control the movement of the device. Fig.1 shows the schematic of PFBR SONAR device. The mechanical assembly holds the ultrasonic sensor at an inclined position facing the crown region of the subassembly. Three ultrasonic sensors are used in PFBR SONAR device. Two inclined sensors (one spare) at the bottom will be focused on the target subassembly crown region, and the third one will be focused on the central canal shroud tube for detecting the self movement of SONAR device. The device consists of a guide tube and a spinner tube, and transducer holder is attached to the spinner tube. Guide tube is stationary while the spinner tube has both translational and rotational movement. SONAR drive

mechanism is responsible for the movement of the device in 'vertical' and 'theta' (azimuthal) axis. The top part of the device is equipped with two stepper motors for sensor positioning. Stepper motor-1 (SM1) is used to move the device in vertical direction whereas the Stepper motor-2 (SM2) is used to rotate the spinner tube.

4. TESTING OF PROTOTYPE SONAR DEVICE

A prototype device, similar to PFBR SONAR device was designed and fabricated for performance testing in water and sodium. Fig.4 shows the drive mechanism upper part of the prototype SONAR device. Stepper Motor-1 (SM-1) is used for vertical movement and Stepper Motor-2 (SM-2) for spinner tube rotation. The objective of the testing was to assess the performance of the device in water and in sodium, qualification of ultrasonic sensors and testing of ultrasonic electronics and data acquisition system. The details of the testing are summarized in the following subsections.
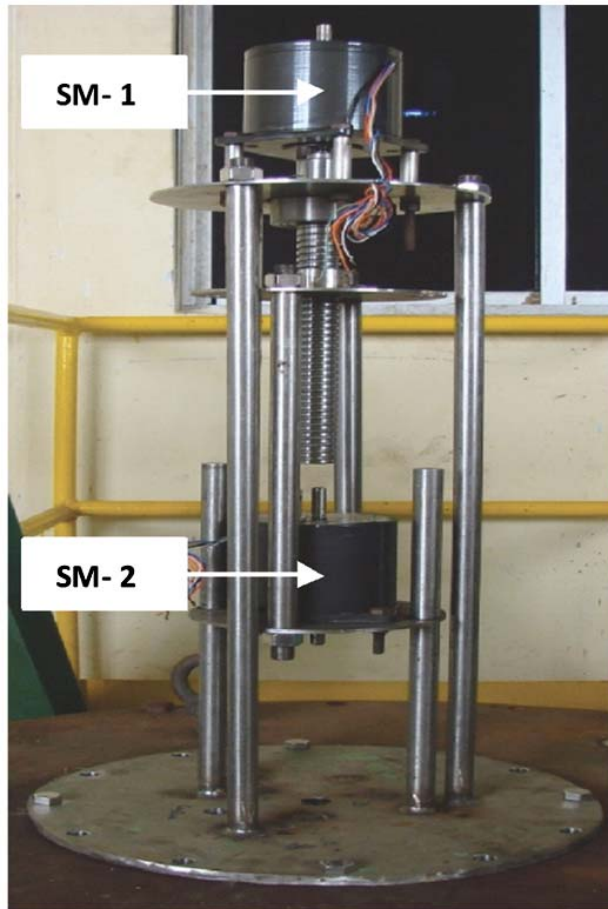
Fig.4 . Prototype Device

4.1 Testing in water

The prototype device was installed in a test vessel filled with water. Figure 5 shows the sensor (S1) focussed on the target in the water test setup. For testing in water, configuration consisting of a target subassembly crown region welded to a SS rod was suspended from the top flange. Ultrasonic waves are generated using the pulser and the received echoes were monitored and recorded. The movement of the target is achieved using an electro-dynamic exciter connected to the assembly.

Fig. 5. Sensor focussed on crown region

4.2 Testing in sodium

Testing of the device in sodium was carried out in sodium Test pot-1of SILVERINA test facility. The test pot is provided with all the necessary instrumentation such as thermocouples, level probes and leak detectors. Figure 6 shows the test setup. Leakage of cover gas is prevented by the O-rings and oil seals. The movement of the transducer inside the vessel was done using the central spinner tube. Fuel subassembly crown region is used for simulating the target subassembly suspended from the top flange and the excitation of the target is done using an electro-dynamic exciter (Fig.7). Measurements were carried out in sodium at 2000C.
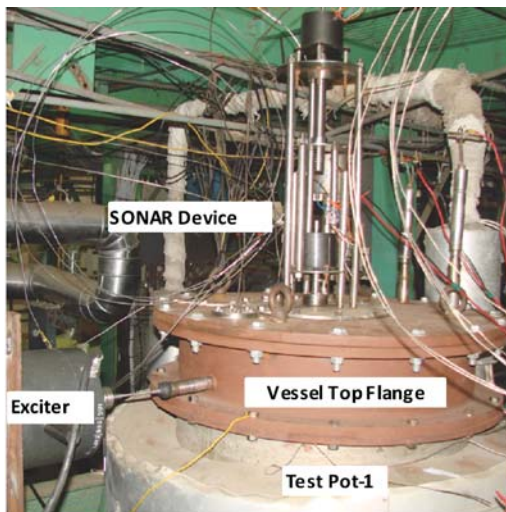
Fig.6 . Test setup for sodium testing   Fig.7 . Electro-dynamic exciter setup for exciting target
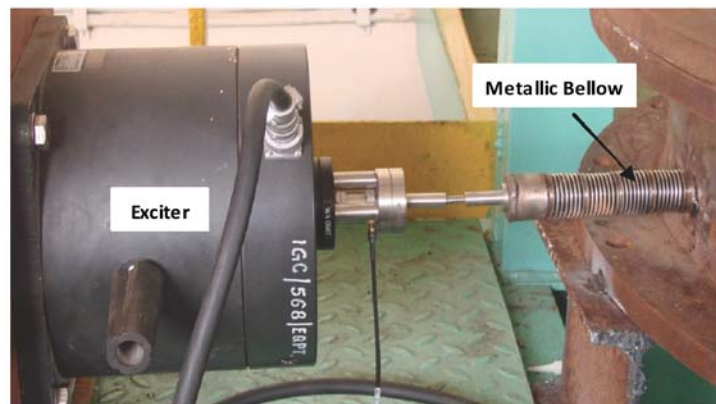
5.   RESULTS AND DISCUSSION

The ultrasonic sensors were excited using the trans-receiver units and the signals were recorded using a high frequency data acquisition system. Using the code written in LabVIEW software, vibration signals were extracted for the recorded data. Figure 8 shows a typical vibration signal extracted from ultrasonic sensors during testing in water for an input frequency of 2 Hz.

It can be clearly seen that the input vibration time signal is faithfully recovered from the train of ultrasonic transmitted pulse and received echoes using the developed software. The frequency spectra of vibration is also calculated from the signal (1.98 Hz) and is plotted (Fig.8). The experiment was repeated for different input frequencies. Figure 9 shows a typical vibration signal extracted from ultrasonic sensors during testing in sodium. The system measured a frequency of 2 Hz from the ultrasonic signal for an input vibration signal of 2 Hz. Denoising technique for excitation frequencies above 4 Hz is under development as echo is found to be distorted.
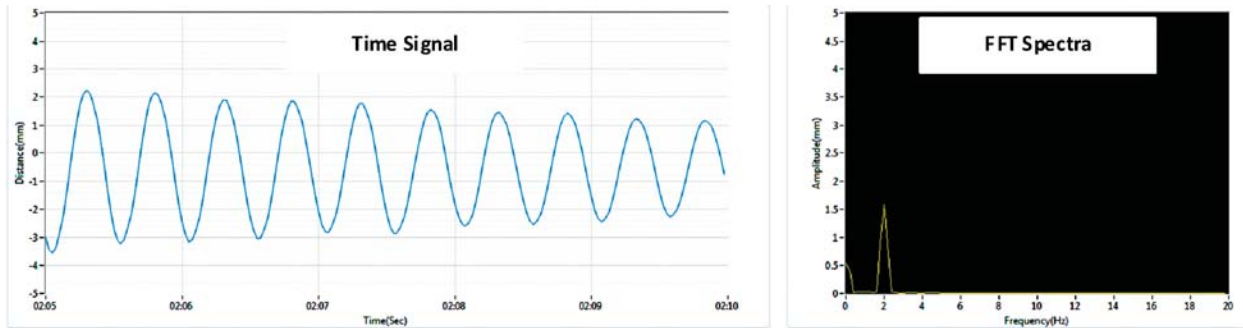
Fig. 8. Extracted vibration time signal and spectra (water).

6. CONCLUSION

Development of SONAR device for fuel subassembly vibration measurement in Prototype Fast Breeder Reactor is in progress. Extensive experiments were carried out in various facilities and the technology was demonstrated. Based on the experimental results, a prototype device was designed, fabricated and tested in water and in sodium. The device is capable of measuring subassembly vibrations faithfully. For high frequency vibration measurements, studies are in progress to improve the detection sensitivity using advanced signal processing techniques and surface profiling. Fabrication of project PFBR SONAR device is in the final stage of completion.
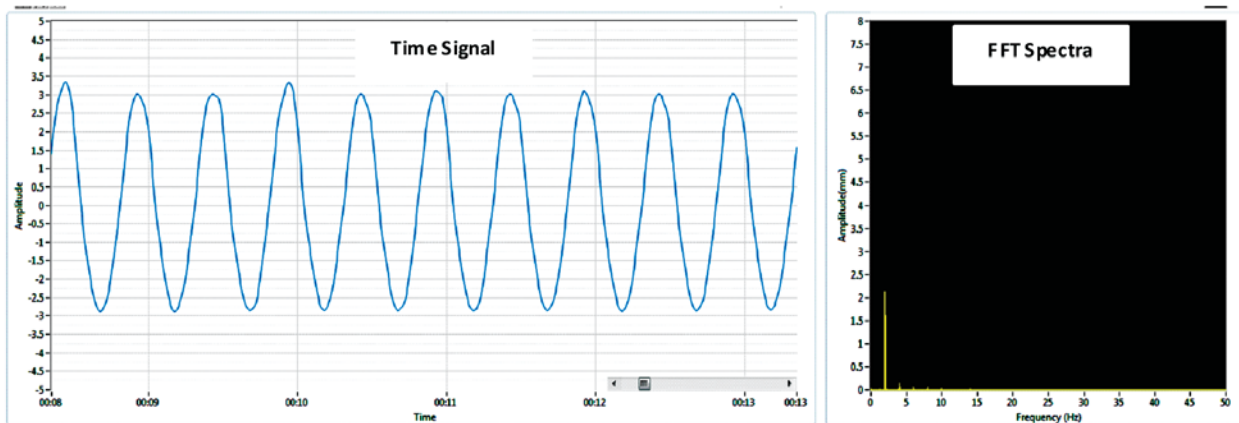
Fig. 9. Extracted vibration time signal and spectra (sodium)

7. REFERENCES

[1]   S.C. CHETAL, *et. al.* 2006. The design of prototype fast breeder reactor, *Nuclear Engineering and Design*, **236**, 852-860.

[2]   V. PRAKASH *et. al.*, 2011, Experimental qualification of subassembly design for Prototype Fast Breeder Reactor, *Nuclear Engineering and Design*, **241,** 3325-3332.

[3]   R.RAMAKRISHNA., *et al.*, 2010. NDE Technique for Reactor Core Vibration Measurement in FBRs, *NDE 2010*, Kolkatta, WB.

Bioacoustic analysis of certain Herpetofauna of the Thar Desert and Central Aravalli of Rajasthan, India

Sharma, K. K., Sharma Vivek, Sharma Neha and Mathur Shikha
Biodiversity Research Laboratory, Department of Zoology
MDS University Ajmer-305009, Rajasthan India
e-mail: kksmds@gmail.com

ABSTRACT

Among herpetofauna (Amphibians and Reptiles) anuran (frogs and toads) vocalization is well organized and produced discrete calls used for communication. However, most reptiles (Testudians, Saurian, Serpents and Crocodilians) produce sound which are not similar to anuran calls. Some snakes produce hissing sounds. Some members of gekkonidae family of lizards and viparidae family of snakes produce sound by rubbing body parts. The vocalization of anurans includes lungs, vocal chords, vocal sacs, trachea, buccal cavity and nostril, in which air flow over the vocal chords in combination with other vocalization components produces the calls. While some snakes have specialized mechanisms for sound production, most species use airflow through the anterior respiratory tract to produce sound. These sounds may be produced by either exhalatory or inhalatory airflow. This airflow in snakes appears to be produced solely by localized movements of the ribs, a system referred to as the costal pump. In some snakes, the defensive hisses exhibit a simple temporal pattern termed a hissing. These hissings are characterized by an initial exhalatory hissing, and a brief pause and then an inhalatory hissing then a second pause or rest period. In anurans vocal sacs enhances transmission of sound. Bioacoustics frequencies, intensities and time intervals of calls vary in different species of different families of herpetofauna. The present study includes methodology of call analysis and call characteristics of anurans (Duttaphrynus melanostictus, Duttaphrynus stomaticus, Fejerverya limnocharis and Microhyla ornata); lizard (Varanus bengalensis) and snakes (Naja naja, Daboia russelli and Echis carinatus). The spectrographic analysis of sound produced by the herpetofauna under the reference show species specific characteristics. This can be studied under the broad heading of Sono-taxonomy i.e. sound based taxonomy.

Sono-taxonomy: The acoustic patterns based grouping of anuran species (sono-taxonomy) does coincide with the traditional taxonomy that is based mainly on morphology (external and internal). However, bioacoustics characteristics can be used as supporting features to the existing taxonomy so that sibling and morphologically similar species can be distinguished with their acoustic specificity. Bioacoustics characteristics of a species can be used not only in identification but also in monitoring of a species in dark, dense and remote areas where visual encounter does not work well.

1. INTRODUCTION

Animals are able to produce extraordinarily diverse vocal signals. They produces the sounds of various intensities and frequencies including the below human hearing rang (infra sounds), human audible range

---

(20Hz to 20 KHz) and also at the ultrasonic ranges (> 200 KHz) (Capranica, 1965; Glaw and Vences, 1994; Narins et al., 2004). Among vertebrates, vocalization is highly developed in anurans, birds, bats, primates, cetaceans, and dolphins while in reptiles it restricted to only certain chirps or hissing sort of acoustics signal. In anurans and birds the primary purpose of vocalization is advertisement. Sound production by animals is primarily a method of advertising the presence of one individual to other conspecifics. Secondarily includes as avoidance of predators and maintenance of territories (Rheinlaender et al., 1979).

The vocalization of frogs have provided a means for studying acoustic communication and, together with other aspects of courtship and mating, have presented the evolutionary biologists with a wealth of material for studies on sexual selection. Vocalization behaviors of anuran amphibians are universally dimorphic sexually. Usually, only male frogs give an advertisement call, while female frog calls are limited to a soft and simple release call which is specifically suppressed during mating. In a very few species female frogs also give mating vocalizations (Duellman and Trueb, 1986).

Species identification in case of anurans includes lots of collection, killing and preservation to confirm only one single anuran species. Several groups of anurans display high levels of morphological homoplasy, which often makes it virtually impossible to distinguish between closely related species on the basis of morphological parameters. Also, in case of dark or dense canopy cover where the visibility is very poor or negligible, it is difficult to observe and identify the anuran species. Advertisement calls characteristic patterns are highly species specific and have great potential to reveal these types of controversial cases. In spite of all these problems specifically for the identification of anuran species, the bioacoustics analysis of advertisement calls can be a good solution.

Most animals communicate using sound, at the time of danger or stress conditions in form of short sequences those known as alarming calls or signals. On the other side long sequences are generated as a part of courtship and known as advertisement calls or mating calls. In many insect and amphibian species (Simmons et al., 2003), they advertise their presence and identity with a single type of utterance which, depends on specific species, might be described as a chirp, click, or whine repeated several times to form a "phrase," with silent gaps between phrases. The utterance, its repetition rate, and the number of repetitions in a phrase are characteristic of species (Sales, 1972; Simmons et al., 2003). Utterances within a species are observed by (Sales, 1972; Gourbal et al., 2004).

Among anurans species specific vocalization of advertisement or matting calls was developed during evolution (Duellman and Trueb, 1986); which helps in successful and higher probability to find a conspecific mate in invisible conditions such as dense foliage or in complete darkness and also helps in search the direction and distance of mate too (Capranica, 1977). Now these days anuran advertisement call analysis based studies are attracted the researchers due to its eco-friendly approach. These types of studies leads to breeding behavior and sound based identification along with monitoring of the anuran population and also help to make conservation strategies (Sharma, 2005).

Vocalization is a conspicuous anuran communication behavior usually used for reproductive and territorial purposes (Duellman and Trueb, 1994), but some frogs may emit different calls during courtship and defense against predation (Wells, 2007). Bogert (1960) defined the sound produced by frogs during attack of predators as "distress call," and its function seems to be alerting neighbors to danger (Wells, 2007). Forti and Bertoluci, (2012) described the characteristics of distress call of *Hypsiboas faber* (Anura: Hylidae) during a predatory attack of *Liophis miliaris* (Serpentes: Colubridae).

Anuran acoustic communications could also be considered as a characteristic feature for identification due to several reasons: Males produce characteristic sound (calls) during breeding season; that play an important role in their courtship and reproductive behavior. Their vocal repertoire consists of a small number of species specific stereotyped sounds which, although complex, may be readily synthesized and used as stimuli in playback experiments in field (Roy, 1994). Such a sound based taxonomic identification of anurans not only helps in identification even of sibling species but also provide tools for their population monitoring and conservation (Sharma, 2005 a, b; Sharma, 2009).

Snakes exhibit variety of interactive behaviors with both predators and conspecifics. In this behavioral

expression continuation, sound production is frequently used as a defensive behavior, and there is negligible evidences are available of intra-specific acoustic communication in snakes. The auditory system of snakes can respond to both ground-borne and air-borne vibrations (Hartline, 1971; Wever, 1978). While some snakes have specialized mechanisms for sound production (Mertens, 1946; Gans and Maderson, 1973; Frankenberg and Werner, 1992; Young, 1997; Young et al., 1999), most species use airflow through the anterior respiratory tract to produce sound (Carpenter and Ferguson, 1977; Greene, 1988).

The present article deals with the call characteristics of the four anurans species *Duttaphrynus melanostictus* (Common Asian Toad), *Duttaphrynus stomaticus* (Marbled Toad) of Bufonidae family; *Fejerverya limnocharis* (Paddy field frog) of Dicroglossidae family and *Microhyla ornata* (Ornate narrow mouthed frog) of Microhylidae family. And hissing characteristics of one lizard species *Varanus bengalensis* (Indian Monitor Lizard) of Varanidae family. Three snake species *Naja naja* (Bi-oscillated Cobra) Elapidae family, *Daboia russelli* (Russell Viper) and *Echis carinatus* (Saw scaled viper) of Viparidae family.

2. METHODOLOGY

Matting calls / advertisement calls of anurans recorded from various parts of Thar Desert and Aravalli mountain ranges of Rajasthan, India during the breeding season of anurans i.e. monsoon. Hissing of snakes and monitor lizard were also recorded at the same time *i.e.* in monsoon.
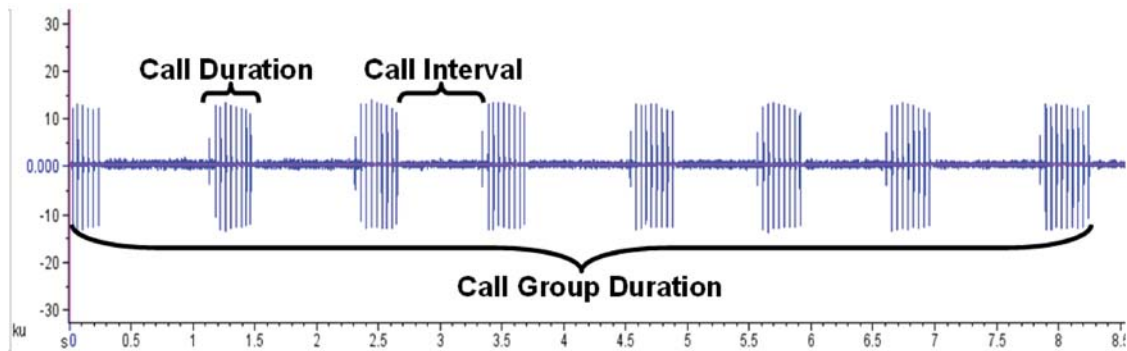

Fig. 1: Call parameters used in the present study: Call group duration, Call Duration and Call interval.
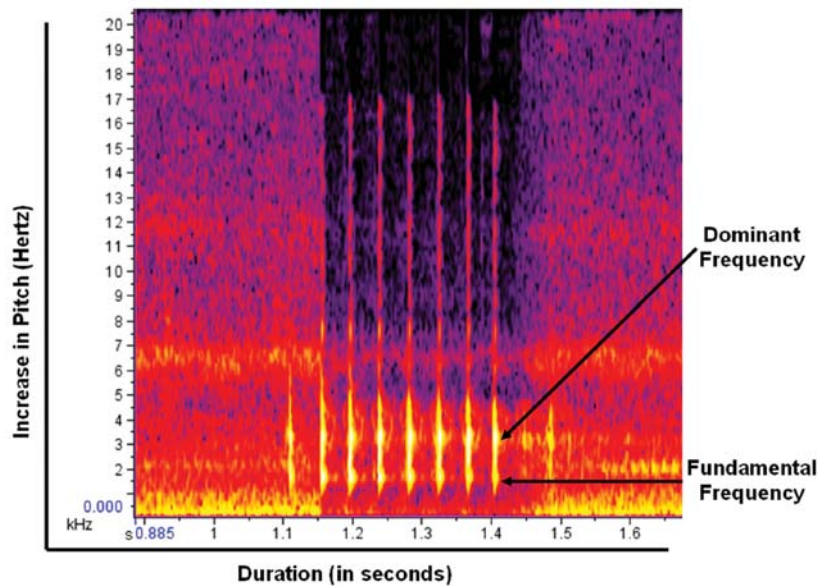

Fig. 2: Fundamental Frequency and Dominant Frequency of a frog call spectrogram.

Vocalization has been studied mainly with reference to communication among the members of a species. Very little is known about the pattern similarities of acoustic communication among different species of a family or among species of different families (sono-taxonomy). A detailed comparative acoustic analysis based on parameters such as number of calls in per call group, call group duration, call group interval, dominant frequency, fundamental frequency, minimum frequency, maximum frequency, harmonics, was carried out, which found in different parts of the Thar desert of Rajasthan and nearby foothills of central Aravalli ranges (Figs 1 and 2). In terms of types of vocal sacs *Duttaphrynus melanostictus, Duttaphrynus stomaticus, Microhyla ornata* are Mono-vocalids; *Fejervarya limnocharis* is Semi-bi-vocalids in nature. While in case of reptiles hissing only dominant frequency, fundamental frequency, minimum frequency, maximum frequency was carried out because there is no clear demarcation of call in hissing pattern (Table 1).

Table 1. Parameters used for the present study: Anuran Calls and Reptiles hissing characterization (+ = Used and - = Not used)

Parameters	Details of Parameters	Anurans	Lizards	Snakes
Call Group Duration	Call group is entire assemblage of acoustic signals produced in sequence from starting to end. It is measured from waveform analyzer screen.	+	-	-
Call Group Interval	Time from beginning of next call group after previous call group. Measured in seconds.	+	-	-
Call Number in Per Call Group	Number of calls in each call group. Measured in numbers n.	+	-	-
Call Duration	Time from beginning to end of one call. Measured in seconds.	+	-	-
Call Interval	Time from beginning of next call after previous call. Measured in seconds.	+	-	-
Fundamental frequency	Fundamental frequency of pulse is oscillations resulting from air passing over the vocal cords and causing them to vibrate. First (lowest-pitched) harmonic usually referred to as the fundamental frequency. Measured in hertz (Hz).	+	+	+
Dominant frequency	Frequency of highest energy sound resulting from resonating of fundamental frequency (or one of its harmonics) with greater emphasis is dominant frequency. This frequency is always a multiple of fundamental frequency. Measured in hertz (Hz).	+	+	+
Minimum frequency	Minimum dominant frequency in pulse or call. Measured in hertz (Hz).	+	+	+
Maximum frequency	Maximum dominant frequency in pulse or call. Measured in hertz (Hz).	+	+	+
Average Power	It is observed in decibel (dB).	+	+	+
Average Entropy	It is observed as μ.	+	+	+

3. GRAPHICAL REPRESENTATIONS OF SOUND

Any acoustic signal can be graphically or mathematically depicted in either of two forms, called *time domain* and *frequency domain* representations. In time domain, instantaneous pressure is represented as a function of time. Signal in time domain is called a *sinusoid* because its amplitude is a sine function of time, characterized by some frequency, which is measured in cycles per second, or Hertz (Hz). Frequency of a sinusoid is easily determined by measuring the length of one period, which is reciprocal of frequency. Amplitude of signal in time domain is measured in pressure units. (Once an acoustic signal has been converted by a microphone

into an electrical signal, amplitude is measured as voltage, which is directly proportional to the sound pressure.) In frequency domain, amplitude of a signal is represented as a function of frequency.

For analysis call characteristics "Sound ruler" (Acoustic analysis Version 0.9.6.0) software was used and for micro-scale analysis of cross sections of spectrograms "Raven Pro 1.4 beta version" (Cornell lab of ornithology) (Charif *et al.*, 2008) was used, spectrum were generated and cross sections views were also compared and also used to find the degree of differences in various observed species of herpetofauna.

4. RESULTS

4.1 Acoustic Analysis

Call characteristics (advertisement / matting calls) of four species were observed. The call characteristics i.e. dominant frequency, fundamental frequency, call duration etc. were found to be highly significant in case of species identification. These properties of calls alongwith the cross sectional view of spectrum of call makes a unique species-specific pattern, which is helpful in species identification of anurans without disturbing them.

- *Duttaphrynus melanostictus* also have median subgular type of external monovocal sac that can be easily spotted during breeding season. Its calls were like strong drumming pattern as "'creo - oo', 'cro - ro - ro - ro - ro' - ……………". *Duttaphrynus melanostictus* prefered to make calls from nearby area of the breeding pool and also changed its direction but intensity to change the direction was very low in comparison to *Bufo stomaticus*. In this species, one individual initiated the calling activity than other joined in as chorus, but within the chorus each individual distinctly advertised its own presence. *D. melanostictus* have the largest call group duration with 17.48 ± 0.51 seconds with an average of 194 ± 11.72 calls in per call group. Call groups were repeated with 2.74 ± 0.19 seconds of call group intervals. During the call groups, call duration was observed as 0.05 ± 0.01 seconds with an average of 0.39 ± 0.01 seconds of call interval. Acoustics analysis of spectrogram showed that *D. melanostictus* produced the call in-between 1636.52 ± 9.28 Hz of minimum frequency and 2325.59 ± 2.78 Hz of maximum frequency. The dominant and fundamental frequencies were found as 2325.59 ± 2.78 Hz and 1162.79 ± 1.39 Hz respectively with an average power of 74 ± 0.32 dB and 2.08 ± 0.02 u of average entropy (Fig. 3).

- *Duttaphrynus stomaticus* have median subgular type of external monovocal sac that can be easily visible during breeding season. It makes call in a particular drumming pattern, which is a general characteristic of most toads of the genus *Bufo*. The call of *Bufo stomaticus* was distinctly softer "cre -

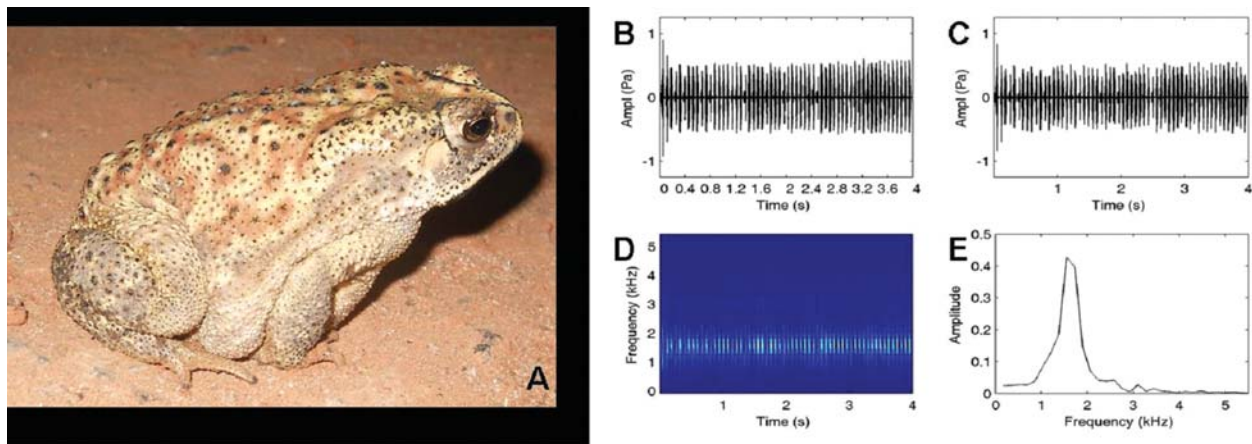

Fig. 3: (A) adult Duttaphrynus melanostictus; (B) Time domain presentation of audio-spectrum; (C) Enlarged view of time domain presentation of audio-spectrum; (D) Frequency domain presentation of audio-spectrum and (E) Cross section of a call of Duttaphrynus melanostictus showing dominant frequency peak.

cre - cre - cre - ...." that can be heard from long distance during the monsoon nights. It usually sits near the water pool and makes the calls; simultaneously it changed its direction of calling to advertise its presence in all possible directions and as far as possible for successful mating. Typically, a single male started the calling than other started emitting chorus. Acoustic analysis of *B. stomaticus* call showed that, it made calls in longer period and in groups. The call group duration measured as 13.03 ± 1.26 seconds with an average of 38.4 ± 3.50 calls in per call group. Call groups repeated or continued within 1.83 ± 0.11 seconds of call group interval. The call duration was observed as 0.27 ± 0.01 seconds with the call interval of 0.07 ± 0.01 seconds. The dominant frequency and fundamental frequency was observed as 2342.75 Hz and 1171.88 Hz respectively. A call showed the range 2276.25 ± 18.37 Hz of minimum frequency and 2456.31 ± 18.76 Hz of maximum frequency with an average power of 73.06 ± 0.22 dB and 2.16 ± 0.02 u of average entropy (Fig. 4).

Fig. 4: (A) pair of Duttaphrynus stomaticus; (B) Time domain presentation of audio-spectrum; (C) Enlarged view of time domain presentation of audio-spectrum; (D) Frequency domain presentation of audio-spectrum and (E) Cross section of a call of Duttaphrynus stomaticus showing dominant frequency peak.

- *Fejervarya limnocharis* have paired subgular external vocal sacs. In this type of vocal sac the sacs are not completely bifurcated. It prefers to make calls while partially submerged into water and surrounded by grass or vegetation. The calls of this species were long series of creaks as cricket
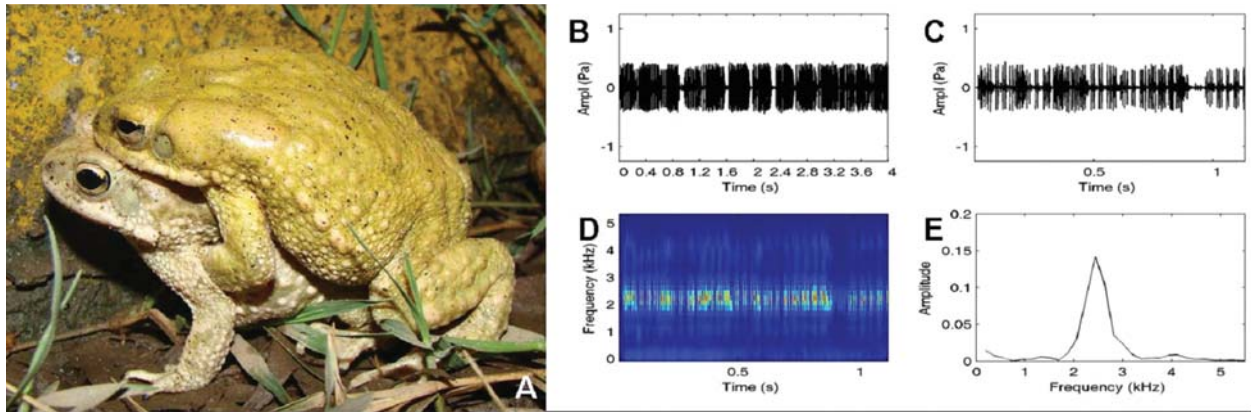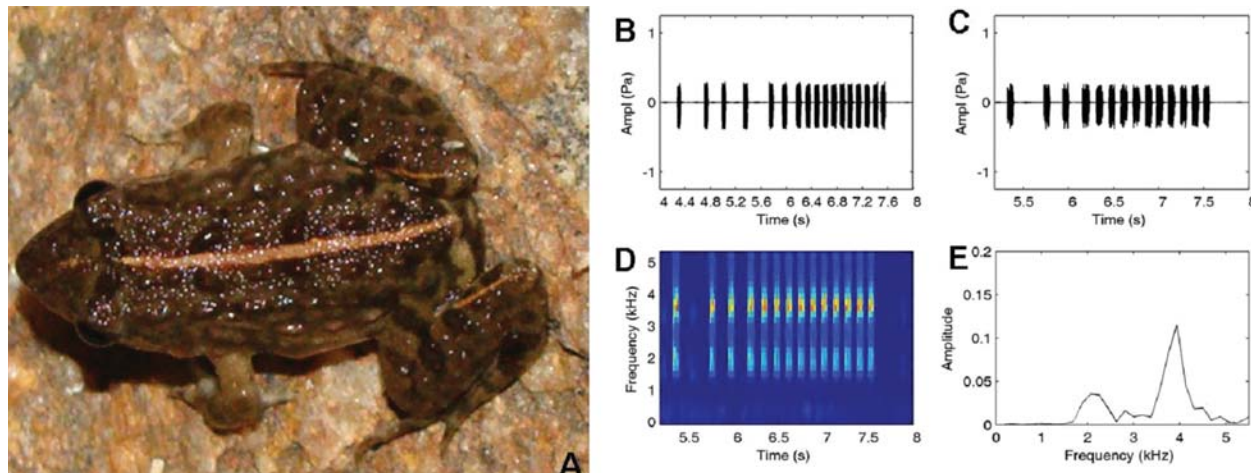

Fig. 5: (A) adult Fejerverya limnocharis; (B) Time domain presentation of audio-spectrum; (C) Enlarged view of time domain presentation of audio-spectrum; (D) Frequency domain presentation of audio-spectrum and (E) Cross section of a call of Fejerverya limnocharis showing dominant frequency peak.

produces. It may be described as in quick succession "creak - creak - creak - ………". This species was rarely found to emit sound solely, most of the time it was found to be calling in large chorus. Call groups were short with 1.87 ± 0.01 seconds with call group interval of 1.37 ± 0.15 seconds. Call group composed of 12 ± 0.76 calls in per call group. The call duration was observed as 0.06 ± 0.002 seconds that repeated with 0.11 ± 0.02 seconds of call interval. *F. limnocharis* produced the calls in between range of 3656.25 Hz of minimum frequency and 3903.41 ± 13.90 Hz of maximum frequency. The fundamental frequency was observed as 1828.125 Hz and the dominant frequency as 3656.25 Hz with the average power of 71.76 ± 0.255 dB with 2.66 ± 0.04 u of average entropy (Fig. 5).

- *Microhyla ornata* possessed median subgular external vocal sac, dark blue or black in color. *M. ornata* made calls after rains, the activity and breeding pattern is restricted to shallow water bodies. It preferred make calls from under bushes or crevices situated near water bodies. Calls of *M. ornata* characterized as shrill resembles the sound produced by dragging a comb on mouth of earthen pot as sharp and long "trrrrk - trrrrk - trrrrk - ……" with regular intervals. Call group duration of *M. ornata* observed as 0.34 ± 0.01 seconds. These call groups were repeated with 1.02 ± 0.03 seconds of call group interval and 8.52 ± 0.15 calls found in each call group. The call duration observed as 0.009 seconds that repeated with 0.03 seconds of call interval. *M. ornata* produced calls in between 3018.75 ± 98.62 Hz of maximum frequency and 2703.75 ± 120.02 Hz of minimum frequency. Fundamental frequency observed as 1430.63 ± 64.56 Hz and dominant frequency found as 2861.25 ± 129.13 Hz with an average power of 64.31 ± 0.16 dB with 3.05 ± 0.06 u of average entropy (Fig. 6).

Fig. 6: (A) adult Microhyla ornata; (B) Time domain presentation of audio-spectrum; (C) Enlarged view of time domain presentation of audio-spectrum; (D) Frequency domain presentation of audio-spectrum and (E) Cross section of a call of Microhyla ornata showing dominant frequency peak.

- Naja naja makes hissing sound to show its presence while disturbed. Hissing is produced as a result of inhale and exhale the breath. When hissing is produced simultaneously it strikes through its hood that appears to attempt for biting in this case the peaks shown in spectrogram are multiple instead of clearly one peak of dominant frequency. In that case the hissing is specific and loud. Hissing was analyzed for this species and found that the this type of hissing ranges in between 1312.50 Hz of maximum frequency and 687.50 Hz of minimum frequency. Fundamental frequency observed as 656.25 Hz and dominant frequency found as 1313.50 Hz with an average power of 37.95 dB with 5.10 u of average entropy (Fig. 7).

- Daboia russelli make hissings for the threatened the predators and show its presence by regularly making acoustics signal with increasing pith of whistle like sound by exhaling the breath. When approaches near to the snake Daboia russelli it strikes suddenly without prior intimation of biting. That's why the peaks shown in spectrogram is in increasing pattern with one peak of dominant frequency at the last of hissing. So the hissing is specific and loud, and hissing section was analyzed

Fig. 7: (A) adult Naja naja; (B) Time domain presentation of audio-spectrum; (C) Enlarged view of time domain presentation of audio-spectrum; (D) Frequency domain presentation of audio-spectrum and (E) Cross section of a hissing of Naja naja showing dominant frequency peak.
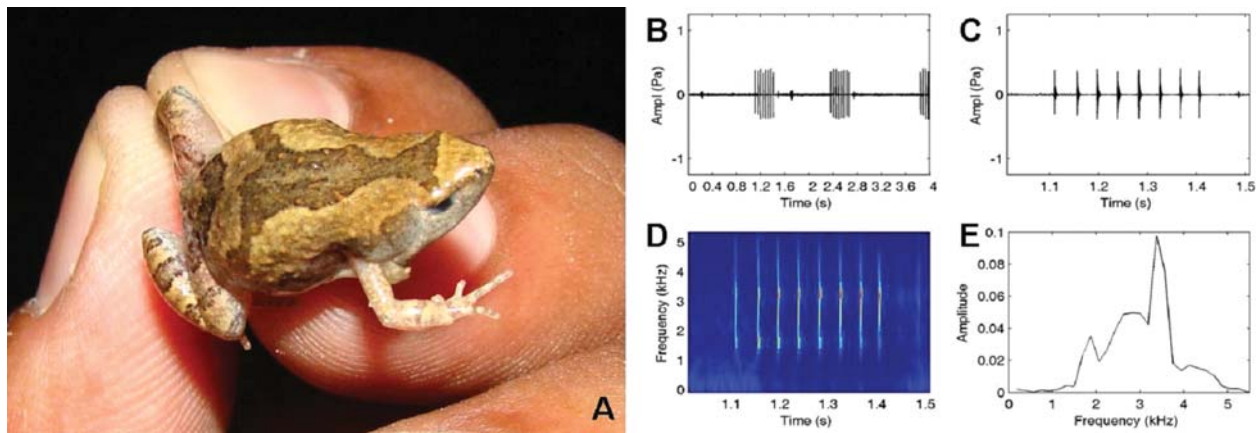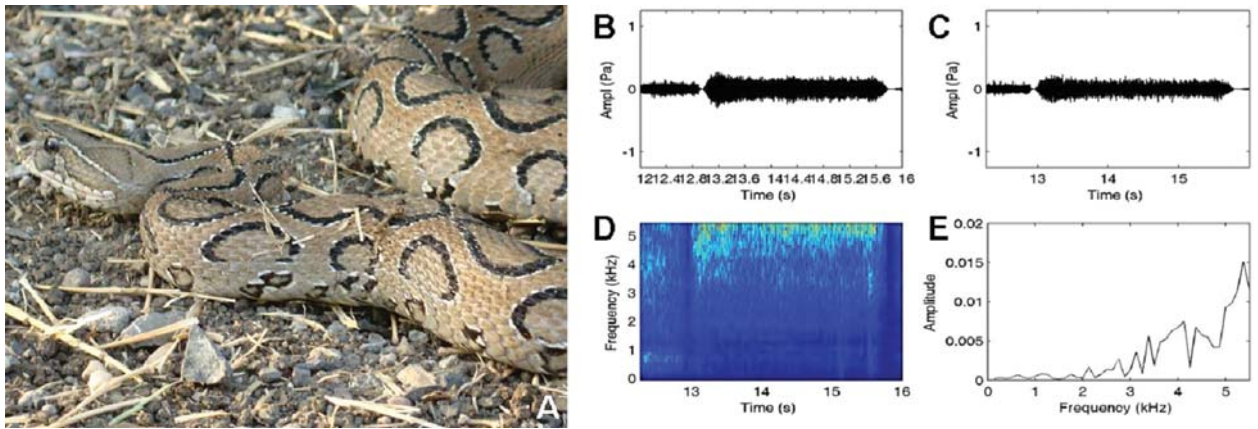

Fig. 8: (A) adult Daboia russelli; (B) Time domain presentation of audio-spectrum; (C) Enlarged view of time domain presentation of audio-spectrum; (D) Frequency domain presentation of audio-spectrum and (E) Cross section of a hissing of Daboia russelli showing dominant frequency peak.

for this species at the time of biting attempt and found hissing ranges in between 7770.83 Hz of maximum frequency and 6854.17 Hz of minimum frequency. Fundamental frequency observed as 3551.91 Hz and dominant frequency found as 7104.17 Hz with an average power of 68.9 dB with 4.85 u of average entropy (Fig. 8).

- Echis carinatus make alarming signals by rubbing its body scales that sound look like the cutting of wood by saw, that's why the common name is saw scaled viper, this signals the predators as a threat and shows his presence by regularly rubbing keeled body scales. When approaches near to the saw scaled viper snake Echis carinatus it strikes on of sudden without prior intimation of biting like Daboia russelli. This sound is loud but at the time of biting attempt it also produces the hissing and is specific but not so loud. This hissing section was analyzed for this species at the time of biting attempt and found hissing ranges in between 4437.50 Hz of maximum frequency and 2562.50 Hz of minimum frequency. Fundamental frequency observed as 1406.25 Hz and dominant frequency found as 2812.5 Hz with an average power of 67.2 dB with 4.94 u of average entropy (Fig. 9).
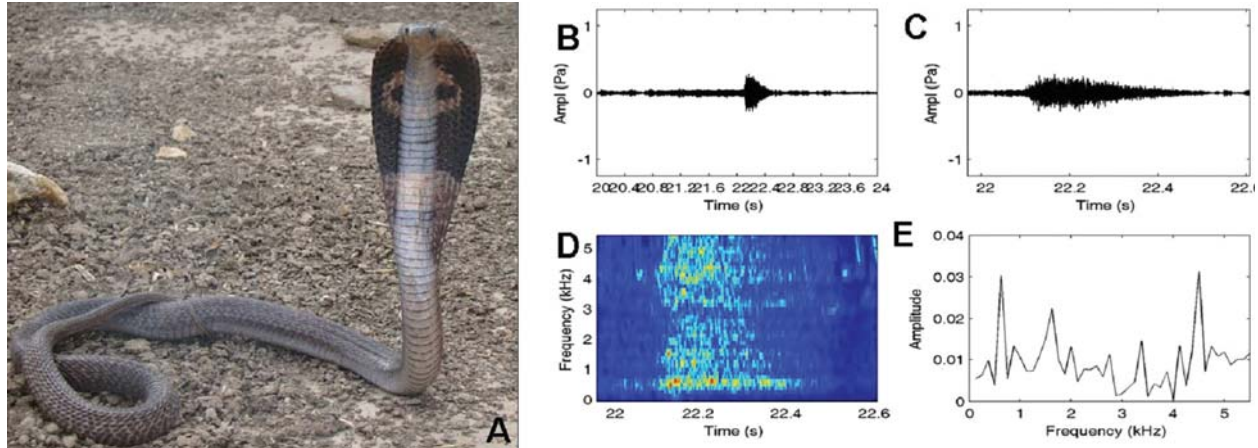
Fig. 9: (A) adults of Echis carinatus; (B) Time domain presentation of audio-spectrum; (C) Enlarged view of time domain presentation of audio-spectrum; (D) Frequency domain presentation of audio-spectrum and (E) Cross section of a hissing of Echis carinatus showing dominant frequency peak.

- Varanus bengalensis have specialized mechanisms for sound (hissing) production and uses airflow through the anterior respiratory tract to produce sound (hissing). These sounds may be produced by exhale or inhale the airflow and air stream generates acoustically loud signals. Varanus bengalensis produces hissing when we approach nearby and that was in continue fashion without any gap. It seems that as the body is very large and the breathing capacity of Varanus bengalensis is also good in volume thus it qualifies him to generate regular hissing. There is no clear demarcation of biting or attacking time hissing thus the complete hissing was analyzed for the Varanus bengalensis (Indian monitor lizard) and we found that hissing ranges in between 468.75 Hz of maximum frequency and 234.37 Hz of minimum frequency. Fundamental frequency observed as 234.37 Hz and dominant frequency found as 468.75 Hz with an average power of 58.3 dB with 4.83 u of average entropy (Fig. 10).
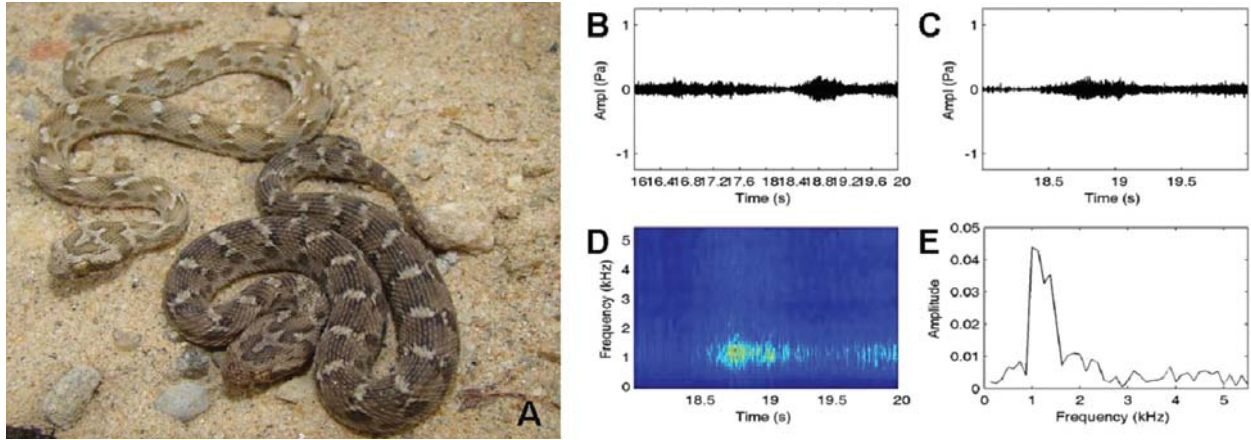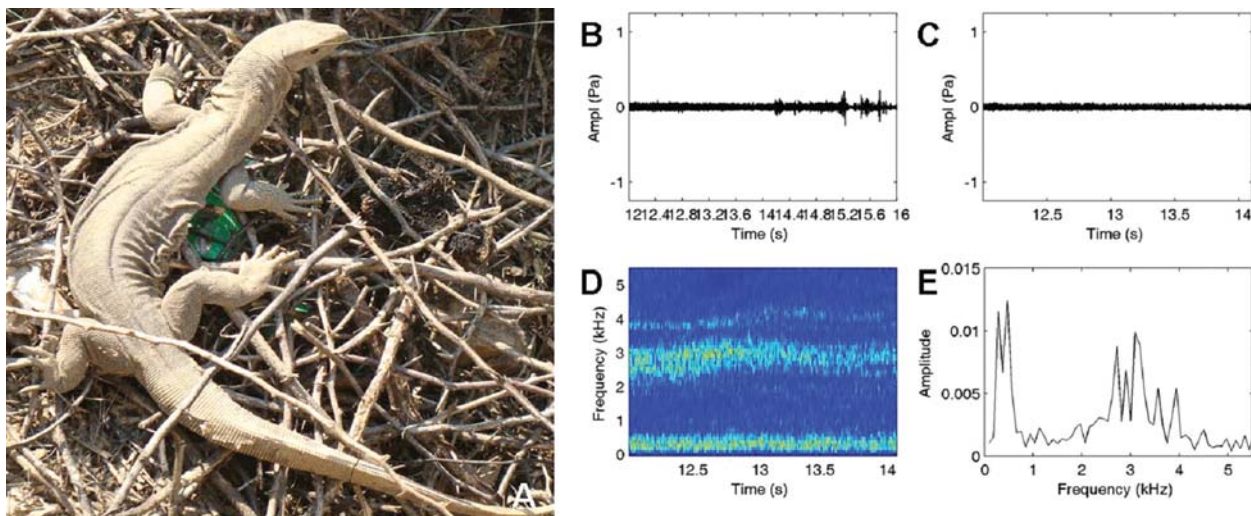

Fig. 10: (A) adult Varanus bengalensis; (B) Time domain presentation of audio-spectrum; (C) Enlarged view of time domain presentation of audio-spectrum; (D) Frequency domain presentation of audio-spectrum and (E) Cross section of a hissing of Varanus bengalensis showing dominant frequency peak.

4.2 Anurans call characteristics and comparative analysis

Duttaphrynus melanostictus having highest number of calls in per call group with 194 ± 11.2 calls while Microhyla ornata having least number of calls in per call group as 8.52 ± 0.15 calls. Call group duration was observed as Duttaphrynus melanostictus showed longest call group duration of 17.48 ± 0.51 seconds and in vice versa case Microhyla ornata having smallest call group duration 0.34 ± 0.01 seconds. Fejerverya limnocharis exemplified highest dominant frequency as 3656.25 Hz and in concern of lowest values of dominant frequency Duttaphrynus melanostictus showed lowest dominant frequency as 2325.59 ± 2.78 Hz. Average power of the advertisement calls of observed anurans Duttaphrynus melanostictus having highest Average power of call as 74 ± 0.32 dB while Microhyla ornata having 64.31 ± 0.16 dB lowest averages power of call.

4.3 Reptiles hissing characteristics and comparative analysis

Daboia russelli exemplified hissing with highest dominant frequency as 7104.17 Hz and in concern of lowest values of dominant frequency Varanus bengalensis showed lowest dominant frequency as 468.75 Hz. Average power of the hissing of observed reptiles Daboia russelli having highest Average power of hissing as 68.9 dB while Naja naja having 37.95 dB lowest averages power of hissing.

5. DISCUSSION AND CONCLUSION

Bioacoustics is a modern tool that does not involve any type of killing, preservation or even capturing of individual species. Bioacoustics or sound based identification of anurans is eco-friendly tool that can resolve problems of identification of species in the case of morpho-variant, cryptic species, and in identification of species in completely dark conditions (Sharma et al., 2011).

Species identification based on acoustic analysis is growing (Heyer *et al.*, 1990; Pombal *et al.*, 1995; Napoli and Cruz, 2005; Weber *et al.*, 2005; Silva-Filho and Junca, 2006; Angulo and Reichle, 2008). Many new species have been detected by their advertisement calls before their genetics were studied (Schneider *et al.*, 1984; Paillette *et al.*, 1992; Schneider and Haxhiu, 1994; Channing *et al.*, 2002). Recent studies have shown that anuran advertisement calls are also helpful in resolving sympatric species cases which are difficult by morphological identification and also helps to identify in large chorus and call alternation conditions too (Bogert, 1960; Wells, 1977; Kanamadi *et al.*, 1994; Grosjean and Dubois, 2006; Vences *et al.*, 2006; Vences *et al.*, 2011).

Acoustic communication is an important and discrete evolutionary unit (Etges, 1987; Cardoso and Vielliard, 1990). Vocalizations of anurans were developed during evolution for successful or higher rate of mating of these tiny creatures in invisible or complete dark conditions (Duellman and Trueb, 1986). Advertisement calls are used in mate attraction, directly linked to their reproductive behavior, highly species specific and potentially under sexual selection (Glaw and Vences, 1994), and maintaining the territory (Duellman and Trueb, 1994; Gerhardt, 1994). Advertisement calls are species specific.

In addition detailed description of anuran advertisement calls has proved to be a powerful tool to determine their taxonomic status. Sharma (2005a) proposed sonotaxonomy based on acoustic characteristics of different species of taxas. Only advertisement calls were recorded of observed 4 species of anurans in the present study. Territorial, distress, release calls or other types of calls which are presented by many anuran species (Wahl, 1969; Kuhn and Schneider, 1984; Schneider, 1990; Kanamadi et al., 1993) were not recorded to avoid confusion.

Calls of anurans have been found to be species specific. Their call patterns are distinct and species specific audio spectrum, cross sections of spectrum which characteristics of spectrograms of advertisement call can be used to identify species and also help in monitoring of population.

Acoustic applications are important in case of species which are not identified by their morphological traits. During present study dominant frequency, fundamental frequency and their harmonics alongwith fundamental features of call (call duration, average power and average entropy) are observed species specific.

Spectral patterns, power spectrum and cross sections of audio-spectrogram of anurans calls and reptiles hissing were found to be highly species specific.

6. REFERENCES

[1] A. ANGULO and S. REICHLE, 2008. Acoustic signals, species diagnosis, and species concepts: the case of a new cryptic species of *Leptodactylus* (Amphibia, Anura, Leptodactylidae) from the Chapare region, *Bolivia. Zoo. J. Lin. Soc.* **152**, 59-77.

[2] C.M. BOGERT, 1960. The influence of sound on the behavior of amphibians and reptiles. In: Animal sounds and communication. Lanyon, W. E. and Tavolga, W. N. (eds.) Washington, *D.C. American Institute of Biological Sciences*, 137-320.

[3] R.R. CAPRANICA, 1965. The evoked vocal response of the Bullfrog: A study of communication by sound. *Res. Monograph* 33 (MIT, Cambridge, MA)

[4] R.R. CAPRANICA, 1977. Auditory processing of vocal signals in anurans, in Taylor, D. H. and Guttman, S. I. (eds.)., The reproductive biology of Amphibians, New York: *Plenum Press*, 337 - 355.

[5] A.J. CARDOSO and J. VIELLIARD, 1990. Vocalizacoes de anfibios anuros de um ambiente aberto, em Cruzeiro do Sul, estado do Acre. Rev. Bras. Zoo. **50** (1), 229-242.

[6] C. CARPENTER and G. FERGUSON, 1977. Variation and evolution of stereotyped behavior in reptiles. *In Biology of the Reptilia,* (ed. C. Gans and D. Tinkle). New York: Academic Press, **7**, 335-554.

[7] A. CHANNING, D. MOYER and M. BURGER, 2002. Cryptic species of sharp-nosed reed frogs in the Hyperolius nasutus complex: advertisement call differences. *African Zoology,* **37**, 91-99.

[8] R.A. CHARIF, A.M. WAACK and L.M. STRICKMAN, 2008. Raven Pro 1.4 User's Manual. Cornell Laboratory of Ornithology, Ithaca, NY.

[9] W.E. DUELLMAN and L. TRUEB, 1986. Biology of Amphibians. *McGraw Hill Book Company*, San Fransisco. xvii+670.

[10] W.E. DUELLMAN and L. TRUEB, 1994. Biology of Amphibians. *John Hopkins University Press*, Baltimore and London.

[11] W.J. ETGES, 1987. Call site choice in male anurans. *Copeia* **4**, 910-923.

[12] L.R. Forti and J. Bertoluci, 2012. Distress call of Hypsiboas faber (Anura: Hylidae) during a Liophis miliaris (Serpentes: Colubridae) attack. *Herpetology Notes*, **5**, 187-188.

[13] E. FRANKENBERG and Y. WERNER, 1992. Vocal communication in the Reptilia - facts and questions. *Acta Zool. Lill.* **41**, 45-62.

[14] C. GANS and P. MADERSON, 1973. Sound production mechanisms in recent reptiles: review and comment. *Am. Zool.* **13**, 1195-1203.

[15] H.C. GERHARDT, 1994. Reproductive character displacement of female mate choice in the gray tree frog, Hyla chrysoscelis. *Anim. Behav.* **47**, 959-969.

[16] F. GLAW and M. VENCES, 1994. A field guide to the Amphibians and Reptiles of Medagascar, 2nd ed. (Vences, M. and Glaw Verlags, F. Köln, Germany).

[17] B.E.F. GOURBAL, M. BARTHELEMY, G. PETIT and C. GABRION, 2004. Spectrographic analysis of the ultrasonic vocalisations of adult male and female BALB/c mice. *Naturwissenschaften* **91**, 381-385.

[18] H. GREENE, 1988. Antipredator mechanisms in reptiles. In *Biology of the Reptilia*, (ed. C. Gans and R. Huey). New York: *Alan R. Liss*., **16**, 1-152

[19] S. GROSJEAN and A. DUBOIS, 2006. Description of advertisement calls of 6 of the Chaparana (Ranidae) from Nepal and India. *Alytes* **23** (3-4), 103 -122.

[20] P. HARTLINE, 1971. Midbrain responses to the auditory and somatic vibration system in snakes. *J. Exp. Biol.* **54**, 373-390.

[21] W.R. HEYER, A.S. RAND, C.A.G. CRUZ, P.L. PEIXOTO and C.E. NELSON, 1990. Frogs of Boraceia. *Arquivos de Zoologia Sao Paulo* **31**, 231-410.

[22] R.D. KANAMADI, C.R. HIREMATH and H. SCHNEIDER, 1993. The advertisement calls of the south Indian frog Ramanella variegata (Microhylidae). *Journal of Herpetology* **27**, 218-219.

[23] R.D. KANAMADI, C.R. HIREMATH and H. SCHNEIDER, 1994. Advertisement calls of two anuran amphibians, Rana tigrina and Tomopterna breviceps. *Journal of Biosciences* **19**, 75-80.

[24] B. KUHN and H. SCHNEIDER, 1984. Mating and territorial calls of the frog Rana ridibunda and their temperature dependent variability: *Zool. Anz.* **212**, 273-305.

[25] R. MERTENS, 1946. Die Warn-und Droh-reaktionen der Reptilien. Senck. *Naturf. Abh.* **471**, 1-108.

[26] M.F. NAPOLI and I.C.S. CRUZ, 2005. The advertisement call of Hyla atlantica Caramaschi and Velosa; 1996, with consideration on its taxonomic status (Amphibian, Anura, Hylidae) *Arq. Mus. Nac.* **63** (2), 283-288.

[27] P.M. NARINS, A.S. FENG, W. LIN, H.U. SCHNITZIER, A. DENZINGER, R.A. SUTHERS and C. XU, 2004. Old World frog and bird vocalization contain prominent ultrasonic harmonics. *Journal of Acoustical Society America.* **115**(2), 910-913.

[28] M. PAILLETTE, M.E. OLIVEIRA, H.D. ROSA and E.G. CRESPO, 1992. Is there a dialect in Pelodytes punctatus from southern Portugal? *Amphibia-Reptilia* **13**, 97-108.

[29] JR. POMBAL, R.P. BASTOS and C.F.B. HADDAD, 1995. Vocalizacoes de algunas especies do genero Scinax (anura, Hylidae) do sudeste do Brasil e comentarios taxonomicos. *Naturalia* **20**, 213-225.

[30] J. RHEINLAENDER, H.C. GERHARDT, D.D. YAGER and R.R. CAPRANICA, 1979. Accuracy of phonotaxis by the green tree frog (Hyla cinerea). *J. Comp. Physiol.* **133**, 247-255.

[31] D. ROY, 1994. Development of hearing in vertebrates with special reference to anuran communication. *J. Biosci.* **19**, 629-644.

[32] G.D. SALES, 1972. Ultrasound and mating behavior in rodents with some observations on other behavioural situations. *J. Zool. Lond.* **168**, 149-164.

[33] H. SCHNEIDER and I. HAXHIU, 1994. Mating call analysis and taxonomy of the water frogs in Albania (Anura: Ranidae). *Zoologische Jahrbucher Systematik* **121**, 248-262.

[34] H. SCHNEIDER, T.S. SOFIANIDOU and P. KYRIAKOPOULOU-SKLAVOUNOU, 1984. Bioacoustic and morphometric studies in water frogs (genus Rana) of Lake Ionnina in Greece, and description of a new species (Anura, Amphibia). *Zeitschrift fur Zoologische Systematik und Evolutionsforschung* **22**, 349-366.

[35] H. SCHNEIDER, 1990. Reproductive behavior and biology of central European water frogs; in *Biology and physiology of amphibians* (ed.) Hanke, W. (Stuttgart: Gustav Fischer Verlag) 29-39.

[36] K.K. SHARMA, 2005a. Sonotaxonomy: sound based taxonomy is a novel and environment friendly approach in systematics. *J. Cell Tiss. Res.* **5** (3), 1-2.

[37] K.K. SHARMA, 2005b. Wildlife monitoring by sound analysis system - An authentic and precise approach in wildlife management. National Conference on Environment and Natural Disaster Management, November 28-30, 2005. *Dept. of Zoology*, University of Rajasthan, Jaipur. **IL-10**, 118.

[38] K.K. SHARMA, 2009. Identification and monitoring the population of anurans of the Thar Desert and nearby vicinity using bioacoustics tools. *Proceedings IBAC*, Lisbon.

[39] K.K. SHARMA, M.C. SATHYANARAYANA, M.A. AKBARSHA, SHARMA VIVEK and N. SHARMA, 2011. Role of Amphibians in the Ecosystem, The Current Threats and Conservation Strategies. International Conference on Ecosystem Conservation and Sustainable Development. 10-12 February, 2011. Organized by Department of Biology, *Ambo University, Ethopia* 163-164.

[40] I.S.N. SILVA-FILHO and F.A. JUNACA, 2006. Evidence of the full species status of Neotropical leaf-frog Phyllomedusa burmeisteri baiana (Lutz, A. 1925) (Amphibia: Anura: Hylidae). *Zootexa* **1113**, 51-64.

[41] A.M. SIMMONS, A.N. POPPER and R.R. FAY, 2003. Acoustic communication. Volume 16, Springer handbook of auditory research. *New York: Springer*, 404.

[42] M. VENCES, F. GLAW and R. MARQUEZ, 2006. The Calls of the Frogs of Madagascar. (3 audio CDs and booklet). Barcelona: Alosa, Sons de la Natura.

[43] M. VENCES, J.S. HAUSWALDT and F. GLAW, 2011. The advertisement call of Guibemantis pulcher, a phytotelmic frog from Madagascar Herpetology Notes, **4**, 377-379

[44] M. WAHL, 1969. Untersuchurgen zur Bio-akustik des wasser-frosches Rana esculenta: *Oecologia* **3**, 14-55.

[45] L.N. WEBER, L.P. GONZAGA and S.P. CARVALHO-E-SILVA, 2005. A new species of Physalaemus Fitzinger, 1826, from the lowland atlantic forest of Rio de Janeiro State, Brazil (Amphibia, Anura, Leptodactylidae), *Arq. Mus. Nac.* **63** (4), 477-684.

[46] K.D. WELLS, 1977. The social behavior of anuran amphibians. *Anim. Behav.*, **25**, 666-693.

[47] K.D. WELLS, 2007. The ecology and behavior of amphibians. The University of Chicago Press.

[48] E. WEVER, 1978. The Reptile Ear. Princeton: Princeton University Press.

[49] B.A. YOUNG, 1997. A review of sound production and hearing in snakes, with a discussion of intraspecific acoustic communication in snakes. *J. Penn. Acad. Sci.* **71**, 39-46.

[50] B.A. YOUNG, K. MELTZER, C. MARSIT and G. ABISHAHIN, 1999. Cloacal popping in snakes. *J. Herpetol.* 55.

Singer's Formant in Hindustani Classical Singers

Namita Joshi[1],Manna A Raj[2] and Vikram Oak[3]

[1]*Bharati Vidyapeeth Deemed University, School of Audiology & Speech Language Pathology, Pune Satara Road, Pune, Maharashtra, India 410043.*
[2]*KochiyilPoovakala Bethel, Pathanamthitta, Kerala, India 689582,*
[3]*Bharati Hospital & Research Centre, Pune Satara Road, Pune, Maharashtra, India 410043,*
e-mail: nj21slp@gmail.com

ABSTRACT

Since last two decades, the research has been concentrated on professional voice; there is a curiosity among researchers to find out whether singers are really special in their voice use than non singers. Many studies have been conducted to know more about what produces the most interesting 'ring' which is called as 'Singer's Formant' (Fs) in the professional singing voice, which makes them to be perceived better. Though there have been studies regarding singer's formant in Indian classical singers, underlying physiological adjustments made by singers and its relation with acoustical features needs to be studied. Knowledge about physiological modifications aids professionals, to provide meaningful and specific guidelines for professional voice care and quality improvement among Indian classical singers. Thus the aims of the present study were to explore the possibility of singer's formant in Hindustani classical singers, to study the physiological adjustments made by the singers and also to find out the effect of number years of experience on acoustical as well as perceptual parameters. 20 Hindustani classical singers and 10 non singers within the age range of 18 -50 yrs were considered for the study. The singers (S) were again grouped into three subgroups based on their years of music experience as S1 (with 0-5 yrs of experience), S2 (with 6-10yrs of experience) and S3 (with >10 yrs of experience). Acoustical as well as perceptual evaluation was carried out for singers and non singers. Following the case history, the acoustical evaluation was carried out on samples of sustained phonation of /a/, and /vandemataram/ (old) song for a minimum of 20 secs. The samples were recorded in a digital tape recorder and it was transferred to LTAS module of CSL - MDVP4500 software. The LTAS parameters considered for the study include: amplitude at 0-2 and 2-4 kHz, mean centre frequency of singer's formant region and singing power ratio. Mean f0 was also measured. The study revealed that S3 (>10 yrs of experience) group had highest amplitude at 2-4 kHz, as well as higher SPR values than compared to S1 and S2. This means that there is occurrence of clustering of formants in the higher harmonics region. But the difference in the parameters was not statistically significant between the groups.The perceptual evaluation was carried out to see for the parameters such as velopharyngeal closure pattern, lateral /pharyngeal wall movement and pharyngeal opening. Nasoendoscopic evaluation was done for all the participants by a well experienced ENT professional. Coronal velopharyngeal closure pattern and lateral pharyngeal wall movement were found to be common in both singers and non singers. The pharyngeal opening was rated as narrow, in between or wider. Inter rater reliability for four perceptual evaluators was found to be good. S3 group had widest pharyngeal opening. The results obtained were in correlation with the results of acoustical analysis. Hence the results of the present study points out the possibility of occurrence of singer's formant in Hindustani classical singers.

The result of the acoustical analysis indicates that there is an effect of years of music experience on the acoustical as well as perceptual parameters. Singers with more than 10 years of experience are special in terms of acoustical and perceptual parameters of voice than non singers. Though the difference between the groups might have not been significant due to the small sample size and unequal distribution of participants within the group. The study can be done on large sample size with the following future implications. The study highlights the possibility of developing training material for singers to improve their pharyngeal widening. It throws light into the future utility of Fs in pathological conditions among Hindustani Classical singers. Study can also be repeated to compare SPR values &nasoendoscopic evaluation between different styles of singing such as Carnatic Vs Hindustani classical singers.

1. INTRODUCTION

Singing as defined is as "sensory motor phenomenon that requires particular balanced physical skill[1]". Maintenance of a better quality and wide range of voice for a longer period is a necessity for singers. Awareness about voice culture is increasing among singers and they often approach professionals (Speech Language Pathologist and Otolaryngologist) for care and maintenance of singing voice. Speech Language Pathologist and Otolaryngologist play a crucial role in assessment & management of singing & speaking voice.Singers are special when compared to non singers due to an exciting "ringing" voice quality during singing performance that helps them to be heard over a large orchestral accompaniment.[2],[3] The author explained about 'brightness in voice' as "singer's formant" which occurs as a result of clustering of higher third, fourth and fifth vowel formants (F3, F4 and F5). In order to find out whether singers are special in their vocal usage, various authors studied following LTAS parameters: amplitude at lower harmonics (0-2 kHz), amplitude at higher harmonics (2-4 kHz), centre frequency of singer's formant and singing power ratio etc.[4],[5],[6],[7],[8],[9]

However, research on vibratory mechanism of vocal folds and its relation to acoustical parameters are rare. Examination of vibratory mechanism of vocal folds can be done using various instruments such as videoflouroscopy, nasoendoscopy, videolaryngoscopy, strobovideolaryngoscopy etc. Researchers have reported an association between pharyngeal widening and production of ringing voice while singing.[10] Singers with widened pharynx were observed to have effective clustering of higher formants and thereby higher singers' formant. Perceptual evaluation has been considered as a gold standard for assessing voice, though the subjectivity can be reduced by complementing it with acoustical evaluation. Singing is a complex act and its uniqueness can be investigated by a combination of perceptual as well as acoustical analysis.

2. NEED OF THE STUDY

In western scenario, research concentrated on finding out singer's formant, centre frequency and singing power ratio (SPR) in singers and non singers. Fsis defined as a pronounced peak of acoustic energy which is located around 3kHz and it is formed by the clustering of the third, fourth and the fifth vowel formants (F3, F4, and F5)[10]. Author hasstated that the centre frequency (frequency at which the highest peak amplitude between 2-4 kHz is obtained) of singer's formant lies between 2.4 - 3.6 kHz in almost all of the singers. [11] In Indian classical singers, there have been attempts to find out the centre frequency of Fs. It was found that maximum energy concentration observed to be around 2500 - 2950 Hz in trained Carnatic singers and around 2300 - 2500 Hz in untrained singers.[12] Fs was located in 2-4 kHz region in Hindustani classical singers and its centre frequency increased with rise in pitch, which was parallel to sung vowels in Western music.[13] It has been found that singer's formant is present in Indian classical singers.[14] Contrary to the above mentioned studies, singer's formant was not found in South Indian classical singers.[15] Though there have been studies regarding singer's formant in Indian classical singers, underlying physiological adjustments made by singers and its relation with acoustical features needs to be studied. The review of literature suggests that there have been very limited number of studies done to explore the physiological differences in singers and non singers

during singing. There have also been limited researches on effect of years of experience on the acoustical and perceptual parameters. Hence the present study was planned to explore the physiological, acoustical and perceptual differences between singers (with varied experience) and non singers.

3. AIM OF THE STUDY

- To explore presence of singer's formant in Hindustani Classical singers.
- To investigate physiological adjustments made by the singers.
- Level of impact of number of years of experience of singing on singer's formant.

4. METHOD

4.1 Participants

A total of 20 Hindustani classical singers (11 males & 9 females) and 10 non singers (5 males & 5 females) were participated for the study. The mean age ranges of singers were 29.15 yrs and that of non singers were 22.5 yrs. The Hindustani classical singers were again divided into three subgroups S1, S2 and S3 according to their years of experience in singing. S1 included those singers who had a formal vocal training of about 0-5 yrs (4 males & 3 females). S2 singers had an experience of about 6-10 yrs (4 males & 3 females). Those singers with more than 10 years of experience were considered in sub group S3 (3 males & 3 females). Non singers were those participants who had not undergone any kind of formal vocal training. Case history revealed that singers in S1 group, used to practice around an average of 2-3 hrs per day. Most of them were students of college of fine arts where they had just started formal training. Whereas singers in group S2, have a practice of singing for 4-5 hours per day. Many of them have an experience of singing in semi classical as well as Indian classical music. Singers in group S3 were the most experienced singers with maximum knowledge about voice culture. They have a practice of more than 6-7 hrs per day. They were involved in some of the voice care practices like drinking sips of water during performances, steam inhalation and omkar practice before daily singing activity (riyaz). All the participants were included only when they did not show any signs of any speech, language, vocal, sensory motor problems at the time of recording. Prior to the recording, all the participants were explained regarding the purpose of the study and the future implications. Consent form was filled by all the participants.

4.2. Procedure

4.2.1 Acoustical Analysis

The stimuli recorded for the particular study was a phonation sample of the vowel /a/, /i/ and /u/ for about 5 seconds and also the well known song /vanðemataram/ for about 20 seconds. The acoustical analysis was carried out on the recorded stimuli to see for the presence of singer's formant. A portable digital tape recorder was used for recording the tasks. The microphone was kept away from the participant at a distance of 10 cm. All recordings were done in quiet environment with the participants seated in comfortable position.

The recordings were transferred to the computer and acoustical analysis was done using Long Term Average Spectrum (LTAS) of CSL 4500 MDVP software at a sampling rate of 44000 Hz.

4.2.2 LTAS Parameters

- Amplitude of highest peak at the lower harmonic (0-2) kHz region and the amplitude of the highest peak at the higher harmonics (2-4) kHz region
- Mean centre frequency of singer's formant: It is the peak frequency of the highest amplitude obtained in region of higher harmonics (2-4 kHz).[6]
- Singing Power Ratio: It is the ratio of amplitude obtained at 2-4 kHz to that of 0-2 kHz. SPR is a parameter that can quantitatively measure the resonant quality of singing voice.[16]

4.2.3 Mean Fundamental frequency (Mean f0)

It isthe lowest frequency in a periodic waveform. [17]

4.2.4 Perceptual Analysis

Nasoendoscopy was carried out to investigate the physiological adjustments made by the singers with respect to the presence of singer's formant when compared to non singers. A 70 degree rigid nasoendoscope (HAWK model) with a diameter of 4mm was used for the analysis. It was kept at 7-8 cm from the opening of the nostrils of the anterior nares. The task of the participant was to phonate /i/ while nasoendoscopy will be done simultaneously with the help of an experienced ENT professional. The videos were saved on a compact CD drive.

Perceptual evaluation of velopharyngeal closure pattern, lateral and posterior wall movement and also the pharyngeal widening was carried out. Four well experienced ENT professionals were asked to rate the nasoendoscopy video samples. All the samples were randomly presented to the raters. The inter rater reliability was estimated to see the correlation between the visual perceptual evaluation. Parameters measured for perceptual (visual) evaluation are as follows:

- Velopharyngeal Closure Pattern and Lateral or Pharyngeal wall Movement: The professionals were asked to rate nasoendoscopic videos on the basis of two parameters. One is velopharyngeal closure pattern: coronal, sagittal, circular and second is the lateral versus pharyngeal wall movement.
- Pharyngeal opening: The ENT professionals were asked to rate the nasoendoscopy samples on a three point rating scale. (1= narrow pharyngeal opening, 2= medium pharyngeal opening, 3= wider pharyngeal opening).

Results of acoustical and perceptual evaluation are tabulated and discussed.

5. RESULTS & DISCUSSION

Recorded sample of all the participants was transferred to CSL-MDVP module for LTAS analysis. The results of acoustical and perceptual analysis are as follows.

5.1. LTAS Parameters

5.1.1. Amplitude at 0-2 kHz and 2-4 kHz: Amplitude of highest peak at the lower harmonics (0-2) kHz region and the amplitude of the highest peak at the higher harmonics (2-4) kHz region were analyzed.
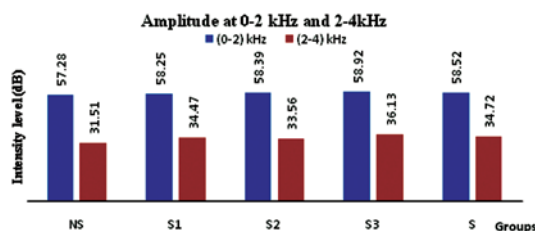

Fig. 1. Mean scores of amplitude at 0-2 and 2-4 kHz for singers and non singers (NS = Non singers. S1= Singers with 0-5 yrs of experience. S2 = Singers with 6-10 yrs of experience. S3 = Singers with > 10 yrs of experience. S= Singers as a group).

The Fig.1.Showed that there was no much difference in amplitude at 0-2 kHz for non singers and singers (as a group). But the amplitude at 2-4 kHz was found to be higher in singers than for non singers. When the comparisons within the group of singers were considered, it was found that amplitude at 0-2 kHz remained almost similar for all the three groups of singers. The amplitude at 2-4 kHz was found to be variable for singers. Higher amplitude was noticed for singers with more than 10 yrs of experience (S3) when compared to singers of 0-5 (S1) & 6-10 (S2) yrs of experience. Although the difference was observed, it was not statistically

significant. The participants in the group S1 and S2, were students of musical institute, and the amount of singing and daily riyaz carried out by them was not as much as group S3. The variability in amplitude at 2-4 kHz may be due to the difference in the number of hours of the riyaz they were doing per day. The findings of the study showed that there is a tendency for the increment in amplitude level at 2-4 kHz as the years of music experience increases. Thus the amount of training and hours of practice per day can be expected to be a supplementary factor for the achievement of significant energy concentration at higher harmonics. The findings of the present study support the observation of a previous studies18 where they have found that as the years of experience or the vocal training increases, amplitude (energy levels) also increases. Authors also observed additional energy concentration in 2-4 kHz region for trained singers when compared to non singers.19,20 The higher amplitude obtained at 2-4 kHz region for singers with more than 10 yrs of experience (S3) can be correlated to pharyngeal widening (supralaryngeal adjustments) observed in the perceptual analysis for S3 group. The results of the present study can be confirmed on a larger sample size. It can also be assumed that rigorous singing training for less than 10 years may be too short time period to expect an effect in the higher harmonic region.

5.1.2 Mean Centre frequency of singer's formant (Fs)

The center frequency of Fs was analyzed to see the frequency at which energy is concentrated.
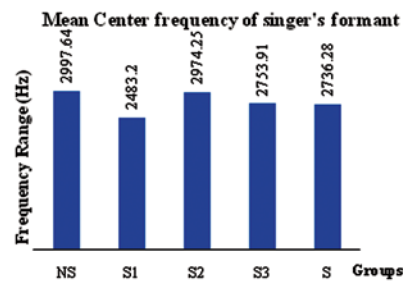

Fig. 2. Mean scores of Fs of singers of each group and non singers. (NS = Non singers. S1= Singers with 0-5 yrs of experience. S2 = Singers with 6-10 yrs of experience. S3 = Singers with > 10 yrs of experience. S= Singers as a group).

In the present study, the maximum energy concentration in singers was observed from 2.1 to 3.4 kHz with the mean centre frequency of 2.4 kHz, 2.9 kHz and 2.7 kHz for S1, S2 and S3 respectively. Though the differences between mean center frequencies for the groups were obtained, it was not statistically significant. The above findings were consistent with the prior investigations,21where it was found that for sopranos and mezzo sopranos, a significant energy concentration is observed in the higher harmonics region which is in 2.8 - 3.4 kHz region (p< 0.05). Singer's formant was observed to be near 3 kHz for a well classically trained bass, baritone, tenor and alto singers' voices.11The present study did not consider the different voice categories in Hindustani classical singers (E.g. Drupad, Khyal, Tumri etc.) like in western studies mentioned above. The group of singers were more heterogeneous and small to generalize the results for range of center frequency in Hindustani classical singers.

5.1.3. Singing Power Ratio (SPR)

It is calculated by the ratio of highest peak intensity level obtained at higher harmonics (2-4) kHz to the highest peak intensity at lower harmonics (0-2) kHz.As shown in Fig.3.among the three groups of singers, S3 (0.6) demonstrated the highest SPR value, than S1 (0.5) and S2 (0.5). In the present study, a tendency of an augmentation in the SPR values was observed as the music training increases. Although, the differences were seen for the groups, these differences were not statistically significant. The results of the present study were similar to that of studies done in past16 who found that professional singers with more years of music experience (>4yrs) had significantly higher SPR values than trained singers with less than 4 years of experience.

The results of the present study were unlike the studies18where they found that SPR scores were significantly lesser for singer group than for non singer group. Higher SPR values in S3 group shows that they had higher energy concentration at 2-4 kHz than 0-2 kHz, which confirms the possibility of formant clustering at higher harmonics. The expertise and self regulating pharyngeal widening in S3 group would have led them to have higher SPR values as compared to S2 and S1. The present study highlights the possibility of obtaining the singer's formant for singers with more than 10 yrs of experience in the region of 2-4 kHz.
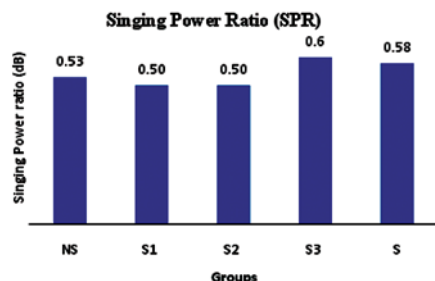

Fig. 3. Mean value scores of SPR of singers of each group and non singers (NS = Non   singers.
S1= Singers with 0-5 yrs of experience. S2 = Singers with 6-10 yrs of experience.
S3 = Singers with > 10 yrs of experience. S= Singers as a group)

5.2. Mean Fundamental frequency (Mean f0)

The fundamental frequencies of the participants wereanalyzed acoustically. The gender wise comparison was done for the parameter of mean f0 between singers and non singers. Independent sample t test was carried out which revealed that there is no significant difference in mean f0 between males and females within the group and across the group. The results of the present study shows that singers were not special than non singers in terms of their mean f0. Mean f0 values for female singers were higher in comparison with female non singers which supports the other studies[22,] where they also found that the mean relative f0 of trained females (soprano, mezzo soprano, and altos) was higher than female non singers. However, the results were not similar for male category where, the male singers were found to have lower f0 values than male non singers. This probably is the result of low magnitude of jaw opening in male non singers during the task of vowel phonation, as also reported.[23] The differences obtained in the present study can be due to the less sample size and unequal distribution of males and females across the groups.

Fig. 4. Mean f0 of males and females in singers and non singers. (NS = Non singers. S1= Singers
with 0-5 yrs of experience. S2 = Singers with 6-10 yrs of experience.
S3 = Singers with > 10 yrs of experience. S= as a group).

5.3. Perceptual parameters

5.3.1. Velopharyngeal closure pattern & lateral / posterior pharyngeal wall movement

The velopharyngeal closure pattern of all the participants were perceptually evaluated with the help of four experienced ENT professionals in Pune. The percentage of occurrence of velopharyngeal closure patterns in

Table 1. Shows the percentage of velopharyngeal closure pattern in singers and non singers.

Pattern	Non Singers	S1 (0-5yrs)	S2 (6-10yrs)	S3 (>10yrs)
Coronal	60%	57.14%	57.14%	66.66%
Sagittal	0%	28.57%	14.28%	16.66%
Circular	40%	14.28%	28.57%	16.66%

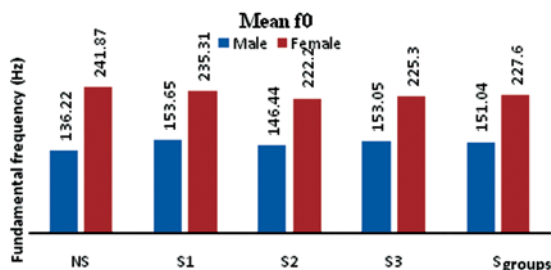Table 2. Shows overall lateral or posterior pharyngeal wall movement in singers and non singers. (NS = Non singers, S1= Singers with 0-5 yrs of experience, S2 = Singers with 6-10 yrs of experience, S3 = Singers with > 10 yrs of experience. S= Singers as a group).

Parameter	Non singers	S1	S2	S3	S
Lateral (LPW) / Posterior Pharyngeal wall (PPW) movement	LPW	LPW	LPW	LPW	LPW

each of the sub group of singers and that of non singers were calculated. As shown in Table 1 for non singers, coronal pattern was observed in 60% of the participants, circular pattern was observed in 40% and none of them had sagittal pattern. For the sub group of singers in S1, 57.14% of the participants had coronal pattern, 28. 57% had sagittal pattern and 14.28% had circular pattern. For sub group S2, coronal pattern was present for 57.14% of participants, sagittal were present for 14.28% and circular was present for 28.57% of the participants. Around 66.66% of the participants of sub group S3 singers had coronal pattern with remaining 16.66% of participants withsagittal as well as circular pattern. As shown in Table2, all the groups had lateral wall movement. The most common velopharyngeal closure pattern was coronal with lateral wall movement across the groups. Hence the results of the present study conclude that singers were not special in the velopharyngeal closure pattern than non singers.

Studies are limited regarding the exploration of velopharyngeal closure pattern as well as lateral or posterior pharyngeal wall movement in singers and non singers.

5.3.2 Pharyngeal Widening

Singer's formant cluster is created in the vocal tract by narrow epilaryngeal tube opening, so that the ratio of the cross sectional area of pharynx is approximately six times greater than that of epilarynx outlet (1:6 ratio)[24]. The maintenance of an enlarged pharyngeal area is essential for the achievement of pharyngeal - laryngeal vestibule area ratio (6:1)[10]. The sample of nasoendoscopy evaluation of singers and non singers were evaluated by four experienced ENT professionals on a three point rating scale (1 = narrow pharyngeal opening, 2= medium pharyngeal opening and 3= wider pharyngeal opening). Inter rater reliability was carried out for the parameter of pharyngeal widening.

Table 3. The overall rating of pharyngeal widening for singers and non singers.

Parameter	NS	S1	S2	S3
Pharyngeal Opening	2	2	2	3

(NS = Non singers. S1= Singers with 0-5 yrs of experience. S2 = Singers with 6-10 yrs of experience. S3 = Singers with > 10 yrs of experience. S = Singers as a whole).   (3=.wider pharyngeal opening 2=medium pharyngeal opening).

As mentioned in table no.11, the group of NS, S1 and S2 were rated 2 for pharyngeal widening which means they had medium pharyngeal opening. S3 group was rated 3, which means they had wider pharyngeal opening. The product moment correlation between each of the raters for pharyngeal widening is significant ($p<0.05$). It can be opined that well trained singers use more efficient supralaryngeal adjustments which

Namita Joshi,Manna A Raj and Vikram Oak

Table 4. Inter Rater Reliability for pharyngeal widening between singers and non singers.

	R1	R2	R3	R4
R 1	--	.525*	.375*	.381*
R 2		---	.588*	.511*
R 3			----	.512*
R 4	.381*	.511*	.512*	----

*indicates correlation is significant at 0.05 level (*R1= Rater 1, R2=Rater 2, R3 = Rater 3, R4 =Rater4*).

enables them to produce a bright vocal quality. The results of perceptual evaluation of pharyngeal widening are in support of acoustical findings of higher SPR values in group S3. Present study postulates the fact that more the number of years of experience, better are the supralaryngeal adjustments and thereby higher energy concentration in the Fs region. The result of the present study is parallel to the results obtained by other authors8where they revealed that trained singers (8-10 yrs of experience in Carnatic singing) showed clustering of higher formants due to widened pharynx.

The results of the study may be contributed to the fact that the singers with less than 10 years of experience are still undergoing formal music training and have not achieved mastery in singing as they are no different in terms of acoustical and perceptual parameters with that of non singers. Hence, singer's formant can be considered as a learned behavior which could be attained only when one masters in making physiological adjustments with more than 10 years of singing experience. Thus pharyngeal widening should be the part of training for professional singers who needs to increase the projection of their voice.

The results of the present study indicate the existence of singer's formant in Hindustani classical singers. The results of the acoustical analysis point out the effect of years of singing experience on all the parameters (LTAS parameters and f0). The S3 group had highest amplitude at 2-4 kHz, had highest SPR values than compared to S1, S2 and implies the formant clustering in higher harmonics. According to perceptual evaluation, S3 group had widest pharyngeal opening which is in correlation with the results of acoustical analysis. Hence the study concludes that singers with more than 10 years of experience are special in terms of acoustical and perceptual parameters of voice than non singers though the significant difference between the groups could not be found due to the small sample size and unequal distribution of participants within the group. The present study suggests that for improving the voice quality in professional voice users, proper physiological adjustments (pharyngeal widening) should be taught. The study highlights the possibility of developing training material for singers to improve their pharyngeal widening. The study points out the need and development of an objective parameter (SPR) for differentiating style of singing in future. It throws light into the future utility of Fs in pathological conditions among Hindustani Classical singers. Study can also be repeated to compare SPR values &nasoendoscopic evaluation between different styles of singing such as Carnatic Vs Hindustani classical singers.

6. REFERENCES

[1] M. BUNCH, 1982. Dynamics of the singing voice. New York: *Springer, Verlag.*

[2] SUNDBERG, J. 1987. The Science of the Singing Voice.Dekalb, Illinois: *Northern Illinois University Press*, 35.

[3] J. SUNDBERG, 1990. "What's so special about singer's?". *Journal of Voice*, **4** (2),107-119.

[4] V.M.O. BARRICHELO, R.J.HEUER, C.M. DEAN, and R.T. SATALOFF, 200). Comparison of singer's formant, speaker's ring, and LTA spectrum among classical singers and Untrained normal speakers. *Journal of Voice* **15** (3),344- 350.

[5] K. GHOSH, 2007. Comparison of acoustic characteristics in female trained (Carnatic Style) singers, untrained singers and non singers. *Unpublished Master's Dissertation.*University of Mysore.

[6] D.S. LUNDY, S. ROY, R. R. CASIANO, J.W. XUE and J. EVANS, 2000.Acoustic analysis of the singing and speaking voice in singing students. *Journal of Voice*, **14** (4), 490 - 493.

[7]   M. SANTHOSH, N. DEVIE and K. YESHODA, 2008. Acoustical analysis of voice of singing students. *Proceedings of the 35th Indian Speech and Hearing Association Conference.*

[8]   R. SHEETAL and K. YESHODA, 2008. Acoustical analysis of singer's voice. *Journal of the Indian Speech and Hearing Association*, **22**, 102 - 105.

[9]   J. SUNDBERG, P. BIRCH, B. GUMOES, H. STAVARD, S. PRYTZ and A. KARLE, 2007. Experimental findings on the nasal tract resonator in singing. *Journal of Voice*, **21** (2), 127 - 137.

[10].   J. SUNDBERG, 1974. Articulatory Interpretation of the 'Singing Formant'. *Journal of Acoustical Society of America*, **55**, 838-844.

[11].   J. SUNDBERG, 2001. Level and Centre Frequency of the Singer's Formant. *Journal of Voice*, **15** (2), 176-186.

[12]   SUJATHA. 1989. Analysis of singing voice. Unpublished Master's Dissertation. *University of Mysore.*

[13]   R. SENGUPTA, (1990). Study on Some Aspects of the "Singers Formant" in North Indian Classical Singing. *Journal of Voice*, **4** (2), 129-134.

[14]   N. DEVIE, 2003. Singer's Formant in Indian classical singers.Carnatic vs Hindustani.Unpublished Master's Dissertation. *University of Mysore.*

[15]   P. BOOMINATHAN, 2004. Do Carnatic singer's have singer's formant? - An exploratory study. *Proceedings of The Frontiers of Research in Speech and Music conference.*

[16]   K. OMORI, A. KACKER, L.M. CARROL, W.D. RILEY and S.M. BLAUGRUND, 1996. Singing power ratio: quantitative evaluation of singing voice quality. *Journal of Voice*, **10** (3), 228-235.

[17]   I. SMITS, P. CEUPPENS and M. S. DE BODT , 2005. A comparative study of acoustic voice measurements by means of Dr. Speech and Computerised Speech Lab. *Journal of Voice*, **19** (2), 187-196.

[18]   C. WATTS, K.B. BURROUHS, ESTIS, J and BLANTON, D. 2006. The singing power ratio as an objective measures of singing voice quality in untrained talented and nontalented singers. *Journal of voice*, **20** (1), 82-88.

[19]   V. OLIVEIRA, R. HEUER, C. DEAN and R. SATALOFF, 2000. Comparison of singer's formant, Speaker's ring and LTA spectrum among classical singers and untrained normal speakers, *Journal of voice*, **15** (3), 344-350.

[20]   K.L.P. REID, P. DAVIS, J. OATES, D. CABRERA, S. TERNSTROM, M. BLACK and J. CHAPMAN, 2007. The acoustic characteristics of professional opera singers performing in chorus versus solo mode. *Journal of Voice*, **21** (1), 35-45.

[21]   S.H. LEE, H.J. KWON, H.J. CHOI, N.H. LEE, S.U. LEE and S.M. JIN, 2008. The Singer's Formant and Speaker's Ring Resonance: A Long - Term Average Spectrum Analysis. *Journal of Clinical and Experimental Otorhinolaryngology*, **1** (2), 92 - 96.

[22]   L. AKERLUND, P. GRAMMING and J. SUNDBERG, 1992. Phonetogram and averages of sound pressure levels and fundamental frequencies of speech: comparison between female singers and nonsingers. *Journal of Voice*, **6** (1),55-63.

[23]   M. LIM, E. LIN AND P. BONES, 2006. Vowel effect on glottal parameters and the magnitude of jaw opening. *Journal of Voice*, **20** (1), 46-54.

[24]   B.B. MONSON, 2007. The 1:6 ratio in vocal pedagogy. *Journal of Acoustic Society of America*, **121** (5).

Understanding Emotional Contagion Associated with Hindustani Classical Ragas: an Analysis of Behaviour and Acoustic Features

Avantika Mathur and Nandini C. Singh

Speech and Language Laboratory, National Brain Research Centre, Nainwal Mode, Manesar 122 050, Haryana, India
e-mail: avantika,nandini}@nbrc.ac.in

ABSTRACT

Music is well known to evoke emotions. The first objective of this study was to understand emotional contagion associated with Hindustani classical *ragas*. The second objective was to study the role of acoustic properties in determining the emotions associated with *ragas*. We conducted an internet based survey in which participants listened to *raga* excerpts played in both *alaap* (slow arrhythmic introductory section) and *gat* (fast rhythmic composition). A total of 164 participants completed the survey. Survey responses showed that despite of cultural differences, participants were able to associate positive and plaintive emotions with different ragas. Analysis of behavioral results showed that the emotions associated with *ragas* when played in *alaap* were 'calm' and 'sad'. However, when played in *gat*, the 'calm' ratings shifted to 'Happy' and 'sad' ratings shifted to 'Longing' or 'Restless'emotions. The results of multiple linear regression analysis indicated that the presence or absence of a subset of major and minor pitch intervals in a *raga* were predictive of ratings on positive and plaintive emotions. The percent mean frequency of occurrence of the major (*shuddh Ni*) and minor (*teevra ma, komal re*) tonic intervals accounted for 90.4% and 86.5% of variance in ratings of 'happy' and 'sad' emotions. This suggests that it is the underlying distribution of specific pitch intervals that listeners associate with positive or plaintive emotions.

1. INTRODUCTION

Music has long been associated with emotional contagion. It is the process by which emotions are induced by a piece of music because the listener perceives the emotional expression of the music and then mimics this expression internally wherein by means of either peripheral feedback from muscles [1][2] , or a more direct activation of relevant emotional representations in the brain [3][4] leads to an induction of the same emotion.

Musical emotions have been extensively studied and many different theories have been proposed to explain the type of emotions induced by music [5]. But, most of work has been centred on western music[6][7]. Music cultures from the eastern hemispheres are unexplored. In this study we identified the emotions induced by music of eastern hemisphere using *ragas* of North India. That North Indian classical *Ragas* are capable of evoking emotions is well documented in North Indian classical music (NICM) theory(Bhatkhande, 1934) but very few attempts have been made to investigate this phenomenon. A *raga* uses a series of five or more musical notes upon which a melody is constructed. However, the way the notes are approached and

rendered in musical phrases and the mood they convey are more important in defining a *raga* than the notes themselves. In theory, a *raga* depicting a particular emotion could evoke multiple emotions in a listener. The basic set of tones and tone-relationships used in Hindustani classical music from which *Ragas* are derived is the 12-tone octave divisions. Each interval is a tone defined by the ratio of its fundamental frequency to the tonic.

However very little empirical work has been done linking the emotions experienced by participants to the acoustic properties of *ragas*. Balkwill and Thompson [9] reported that Japanese participants were sensitive to the intended emotions of *ragas* and this sensitivity was associated with the underlying acoustic cues. Another study by Chordia et. al. [10], that characterized the emotional responses of listeners to five different *ragas* found that the interplay between the major and minor intervals predicted the variance associated with happy and sad ratings of participants. The primary predictors of emotion were pitch-class distribution, pitch-class dyad entropy, overall sensory dissonance, and note density, which in combination explained 33% and 28% of response variance in happy and sad ratings. Although the explanatory power of these models was limited, the results suggested that *ragas* do consistently elicit specific emotions that are linked to musical properties. However the role of rhythm in emotion perception of *ragas* has not been studied so far.

The first objective of this study was to to understand emotional contagion associated with Hindustani classical *ragas*. In this study we used both alaap (slow arrhythmic introductory section of a *raga*) and gat (faster composition with a rhythmic accompaniment) of *ragas* to understand the role of rhythm in emotion perception. The second objective was to establish the role of acoustic properties of Hindustani classical *ragas* in recognising the emotions associated with them. As a first step in this direction, we conducted an internet based survey to investigate emotional contagion associated with twelve North Indian classical *Ragas.*

3. MATERIALS AND METHODS

Three minute instrumental renditions of twelve Hindustani classical *Ragas* were composed and played by a professional musician on *sarod* and digitally recorded in both *alaap* and *gat*. *Ragas* were chosen to induce both positive and plaintive emotional states (Table 1). It was also ensured that all the pieces in *gat* were provided similar accompaniment on tabla in *teen taal*. A detailed questionnaire to ascertain demographic information, details of music preference and training was implemented before starting with the survey. Participants were instructed to listen to the *Raga* excerpts for a minimum of one minute and rate each *raga* on all of the following emotions on a 0-4 Likert scale (with 0 being 'not at all felt' to 4 being 'felt the most'). The emotions were: happy, romantic, devotional, calm/soothed, angry, longing/yearning, tensed/restless, and sad. The survey is available at http://emotion-in-music.nbrc.ac.in/p1/.

The results of the survey were analysed using SPSS v20 as described below:

3.1 Behavioral data analysis

Average ratings for each emotion for all *ragas* with positive and plaintive intended emotion played in *alaap* and *gat* were computed. Following this, a confusion matrix representing the average ratings of emotional responses provided by the subjects were plotted against the intended emotion of *ragas*.

3.2 Acoustic Analysis

In order to determine the underlying relationship between the tonality of *Raga* and its intended emotion the tonal structure of different *Ragas* was assessed. The tonic interval is a tone defined by the ratio of its fundamental frequency to the tonic (*Sa*). In the notation used the 7 *shuddha swaras* are denoted by capital letters (S, R, G, M, P, D, N) , 5 *komal swaras* and *1tivra swara* are *denoted* by small letters (r, g, m, d, n) .

Pitch was extracted using Melodia- Melody extraction toolbox for every 30 ms window for all the ragas [11] . The pitch class distributions for tonic intervals were calculated by making histograms of the pitch values calculated in cents. The bins corresponded to each note of three octaves centered around tonic for that segment. The three octaves were then folded into one and the values were normalized to create pitch-class distributions. The bin counts were averaged across *ragas* with positive and plaintive intended emotion

Table 1. The table lists the ragas played by the artist, thaat of the ragas, the scale used by artist and the emotion intended by the artist. The thaat of ragas refers to the musical scale comprising of seven notes presented in their order of ascent.

S. No	Raga	Thaat	Scale used by Artist							Intended Emotion	
1	Tilak kamod	Khamaj	S	R	G	M	P	D	N	Positive	Happy/Romantic/Peaceful
2	Hansadhwani	Bilawal	S	R	G		P		N	Positive	Happy/Romantic/Peaceful/ Devotional
3	Desh	Khamaj	S	R	G	M	P	D	n/N	Positive	Happy/Romantic/Peaceful
4	Yaman	Kalyan	S	R	G	m	P	D	N	Positive	Devotional/Romantic/Peaceful
5	Rageshree	Khamaj	S	R	G	M		D	n	Positive	Happy/Romantic/Peaceful
6	Jog	Kafi	S		g/G	M	P		n	Positive	Happy/Romantic/Peaceful
7	Marwa	Marwa	S	r	G	m		D	N	Plaintive	Sad/Tensed/Devotional
8	Lalit	Marwa	S	r	G	M/m	P	d	N	Plaintive	Sad/Romantic/Peaceful
9	Malkauns	Bhairavi	S		g	M		d	n	Plaintive	Sad/Romantic/Peaceful/ Devotional
10	Shree	Purvi	S	r	G	m	P	d	N	Plaintive	Sad/Anger/Devotional
11	Basant Mukhari	Bhairav	S	r	G	M	P	d	n	Plaintive	Sad/Romantic/Peaceful
12	Miyan ki todi	Todi	S	r	g	M/m	P	d	N	Plaintive	Sad/Tensed/Devotional

to obtain average distributions of interval size. The differences between emotional conditions for each 100 cent bin were evaluated for statistical significance using two tailed Mann-Whitney U-test [8].

3.3 Regression Analysis

Stepwise multiple linear regression analysis was conducted in order to determine the variance of the emotional responses explained by the mean frequency of occurrence of the tonic intervals.

4. PARTICIPANT DETAILS

A total of 164 participants took the survey (F = 85, M = 79). The percentage of participants in the age range <20, 20 - 40, 40-60, >60 was 6.1%, 3.7%, 61.6%, 28.0% respectively. People from different cultural backgrounds participated in the survey. The percentage of participants from Asia primarily India was 65.24 %, America was 10.37 % and Europe was17.68 %.

5. RESULTS AND DISCUSSION

5.1 Behaviour

The confusion matrix representing the average ratings of emotions for positive and plaintive *ragas* across *alaap* and *gat* are shown in Fig 1A and Fig 1B respectively. The average ratings of emotion are colour coded; the intensity of colour represents the weightage of ratings. The highest average rating for ragas whose intended emotion was positive when played in *alaap* was for 'calm/soothing' but when played in *gat* shifted to 'happy'. The highest average rating for ragas whose intended emotion was plaintive was for 'sad'' but when played in gat shifted to 'Longing/Yearning' or 'Tensed/Restless'.

5.2 Acoustic

The percent mean frequency of occurrence of tonic intervals averaged across *alaap* of *ragas* whose intended emotion was positive and plaintive is shown in Fig 2 .The analysis of tonic intervals revealed that the positive
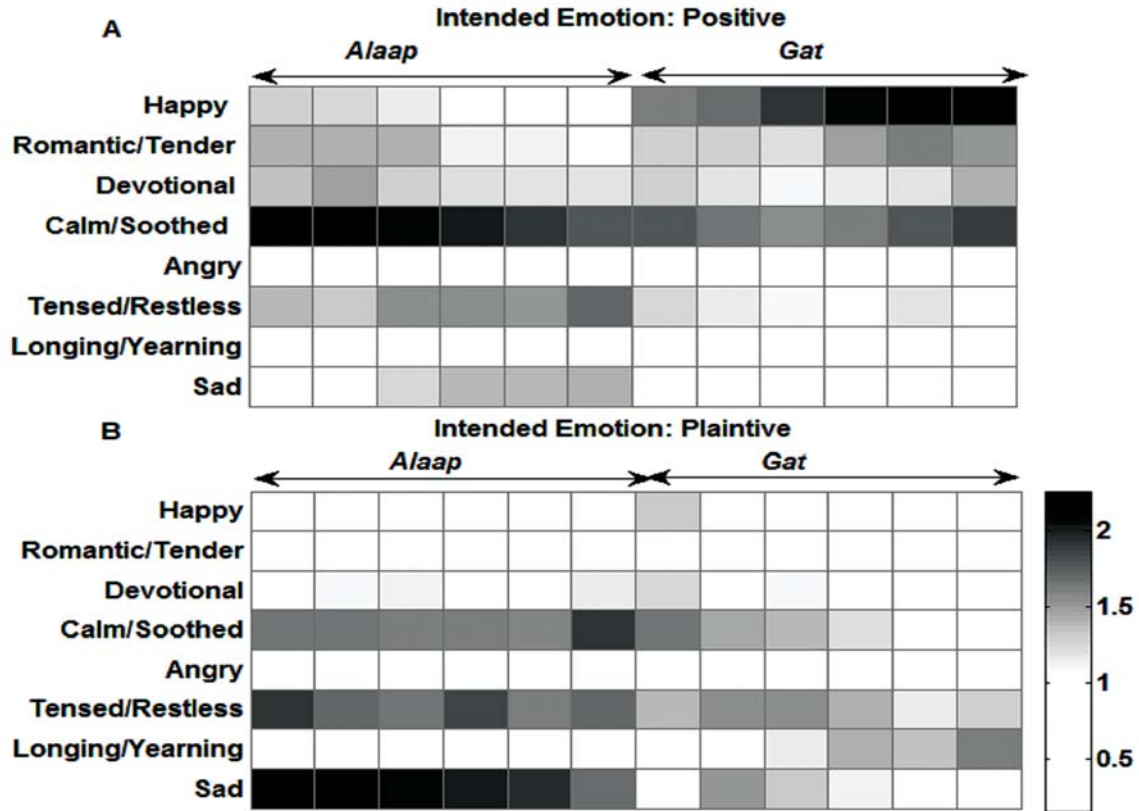
Fig. 2. The percent mean frequency of occurrence of tonic intervals averaged *across* alaap of *ragas* whose intended was positive (red) and plaintive (blue).

ragas are characterized by more major intervals (*shuddh swaras*) while plaintive ragas are characterized by more minor intervals (*komal swaras*). The two-tailed Mann-Whitney U test was conducted to assess statistical significance of the differences in the mean frequency of occurrence of major and minor intervals in positive and plaintive *ragas*. The results of the test revealed that the mean frequency of occurrence of major second (*shuddh Re* ($z = -1.92$, p ?.05) and major third (*shuddh Ga* ($z = -2.24$, p <.05) was significantly higher in ragas whose intended emotion was positive. Also, the mean frequency of occurrence of minor second (*komal re* ($z = -2.88$, p <.05)) and minor sixth (*komal dha*($z = -2.88$, p <.05)) was significantly higher in plaintive ragas. The results remained consistent for gat of ragas.

5.3 Regression Analysis

Stepwise multiple regressions were performed to identify the tonic intervals that best predict ratings of each emotion. The tonic intervals minor second (*komal re*), major seventh (*shuddh Ni*) and triton (*tivra Ma*) explained 90 % of variance for ratings for happy emotion ($R^2 = .90$, $F (3, 8) = 25.05$, $p < .001$). The percent mean frequency of occurrence major seventh (*shuddh Ni*) was positively correlated and percent mean frequency of occurrence minor second (*komal re*) and triton (*tivra Ma*) was negatively correlated with average rating for happy emotion. All three variables added statistically significantly to the prediction of ratings for happy emotion, $p < .001$.

The tonic intervals minor second (*komal re*) and major seventh (*shuddh Ni*) explained 86 % of variance ratings for sad emotion ($R^2 = .86$, $F (2, 9) = 28.91$, $p<0.001$). The percent mean frequency of occurrence minor second (*komal re*) was positively correlated and percent mean frequency of occurrence major seventh (*shuddh*
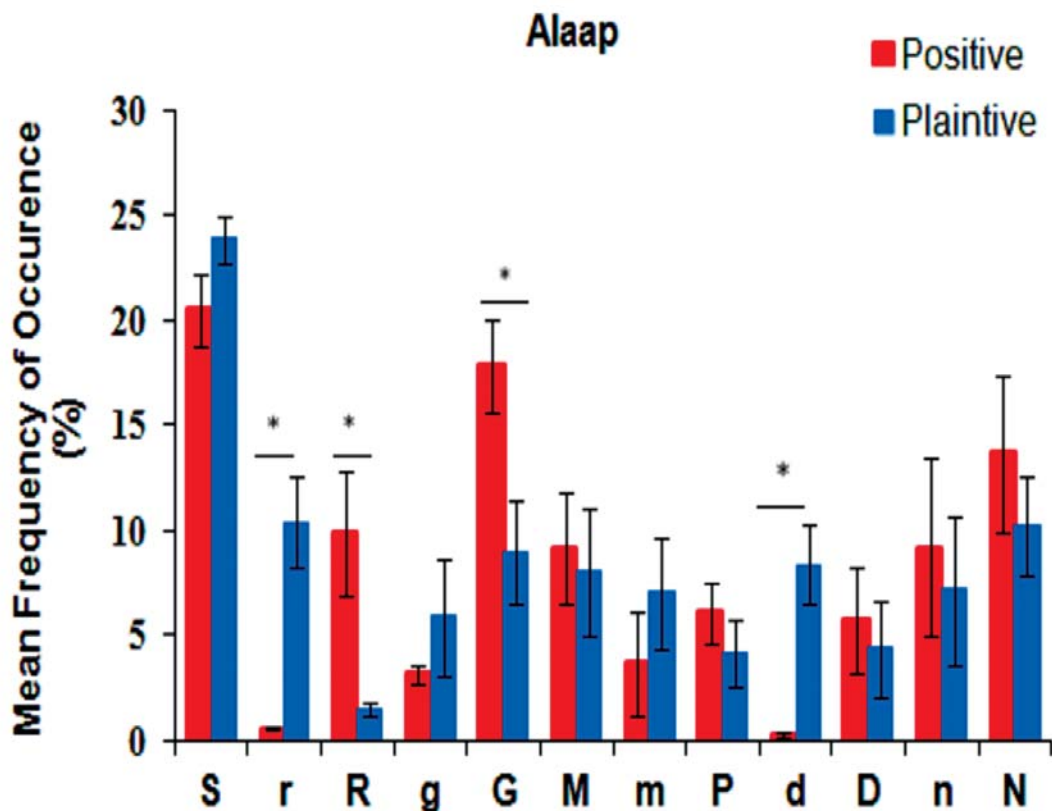
Fig. 2. The confusion matrix representing the average ratings of participants for *alaap* (N=121-141) and *gat* (N=121-143) of *ragas* with positive (Fig 1 A) and plaintive (Fig 1 B) intended emotion.

Ni) was negatively correlated with average ratings of sad emotion. Both the variables added statistically significantly to the prediction of ratings for sad emotion, $p < .001$.

The results of regression analysis are reported in Table 2.

Table 2. Results of Stepwise multiple linear regressions performed in order to determine the variance of the emotional responses explained by all the tonic intervals. (*p<0.05, **p<0.001)

Happy	Romantic	Devotional	Calm	Angry	Longing	Tensed	Sad
N,	r,	R,	N,	r,	R,	r,	r,
? = 0.54 *	β = -0.88 **	β = 0.96 **	β = 0.59 **	β = 0.58 *	β = -0.78 *	β = -0.78 *	β = 0.86 **
r,		M,	r,	d,			N,
β = -0.68 **		β = 0.40 *	β = -0.69 **	β = 0.48 *			β = -0.38*
m,			m, β = -0.33 *				
β = -0.35 *							
R^2 = 0.90	R^2 = 0.77	R^2 = 0.77	R^2 = 0.95	R^2 = 0.80	R^2 = 0.62	R^2 = 0.62	R^2 = 0.86
F(3,8)	F(1,10)	F(2,9)	F(3,8)	F(2,9)	F(1,10)	F(1,10)	F(2,9)
= 25.05,	= 33.56,	= 15.31,	= 51.47,	= 18.30,	= 16.02,	= 16.09,	= 28.91,
p<0.001	p<0.001	p<0.001	p<0.001	p<0.001	p<0.05	p<0.05	p<0.001

6. CONCLUSIONS

The findings of our behavioural survey showed that different *Ragas* evoke a different set of emotional responses belonging to positive and plaintive categories. Our results also suggest that perception of emotion in *ragas* transcends culture boundaries and thereby indicates that it is the underlying acoustic properties of the *ragas* that listener's indentify as cue for judging the underlying emotions. Analysis of behavioural results showed that *ragas* when played in *alaap* were given highest ratings for 'calm/soothing' and 'sad' emotions and when the same *ragas* were played in *gat* the highest ratings shifted from 'calm/soothing' to 'Happy' and from 'sad' to 'Longing/Yearning' or 'Tense/Restless'emotions. The correlation of acoustic properties of *ragas* with behavioural data suggests that it is the underlying distribution of notes (specific pitch intervals) of a *Raga* that listeners associate with positive or plaintive emotions and presence of rhythm enhances that perception.

The positive *ragas* have high mean frequency of occurrence major intervals (*shuddh swaras*) where as plaintive ragas have high mean frequency of occurrence minor intervals (*komal swaras*). These results are consistent with western music literature where major and minor modes have been associated with positive and negative valence respectively. It is the presence of specific pitch intervals in melodic composition of *raga* that listeners associate with emotions. The regression models suggest that within the subset of *ragas* used in our study the *ragas* with presence of *shuddh Ni*, absence of komal re and *tivra Ma* (*raga* Hansdhwani and *raga* Tilak Kamod) are associated with 'happy' emotion where as *raga* with presence of komal re and absence of *shuddh Ni* (*raga* Basant Mukhari) is associated with 'sad' emotion.

To sum up, the present study confirms and extends previous work on the induction of emotion during music listening. The ragas chosen for this experiment have proved suitable for the induction of emotions as assessed by subjective ratings. One intriguing question for the guidance of future research is the neural representation of musically induced emotions by Hindustani classical *ragas.*

7. REFERENCES

[1] S. KHALFA, M. ROY, P. RAINVILLE, S. DALLA BELLA and I. PERETZ, 2008. Role of tempo entrainment in psychophysiological differentiation of happy and sad music? International journal of psychophysiology. *Journal of the International Organization of Psychophysiology* **68** (1), 17-26.

[2] V.N. SALIMPOOR, M. BENOVOY, G. LONGO, J.R. COOPERSTOCK and R.J. ZATORRE, 2009. The rewarding aspects of music listening are related to degree of emotional arousal. *PloS one* **4** (10), e7487.

[3] S. KOELSCH, T. FRITZ, D.Y.V. CRAMON , K. MÜLLER and A.D. FRIEDERICI . 2006. Investigating emotion with music: an fMRI study. *Human brain mapping* **27** (3), 239-50.

[4] M.T. MITTERSCHIFFTHALER, C.H.Y. FU , J.A. DALTON , C.M. ANDREW and S.C.R.WILLIAMS, A 2007. functional MRI study of happy and sad affective states induced by classical music. *Human brain mapping* **28** (11), 1150-62.

[5] P.N. JUSLIN and D. VÄSTFJÄLL, 2008. Emotional responses to music: the need to consider underlying mechanisms. *The Behavioural and brain sciences* **31** (5), 559-75; discussion 575-621.

[6] M. ZENTNER, D. GRANDJEAN and K.R. SCHERER, 2008. Emotions evoked by the sound of music: characterization, classification and measurement. *Emotion* (Washington, D.C.) **8** (4), 494-521.

[7] S. VIEILLARD, I. PERETZ, N. GOSSELIN, S. KHALFA, L. GAGNON and B. BOUCHARD, 2008. Happy, sad, scary and peaceful musical excerpts for research on emotions. *Cognition & Emotion* **22** (4), 720-752.

[8] D.L. BOWLING, J. SUNDARARAJAN, S. HAN and D. PURVES, 2012. Expression of emotion in Eastern and Western music mirrors vocalization. *PloS one* **7** (3), e31942.

[9] W. F. THOMPSON and R.I.E. MATSUNAGA, 2004. Recognition of emotion in Japanese , Western , and Hindustani music by Japanese listeners 1. **46** (4), 337-349.

[10] P. CHORDIA and A. RAE, Understanding Emotion In Raag?: An Empirical Study Of Listener Responses.

[11] J. SALAMON, E. GÓMEZ, 2012. Melody Extraction From Polyphonic Music Signals Using Pitch Contour Characteristics. **20**(6), 1759-1770.

A Comparision between Acoustic Absorption Coefficient and Trasmistion Loss Analysis of Multi-Layer Absorbers

Mahavir Singh and Gurbir Singh

Acoustics, Ultrasonics & Vibration (AUV) Section, CSIR-National Physical Laboratory,
Dr. K. S. Krishnan Road, New Delhi 110 012, India
e-mail: mahavir.acoustics@gmail.com

ABSTRACT

A comparison between practical acoustic sound absorption coefficient and transmission analysis of multi-layer absorber as the filler with and without perforated panels were studied this paper. Experimental data obtained using reverberation room test method were compared with data from numerical simulation. The innovative sound absorption panel was developed and fabricated using treated absorber layers as sound absorption materials. The outer layer of the panel was fabricated from absorber/polyester composite panel. This innovative acoustic panel was tested at acoustic lab of Acoustics, Ultrasonics and Vibration (AUV) Standards at CSIR-National Physical Laboratory, New Delhi using ISO 354 standard for noise absorption coefficient and ISO 717-1 standard for the sound transmission loss (TL). Simulation study was also conducted for the sound absorption panel. For the sound absorption coefficient, the experiment gives the value between 0.70 and 0.80 for the frequency range of 1000 to 1800 Hz while the sound absorption coefficient obtained from simulation gives 0.7 to 0.85 for the frequency range of 500 to 2500 Hz. TL gives an average of 20 dB for the panel. The results showed that the sound absorption coefficient obtained through both the experimental and simulation methods were comparable to those use commercially in the market such as rock wool and synthetic absorber.

1. INTRODUCTION

Currently, commercially available sound absorption materials for acoustic treatment used in the building construction industry consisted of glass-or mineral-fibre materials. However, they are growing concern in health and safety related issue due to the potential health risks associated to these fibres when exposed to human such as the effect from fibre shedding from glass-or mineral fibre materials to human lungs and eyes. These issues provide an opportunity for alternative materials from organic fibres to be developed as replacement materials. In India, agricultural waste such as coir fibres, rice fibre and oil palm frond fibre are abundance and usually burnt or used as an agricultural by-products. Recently, natural fibres from agriculture are increasingly being investigated for various usage in many structural and non-structural applications such as a substitute for synthetic fibres in composite materials and lining for automotive components. However, natural fibres such as coir fibre are also suitable as a substitute to synthetic fibres and wood-based materials for acoustic absorption purposes. These fibres have many advantages because they are cheaper, renewable and abundance, non-abrasive and does not give rise to health and safety issue during processing and handling [3-5,12]

Researcher [6] has developed particle composite boards from agricultural waste products using combinations of durian peel and coir fibre straw particles instead of wood as an insulation board in wooden construction industry. Researchers [14] study the acoustic properties of rice straw-wood particle composite boards and found that the sound absorption coefficient in the frequency range of 500 to 8000 Hz is higher than other wood-based materials which are due to the low specific gravity of the composite boards.

To improve the acoustic properties further, perforated plate design is used in the construction of the panels. Researcher [7] studied the effect of the perforated plate, airspace layers and porosity on the acoustic properties of materials. He found that the porosity of the perforated plate and the density of the porous material would significantly affected the acoustic impedance and sound absorption coefficient of the panel in which case the frequency b and near the resonance frequency achieved high acoustic absorption. Some researcher [8] reported that the acoustic absorption of multi-layer materials is better with perforated plate backed with airspaces.

The main parameter that is critical in the determination of the acoustic properties is the acoustic absorption coefficient properties and transmission loss index. These parameters were determined using the tests carried out in the reverberation chamber method at the Acoustic Lab, CSIR-NPL, New Delhi. Computer simulation (using the dBBAT132 program) was carried out to determine the reference acoustic parameters. The acoustic properties of the rock wool materials were also determined as a comparison. The fibres arrangements in the plate were studied using the scanning electron microscope. Latex was used to provide the necessary cohesion between the coir fibres so that its arrangement can be moulded into square layers for the acoustic testing purposes. The latex was shown to have no influence on the sound absorption properties due to the small influence on the fibres physical characteristics. Other usage of natural fibre is in applications to reduce sound propagation in automotive interior spaces or to improve the control of outdoor noise propagation [7].

The aim of this research was to study the potential use of the multi-layer absorbers as a sound absorption material to replace synthetic materials such as glass, mineral wool, felts or polyester fibre in commercial applications. This study investigated the sound absorption properties of the coir fibres together with the characteristics of the coir fibres and its fibre arrangement as the data were important to optimize the acoustic properties of the panel. The characteristics and arrangement of the fibre were found to influence the acoustic properties of the panel [10]. The use of natural fibres as sound absorption materials will be good for environment as it is biodegradable and exposed no potential health risk.

2. MATERIAL AND METHODS

There are two main parts in carrying out this research. The first is to fabricate the composite panel box using coir/polyester composites and the second is to use treated coir fiber as the absorption materials. The combination of high quality natural fiber/polyester composite and coir fiber as the absorption material gives the panel a good absorption characteristic. The outer layer of the sound absorption panel is fabricated with polyester resin reinforced with coir fiber to make the composite strong and stiff. Perforated panel design requires holes to be drilled on the panels surface in order to give more advantages in acoustic part by decreasing the optimum absorption coefficient to the lower frequency [13].

2.1 Noise absorption coefficient

2.1.1 Experiments using reverberation room

Experiments using the reverberation room have been performed to calculate the noise reduction coefficient (NRC). The test was performed using ISO 354 (1985) standard for noise absorption coefficient. The required inputs are reverberation time for empty room, RT0 and reverberation time for room with sample, RTm. Parameter needed for the experiment are volume for an empty rever-beration room and testing area for the sample. Figure 1 shows the schematic drawing of the experimental setup and Figure 2 shows the sound absorption perforated panel using coir fibre as the absorption material. The tests were carried out at the Acoustic Lab in the CSIR-NPL, New Delhi.
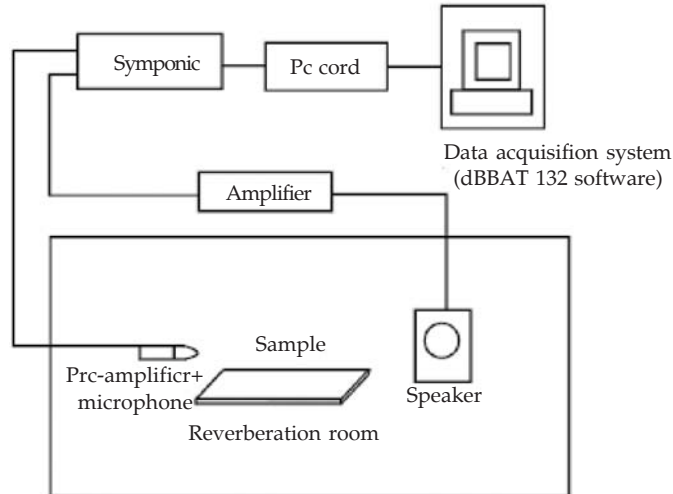
Fig. 1. Schematic configuration absorption coefficient test in the reverberation room
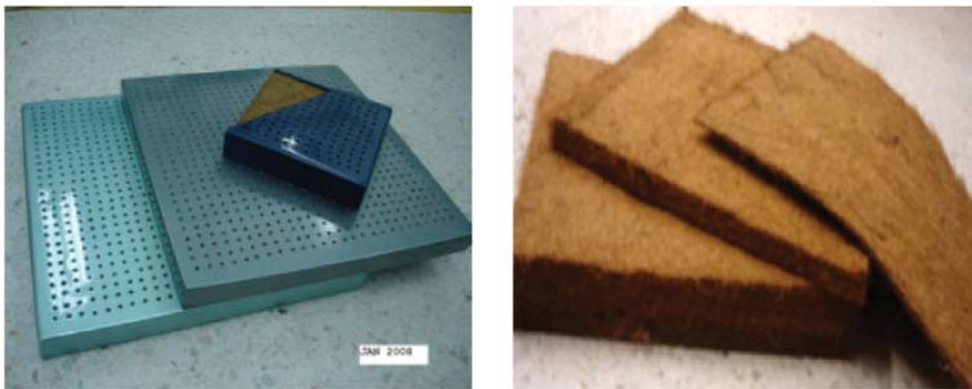

Fig. 2. Sound absorption perforated panel using coir fibre as an absorption material

2.1.2 Simulation program

For the simulation works, absorption coefficients of panels were calculated by the computer [4]. This program implements the transfer matrix method for a number of materials, including porous material and perforated plates (slotted, with circular holes etc.). The program calculates the absorption coefficient, impedance and sound reduction index. Calculation can be performed at single frequencies or as mean values in 1/3 octave frequency. Simulation program has also been used to estimate the acoustic performance of materials with and without airspaces [4].

2.2 Noise absorption coefficient

Experiments for the transmission lost have been conducted at acoustic lab, CSIR-NPL, New Delhi which consisted of reverberation chambers method using the ISO 717-1 standard [4]. The composite panel was placed between the two rooms and a noise source was given from the small reverberation room.

3. RESULT AND DISCUSSION

3.1 Sound absorption coefficient

Simulations works have been conducted in order to predict the sound absorption coefficient of the panel before the experimental tests were conducted. The simulation for the noise absorption coefficient of the

plain coir fiber and coir fiber with perforated panel were calculated using computer program. In the simulation works, absorption coefficients of the panels were calculated by the computer program. This program also had been used for simulations to estimate the acoustic performance of constructions combining different material layers by other researchers This program implements the transfer matrix method for a number of materials, including porous materials and perforated plates (slotted, with circular holes or microperforated etc.). Program does the job of calculating absorption coefficient, impedance and sound reduction index for such constructions. Calculations may be performed at single frequencies or as mean values in 1/3-octave bands, in both cases for a free field sound incidence as well as in diffuse field. Figure 3 shows the result obtained for the noise absorption coefficient for multi-layer coir fibre with and without composite perforated panel. The coir fiber with perforated panel shows higher coefficient index compared to the plain coir fiber for the range of 500 Hz until 2500 Hz. For the frequency range of more than 2500 Hz, the coir fiber without panel gives higher coefficient index. The highest coefficient index for coir fiber with perforated panel is in the range of 0.7 to 0.85 for the frequency range of 500 Hz until 2500 Hz while for the coir fibre without panel, it is around 0.8 for the range 2500 Hz until 5000 Hz.

3.2 Sound transmission loss

The experimental results of the transmission loss for the composite perforated panel have an average value of 20 dB. Several other tests have also been carried out to compare the results. Figure 5 shows the result of transmission lost versus frequency for the coir fibre in the composite perforated panel. Figure 6 shows the comparison for several other composite perforated panels using different type of natural fibre materials. For the first 12 data point, the composite perforated panel with coir fiber gives the comparable transmission lost compared to other samples. Beginning from No.12 to 16, for the range of 630 Hz until 1600 Hz, the composite gives higher value of transmission lost compared to the curve for composite with coir fiber without perforated panel and from No. 17 until 27, it is giving the highest transmission lost compared to the other samples.

Composite with oil palm fiber sample shows the optimum value from the 6th data (160 Hz) until 8th data (315 Hz). For the fourth sample (coir fibre without composite perforated panel), the optimum value for transmission lost index appears from the range 16th data (1600 Hz) until 24th data (10 kHz). In the case of
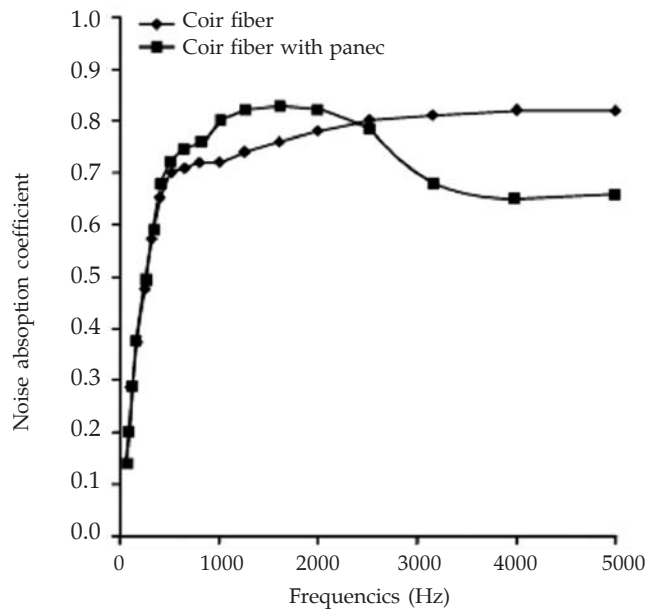

Fig. 3. Comparison of simulation values for noise absorption coefficient between coir fibre with and without composite perforated panel
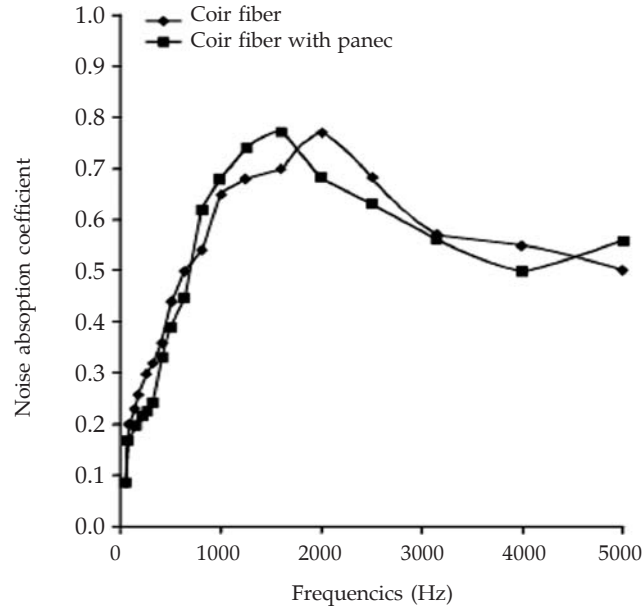
Fig. 4. Comparison of experimental values for noise absorption coefficients between coir fibre with and without composite perforated panel
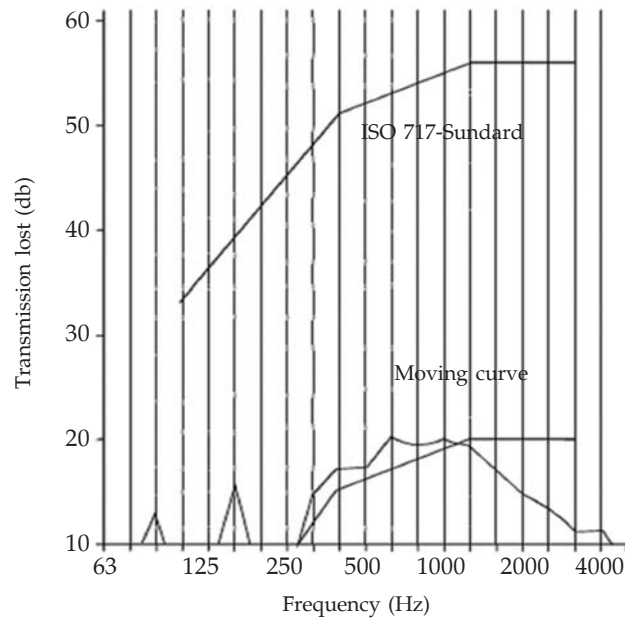

Fig. 5. Transmission lost versus frequency for coir fibre in composite perforated panel

perforated facing, the structure promotes the sound absorption coefficients in the low-frequency region, but it has the reverse effect in the high frequency region. Therefore, many considerations are required for the purpose of sound control; on the other hand, the multi-layer coconut coir fiber contributed to increase the sound absorption coefficients. This provides a reliable guidance for the design of multi-layer sound absorbers.
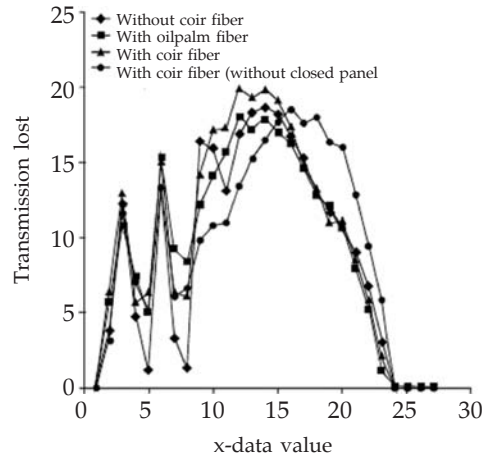
Fig. 6. Comparison of transmission lost index for different configuration of coir fibre and oil palm fibre

4. CONCLUSION

In this study multi-layer absorber has been introduced as one of the sound absorption material. The results form the simulation and experimental tests show that it has good acoustic properties and has a high potential to be an alternative replacement of synthetic based commercial product. By introducing the composite perforated panel made from fibre-reinforced polymeric materials, the innovative sound absorption panel shows a good potential to be an environmentally friendly product. As one of the green technology product, this innovative absorption panel has a bright future because they are cheaper, lighter and environmentally superior compare to glass fiber and mineral based synthetic materials. The results of the acoustic properties obtained shows that the coir fibre gave a good sound absorption coefficient and transmission loss index value. The fibres arrangement in the coir fibre can be modified in order to control the sound absorption properties. This will allow the coir fibre to be used in applications to reduce sound propagation in interior spaces or to improve the control of outdoor noise propagation. Further works can be carried out to optimize and increases the performance of the coir fibres.

5. REFERENCES

[1]   MAHAVIR SINGH, DHARAM PAL SINGH and OMKAR SHARMA, 2010. Airborne Sound Transmission in Lightweight Wall Design Structures for Residential and Commercial Buildings, *Proc. of the 20th International Congress on Acoustics (ICA-2010), Sydney*, 1-6.

[2]   MAHAVIR SINGH, OMKAR SHARMA and DHARAM PAL SINGH, 2010. Controlling Reverberant Noise in Rooms using Sound Absorptive Materials, *Proc. of National Symposium on Acoustics (NSA2010), Rishikesh*, 73-78.

[3]   MAHAVIR SINGH, OMKAR SHARMA and DHARAM PAL SINGH, 2011. Room Acoustics - Design for Internal Acoustic Quality, *Journal of the Acoustical Society of India*, **38** (1), 3-10.

[4]   MAHAVIR SINGH, 2011. Sound Transmission through Building Elements, *Proc. of Indo-US Work shop on Nanosonic & Ultrasound (IUWONU2011) and International Conference on Nanotechnology & Ultrasound (ICNU2011), Trichy*, 52 -70.

[5]   MAHAVIR SINGH, OMKAR SHARMA and DHARAM PAL SINGH, 2011. Experimental Investigations of the Sound Transmission Loss of Window Panels, *Proc. of 1st National Conference on Advances in Metrology* (*AdMet-2011*), *Banglore*, 1-6.

[6]   MAHAVIR SINGH, OMKAR SHARMA and DHARAM PAL SINGH, 2011. Acoustic Comfort - Noise Control for Buildings, *New Dimensions of Physics of Proc. of National Conference on Ultrasonics (NCU-2011), Jhansi*, 1-14.

[7]   MAHAVIR SINGH, OMKAR SHARMA and DHARAM PAL SINGH, 2011. Sound Transmission through Cavity Walls Constructed from Gypsum Board, GESTS Int'l Trans. *Acoustics Science and Engr.*, **15**(3), 107-112.

[8]   MAHAVIR SINGH, DHARAM PAL SINGH and OMKAR SHARMA, 2011. Sound Insulation Performance of Double-leaf Structures, *Acoustic Waves of Proc. of National Symposium on Acoustics* (*NSA2011*), *Bundelkhand*, *15-24* (*Received a Best Paper Award*).

[9]   MAHAVIR SINGH, OMKAR SHARMA and DHARAM PAL SINGH, 2011. Sound Transmission Loss of a New Designed Lightweight Partition, *Acoustic Waves of Proc. of National Symposium on Acoustics* (*NSA2011*), Bundelkhand, 62-77.

[10] MAHAVIR SINGH, 2012. Development of Lightweight Sandwich Material as Acoustic Partitions for Building Applications, *Proc. of National Seminar on Material Characterization by Ultrasonics* (NSMCU2012), *New Delhi*, 1-10.

[11] DHARAM PAL SINGH and MAHAVIR SINGH, 2012. Acoustic Properties of Coconut Coir Fiber Sound Absorptive Material, *Proc. of National Seminar on Material Characterization by Ultrasonics* (*NSMCU2012*), *New Delhi,* 1-7 (Received a Best Paper Award).

[12] MAHAVIR SINGH and DHARAM PAL SINGH, 2012. Evaluating Accurate Value of the Reverberation Chamber Sound Absorption Coefficient, *Proc. of National Symposium on Acoustics* (*NSA2012*), *Tiruchengode*, 45-53.

[13] MAHAVIR SINGH, 2013. Acoustics Properties of New Rice Husk Sound Absorptive Material, *Proc. of International Conference on Advances in Building Sciences* (*BTCM 2013 Confeences*), Chennai, 257-264.

[14] MAHAVIR SINGH AND DHARAM PAL SINGH, 2013. Acoustic Metrology of Agricultural Waste Material as a Sound Absorber, *Proc. of 8th International Conference on Advances in Metrology"* (*AdMet-2013*), New Delhi, 189-190.

Acoustical Society of India
(Regn. No. 65-1971)

New Executive Council (2014 - 2016)

President	:	**Prof. V. R. Singh**
		[PDM EI, New Delh-NCR; vrsingh@yahoo.com; +91-98 11 57 46 36]
Vice President	:	**P. V. S. Ganesh Kumar**
		[NSTL, Vizag; gkpakki@rediffmail.com; +91-98 66 40 08 94]
General Secretary	:	**Dr. Mahavir Singh**
		[CSIR-NPL, New Delhi; mahavir@nplindia.org; +91-98 71 69 33 46]
Jt. Secretary	:	**Dr. I. Johnson**
		[SJC, Trichy; jnaadarsh@hotmail.com; +91-94 42 90 48 20]
Treasurer	:	**Dr Yudhisther K Yadav**
		[CSIR-NPL, New Delhi; ykyadav@nplindia.org; +91-98 71 38 47 01]
Editor in Chief	:	**Dr. B. Chakraborty**
		[CSIR-NIO, Goa; bishwajit@nio.org; +91-98 90 00 87 25]
Council Members	:	**Dr. (Mrs.) Rita Paikarey**
		[RU, Cuttack; r_paikaray@rediffmail.com; +91-94 37 14 71 50]
		Dr. Rajiv K. Upadhayay
		[AU, Aligarh; rku8@rediffmail.com; +91-94 12 97 28 90]
		Dr. S. K. Shrivastava
		[BU, Jhansi; sksphys@yahoo.com; +91-94 15 05 55 65]
		Dr. Alok Kumar Gupta
		[NIOS, Noida; alokphy@gmail.com; +91-98 18 93 69 66]
		Dr. V. Rajendran
		[Imm. Past President; veerajendran@gmail.com; +91-99 94 13 03 03]
Co-opted Members	:	**Dr. S. Kandaswamy**
		[PSS Associates, Chennai; kanda_swamy@hotmail.com; +91-98 40 80 71 00]
		R. N. Jindal
		[MoEF, New Delhi; rnjindal@yahoo.com;+91-98 68 11 30 36]

INFORMATION FOR AUTHORS

ARTICLES

The Journal of Acoustical Society of India (JASI) is a refereed publication published quarterly by the Acoustical Society of India (ASI). JASI includes refereed articles, technical notes, letters-to-the-editor, book review and announcements of general interest to readers.

Articles may be theoretical or experimental in nature. But those which combine theoretical and experimental approaches to solve acoustics problems are particularly welcome. Technical notes, letters-to-the-editor and announcements may also be submitted. Articles must not have been published previously in other engineering or scientific journals. Articles in the following are particularly encouraged: applied acoustics, acoustical materials, active noise & vibration control, bioacoustics, communication acoustics including speech, computational acoustics, electro-acoustics and audio engineering, environmental acoustics, musical acoustics, non-linear acoustics, noise, physical acoustics, physiological and psychological acoustics, quieter technologies, room and building acoustics, structural acoustics and vibration, ultrasonics, underwater acoustics.

Authors whose articles are accepted for publication must transfer copyright of their articles to the ASI. This transfer involves publication only and does not in any way alter the author's traditional right regarding his/her articles.

PREPARATION OF MANUSCRIPTS

All manuscripts are refereed by at least two referees and are reviewed by the Publication Committee (all editors) before acceptance. Manuscripts of articles and technical notes should be submitted for review electronically to the Chief Editor by e-mail or by express mail on a disc. JASI maintains a high standard in the reviewing process and only accept papers of high quality. On acceptance, revised articles of all authors should be submitted to the Chief Editor by e-mail or by express mail.

Text of the manuscript should be double-spaced on A4 size paper, subdivided by main headings-typed in upper and lower case flush centre, with one line of space above and below and sub-headings within a section-typed in upper and lower case understood, flush left, followed by a period. Sub-sub headings should be italic. Articles should be written so that readers in different fields of acoustics can understand them easily. Manuscripts are only published if not normally exceeding twenty double-spaced text pages. If figures and illustrations are included then normally they should be restricted to no more than twelve-fifteen.

The first page of manuscripts should include on separate lines, the title of article, the names, of authors, affiliations and mailing addresses of authors in upper and lowers case. Do not include the author's title, position or degrees. Give an adequate post office address including pin or other postal code and the name of the city. An abstract of not more than 200 words should be included with each article. References should be numbered consecutively throughout the article with the number appearing as a superscript at the end of the sentence unless such placement causes ambiguity. The references should be grouped together, double spaced at the end of the article on a separate page. Footnotes are discouraged. Abbreviations and special terms must be defined if used.

EQUATIONS

Mathematical expressions should be typewritten as completely as possible. Equation should be numbered consecutively throughout the body of the article at the right hand margin in parentheses. Use letters and numbers for any equations in an appendix: Appendix A: (A1, (A2), etc. Equation numbers in the running text should be enclosed in parentheses, i.e., Eq. (1), Eqs. (1a) and (2a). Figures should be referred to as Fig. 1, Fig. 2, etc. Reference to table is in full: Table 1, Table 2, etc. Metric units should be used: the preferred from of metric unit is the System International (SI).

REFERENCES

The order and style of information differs slightly between periodical and book references and between published and unpublished references, depending on the available publication entries. A few examples are shown below.

Periodicals:
[1] S.R. Pride and M.W. Haartsen, 1996. Electroseismic wave properties, *J. Acoust. Soc. Am.*, 100 (3), 1301-1315.
[2] S.-H. Kim and I. Lee, 1996. Aeroelastic analysis of a flexible airfoil with free play non-linearity, *J. Sound Vib.*, 193 (4), 823-846.

Books:
[1] E.S. Skudzryk, 1968. *Simple and Comlex Vibratory Systems*, the Pennsylvania State University Press, London.
[2] E.H. Dowell, 1975. *Aeroelasticity of plates and shells*, Nordhoff, Leyden.

Others:
[1] J.N. Yang and A. Akbarpour, 1987. Technical Report NCEER-87-0007, Instantaneous Optimal Control Law For Tall Buildings Under Seismic Excitations.

SUMISSIONS

All materials from authors should be submitted in electronic form to the JASI Chief Editor: Dr Mahavir Singh, Acoustics, Ultrasonics & Vibration Section, CSIR-National Physical Laboratory, Dr. K. S. Krishnan Road, New Delhi-110 012 (email: mahavir@nplindia.org Tel: +91-11-4560.8317, Fax: +91-11-4560.9310). For the item to be published in a given issue of a journal, the manuscript must reach the Chief Editor at least twelve week before the publication date.

SUMISSION OF ACCEPTED MANUSCRIPT

On acceptance, revised articles should be submitted in electronic form to the JASI Chief Editor (mahavir@nplindia.org)

JOURNAL OF ACOUSTICAL SOCIETY OF INDIA

A Quarterly Publication of the JASI
http://www.acousticsindia.org

Journal of Acoustical Society of India

The Refereed Journal of the Acoustical Society of India (JASI)

The Journal of Acoustical Society of India is a refereed journal of the Acoustical Society of India (ASI). The ASI is a non-profit national society founded in 31st July, 1971. The primary objective of the society is to advance the science of acoustics by creating an organization that is responsive to the needs of scientists and engineers concerned with acoustics problems all around the world.

Manuscripts of articles, technical notes and letter to the editor should be submitted to the Chief Editor. Copies of articles on specific topics listed above should also be submitted to the respective Associate Scientific Editor. Manuscripts are refereed by at least two referees and are reviewed by Publication Committee (all editors) before acceptance. On acceptance, revised articles with the text and figures scanned as separate files on a diskette should be submitted to the Editor by express mail. Manuscripts of articles must be prepared in strict accordance with the author instructions.

All information concerning subscription, new books, journals, conferences, etc. should be submitted to Chief Editor:

Acoustics, Ultrasonics & Vibration Section, CSIR-National Physical Laboratory, Dr. KS Krishnan Road, New Delhi 110 012, Tel: +91.11.4560.8317, Fax: +91.11.4560.9310, e-mail: mahavir@nplindia.org

Annual subscription price including mail postage is Rs. 2000/= for institutions, companies and libraries and Rs. 2000/= for individuals who are not ASI members. The Journal of Acoustical Society of India will be sent to ASI members free of any extra charge. Requests for specimen copies and claims for missing issues as well as address changes should be sent to the Editorial Office:

Acoustics, Ultrasonics & Vibration Section, CSIR-National Physical Laboratory, Dr. KS Krishnan Road, New Delhi 110 012, Tel: +91.11.4560.8317, Fax: +91.11.4560.9310, e-mail: mahavir@nplindia.org

Journal of Acoustical Society of India (JASI)

JASI

A quarterly publication of the Acoustical Society of India

Volume 41, Number 4, October 2014

EDITORIAL

ARTICLES

INFORMATION

Reverberant Noise Control in Rooms

For a given noise source the behaviour of the sound it emits and the noise levels it produces within a room are largely determined by the sound absorbing properties of the materials in the room. The problem of noise transmitted to adjacent rooms is determined by the sound insulating properties of the walls and is not dealt with in this note. For many rooms where the exact behaviour of the sound need not be examined as critically as, for example, in a lecture theatre or a conference hall, sound absorbing materials are used mainly to reduce reverberant noise levels. This paper provides some information to aid in the design of such rooms. The sound absorption coefficient for a material is the fraction or percentage o incident sound energy that is absorbed by the material. The absorption coefficient depends on the sound frequency and values are usually provided in the literature at the standard frequencies of 125, 250, 500, 1000, 2000 and 4000 Hertz. The noise reduction coefficient (NRC) is the average of the values from 250 to 2000 Hz, inclusive, rounded to the nearest 0.05. Absorption coefficients are sometimes expressed as percentages. The sound absorption for a sample of material or an object is measured in sabins or metric sabins. One sabin may be thought of as the absorption of unit area (1 m^2 or 1 ft^2) of a surface that has an absorption coefficient of 1.0 (100 per cent). When areas are measured in square metres, the term metric sabin is used. The absorption for a surface can be found by multiplying its area by its absorption coefficient. Thus for a material with absorption coefficient of 0.5, 10 sq ft has a sound absorption of 5 sabins and 100 m^2 is 50 metric sabins. The total absorption in a room can be estimated by multiplying the area of each surface by an estimated absorption coefficient for that surface and then adding together the contributions from each surface. When a source of sound in a 'live' room is turned off, a noticeable time elapses before the noise becomes inaudible. The less sound absorbing material there is in a room the longer the sound takes to die away. The reverberation time is defined as the time in seconds required for decaying sound to decrease in level by 60 decibels (dB). Since the sound absorption in the room depends on the frequency of the sounds being considered, so also does the reverberation time.

Hard surfaces such as glass, concrete, brick, wood and plaster reflect almost the entire sound incident on them. In contrast with this, soft porous materials such as glass or mineral wool, soft fabrics, clothing, people, and even the air, will absorb sound. In an extremely 'live' or reverberant room where the surfaces are all good sound reflectors, noise can build up to produce unpleasantly high sound levels and the sound field is constant in level for all distances greater than a few metres from the source. The reverberation times in such rooms can be from 5 to 10 seconds long or more making speech at distances of more than a few metres difficult to understand. In a reverberant room the two quantities, absorption and reverberation time, T, in seconds, can be related by the equations $T = 0.616\ V/A$ or $A = 0.161\ V/T$ where, V is the volume of the room in cubic metres and A is the total absorption in it in metric sabins (square metres) in the frequency band being considered. In an extremely absorptive environment the sound level decreases by 6 dB each time the distance from a small source is doubled. There are no reflections, no reverberation and all sound comes directly from the source. This is known as free field behaviour.

In typical rooms the behaviour of the sound field can be described approximately with reference to a critical distance D (metre). Within the critical distance the sound field behaves as in the free field case just described, as if there were no reflecting surfaces. This region is called the near field. Beyond the critical distance, in the region called the reverberant field, the sound pressure level remains constant. The critical distance is given approximately by $D = \sqrt{A/2}$ where, A is the total absorption in the room in metric sabins.

Mahavir Singh

Wavelet Based HRV Extraction

Veena N.Hegde[1], Ravishankar Deekshit[2] and P.S.Satyanarayana[3]
Associate Professor, Department of Instrumentation Technology
B.M.S College of Engineering, Bangalore, India
e-mail: veena.bms@gmail.com

ABSTRACT

This paper provides a novel approach for extracting Heart Rate Variability(HRV) from ECG. The instantaneous angular frequency of the heart is extracted using the phase change of the ECG signal that is filtered through Multi -Resolution Array(MRA) filter bank of Wavelets. The instantaneous heart's frequency thus obtained represents HRV which is a strong indicator of heart diseases or impending abnormalities of cardiovascular system. The proposed wavelet function specific to every ECG sample is a modified Gabor wavelet which is made self-adaptive to extract the instantaneous frequency of the heart or HRV.The HRV thus obtained is more accurate and compact compared to that obtained using the traditional method of R peak detection. The method proposed is robust as wavelet transform is tuned toextract only the required frequency eliminating the rest. The technique proposed does not require re-sampling. The Spectrogram using CWT is used to define the driver function for the adaptive modified Gabor wavelet which does fine extraction of HRV. The method proposed has been tested with the spectral response of HRV obtained both for normal and abnormal samples of ECG signals from MIT data base.

Key words: MRA,HIF, HRV, CWT, Modified Gabor function

1. INTRODUCTION

The Heart Rate Variability (HRV) is used as a tool to detect the cardiac diseases and diabetic conditions. It is also a strong indicator of the nervous system balance exhibited by the Autonomous Nervous System (ANS). The spectral characteristics of HRV and their frequency deviations have become importantanalysing patterns of abnormalities in cardiovascular system [1]. The short term HRV and its spectral analysis have proved better in some of the situations replacing the long term holter recordings [2]. The accurate extraction of HRV has become a challenging task. Traditionally HRV have been obtained by using the R peak detection and consecutive distance measurements of R peaks in ECG. Though ECG has R peak as the most prominent wave element, the threshold applied to detect the peak has to be carefully chosen in calculating HRV for heart patients with atrial fibrillation or myocardial infarction [3].The spectral analysis carried outon the HRV data extracted by the R peak detection method by applying the Fourier Transform needs resampling which is an additional burden [4].The parametric analysis of HRV uses mathematical modelling where the model order selection is a critical issue[5]. Though the resampling issue of HRV spectral response is addressed by various resampling techniques such as cubic spline [6], Lomb periodogram and interpolation[7], the R to R distance consideration in case of occurrences of ectopic beats [8] is still a challenge. The accuracy of HRV obtained using the traditional technique without resampling will lead to totally wrong diagnosis if employed. Hence the necessity for having an alternative technique for HRV extraction has been addressed in this paper by providing a novel approach of phase modulation principle.

The paper has been organized in following sections. Section 2 provides the mathematical background for the filterbank generated using wavelet transform, to extract the fundamental frequency of the heart as HRV. It also gives the method of extracting the instantaneous angular frequency of a signal using the phase modulation approach. The data base, the data characteristics and the traditional method of obtaining the HRV are discussed in Section 3.Section 4 provides the HRV extraction from ECG. Section 5 gives the results obtained by applying the proposed method and comparison of the proposed method with the traditional ones. The discussions based on the results and conclusions arrived at are given in section6and section 7 respectively.

2. WAVELET BASED HRV EXTRACTION

Traditionally HRV being a discrete signal is defined from ECG as HRV= $[t_1/60, t_2/60 \ldots t_n/60]^T$ where t_1, $t_2 \ldots t_n$ are the distances between the R to R peaks of consecutive ECG beats. As R to R distances are not same due to the changes in the intrinsic firing system of the heartbeat, the HRV is not stationary. It possesses modulations in case of the exercising effects, sleep Apnea or heart diseases. By taking the spectral characteristics of short time HRV for analysis, it is found that it can be strong indicator of heart diseases [9]. The spectral response of HRV obtained through this ideal method needs re-sampling [10]. Instead heart may be thought of as a stable system generating heart beats at every 'T' seconds witha corresponding fundamental frequency ω_0. This implies that there has to be a spectral peak at ω_0, $2\omega_0$, $3\omega_0$ etc. But the ECG consists of harmonic components and it is necessary to extract ω_0 from the signal. One way to extract ω_0 is

by spectral analysis of HRVin which case a short duration of ECG signalx(t)is sufficient for this purpose unlike long time holter recordings as used by traditional methods.

The heart beats at a rate which varies with respect to time. Hence heart can be modelled to be frequency modulated system. The modulation in heart's fundamental frequency may be due to exercise, respiratory pattern getting reflected in HRV or due to some of the heart diseases. In all these cases, the time period between the consecutive heart beats is different. The frequency modulation of any signal can be known by extracting its instantaneous frequency (IF) [11]. Further as referred in literatures [12] and [13] the instantaneous frequency measurement is possible by knowing its phase modulations.That is, for a signal $x(t)$, IF is function of time .If the signal is real as is the case with most of the physiological signals, for a given real signal $s(t)$, a unique representation of its corresponding imaginary signal may be obtained from its Hilbert Transform (Imaginary part of the real signal). The analytic signal $x(t)$ is then given by

$$x(t) = s(t) + \text{Hilbert } (s(t)) \tag{1}$$

The corresponding phase of the analytic signal is given by

$$\phi(t) \tag{2}$$

$$= tan^{-1} \frac{Hilbert[s(t)]}{s(t)}$$

and the IF is formally defined as [14]

$$f_i(t) = \frac{1}{2\pi} \frac{d\phi(t)}{dt} \tag{3}$$

Here $f_i(t)$ is the IF of the signal and $\phi(t)$ represents the phase of the analytic signal. The definition of IF may be extended to the discrete time signal $z(n)$, based on central difference of the phase and is given as:

$$f_i(n) = \frac{f_s}{4\pi} \left(\left[arg(z(n+1)) - arg(z(n-1)) \right] \right)_{Mod2\pi} \tag{4}$$

Here $\frac{f_s}{4\pi}$ is the sampling frequency, the notation Mod2π represents 2π periodicity of the signals. The

$arg[z(n)] = tan^{-1} \frac{Im[z(n)]}{Re[z(n)]}$ represents phase of $Z(n)$.

3. PROPOSED METHOD OF IF EXTRACTION OF THE HEART

The ECG signal as explained in section 2 exhibits multiple peaks in its spectrum indicating the existence of multiple frequencies. The effective way for filtering the original ECG signal is to have ECG with only the fundamental frequency. The filtering is carried out by passing the signal through a set of wavelet band-pass filters designed specifically for the incoming ECG, modifying the Gabor function [14]. This section gives the procedure and designing involved in obtaining MRA filterbanks of wavelet filter bank proposed.Initially, the extraction of HRV estimation of scalogram using Wavelet transform is as a first step. The Continuous Wavelet Transform (CWT) is selected for this purpose. The CWT of a time varying signal $x(t)$, is the inner product of $x(t)$ and $\psi\left(\dfrac{t\text{-}\tau_0}{s_0}\right)$ where $\psi(t)$ is the Mother Wavelet chosen. Normalising the term $\psi\left(\dfrac{t\text{-}\tau_0}{s_0}\right)$ it is seen that the inner product of the two is resulted as:

$$CWT < x(t)\psi\left(\frac{t-\tau_0}{s_0}\right) >= \int_{-\infty}^{+\infty} x(t)\overline{\psi\left(\frac{t-\tau_0}{s_0}\right)}dt \tag{5}$$

Here, $\overline{\psi\left(\dfrac{t-\tau_0}{s_0}\right)}$ indicates the complex conjugate of the translated and scaled wavelet function. Applying the Parseval's theorem, inner product in time domain is same as multiplication of FT of $x(t)$ and $\overline{\psi\left(\dfrac{t-\tau_0}{s_0}\right)}$. If the FT of $x(t)$ is denoted as $\tilde{x}(t)$ then the FT of the scaled and translated Wavelet can be represented as follows:

$$\frac{1}{\sqrt{s_0}}\psi\left(\frac{t-\tau_0}{s_0}\right) \leftrightarrow \sqrt{s_0}\hat{\psi}(s_0\omega)e^{-j\omega\tau_0} \tag{6}$$

The CWT of a time varying signal $x(t)$ represented as CWT $(x,\psi)(\tau_0,s_0)$ is given by:

$$CWT(x,\psi)(\tau_0,s_0) = \frac{1}{2\pi}\int_{-\infty}^{+\infty} \tilde{x}(\omega)\sqrt{s_0}\hat{\psi}(s_0\omega)e^{-j\omega\tau_0} dw \tag{7}$$

It is seen from (7) that CWT is a function of 'τ_0' at the scale 's_0'. The frequency and time resolution are provided by 's_0' and 'τ_0' respectively. Further it is seen that second derivative of Gaussian Wavelet known as Mexican Hat can.

only make the integration in (7) converge The Fig.1 shows the Mexican Hat Wavelet and its FT respectively. Generalizing (7) in discrete domain, the Gaussian Wavelet is expressed as follows.

$$\psi_0(n) = \frac{(-j^m)}{\sqrt{\Gamma\left(m+\frac{1}{2}\right)}}\frac{d^m}{d\eta^m}(e-\eta^2/2) \tag{8}$$
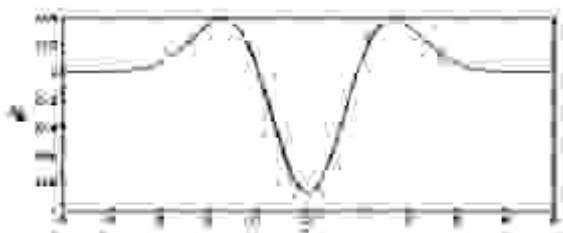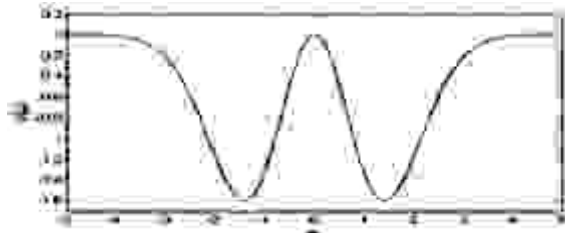

Fig. 1. Mexican Hat Wavelet

Fig. 2. Frequency domain Mexican Hat Wavelet.

Where $\psi_0(\eta)$ is the mother Wavelet, 'm' is the degree of Gaussian Wavelet and can vary from 2 onwards. Further extending the same CWT concept to a discrete sequence 'x_n',sas most of the biomedical signals are stored in digital form for processing, it is defined as the convolution of 'xn'with a scaled and translated version of $\psi_0(\eta)$:

$$W_n(s) = \sum_{n=0}^{N-1} x_n \psi^* \left[\frac{(n'-n)\Delta t}{s} \right]$$

(9)

Here the (*) indicates the complex conjugate. By varying the wavelet scale 's' and translating along the localized time index 'n', one can construct an image showing variation of the amplitude of any feature versus the scale and also variation of this amplitude versus time. To approximate the CWT, the convolution (shown in equ.10) using DFT)is carried outN times for each scale, where N alsois the number of points in the time series.. The DFT of 'xn'is

$$X_k = \sum_{n-o}^{N-1} x_n$$

(10)

Here,k = 0 … N-1 is the frequency index. In the continuous limit, the Fourier transform of a function $\psi(t/h)$ is given by $\psi(s\omega)$. By the convolution theorem, the wavelet transform is the inverse Fourier transform of the product:

$$W_n(s) = \frac{1}{N} \sum_{k-o}^{N-1} X_k \psi^* (s\omega_k) e^{in\Delta t\omega k}$$

(11)

and

$$\omega_k = \left\{ \frac{2\pi k}{N\Delta t} : k \le \frac{N}{2} \text{ and } \omega_k = \left\{ -\frac{2\pi k}{N\Delta t} : k > \frac{N}{2} \right.\right.$$

(12)

Using (11) and a standard Fourier transform routine, one can calculate the continuous wavelet transform (for a given s) at all 'n'simultaneously and efficiently. To ensure that the wavelet transform (11) at each scale 's'are directly comparable to each other and to the transform of other time series, the wavelet function at each scale 's'is normalized to have unit energy as:

$$\bar{\psi}(s\omega_k) = \left[\frac{2\pi k}{N\Delta t} \right]^{\frac{1}{2}} \psi(s\omega_k)$$

(13)

The wavelet transform is weighted only by the amplitude of the Fourier coefficients and not by the wavelet function. If one is using the convolution formula (11), the normalization is:

$$\psi \left[\frac{n'-n}{s} \right] = \left[\frac{\Delta t}{s} \right]^2 \psi_0 \left[\frac{(n'-n)\Delta t}{s} \right]$$

(14)

Since the Wavelet function is in general complex, the Wavelet Transform spectrum $W_N(s)$ is also complex. The transform can then be divided into the real part, $R(W_N(s))$ and imaginary part, $I(W_N(s))$, or amplitude, $|W_N(s)|^2$,and phase,$\tan^{-1} \left\{ \frac{I(W_N(s))}{R(W_N(s))} \right\}$. Finally, one can define the Wavelet power spectrum as,

$$W_n(s) = \frac{1}{N} \left| \sum_{k=0}^{N-1} X_k \psi^* (s\omega_k) e^{j\omega_k \pi \Delta t} \right|^2$$

(15)

For real-valued wavelet functions such as the Discrete Gaussian Wavelet (DGW) the imaginary part is zero and the phase is undefined. To make it easier to compare different wavelet power spectra, it is desirable to find a common normalization for the wavelet spectrum. From the wavelet spectrum, the frequency values corresponding to the maximum magnitude at each time points are obtained in a given frequency range and this function is termed as driver function$\delta(t)$. '

$$\delta(t = \arg\max\left(W_n(s)\Big|_{\delta(t-)-a}^{\delta(t-)+a}\right) \qquad (16)$$

The value of α is decided upon the frequency search range that is selected as 0.3 Hz to 0.5 Hz. At every time instant t, the previous driver function value $\delta(t-)$ is considered along with the search range of frequency, $\delta(t-)-\alpha$ to $\delta(t-)+\alpha$, to decide the driver function value $\delta(t)$. Thus the driver function is derived recursively and is anonlinear function of $W_n(s)$. With the modulations in ECG due to various reasons, the scalogram maximum may shift with respect to time. At one time instant the maximum may correspond to maximum frequency at some other time instances it may not. However since the eq. (16) is recursive there will not be any drastic shift in the in the frequency captured as the HRV does not change drastically.Finally the instantaneous frequency is computed using the set of band-pass filters,centeredat the frequency provided by the driver function at different time instants. It has been carried out using wavelet filterbank, where central frequencies of band pass filters during selected time intervals have been derived by the driver functions to provide the necessary time frequency resolutions.The modified Gabor wavelet applied for this purpose is given by:

$$\psi(t) = \frac{1}{2\pi}\frac{d}{dt}\left[\exp\left(-\pi\left\{\frac{\overline{\delta(t)}}{2}t\right\}^2\right)\cos\left(2\pi t\int_0^\Omega \delta(\tau)d\tau\right)\right] \qquad (17)$$

$$\overline{\delta(t)} = \frac{1}{2\Omega}\sum_\Omega \delta(t) \qquad (18)$$

The signal filtered in the interval is given by

$$s_\Omega(t) = \int x_\Omega(\tau)\psi(t-\tau)d\tau \qquad (19)$$

The HIF or HRV is then calculated using eq.(2) for each band pass filter output in the filter bank.
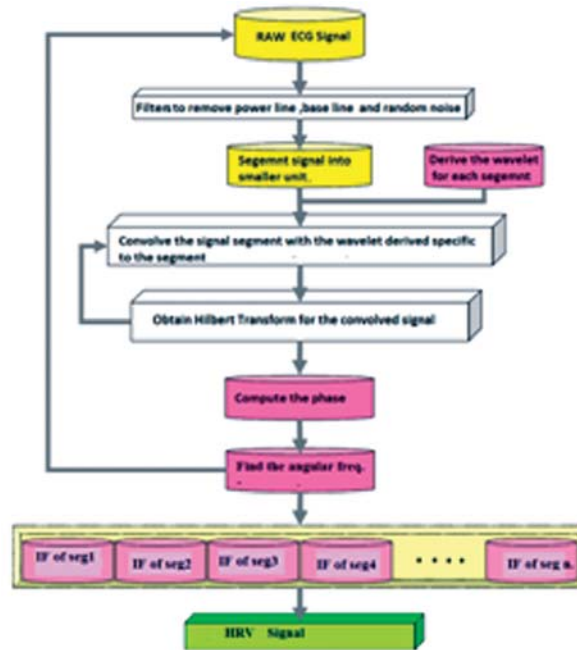
4. PHYSIOLOGICAL CORRELATES OF HRV

Fig. 2. Proposed algorithm flow.

Fig. 2 indicates the flow chart for the implementation of the proposed algorithm to extract HRV from raw ECG.

Though the cardiac automaticity is intrinsic to pacemaker tissues, the HR and Rhythm are largely under the control of autonomic nervous system. The sympathetic influence on HR mediated by release of epinephrine and the autonomic neural regulation of both the heart and circulatory system determines the normal HRV. The instantaneous HR is strongly dependent on a variety of neural, hormonal, and myocardial factors. In cardiac patients the HRV pattern is affected substantially whenever the SA node fails to operate at intrinsic rate. The HRV may be reflected by Day-Night periodicity, as respiratory arrhythmia or ten seconds rhythm and slower fluctuations. Respiratory sinus arrhythmia is characterized by Tachycardia during Inspiration and Bradycardia during expiration causing heart rate variability. Stimulation frequencies elicit corresponding HR oscillations. Cardiac sympathetic and parasympathetic neuronal activity contains frequency components at the heart rate and the respiratory rate. The resonance frequency of the Baro-receptor heart rate reflex and resonance frequency of the slower blood pressure regulating system occur in the same frequency range as HR. The SA node responds to all these frequencies with corresponding fluctuations in the heart rate [10-12]. Perturbations of sympathetic nervous system interventions that increase the sympathetic nerve activity increase the Low Frequency (LF) power of HR: Coronary artery occlusion, Exercise, Upright tilt, Mental arithmetic stress, are the major interventions that would affect the LF power of HR. High frequency(HF) components of HRV are affected only by parasympathetic activities. LF/HF ratio greater reflects sympathetic dominance, smaller values reflect the parasympathetic dominance. Spectral power of LF/HF ratio of HR indicates the cardiac autonomic balance. Therefore, HRV analysis has numerous clinical applications, specifically in the fields of physiology, biochemistry, and pharmacology.

Fig. 3 shows the spectral regions of a healthy heart. As seen from the figure the LF region is below 0.15
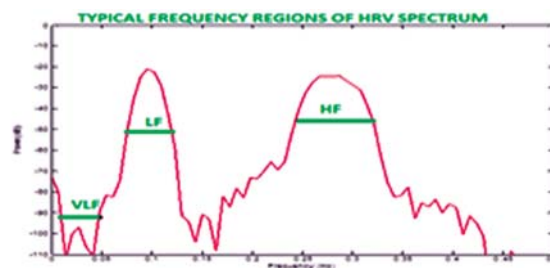

Fig. 3. Typical spectral regions of HRV indicating a healthy condition of the heart.

Hz. The Major frequency content is seen in HF region. These frequency regions get shifted in case of different abnormal HRVs.

5. RESULTS

The simulation of the traditional and the proposed method of HRV extraction are carried out using the ECG data samples available in the MIT/BIH data base. The traditional method is tested with the data file samples 105, 117 from MIT/BIH library. The 105 data sample has maximum number of the normal beats, while the sample 117 is the samples with abnormal beats. The wavelet filtering method is tested with different data samples of MIT/BIH data base having the beats representing VT, VF and CHF. The verification of the proposed method is done with the R-R time series data sets availablein Physiobank toolkit. The ECG signal is filtered
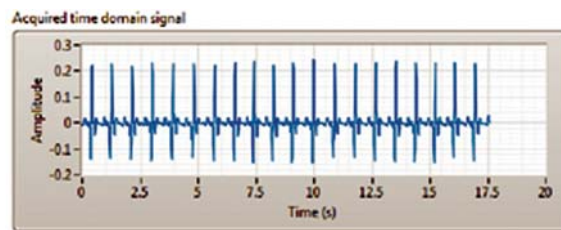

Fig. 4. ECG signal after pre-processing with different filters.

through a band pass filter with lower and upper cut off frequencies of 0.5 Hz and 49.5 Hz in case of normal ECG signal and with a cutoff frequencies of 0.5 Hz and 200 Hz in case of abnormal ECG.

Fig. 4 shows ECG signal (file 105 from MIT data base) that has been pre-processed with various filters to remove the power line interference, base line wander and random noise. The duration of the data is 17.5 seconds with the sampling rate of 360 Hz. Fig.5 shows the HRV derived from re-sampling (traditional) method for time duration of 60 seconds. The Computation of HRV is based on the eq. (1) and Resampling rate of 4Hz is used using linear interpolation.

To illustrate the necessity of resampling in the traditional method, a data sample 122 from MIT data
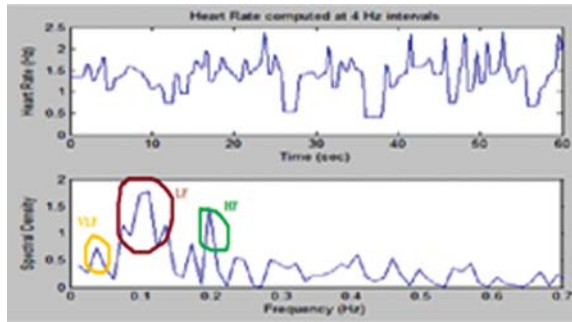

Fig. 5. HRV obtained from the traditional method with the frequency regions of the HRV spectrum.

base was considered. As seen in Fig. 5, the R to R distances are different and can be represented by the counts as shown in the histogram for a time interval. Fig. 5 indicates the HRV and its spectrum without resampling. The spectrum is spread fully on 0 to 1 normalised frequency axis, which can lead to wrong diagnosis. The significance of resampling and true HRV spectrum are shown in Fig. 6.

The modified Gabor wavelet (eq. 17) is the mother wavelet which is obtained by passing the driver $\delta(t)$
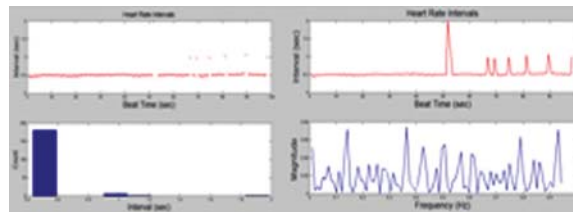

Fig. 6. Tachogram and the distribution of R-R intervals on a histogram for a data sample 122 and the HRV spectrum before resampling
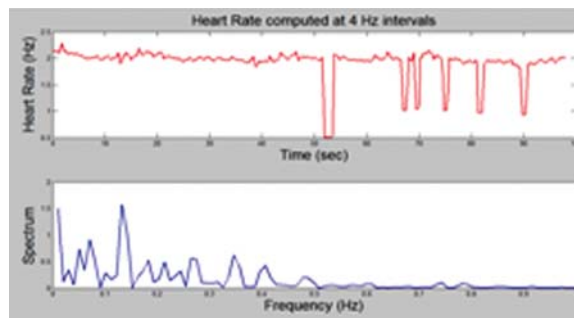

Fig. 7. HRV and its spectrum after resampling (ECG 122)

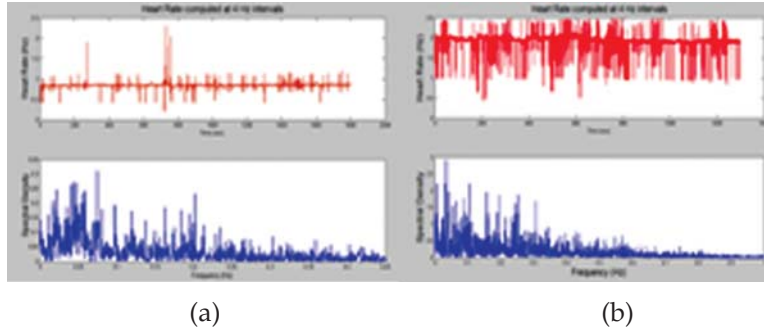(a)   (b)

Fig. 8. The HRV and its spectra obtained for the ECG data (a) 105 and
(b)112 from traditional method for the ECG data for longer

to the equation. The Fig. 7 shows its scalogram for the data sample 105 shown in Fig. 4.

The driver function for one segment of data is calculated using the frequency variation of Fig. 9. The
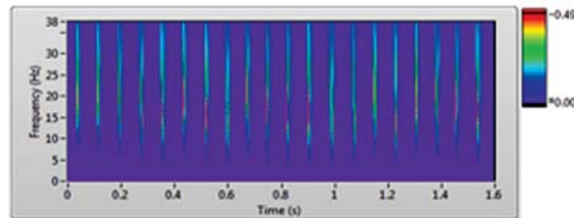
Fig. 9. Scalogram using Mexican Hat (CWT) to identify the frequencies over time in ECG (105)

frequency contents of the ECG sample range from 1 to 45 Hz as shown in the figure. The driver function is calculated by averaging the frequencies computed based on eq. (16).

Fig. 11 shows the time domain wavelet band-pass filter formed by passing driver function constructed
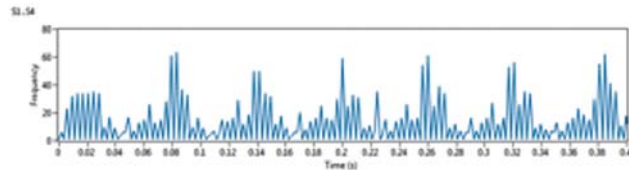
Fig. 10. The variation of ECG frequency over time for a segment of ECG (105 data sample)
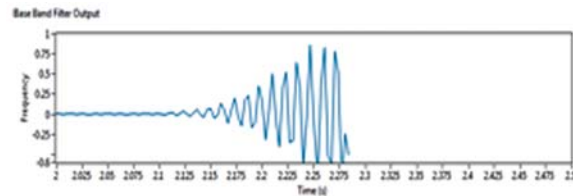
Fig. 11. 11 Sample of a wavelet band pass filter output, indicating an adapted wavelet

from ECG segment to Gabor wavelet equation. The shape of the wavelet every time is adapted to the variable IF.
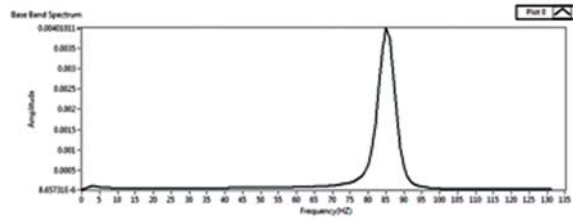
Fig. 12. The spectrum of Band-pass filter for the wavelet function derived for ECG 105

The frequency domain characteristics of this band-pass filter is as shown in Fig.12. It can be seen from Fig 12, and Fig.13 that for the same signal the band-pass filter width can be changed as the central frequency of the band-pass filter is shifted.
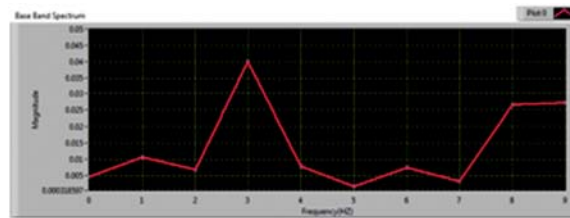
Fig. 13. Self adaptation of the wavelet band-pass filter for different segements of the signal (ECG 105)
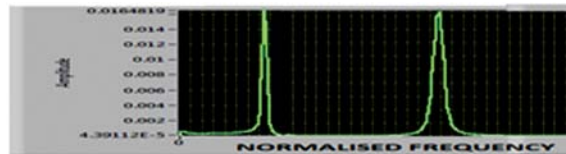
Fig. 14. Response of band -pass filter at different time durations for the same signal ECG (105) on a normalised scale
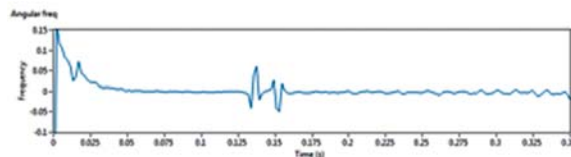
Fig. 15. HRV obtained by the proposed wavelet method

Fig.13 and Fig 14 show the wavelet band pass filter responses for CEG signal considered as an example to illustrate the proposed, multi-resolution filter bank concept As seen in the figures there is shift in the central frequency of each of the band pass filter with respect to time. Fig.15 shows the HRV extracted from the one such band pass filter, filtering a short duration signal. Fig. 16 and Fig.17 show the HRV and its spectrum obtained for the long duration ECG 105. It is seen from these figures that the spectrum obtained for the HRV in the proposed is more accurate and clear compared to the same shown in Fig.5 obtained from the traditional method.
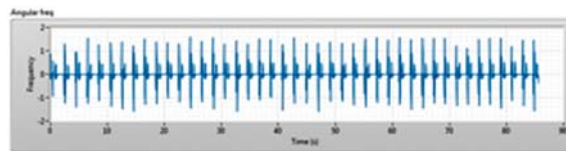
Fig. 16. The HRV extracted from the proposed wavelet method from the ECG sample 105.
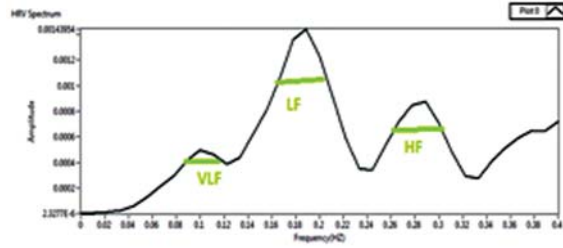
Fig. 17. The PSD of HRV obtained for the sample in Fig. 13 with different frequencies.
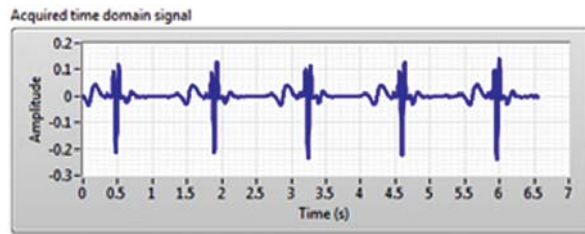
Fig. 18. The ECG sample 117 after noise cancellation

Fig. 18 shows an ECG data (117) after noise cancellation. Fig. 19 shows the wavelet band-pass filterapplied for a segment of ECG form the data sample 117. The band pass filter has different central frequency as compared to that in Fig. 12 , since the driver function tuning the band pass filter is derived to be different for this sample of ECG.
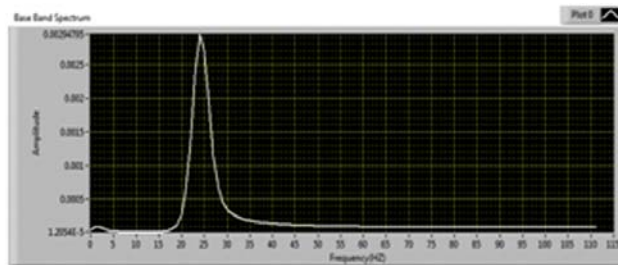
Fig. 19. The wavelet band pass filter derived for the abnormal segment of ECG (117).

The HRV derived from the proposed method by passing the ECG through this band pass filter is shown in Fig. 19. The subsequent scalogram and the HRV are seen in Fig. 20 and Fig. 21 respectively. The Fig. 20 shows PSD for the HRV of the abnormal ECG (117). As seen from the PSD plot the regions of LF is shifted as compared to the normal plot in Fig. 14. The HF is within 0.3 Hz indicating there is a reduced frequency spread for the HRV. It is possible to have inferences about the cardiac conditions and status of ANS based on the frequency leakages and spreads within the frequency regions of HRV.
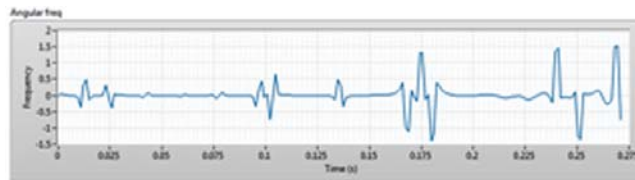
Fig. 20. HRV obtained for the data sample ECG (117)
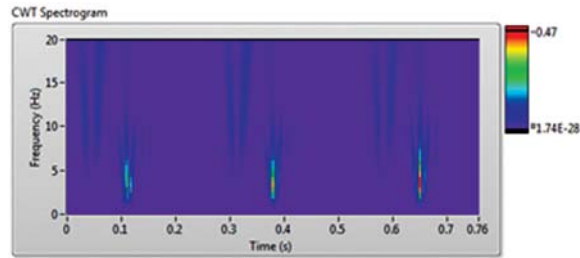
Fig. 21. Scalogram of the ECG sample (117) using Mexican Hat CWT.
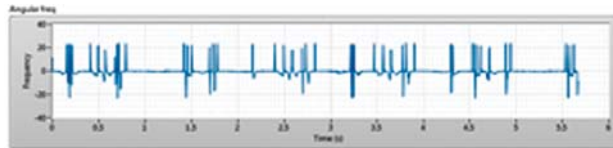
Fig. 22. HRV obtained by the proposed method for ECG(117).
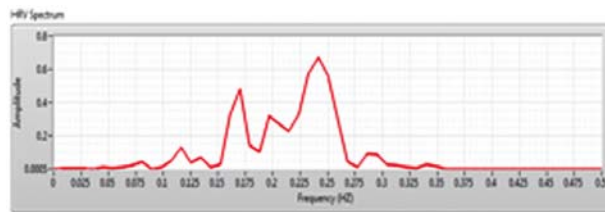
Fig. 23. PSD for the HRV data shown in Fig 22.

6. DISCUSSIONS

The major frequency regions pf HRV power spectrum are categorized into three major parts. Very low-frequency region(VLF),Low frequency region(LF) and High frequency region (HF). The range of VLF is less than 0.04 Hz while the LF ranges from 0.04 Hz to .15 Hz and subsequently HF ranges from .15 Hz to .40 Hz. If traditional method of R peak detection is employed, it essentially requires longer number of data samples and is also expensive in terms of memory requirement and sampling frequency. The method proposed here is highly compact as it directly gives HRV. The same techniques of spectral content identifications for different spectral regions of PSD can be extended to the proposed method. Since the angular fundamental frequency measure is a direct computation of HRV in HZ, which otherwise in traditional method is obtained as inverse of time difference between consecutive R peaks, makes the method easier and direct.

The sampling rate of ECG differs in case of disused hearts and during exercises. Hence the re-sampling rate selection in traditional method is a critical issue. In case of proposed method, the sampling frequency can be changed by examining the input samples at the beginning. There are two stages of IF extraction. During the first stage without being particular about the time-frequency resolution, CWT scalogram is obtained for the ECG signal. In second stage modification of the Wavelet equation using the driver function derived from the first stage is carried out. As seen, the band pass filters with their central frequencies show the accuracy and smoothness obtained while adapting to the fundamental frequency. The main advantage of this method is the automatic averaging provided in the second stage which generates the adaptive daughter wavelets,when every segment of signal is considered.

The proposed method has been tested with different ECG data available in MIT data base. The data samples 100, 104, 106 though have more normal beats, have modulations due to the intrinsic behaviour of Sino Atrial (SA) node. The data samples 122, 132 and 143 etc. represent heart diseases withthe absence of P

wave, elevated ST segment, increased T wave etc. But as far as the R peaks are concerned, still they havefewer modulations. Hence the spectral analysiscan only provide the cardiac conditions as explained in this method.Further the method is more robust as it was tried on samples of ECG both with and without noise cancellation where the spectral behaviour was unchanged. The method is for direct extraction of the fundamental frequency named to be HRVcan easily be extended for other physiological signals and their frequency modulations and could provide more features of physiological interest.

7. CONCLUSION

The heart rate variability of a person, without any stress or anxiety has frequency, with fewer modulations. In situations of heart diseases or stress the normal HRV exhibiting stable oscillations is not possible. Then the HRV becomes non-stationary whose frequency variation can only be analyzed by time frequency analysis techniques. As an enhancement to the existing approach of obtaining HRV from ECG, HIF extraction method using phase modulation is proposed and tested. The adaptive modified Gabor wavelet filter makes the HIF estimation more robust. The proposed method is tested with existing state of art technique and is verified for both normal and different abnormal ECG signals for HRV extraction.Though the derivations are given with respect toGabor wavelet the same formula may be used with any wavelet including Haar wavelet to get the same result.

8. REFERENCES

[1] KO KEUN KIM, JUNG SOO KIM, YONG GYU LIM and KWANG SUK PARK, 2009. "The effect of missing RR-interval data on heart rate variability analysis in the frequency domain". *Physiol. Meas*. **30**, 1039-1050.

[2] S. AIF AHMAD, ANJALI TEJUJA, KIMBERLEY D NEWMAN, RYAN ZARYCHANSKI and ANDREW JE SEELY, 2009. "Clinical review: A review and analysis of heart rate variability andthe diagnosis and prognosis of infection" *Critical Care* **13**, 232

[3] HELONG LI, SAM KWONG, LIHUA YANG, DAREN HUANG, and DONGPING XIAO, 2011. "Hilbert-Huang Transform For Analysis Of Heart Rate Variability In Cardiac Health", *IEEE/ACM Transactions On Computational Biology and Bioinformatics*, **8** (6).

[4] KO KEUN KIM, JUNG SOO KIM, YONG GYU LIM2 and KWANG SUK PARK, 2009. "The effect of missing RR-interval data on heart rate variability analysis in the frequency domain", *Physiol. Meas.* **30**, 1039-1050.

[5] PABLO LAGUNA, GEORGE B. MOODY, and ROGER G. MARK, 1998. "Power Spectral Density of Unevenly Sampled Data by Least-Square Analysis: Performance and Application to Heart Rate Signals", *IEEE Transactions on Biomedical Engineering*, **45**, (6).

[6] KRISTIAN SOLEM, PABLO LAGUNA, JUAN PABLO MART´INEZ and LEIF S¨ORNMO, 2008. "Model-Based Detection of Heart Rate Turbulence", *IEEE Transactions On Biomedical Engineering*, **55** (12).

[7] REN-GUEY LEE, I-CHI CHOU, CHIEN-CHIH LAI, MING-HSIU LIU, and MING-JANG CHIU, 2005. "A Novel QRS Detection Algorithm Applied To The Analysis For Heart Rate Variability Of Patients With Sleep Apnea", *Biomed Engg. Appl. Basis Comm*. **17** (5).

[8] R. U. ACHARYA, C. M. LIM, and P. JOSEPH, "Heart rate variability analysis using correlation dimension and detrended fluctuation analysis", *ITBM-R*

[9] LEON COHEN, 1989. "Time-Frequency Distributions-A Review", *Proceedings of the IEEE*, **77** (7).

[10] SIMONE POLA, ALBERT0 MACERATA, MICHELE EMDIN and CARLO MARCHESI, 1996. "Estimation of Power Spectral Density In Nonstationary Cardiovascular Time Series: Assessing the Role of the Time -Frequency Representations (TFR)", *IEEE Transactions On Biomedical Engineering*, **43**(1).

[11] MICHAEL G.ROSENBLUM, JURGEN KURTHS, ARKADY PIKOVSKY,CARSTEN SCHAFER, PETER TASS and HANS-HENNING ABEL, 1998. "Synchronization in noisy system and cardiorespiratory Interaction", *IEEE Engineering in Medicine and Biology*.

[12] LUNJI QIU and GANG LI "Representation of ECG Signals Based on the Instantaneous Frequency, Estimation". *Proceedings of ICSP'96*

[13] M. ANNA BIANCHI, LUCA MAINARDI, ETTORE PETRUCCI, G. MARIA SIGNORINI, MAURO MAINARDI and SERGIO CERUTTI, 1993. "Time- Variant Power Spectrum Analysis for the Detection of Transient Episodes in HRV Signal", *IEEE Transactions On Biomedical Engineering*. **40**. (2).

[14] ALLAN KARDEC BARROS and NOBORU OHNISHI, 2001. "Heart Instantaneous Frequency (HIF): An Alternative Approach to Extract Heart Rate Variability", *IEEE Transactions on Biomedical Engineering*, **48**(8).

Sodar Mixing Height Estimates and air Pollution Characteristics Over Delhi a Big City During Spring and Summer

Kirti Soni[1], Mahavir Singh[1], Gurbir Singh[1] and Sanjeev Agarwal[2]

[1]*Acoustics, Ultrasonics and Vibration Standard and Electronics & Instrumentation Cell*
CSIR-National Physical Laboratory, New Delhi-110012
[2]*Central Pollution Control Board,PariveshBhawan, CBD-cum-Office Complex*
East Arjun Nagar, Delhi - 110 032, INDIA
e-mail: 2006.kirti@gmail.com

ABSTRACT

The concentration of atmospheric pollutants such as SO_2, NO_2, SPM (Suspended Particulate Matter), RSPM (Respirable Suspended Particulate Matter) is affected by atmospheric flows and by dispersion within the atmospheric boundary layer. The height of the atmospheric boundary layer, i.e., mixing height is an important parameter that describes the structure of the lower atmosphere. Mixing height defines the volume available for the dispersion of pollutants by convection or mechanical turbulence. The influence of the atmospheric boundary layer (ABL) on the ground concentrations of the main air pollutants and meteorological parameters such as Temperature, Wind speed and Relative humidity have been analyzed over Delhi during Spring and Summer seasons. This study presents results of monthly and Spring - Summer seasonal variations of NO_2, SO_2, SPM and RSPM concentrations as well as the influence of meteorological parameters on observed mixing height generated from SODAR (Sound Detection and Ranging). Good correlation has been observed for mixing height with Temperature (R = 0.582) and wind speed (R = 0.437). Temperature and wind speedare influencing positively to the mixing heights during the Spring and Summer seasons. The convective boundary layer height growths and falls during the day time depending on the increase and decrease of surface temperature due to solar heating of the ground. The variation in surface temperature controls the existence of atmospheric convection; therefore it strongly affects the mixing height. The negative correlation (R=0. 598) has been found between mixing height and relative humidity (RH), indicates that as the humidity increases mixing height decreases. In addition, temporal variation of mixing layer height with the meteorological parameters between daytime and nighttime have also been studied. On the other hand, low correlations have been observed between all air pollutant concentrations and mixing height in Spring and Summer seasons R= 0.21 (SO_2), R= 0.145 (NO_2), R= 0.085 (SPM) and R= 0.277 (RSPM). Furthermore, positive correlations have been observed for NO_2, SPM and RSPM concentrations whereas negative correlation has been found in SO_2 concentrations.

1. INTRODUCTION

The height of the atmospheric boundary layer (ABL) or mixing height (MH) is animportant parameter describing the structureof the lower atmosphere, and its understanding is of specific importance for several applications for example environmental monitoring, the prediction of air pollution, weather forecasting or as a scaling parameter for the description of vertical profiles.[1] The mixing height (MH) is a key parameterin air pollution models determining the volume available forpollutants to dispersion [2] and the structure of turbulence in the boundary layer[3]. It plays an important role in dispersion of pollutants and is one of the factors that determine the pollution potential. The major air pollutant, which could cause potential harm to human health has been included are SO_2, NO_2 and particulate matter (SPM and RSPM) etc. The aim described in this paper, is to compareand correlate the concentration of air pollutants and meteorological parameters (wind speed, wind direction temperature etc.) with mixing height.

2. DATA

The observation site was Delhi (28.38°N, 77.12°E, 300 m a.s.l.), the capital city of India, which is not only one of the most densely populated areas but also one of the most highly polluted mega-cities in the world. The mixing height has been measured using the monostatic SODAR. In SODAR highly directional short bursts of sound energy are radiated into the atmosphere, which, after scattering from atmospheric fluctuations of eddy sizes within the inertial subrange (0.1-10 m), are received back by the receiving antenna. The signals are processed to produce an online facsimile display of the dynamics of atmospheric boundary layer (ABL) thermal structures. The echogram structural details are used to derive the mixing height of the ABL. The SODAR was operated at a frequency of 2.25 kHz with a100-ms pulse duration, a cycle time of 6s and electrical power of 100 W. The antenna was a parabolic dish 1.22 m in diameter and the beam width was 15°. The mixing height was obtained using the empirical relationship given by Singal *et al*. [4].

3. RESULTS AND DISCUSSION

The hourly variation of mixing layer during daytime and night time have been studied. Figure 1 shows the temporal variation of mixing height in spring and summer months. As shown in Fig. 1, the mixing layer height increased from 8:00, and reached the maximum at 14:00 then; it decreased from 14:00 till 19:00, and tended to be invariable from 20:00. The convective boundary layer height growths and falls during the day time depending on the increase and decrease of surface temperature due to solar heating of the ground. The variation in surface temperature controls the existence of atmospheric convection; therefore it strongly affects the mixing height. The hourly values of the mixing layer height indicated a similar trend in both the seasons.

The wind speed and temperature played an important role in the alteration of mixing layer height. Figures 2(a) and 2(b) show the correlation between the wind speed and temperature with mixing height. Good correlation have been observed for mixing height with Temperature (R = 0.582) and wind speed (R = 0.437).
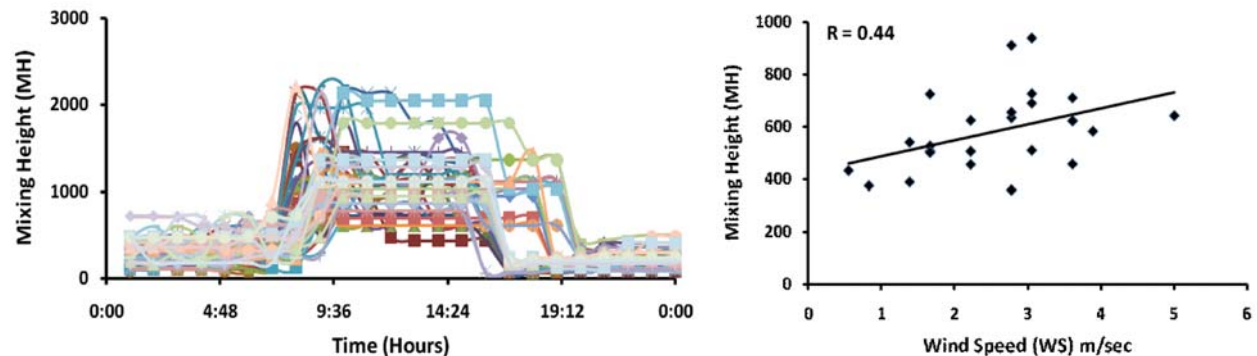
Fig. 1. Variations of hourly MH in Spring and Summer seasons at Delhi during 2009.

Temperature and wind speed are influencing positively to the mixing heights during the Spring and Summer seasons. Furthermore, the mixing layer height also had relatively high correlation coefficients with relative humidity. Figure 2(c) shows the scatter plot between relative humidity and mixing height. The strong negative correlation (R=0.598) has been found between mixing height and relative humidity (RH), indicates that as the humidity increases mixing height decreases.
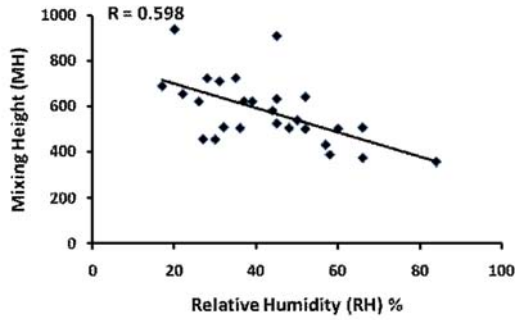
Fig. 2(a) Scatter plot between Wind speed and mixing height.
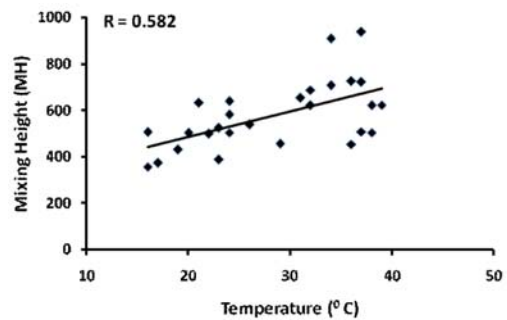
Fig. 2(b) Scatter plot between Temperature and mixing height.
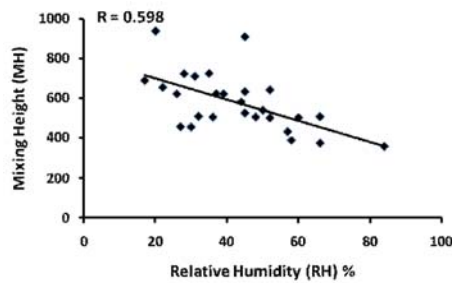
Fig. 2(c). Scatter plot between Relative humidity and mixing height.

On the other hand, correlations between the air pollutants with mixing height have also been studied. Low correlations have been observed between all air pollutants concentrations and mixing height in Spring and Summer seasons R= 0.21 (SO_2), R= 0.145 (NO_2), R= 0.085 (SPM) and R= 0.277 (RSPM). Furthermore, positive correlations have been observed for NO_2, SPM and RSPM concentrations whereas negative correlation has been found for SO2 concentrations. M concentration and mixing height.
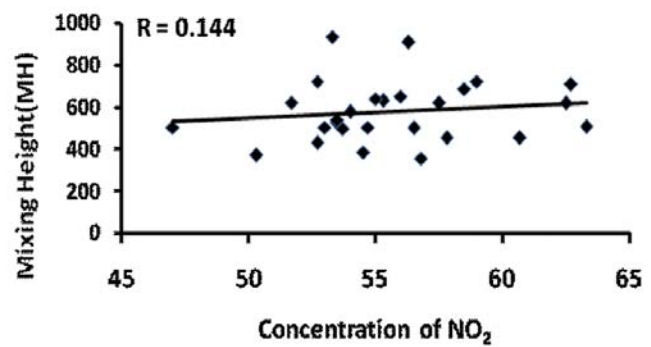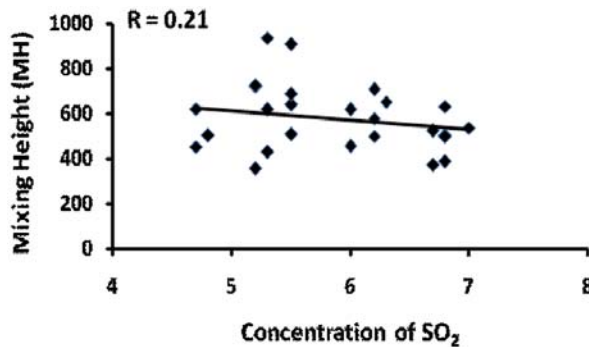
Fig. 3 (a&b) Scatter plot between SO_2 concentration and mixing height.
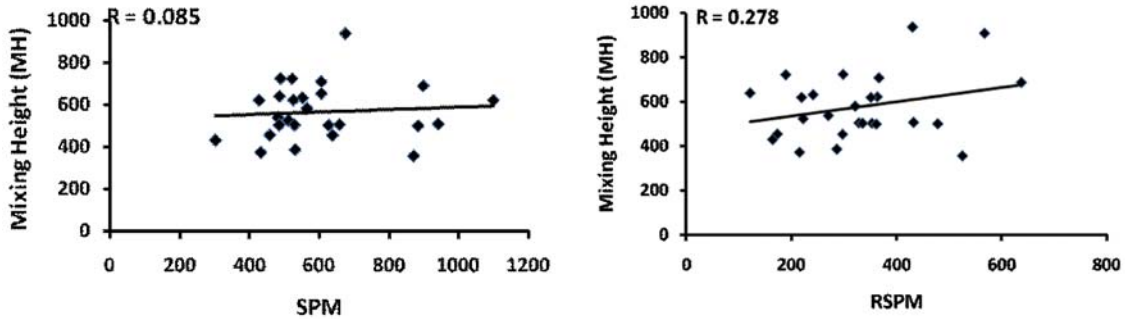
Fig. 3 (c&d). Scatter plot between SPM concentration and mixing height.

4. CONCLUSION

This study presents results of monthly and Spring - Summer seasonal variations of NO_2, SO_2, SPM and RSPM concentrations as well as the influence of meteorological parameters on observed mixing height generated from SODAR (Sound Detection and Ranging).

- Good correlations have been observed for mixing height with Temperature and wind speed.
- Temperature and wind speed are influencing positively to the mixing heights during the Spring and Summer seasons.
- The negative correlation has been found between mixing height and relative humidity.
- Positive correlations have been observed for NO_2, SPM and RSPM concentrations whereas negative correlation has been found for SO_2 concentrations.

5. REFERENCES

[1]   BEYRICH, 1997. Mixing height estimation from sodar data — a critical discussion*. *Atmospheric Environment* **31** (23), 3941-3953.

[2]   P. SEIBERT, F. BEYRICH, S.E. GRYNING, S. JOFFRE, A. RASMUSSEN and TERCIER, 2000. Ph.: Review and Intercomparison of Operational Methods for the Determination of the Mixing Height, Atmos. *Environ.*, **34**(7), 1001–1027.

[3]   R. HASHMONAY, A. COHEN, and U. DAYAN, 1991. Lidar observations of atmosphere boundary layer in Jerusalem, *J. Appl. Meteorol.*, **30**, 1228–1236.

[4]   S.P. SINGAL, B.S. GERA, and D.R. PAHWA, 1994. Application of SODAR to air pollution meteorology. *International Journal of Remote Sensing*, **15**, 427–441.

Investigation of Auditory Nuclei Generating Binaural Masking Level Difference: a Frequency Following Response Study

Sreekesh Nambiar[1], Suhani Sharma[2] and Rashmi Bhat[1]
[1]Dr. S.R.C. Institute of Speech and Hearing
[2]All India Institute of Speech and Hearing
e-mail: sreekesh.nambiar@gmail.com

ABSTRACT

Binaural masking level difference (BMLD) refers to the improved signal detection in presence of noise when either signal or noise go out of phase in one ear with respect to the other. BMLD is considered to be result of the binaural interaction occurring at the level of brainstem. Jenkins and Masterton (1982) suggested MSO neurons to be the probable site of BMLD generation in human. Animal studies in single cell chinchilla and guinea pig have shown lower brainstem to be the site of generation of BMLD (Palmer, Jiang, and McAlpine, 1999). However, these results cannot be implicated to humans directly. Few electrophysiologic studies had aimed to locate site of origin of BMLD in adults. But this issue always remained a matter of discrepancy across researcher. Kevanishivili and Lagidze (1987) used auditory brainstem responses (ABR), middle latency responses (MLR) and slow cortical potentials (SCPs) to estimate site of BMLD origin, they concluded it to be generating from auditory cortical areas. Wong and Stapels (2004) suggested the same using auditory steady state potential (ASSR) as investigating tools. Wilson and Krishnan (2005) recorded BMLD from the auditory brainstem using brainstem evoked potentials (FFRs) but their findings could not be validated as they did not measure and correlated behavioral BMLDs to FFR BMLDs. **Need for study**: This study was undertaken to investigate FFR BMLD at the brainstem level and correlate the results with that of behavioral BMLD measure to validate the finding of FFR. Results of this study will provide a critical insight on the site of origin of BMLD.**Aim and Objective**: To systematically measure Binaural masking level difference behaviourally and electrophysiologically using Frequency Following Response in all participants. **Methods:** Participants: 20 adults (10 males and 10 females) within the age range of 23-30 years participated in this study. All subjects had normal hearing (<20 dB HL) thresholds at octave frequencies from 250 to 8000Hz.Procedures and instrumentation: FFRs were recorded using 500Hztone burst stimulus at 70 dB HL in the So and S π conditions. A 40 msec duration white noise was generated using Adobe Audition. Both the stimulus and noise were routed independently to each ear through two independent programmable attenuators. The six different experimental conditions in which FFR were recorded were So, S π , SoNo, SoN and S π No.All neural responses were transformed from the time domain to frequency domain using fast fourier's transformation (FFT) for different conditions. BMLD amplitude for FFR is obtained from differences between SoNo and SoNπ and SoNo and Sπ Noconditions.Behavioural BMLD threshold were measured using OB 922 diagnostic audiometerfor the same conditions as for FFR BMLD. **Result and Discussion:** FFRs were present in all the individuals for all the BMLD conditions in both frequency and time domain. There was no significant difference between the So and Sπ conditions. Significant differences were obtained between SoNo

and SoNπ and SoNo and Sπ Noconditions. Further, no correlation was evident for behavioural BMLD thresholds and FFR BMLD amplitudes. Conclusion: The results of this study revealed that lower auditory brainstem do preserve phase locked neural activity relevant to BMLDs.But no correlation of FFR BMLDs with behavioral FFR uncertainthe role of auditory brainstem in the generation of BMLDs.

1. INTRODUCTION

Binaural masking level difference (BMLD) refers to the improved signal detection in presence of noise when either signal or noise go out of phase in one ear with respect to the other. Masked threshold are determined for many condition by manipulating the phase, intensity, duration, bandwidth, modulation, etc. of both or either signal or noise. Behaviourally, BMLD is calculated as the improvement in the threshold of signal detection in noise in diotic condition (SoNo) compared to dichotic conditions (SoNπ and (SπNo).BMLD depends on different signal and noise conditions (homophasic and antiphasic) and also on the frequency of the signal. Larger BMLD (typically 10-15 dB) are obtained with low signal frequencies and becomes smaller with increasing frequencies reaching a minimum of 3 dB with signals at approximately 1500 Hz (Henning, 1974a).

BMLD is considered to be result of the binaural interaction occurring at the level of brainstem. The reason for the differences in the detectability of the various BMLD conditions is mostly because of the capacity of our auditory system to use binaural cues in order to detect signals in noise, especially the interaural time difference cues (ITD; Moore, 1995; Yost, 2006). Jenkins and Masterton (1982) suggested MSO neurons to be the probable site of BMLD generation in human as many single neurons in this nucleus respond to low frequency stimulation and receive bilateral excitatory inputs. Also unit responses show many ITD sensitive neurons in MSO.

Animal studies in single cell chinchilla and guinea pig have shown lower brainstem to be the site of generation of BMLD (Palmer, Jiang, and McAlpine, 1999). However, these results cannot be implicated to humans directly. Few electrophysiologic studies had aimed to locate site of origin of BMLD in adults. But this issue always remained a matter of discrepancy across researcher. Kevanishivili and Lagidze (1987) used auditory brainstem responses (ABR), middle latency responses (MLR) and slow cortical potentials (SCPs) to estimate site of BMLD origin, they concluded it to be generating from auditory cortical areas. Wong and Stapells (2004) suggested that processing of BMLD in the brain occurs in the pathway other that auditory brainstem, probably in the auditory cortex using 80-Hz ASSR. . Only one study, Wilson and Krishnan (2005) reported BMLD from the auditory brainstemusing frequency following response (FFRs).

2. NEED FOR STUDY

This study was undertaken to investigate the existence of BMLD at the level of auditory brainstem using FFR andto correlate the results with that of behavioral BMLD measure to validate the finding of FFR. Results of this study will provide a critical insight on the site of origin of BMLD in human auditory system.

3. AIM

To systematically measure binaural masking level difference electrophysiologically using frequency following response and behaviourally in all participants.

4. OBJECTIVE

(1) To determine if behavioural condition of BMLD (SoNo, SoN and S No)will generate FFR.

(2) To investigate if behavioural and FFR BMLDs correlates.

5. METHODS

5.1. Participants

20 adults (10 males and 10 females) within the age range of 23-30 years participated in this study. All subjects had normal hearing (<20 dB HL) thresholds at octave frequencies from 250 to 8000Hz. They had normal middle ear function as assessed by tympanometry and acoustic reflex threshold. There was no history of associated otological or neurological disorders.

5.2. Procedures and instrumentation

FFRs were recorded using 500Hz tone burst stimulus at 70 dB HL in the So and Sπ conditions. A 40 msec duration white noise was generated using Adobe Audition. Both the stimulus and noise were routed independently to each ear through two independent programmable attenuators. The six different experimental conditions in which FFR were recorded were So, Sπ, SoNo, SoNπ and SπNo. All neural responses were transformed from the time domain to frequency domain using fast fourier's transformation (FFT) for different conditions. Behavioural BMLD threshold were measured using OB 922 diagnostic audiometer for the same conditions as for FFR BMLD.

5.3. Result and Discussion

FFR for So, Sπ, SoNo, SoNπ and Sπ No conditions was obtained from 20 adults listeners. BMLD for FFR in SoNπ and Sπ No condition was calculated by subtracting the FFR amplitude for SoNo condition from SoNπ and Sπ No conditions, respectively. Behaviorally BMLD for SoNπ and Sπ No conditionwas calculated by subtracting the masked threshold of SoNo condition from SoNπ and Sπ No conditions, respectively.

Paired T-Test was used to investigate the effect of various condition of signal and noise (So, Sπ, SoNo, SoNπ and Sπ No)on BMLD. Also we ran paired T-Test to see the differences in FFR BMLD and behavioural BMLD obtained for both SoNπ andSπ Nocondition.

Results showed that there was no significant difference between FFR amplitudes obtained from So and Sπ conditions (p = .227). Significant differences were obtained between SoNo and SoNπ (p = .000) &SoNo and S Noconditions p = .000). Means of FFR amplitudes for So, Sπ, SoNo, SoNπ and Sπ No conditions are shown in figure 1.

These findings are consistent with the finding of Wilson and Krishnan (2005). These results confirm that FFR can be elicited from different conditions that are used to measure BMLD behaviourally. Significant
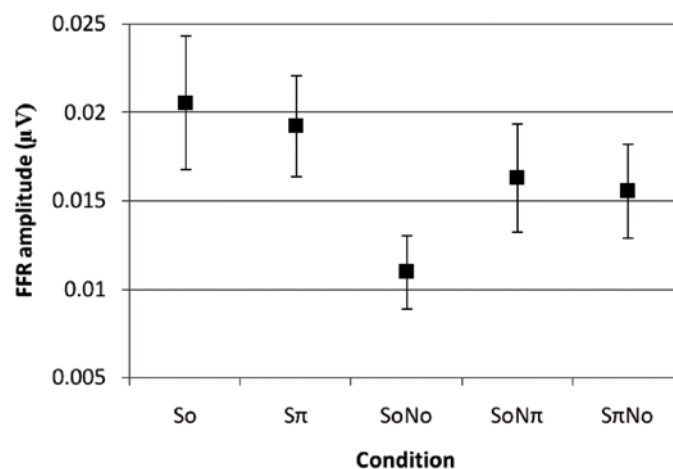
Fig. 1. Mean and standarddeviartion of FFR at various condition of
signal and noise So, S., SoNo, SoN. and S.No.

differences between SoNo and SoNπ and SoNo and Sπ Noshowed that it is possible to measure BMLD electrophysiologically using FFR.

No significant differences were found between BMLD obtained forSoNπ and Sπ Noconditions both behaviourally (p = .109) and electrophysiologically using FFR (p = .294; Figure 2). Wilson and Krishnan (2005) found significant greater FFR BMLD forSoNπ compared toSπ Nocondition. Also behavioural BMLD reported by Durlach and Colburn (1978) showed significantly greater BMLD for Sπ Noin contrast to SoNπ condition. This finding of this contradictory to the above mentioned FFR and behavioural studies. These can be because of the high intra subject variability in the measure of FFR and behavioural BMLD of the listeners participated in the study. However their respective means showed some difference.
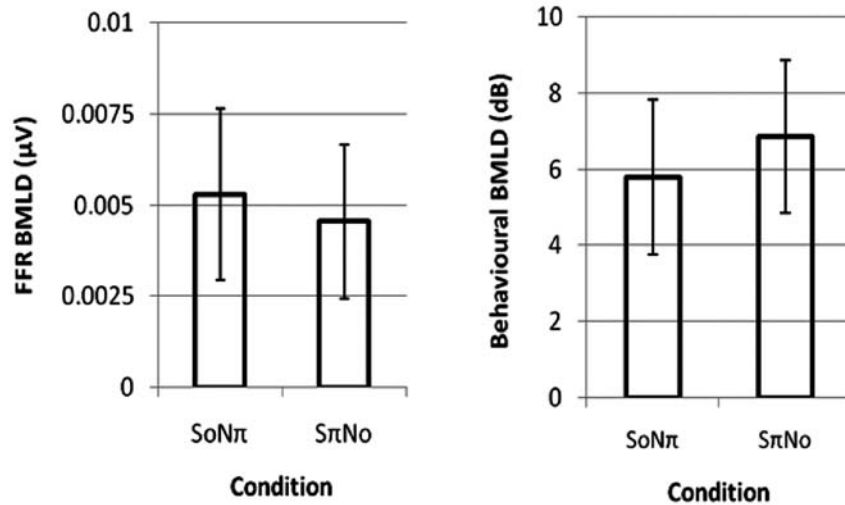
Fig. 2. Mean and standard deviation of the BMLD obtained for SoN. and S.No condition using FFR (left) and behaviourally (right)
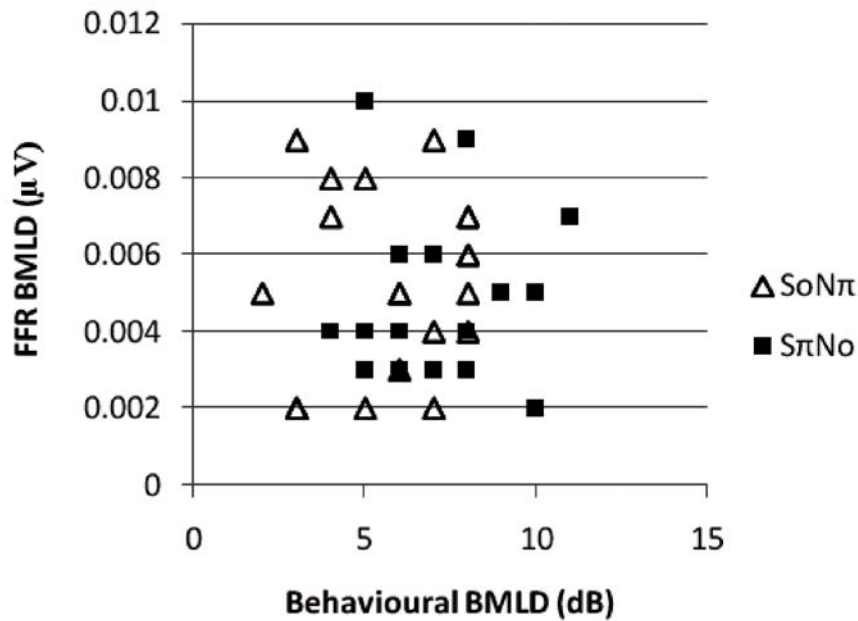
Fig. 3. Relation between FFR BMLD and behavioural BMLD.

A pearson correlation coefficient was obtained to determine the relation between FFR and behaviour BMLD for both SoNπ and Sπ Noconditions (Figure 3). No significant relation was found between FFR and behaviour BMLD. Wilson and Krishnan (2005) found a significant correlation between FFR and behavioural BMLD.These resultsuncertain the place of origin of BMLD in the human auditory system. Also it would highlights that different auditory nuclei may be responsible for FFR and behavioural BMLD.

6. CONCLUSION

The results of this study revealed that lower auditory brainstem do preserve phase locked neural activity relevant to BMLDs. It was revealed that BMLD can be electrophysiologically elicited using FFR. But no correlation of FFR BMLDs with behavioral FFR uncertain the role of auditory brainstem in the generation of BMLD. Further investigation on a large group and of different age groups is required to establish these finding.

7. REFERENCES

[1]. W.M. Jenkins and R.B. Masterton, 1982. Sound localization: effects of unilateral lesions in the central auditory system. *J Neurophysiol* **47**, 987–1016.

[2]. Z. Kevanishvili and Z. Lagidze, 1987. Masking level difference: an electrophysiologic approach. *Scan Audiol* **16**, 3–11.

[3]. J.R. Wilson and A. Krishnan, 2005. Human Frequency-Following Responses to Binaural Masking Level Difference Stimuli. *J Am AcadAudiol* **16**, 184–195.

[4]. G.B. Henning, 1974a. Lateralization and the binaural masking-level difference.*J AcoustSoc Am*. **55**(6), 1259-1262.

[5]. N.I. Durlach and H.S. Colburn, 1978. Binaural phenomena. In: Carterette EC, Friedman MP, eds. *Handbook of Perception.* Hearing. New York: Academic Press, **4**, 428–446.

[6]. D. McAlpine, D. Jiang and A.R. Palmer. 1999. Binaural masking level differences in the inferior colliculus of the guinea pig. *J AcoustSoc Am* **100**, 490–503.

[7]. A.R. Palmer, D. Jiang and D. McAlpine, 1999."Desynchronizing responses to correlated noise: a mechanisms for BMLD at the inferior colliculus", *J. Neurophysiol* 81, 722-734.

[8]. B.C.J. Moore, 1995. *Hearing*. San Diego, CA: Academic press

[9]. W.A. Yost, 2006. *Fundamentals of Hearing*. San Diego, CA: Academic press

[10]. W.Y. Wong and D.R. Stapells, 2004.Brain stem and cortical mechanisms underlying the binaural masking level difference in humans: an auditory steady-state response study. *Ear and Hearing*. **25** (1), 57-67.

Experimental Investigation of Different Acoustic Streaming Flows Inside a Standing wave Thermoacoustic Machine

Yasser Rafat and Luc Mongeau

Department of Mechanical Engineering, McGill University, Montréal, Q.C, Canada
e-mail: yasser.rafat@mail.mcgill.ca

ABSTRACT

In this study different kind of acoustic streaming flows within a standing wave thermoacoustic machine were identified. Experimental study was performed using Particle Image Velo-cimetry (PIV). A rectangular Plexiglas resonator was used as an idealised standing wave thermoacoustic machine. Rayleigh acoustic streaming was studied in an empty resonator. Acoustic streaming generated due to interaction of standing wave with thermoacoustic core was also studied. Simplified components were used to model the stack and heat exchangers. Two different stack configurations were studied. The acoustic streaming near the stack edges and in between the stack plates was studied. Acoustic streaming around a cylinder was also studied at different excitation frequencies and acoustic amplitudes. It was found that complex streaming environments appears due to presence of thermoacoustic core elements.

1. INTRODUCTION

Large amplitude acoustic standing waves give rise to steady, circulatory flow structures, which are called acoustic streaming. The phenomenon of streaming was first reported by Faraday[3] while observing sand patterns on vibrating elastic plates. Acoustic streaming is produced by time averaged Reynolds stresses, defined as the mean value of the acoustic momentum flux. The dissipation of the acoustic energy flux allows gradients in the momentum flux which in turn forces acoustic streaming[5]. Lord Rayleigh was the first to propose a mathematical model for boundary layer driven acoustic streaming in a wide channel. He assumed the boundary layer thickness to be negligible in comparison to the channel width, and the wavelength to be large compared to the tube radius[11].

The interaction of large amplitude oscillating acoustic flows with the stack and heat exchangers creates complex flow patterns such as streaming, vortex shedding and transition to turbulence. Streaming and edge effects are expected to influence strongly the overall efficiency of thermoacoustic systems[2, 6.] Streaming flows[10] contribute significantly to heat transfer. An experimental study[8] of the effects of acoustic streaming on heat transfer reported that heat transfer occurs principally from the leading and trailing edges of the suspended object, where the thermal boundary layer is thin and the local streaming velocity is large. The radial heat transfer in a resonance tube with undisturbed flow is ineffective compared to the effects arising from edges. He found that acoustic streaming occurring at edges of the suspended rigid body enhances the heat transfer much more than the Rayleigh streaming. He also suggested that this streaming is localised near the body edges. Moreau *et al.*[7] employed LDA to study the effect of stack on Rayleigh streaming and found

that the magnitude of the streaming velocities in the vicinity of the stack ends is very high when compared with Rayleigh streaming. The streaming flow near edges of single flat spoiler was studied by Aben et al. [1]. They employed PIV for studying the streaming flow.

2. METHODOLOGY

The experimental setup was explained in detail in a previous study12. Initially, the resonator was excited at an acoustic frequency of 1658 Hz which corresponds to a wavelength of 0.2 m. The camera field of view was 0.1 m × 0.8 m. This selection of acoustic wavelength and camera field of view allowed for capturing more than a complete streaming cell in the field of view. The first stack configuration used is shown in Figure 1. a. It was made of ceramic with square pores of 0.12 mm. The length of stack was 1 cm. The second stack configuration is shown in Figure 1. b. Two different plate gaps were used for this stack configuration with a plate gap of 1 mm and 2 mm. These stacks were fabricated from glass plates used in microscope slides. Each plate had a dimension of 40 × 25.4 × 1 mm.

(a)   (b)
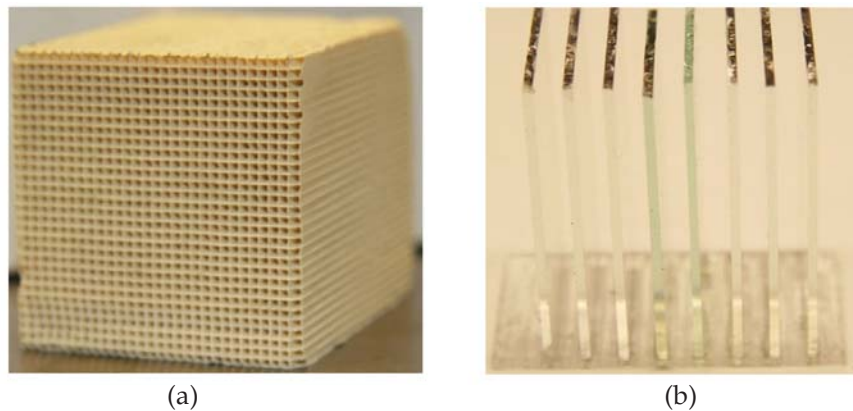
Fig. 1. Ceramic stack. (a) Front view. (b) Perspective view

The first order instantaneous and second order streaming velocities were simultaneously captured by phase locked ensemble average method. Both the laser and camera were synchronised by the pressure signal at the hard end of the resonator. The PIV system would capture images at the phase corresponding to the maximum acoustic velocity. The sampling rate was same as the acoustic excitation frequency. Three hundred images were captured and the final velocity was found after ensemble averaging 300 velocity vector maps. All the vectors shown in the following results are for ensemble averaged velocities.

3. RESULTS AND DISCUSSION

The acoustic and streaming velocity vector map of the acoustic flow at 1658 Hz are shown in Figure 2.a and Figure 2.b respectively. The maximum ensemble averaged acoustic velocity magnitude was 1 m/s and the maximum ensemble averaged streaming velocity magnitude was 0.005 m/s. The streaming velocity vector map shows a complete streaming cell in center and partial streaming cell in front and wake.

In order to study the effect of stack on the Rayleigh streaming, the stack shown in Figure 1.a was introduced at two locations. The first location of stack was at x=λ/4 from velocity antinode. At this location there was maximum acoustic velocity and minimum Rayleigh streaming velocity as shown in Figure 2. The resulting streaming velocity vector map for first stack location is shown inFigure 3.a. Previous experimental studies[7] have suggested change in the streaming velocity magnitudes and shape of Rayleigh streaming cell near the stack edges. Similar results were observed during our experiments. Comparison between the streaming velocity vector map of Figure 2.b andFigure 3.a reveal that the shape of the streaming cell was changed. In the absence of stack the horizontal dimension of the streaming cell is such that there were two streaming cells formed along the resonator width; while in the presence of stack there was only one streaming

(a)   (b)
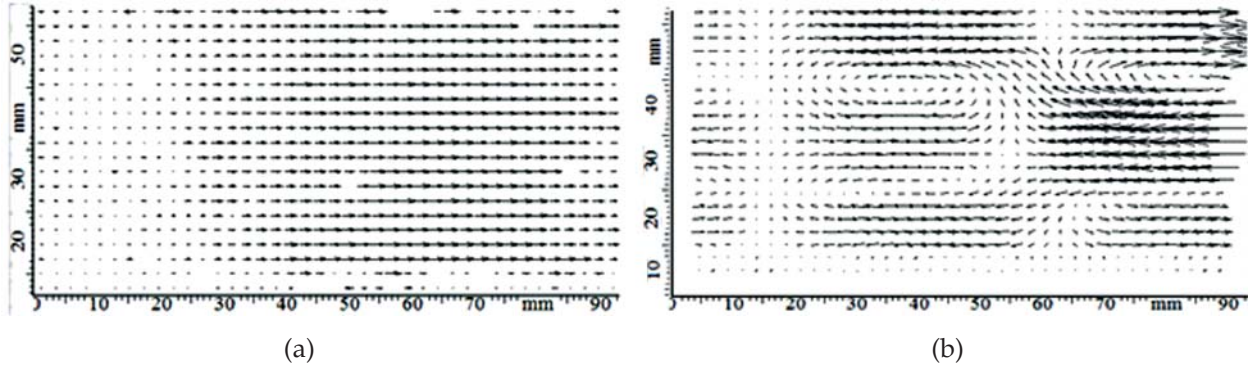
Fig. 2. Velocity vector map at 1658 Hz without stack. (a) Acoustic velocity (b) Streaming velocity

(a)   (b)
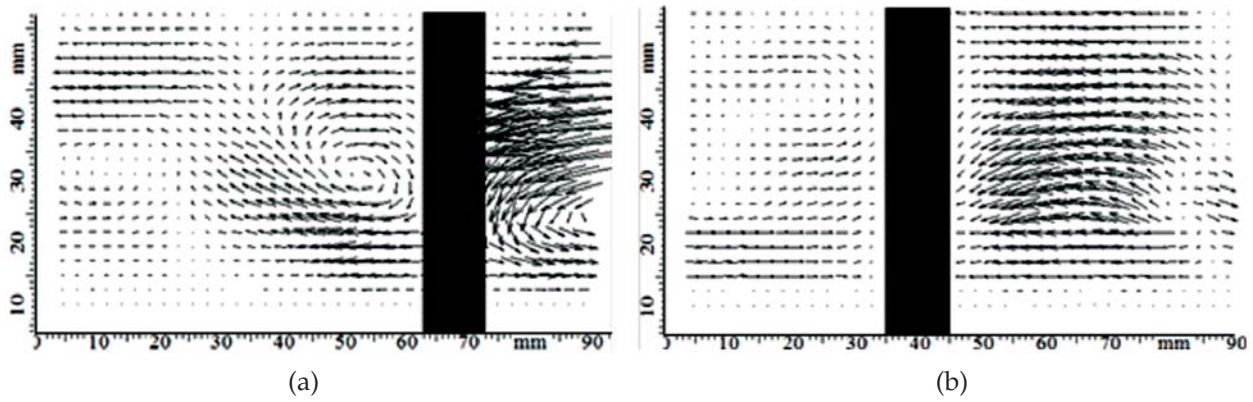
Fig. 3. Streaming velocity. (a) First location (b) Second location

cell in the transverse direction. The longitudinal dimension of the steaming cell was not affected by the presence of the stack.

The second location for the stack was at x=λ/8 away from the acoustic velocity antinode. At this location the streaming velocity amplitude was maximum the acoustic velocity was less than half the peak amplitude. The velocity vector map for acoustic streaming in Figure 3.b shows different shapes of streaming cells on the either side of the stack. As with the previous stack location, the streaming velocity amplitude on the right side of the stack was more than on the left side. This may be attributed to the fact that the acoustic velocity amplitude on the right side was more. The difference in the streaming velocity amplitude on either side of the stack was more pronounced in the second location which again can be attributed to the larger difference in acoustic velocity amplitude on either side of the stack for the second stack location. Due to the presence of stack, the Rayleigh streaming cell was completely disturbed and a different streaming pattern was observed. Near the edges of the stack, data cannot be taken due to flaring of the images. The flaring occurred due to reflection of the laser light from the stack wall. From these results it can inferred that stack presence completely changed the streaming environment both in terms of streaming velocity amplitude and the resulting streaming cell shape. It is therefore necessary to characterise this form of streaming to better understand its effect on the heat transfer between the heat exchanger and stack. For understanding the streaming flow which results due to interaction of stack with standing wave velocity data near the stack edges and in between the stack plates is required.

Acoustic streaming near the stack end and in between the plates was observed for the two glass stacks with plate gap of 1 and 2 mm as shown in Figure 1.b. The flow was excited at 245.5 Hz which corresponds to resonator length of 3λ/4. The peak acoustic velocity amplitude, u_{ac} was 3.4 m/s. The stack center was located

at a distance of $3\lambda/8$ from the hard end. The stacks had a gap, g of 1 mm or $7\delta_v$ and 2 mm or $14\delta_v$ in between the plates. The streaming velocity for the stacks with gap of 1 and 2 mm are shown in Figure 4.a and Figure 4.b respectively. In their analytical work Hamilton *et. al*[4] studied acoustic streaming in channels with arbitrary width. They concluded that for channel width less than $10\delta_v$ classical Rayleigh streaming was not observed and only inner streaming vortex was present and even for channel width of $20\delta_v$, inner streaming vortex occupied 10% of the channel. In the case of resonator with stack, there would be a transition region near the stack ends. The transition region coupled with the stack length would determine the overall streaming environment inside the stack and near its ends. The streaming velocity results for the stack, $g=7\delta_v$ presented in Figure 4.a show presence of a single streaming cell as predicted by analytical study. The magnitudes of the streaming velocity both inside the stack and near the stack ends were higher when compared with streaming velocity away from the stack. The streaming velocity results obtained for the stack, $g=14\delta_v$ show presence of more than one streaming cell inside the stack near the end. Since the plate gap was more than $7\delta_v$, a distinct outer streaming vortex was observed. The results presented here were in accordance with the analytical studies.
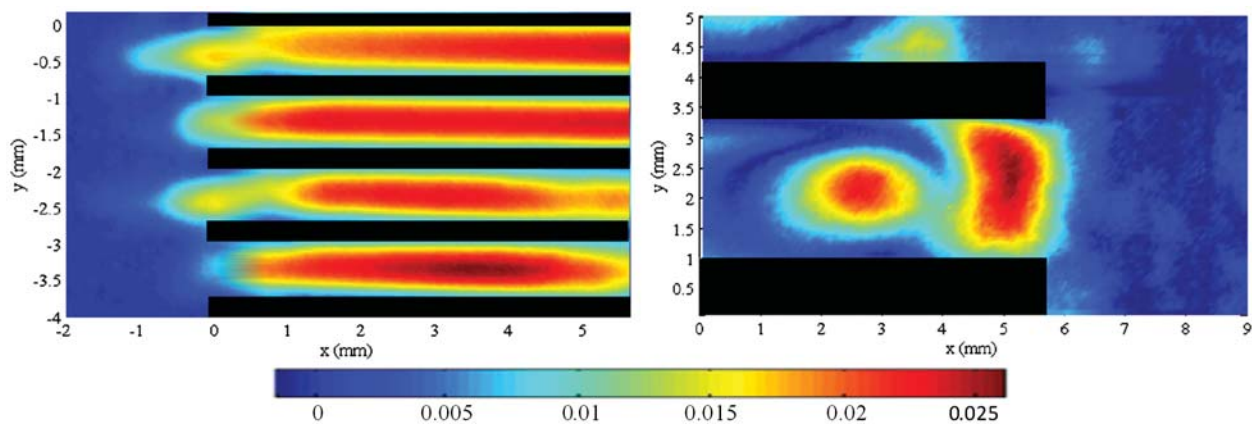
Fig. 4. 4Streaming velocity for glass stack in m/s
(a) 1 mm gap between plates (b) 2 mm gap between plates

In a thermoacoustic core, heat exchangers are located at either side of the stack. A simple fin tube heat exchanger has parallel plates like the stack and tubes perpendicular to the axial flow direction. In the present study a single transparent glass cylinder was used in order to idealise the tubes in a fin tube heat exchanger. The cylinder was 1 mm in diameter and the length was equal to the resonator width. The flow was excited at 85 Hz and 100 Hz. The streaming velocity flow inside a resonator resulting from interaction of acoustic standing wave with a circular cylinder is presented in Figure 5andFigure 6. At 85 Hz the streaming flow was studied for various acoustic velocity amplitudes at the location of the cylinder. For low acoustic amplitude at cylinder location, the streaming vortices were not fully developed as evident from Figure 5.a. Fully developed streaming cells were observed at higher velocity amplitudes as shown in Figure 5.b and Figure 6respectively. In a fully developed streaming flow four vortices were observed, one in each quadrant. The streaming behaviour observed in this study is similar to the analytical results presented by Nyborg[9].

4. CONCLUSION

In this study attempts were made for characterising the acoustic streaming flow present in relatively realistic thermoacoustic machines. It was found that presence of stack changes the streaming flow from Rayleigh streaming observed in an empty resonator. Higher magnitudes of streaming velocities were observed near the stack end and inside the stack. The results presented here for the two stacks with different plate gap were similar to the analytical results. The difference between the experimental results and the analytical results was due to the absence of the effects of the transition region in the analytical model. The streaming

(a)   (b)
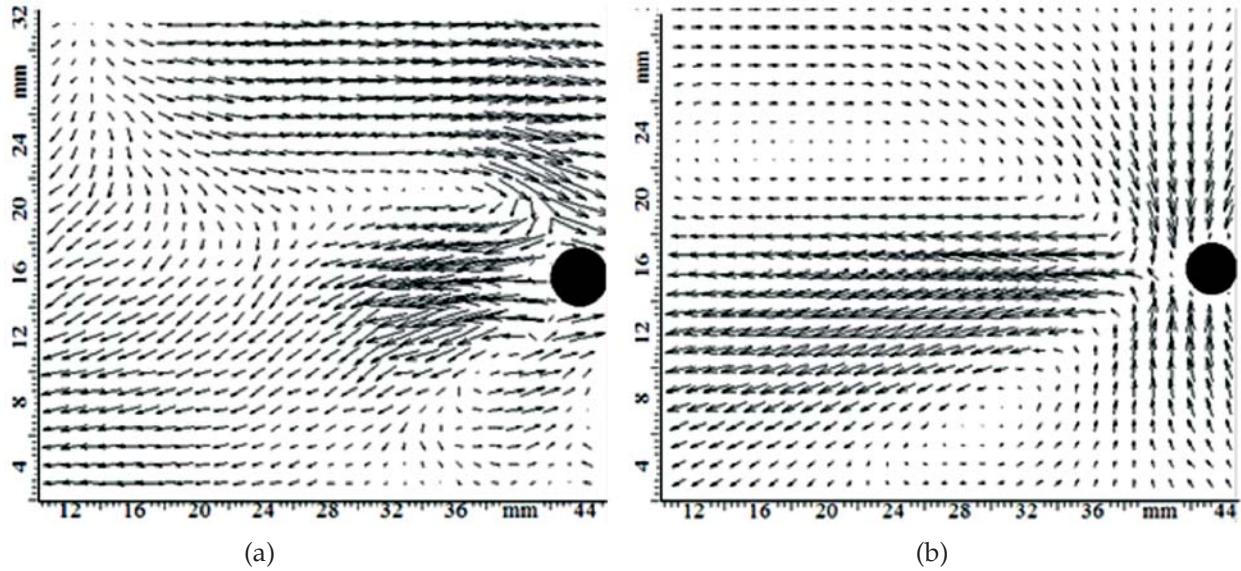
Fig. 5. Streaming around a cylinder at 85 Hz. (a) u=0.34 m/s (b) u=0.76 m/s
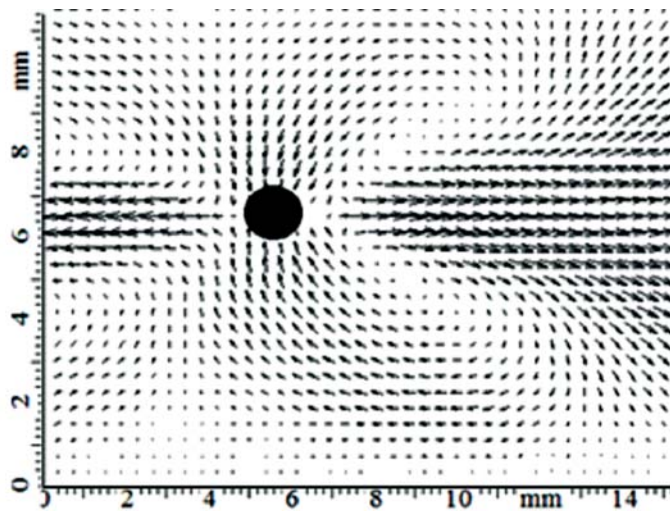
Fig. 6. Streaming around a cylinder at 100 Hz. u=0.57 m/s

flow structures resulting from the presence of a circular cylinder were completely different from either Rayleigh streaming or streaming due to stack. Four circulation regions were observed.

In this study simple objects were introduced in the resonator and the resulting streaming flow structures were observed to be very different from Rayleigh streaming. A real thermoacoustic core would have both stack and heat exchangers and their interaction with each other would create a very complex streaming environment. Thus, a simple Rayleigh streaming model cannot be used for characterising the overall streaming flow behaviour inside a standing wave thermoacoustic machine.

5. REFERENCES

[1] P.C.H. ABEN, P.R. BLOEMEN and J.C. H. ZEEGERS, 2009. '2-D Piv Measurements of Oscillatory Flow around Parallel Plates', *Experiments in Fluids*, **46**, 631-41.

[2] A. BERSON, M. MICHARD and P. BLANC-BENON, 2008. 'Measurement of Acoustic Velocity in the

Stack of a Thermoacoustic Refrigerator Using Particle Image Velocimetry', *Heat and Mass Transfer/ Waermeund Stoffuebertragung,* **44**, 1015-23.

[3] M. FARADAY, 1831. 'On a Peculiar Class of Acoustical Figures; and on Certain Forms Assumed by Groups of Particles Upon Vibrating Elastic Surfaces', *Philosophical Transactions of the Royal Society of London* **121**, 299-340.

[4] M.F. HAMILTON, Y.A. ILINSKII and E.A. ZABOLOTSKAYA, 2003. 'Acoustic Streaming Generated by Standing Waves in Two-Dimensional Channels of Arbitrary Width', *Journal of the Acoustical Society of America,* **113**, 153-60.

[5] SIR JAMES LIGHTHILL, 1978. 'Acoustic Streaming', *Journal of Sound and Vibration,* **61**, 391-418.

[6] X. MAO and A.J. JAWORSKI, 2010. 'Application of Particle Image Velocimetry Measurement Techniques to Study Turbulence Characteristics of Oscillatory Flows around Parallel-Plate Structures in Thermoacoustic Devices', *Measurement Science and Technology,* **21**.

[7] S. MOREAU, H. BAILLIET and J.C. VALIERE, 2009. 'Effect of a Stack on Rayleigh Streaming Cells Investigated by Laser Doppler Velocimetry for Application to Thermoacoustic Devices', *Journal of the Acoustical Society of America,* **125**, 3514-17.

[8] G. MOZURKEWICH, 2002. 'Heat Transport by Acoustic Streaming within a Cylindrical Resonator', *Applied Acoustics,* **63**, 713-35.

[9] W.L. NYBORG, 1965. 'Acoustic Streaming', in *Physical Acoustics Principles and Methods*, ed. by Mason W. P. (New York: Academic Press), 290-95.

[10] I. P.AEK, J.E. BRAUN and L. MONGEAU, 2005. 'Characterizing Heat Transfer Coefficients for Heat Exchangers in Standing Wave Thermoacoustic Coolers', *Journal of the Acoustical Society of America,* **118**, 2271-80.

[11] LORD RAYLEIGH, 1884. ' On the Circulation of Air Observed in Kundt's Tubes, and on Some Allied Acoustical Problems', *Philosophical Transactions of the Royal Society of London,* **175**, 1-21.

[12] IDA REYT, YASSER RAFAT, LUC MONGEAU, RANI TAHER and HELENE BAILLIET, 2012. 'Piv Measurements of 3-Dimensional Acoustic Rayleigh Streaming in a Square Cross-Section Standing Wave Resonator', *Acoustics 2012 Nantes.*

Pre-Restoration Subjective Acoustic Comfort in the Goan Church of Nossa Senhora do Pilar

Menino Allan S. M. Peter Tavares, António P. O. Carvalho[1],
S. Rajagopalan[2] and Satish J. Sharma[3]
[1]*Laboratory of Acoustics, Faculty of Engineering,*
University of Porto, Porto-4200-465, Portugal
[2]*Department of Physics, Nagpur University, Nagpur-440 033, India*
[3]*Department of Electronics, Nagpur University, Nagpur-440 033, India*
e-mail: allan.wholysound@gmail.com

ABSTRACT

This study at the Church of Nossa Senhora do Pilar, built in 1613 by the Spanish Capuchos Franciscan, investigates the acoustic effect of music on the subjective comfort of a listener in a worship space. The results presented describe the effect of variations in the type of music rendered (in the form of live music from the cello, clarinet and the ensemble) from two music sources sites (the nave and the choir loft, of the church) on the subjective acoustic comfort of listeners in the church of Nossa Senhora do Pilar (a significant Catholic church of Goa, India). The subjective acoustic comfort of the listeners for different music types at the two music sources was measured through the *Acoustic Comfort Impression Index* (ACII). This index for subjective acoustic comfort was derived as a difference between desirable Subjective Acoustic Impressions such as of Intimacy, Envelopment, Reverberance, Loudness, Clarity, Directionality, Balance and undesirable Subjective Acoustic Impressions such as of Echoes and of Background Noise. The derived acoustic comfort impression index also took into account the requisite of reverential awe; intelligibility for sacred speech, music, singing and the sacred silence that characterizes a worship space. Although the sacred music rendered by the ensemble seems to have elicited better scores of Acoustical Comfort Impression Index (ACII) among the listeners, yet there is no significant difference between the means of the listeners acoustical comfort impressions by the ensemble, cello or clarinet (p = 0.43). Amongst the two music source locations, although the Acoustical Comfort Impression Index (ACII) seems to favor the choir loft location, the music rendered therein is only 80% significantly more effective than the music rendered from the nave floor location (p = 0.20).

1. INTRODUCTION

The desire for religious comfort and solace brings a devotee to a worship space. A good acoustic ambience facilitates the experience of subjective comfort in a worship space thus enabling *Active, Conscious and Total Participation* of the devotee in community worship [1]. This study investigates the acoustic effect of music on the subjective comfort of a listener in a worship space to determine as to what type of music would be acoustically preferred in order to make the sacred liturgy in a worship space a genuine celebration of 'Comfort' and 'Solace'. The results presented here describe the effect of music rendered by the cello, clarinet and the ensemble from different source locations (namely, the nave and the choir loft of the church) on the subjective

acoustic comfort of listeners. Reverential Awe, Intelligibility and Silence as constituted of subjective acoustic impressions are hypothesized as determinants of 'comfort' in a worship space. The net desired effect is named as *Acoustic Comfort Impression* (ACI) and indexed as *Acoustic Comfort Impression Index* (ACII). This study shows an advancement in the comprehension of ACII as compared to what was presented earlier [2].

2. THE CHURCH OF NOSSA SENHORA DO PILAR: THE SAMPLE CHURCH

The Church of Nossa Senhora do Pilar, built in 1613 by the Spanish *Capuchos* Franciscan, lies atop a hillock that rises alongside one of the largest reclaimed khazan lands of Goa. Its small nave has a high plain barrel vaulted ceiling while its diminuted sanctuary's roof, like the other earlier churches of the konkan [3], is covered with a finely coffered barrel vault. The paintings on wood and canvas which decorate the church were done by local and possibly Chinese artists [4]. The present choir stall at the entrance of the church seems to be a later addition or a renovation of the original. The church has undergone a number of improper interventions causing visual and acoustical damage to the interior worship space of the church [5]. The church is presently in the process of restoration. The church before and during restoration is shown in Figure 1.

Fig. 1. Nossa Senhora do Pilar church (Goa, India) during and before restoration.Some important architectural details of Nossa Senhora do Pilar church are shown in Table 1.

Table 1. Architectural details of Nossa Senhora do Pilar church (Goa, India)

ARCHITECTURAL MEASURES	DESCRIPTION	UNITS	VALUES
Total Floor Area	ATOT	m^2	400
Nave Floor Area	ANV	m^2	130
Maximum Height	HMAX	m	15
Maximum Length	LMAX	m	30
Total Volume	VTOT	m^3	3457
Nave Volume	VNV	m^3	837
Total Average Height	HAVG	m	9
Maximum Nave Width	WNV	m	9
Average Width	WAVG	m	8

The ground floor plan of the church shown in Figure 2 reveals the diminuted sanctuary style of the church.

3. METHODOLOGY

3.1 Listeners and Music sources

Nineteen trained normal listeners were spatially seated into four seating zones within the church. Two locations in the church were chosen as music sources. The first location, labelled as 'Music Source A' (MA)
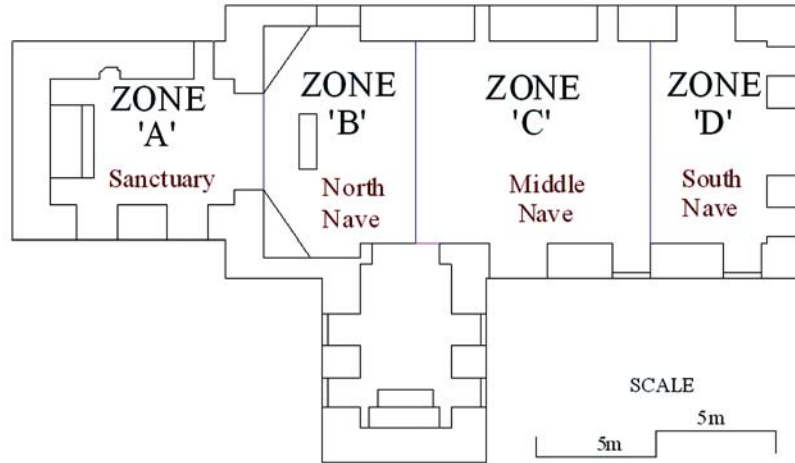
Fig. 2. Ground Floor plan with the zones demarcation (Floor plan courtesy: Engr.Thomas D'Costa)

was the floor of the North East nave - sanctuary corner of the church (Ground floor) and the second location, labelled as 'Music Source B' (MB) was the floor of the Choir Loft of the church (First floor). The musical instruments that were tested in this church are cello (P), clarinet (Q) and an ensemble of cello, clarinet, violins and guitar (R). The locations of the music sources (MA and MB) and listeners seating for the subjective acoustic tests are shown in Figure 3.
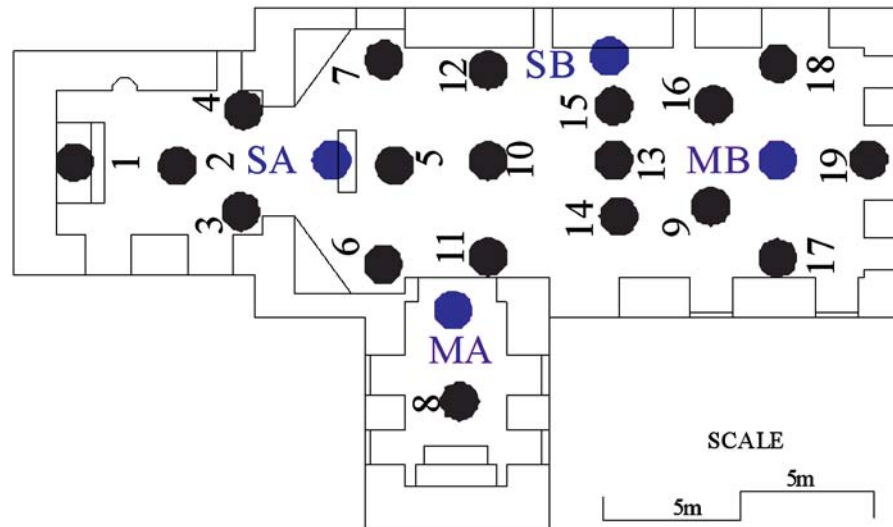
Fig. 3. The locations of Listeners and Music Sources in the Nossa Senhora do Pilar church (Goa, India).

The cellist played "Bach's Suite No. 2". The clarinet player rendered the tune of the "Motet: Fera Pessima" a traditional Christian Lenten hymn. The ensemble played a Goan devotional classic "Piedade Saibinni in minor and major".

3.2 Subjective Evaluation method

The acoustic evaluation sheet [6] [7] given to the listeners was interpreted to accommodate parameters of worship. The experience of reverential awe was expressed as an average of the following desirable Subjective

Acoustic Impressions (SAI): Subjective Acoustic Impression of Intimacy (SAI$_{INT}$), Subjective Acoustic Impression of Envelopment (SAI$_{ENV}$), Subjective Acoustic Impression of Reverberance (SAI$_{REV}$), Overall Subjective Acoustic Impression (SAI$_{OVER}$).The quality of Intelligibility of speech, singing and music was judged as an average of the following desirable Subjective Acoustic Impressions (SAI): Subjective Acoustic Impression of Loudness (SAI$_{LOUD}$), Subjective Acoustic Impression of Clarity (SAI$_{CLAR}$), Subjective Acoustic Impression of Directionality (SAI$_{DIR}$), Subjective Acoustic Impression of Balance (SAI$_{BAL}$). The quality of silence was judged from the following undesirable Subjective Acoustic Impressions (SAI): Subjective Acoustic Impression of Echoes (SAI$_{ECHO}$) and Subjective Acoustic Impression of Background Noise (SAI$_{NOIS}$).

3.3 Derivation of Acoustic Comfort Impression Index (ACII)

The Acoustic Comfort Impression Index (ACII) measures the subjective comfort induced by the acoustics inside the worship space. This subjective acoustic comfort enables the necessary disposition to worship. A difference was drawn between the Desired Subjective Acoustic Impressions (DSAI) in worship space and the Undesired Subjective Acoustic Impressions (USAI) in a worship space in order to acoustically comprehend and optimize this 'Religious Feeling of Comfort and Solace'.

The Desired and Undesired Subjective Acoustic Impressions (DSAI and USAI) were evaluated as averages of the desired eight SAI and the undesired two SAI respectively. The net difference score between the desired and the undesired on a semantic scale of 1-7 was averaged and coded as the *Acoustic Comfort Impression* (ACI) of the worship space.

Finally The *Acoustic Comfort Impression Index* (ACII) at each zone of the worship space was evaluated using equation 1, for different music types: cello (P), clarinet (Q) and ensemble (R) and for different music sources: floor of the nave (MA), and floor of the choir loft (MB).

$$ACLL_{0-1} = \frac{ACLL_i + ACLL_{mux}}{\Delta ACLL_i} \tag{1}$$

where,

$$-1 \leq ACII_i = \text{Calculated value} \leq +1$$
$$ACII_{max} = \text{Maximum value} = 1$$
$$\Delta\, ACII_i = \text{range value} = 2$$

The subjective data was analyzed using *Excel, Origin 6.1 and Origin 8.*

4. RESULTS

The effect of different music source locations (within a church) and the effect of different music types on the subjective acoustical comfort of the listeners is assessed through the results of the ANOVA tests on the means of the populations of *ACII* averaged across 18 listener locations in the church as shown in Table 2.

Table 2. ANOVA tests on means of ACII populations in the church

ANOVA TEST ON MEANS OFACII FOR DIFFERENT MUSIC TYPES AND DIFFERENT MUSIC SOURCES							
TYPE	Data	Mean	SD	SE	N	F value	p value
ACII	P	0.41	0.11	0.03	18	0.85	0.43
	Q	0.45	0.18	0.04	18		
	R	0.48	0.20	0.05	18		
ACII	MA	0.70	0.13	0.03	18	1.69	0.20
	MB	0.75	0.11	0.03	18		

5. CONCLUSION

Although the sacred music rendered by the ensemble seems to have elicited better scores of *Acoustical Comfort Impression Index* (ACII) among the listeners, yet there is no significant difference between the means of the listeners acoustical comfort impressions by the ensemble, cello or clarinet (p = 0.43). Amongst the two music source locations, although the *Acoustical Comfort Impression Index* (ACII) seems to favor the choir loft location, the music rendered therein is only 80% significantly more effective than the music rendered from the nave floor location (p = 0.20).

6. REFERENCES

[1]   Vatican II, 1963. *Sacrosanctum concilium*, 4 Dec. 1963, article **14**, 34.

[2]   M.A.P.S. TAVARES, S. RAJAGOPALAN and S. SHARMA, 2007. Comparative Acoustical Studies of Two Goan Churches, Proceedings of the 19th *International Congress on Acoustics,* 2007, Madrid, Spain; *J. Revista de Acústica*, **38**, 3.

[3]   J. PEREIRA, 2000. *Baroque India; The Neo-Roman Religious Architecture of South Asia: a global stylistic survey*, Aryan Books International, New Delhi.

[4]   C. J. COSTA and S. MASCARENHAS, 2009. Ed., *Pilar; a guide book, Pilar Publications*, Pilar.

[5]   R. GETTU, M. SANTHANAM, A. MENON and R. G. PILLAI, 2013. Ed., *Rehabilitation and Restoration of Structures* IIT Madras, Chennai, 335-345.

[6]   P. O.ANTÓNIO CARVALHO, 1996. Analysis of subjective acoustic measures and speech intelligibility in Portuguese churches, *Proceedings of 131st Acoustical Society of America meeting*, Indianapolis (USA).

[7]   M.A.P.S. TAVARES, 2009. *Acoustical Studies of Worship Spaces*, Ph.D. thesis, Nagpur University, India.

Moisture Detection in the Delaminated Regions of the Hydrophone Encapsulant Material by Infrared Thermography

Sherin Joseph, P.N. Vinod and Reji John
Naval Physical and Oceanographic Laboratory,
Thrikkakara P.O, Kochi - 682021.

ABSTRACT

In this study, the water ingress through the delaminated regions of the rubber encapsulant material in the piezoelectric transducers used for the underwater applications has been studied by infrared thermography. The external heating was applied to the surface of the specimen being tested and the variations in the surface temperature were monitored by means of IR thermography technique. The delaminated regions of the transducers are characterized by hot spot regions in the thermal images. The water ingress was studied in the delaminated regions in the encapsulant of the transducer. The study was also extended to conduct on control samples by using known volume of the water injected into the defect sites and monitor the area by taking IR thermal images. In both cases, the presence of the water ingress regions is clearly observed as cooler regions due to the high specific heat capacity of the water. The maximum thermal contrast corresponding to these cooler regions are calculated and correlated with the volume percentage of the water present.

1. INTRODUCTION

The neoprene rubber is generally used to encapsulate the piezoelectric transducers used for underwater applications [1]. Delamination of the adhesive joints of the encapsulant and intrusion of the water through the delaminated regions are the main reasons for the failure of the sensors. The water intrusion through delaminations can further lead to loss of the adhesion, formation of osmotic blisters, and establishment of a pathway for corrosive ions [2], resulting in derated performance of the acoustic sensors. This emphasizes the need for the application of a reliable nondestructive testing (NDT) tool for early detection of anomalies present in the sensor before irreversible catastrophic failure occurs. In this study, the water ingress through the delaminated region in the piezoelectric transducers has been studied by infrared thermography. The quantitative measurement of the presence of water ingress is necessary in order to get a qualitative value of the water trapped inside. However, quantification of the water ingress inside the delaminated areas in the underwater transducer is not straight forward. Therefore, study was also extended to conduct on control samples by using known volume the water injected into the defect sites and monitor these areas by IR thermal imaging.

The basic principle of the thermography is that the front surface of the inspected structure is externally heated with a short pulse of heat, and the generated heat at the front surface propagates to the interior of the sample because of the heat conduction. The evolution of the surface temperature as a function of time depends on the heat diffusion inside the structure which is affected by the presence of defects in the structure. The

---

transient heat diffusion equation, in 1D through the homogeneous solid with uniform properties is obtained by Fourier law of the heat conduction in solids [3],

$$\frac{\partial^2 T(z,t)}{\partial z^2} = \frac{k}{\rho C} \frac{\partial T(z,t)}{\partial t} \tag{1}$$

where T(z,t) is the temperature field, k is the thermal conductivity of the material, is the volume density and C is the specific heat capacity of the material. In the case of constant heating (Q) flux applied to the surface of a semiinfinite isotropic medium, the temperature decreases approximately as as predicted by the 1D solution of the Fourier equation for the propagation of the heat by conduction [4],

$$T = T_o + \frac{Q}{e\sqrt{\pi t}} \tag{2}$$

where T_o is the initial temperature and Q is the input energy (Joules).
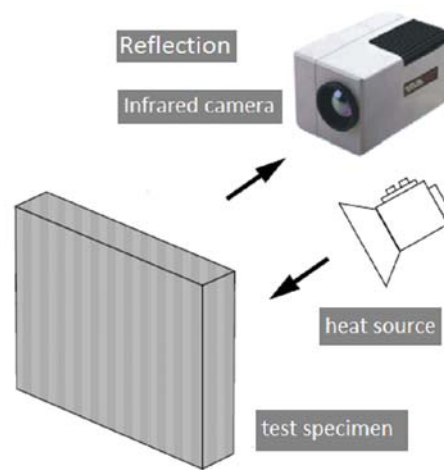
Fig. 1. Experimental set up for thermographic measurement.

2. EXPERIMENTAL

The experimental setup, which comprised a heat source, a long wave infrared camera SC 3000 (FRIR, Sweden) and a specimen holder as shown in fig 1. The infrared camera uses a cooled gallium arsenide (GaAs) quantum well infrared photodetector (QWIP) of 8-9 µm wavelength with a frame rate of 50 Hz and a focal plane array pixel format of 320 (H) x 240 (V). The position of the heating source and the infrared camera are depended on the minimum focal length of the employed lens and on the desired field of view. The encapsulated sensor was thermally heated and thermal images were captured during the cooling phase. The IR image of delaminated areas of the rubber encapsulant was taken by externally heating the surface of the transducer. The IR images were captured in the reflection mode during the cooling down process. Thereafter, these samples are placed in water to induce the water ingress through the delaminated regions. In control samples, the thermographic measurements were carried out for different known volumes of the water introduced.

3. RESULTS AND DISCUSSION

Figure 2 shows the infrared thermal image of the transducer. The thermal image of the inspected transducer shows a clear bright spots indicating the delaminated areas at the interface of the encapsulant material and ceramic stacks or metal structure of the transducer. The efficacy of thermography was evaluated by following a trajectory on the thermal image of the specimen; along with the temperature variations in the specimens were recorded. The trajectory is usually a straight line as shown in the figure 2. The thermal decay curve

along the straight line in the fig 2 indicates the distribution of the temperature as a function of the pixel position. The heat flow in the inspected structure is altered due to the presence of defects. The defect sites acts as a barrier to the thermal diffusion, thereby generating a thermal gradient in or around the region of the defect. As a result, the diffusion rate of the heat flux is reduced at this specific location and these regions cools much slower than its surroundings areas. Hence, these regions appear as hot spots in the captured thermal images.
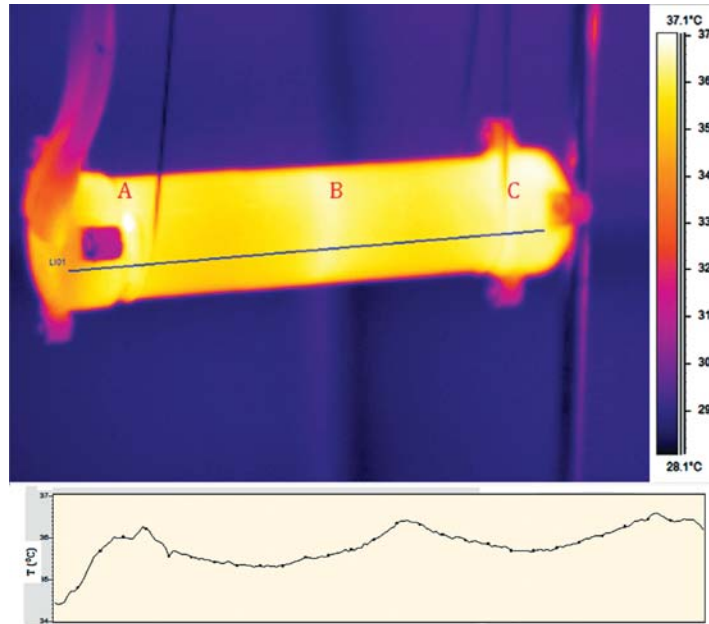
Fig. 2. The infrared thermal image of the delaminated regions in the transducer tested. The temperature profile along the line indicates the higher temperature at the delaminated regions.

The thermal contrast based techniques is considered as the best method to analyse captured thermal images. The absolute thermal contrast, $C^a(t)$ at a location of pixel at time 't' is calculated using the expression [6]

$$C^a(t) = \Delta T(t) = T(t) - T_s(t) \tag{3}$$

where T(t) is the temperature at time t at p and $T_s(t)$ is the average temperature at time t for the sound area in the IR thermal image. The delaminated area of the encapsulant in the hydrophone was characterized by plotting the temperature -time decay curves. Figure 3 shows the typical example of the temperature - time decay plot of the site marked as A in the thermal image. For example, thermal contrast corresponding to delaminated area marked as A in the IR image given in figure 2 was calculated by using eq (3). Figure 4 shows the calculated value of the absolute thermal contrast as a function of time.

The detection of water ingress through delaminated areas in the hydrophone by infrared thermography technique relies on the fact that a delaminated area where the water ingress takes place appears darker than the surrounding areas due to the higher specific heat capacity of the water [5]. Hence, a change in the thermal effussivity, e (W s^{½} m^{-2} K^{-1}) of the material is observed. The thermal effussivity is a property that measures the ability of the material to exchange heat energy with its surroundings and is defined by

$$e = \sqrt{k \rho C} \tag{4}$$

where, k is the thermal conductivity, ρ is the mass density and C is the specific heat capacity of the material. Therefore, presence of the water ingress in the material will appear cooler due to the higher specific
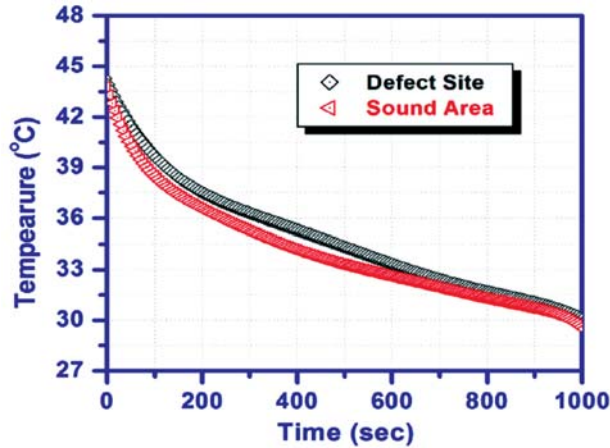
Fig. 3. The temperature decay curves at the defected and non-defected region.
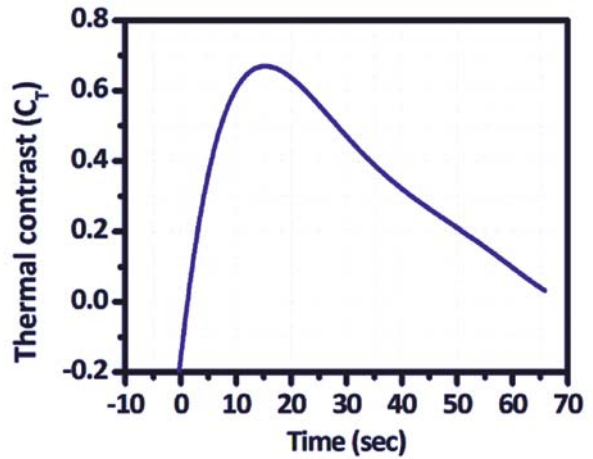
Fig. 4. Thermal contrast as a function of the time.

heat capacity of the water. These regions can be easily monitored by using an infrared thermal imaging system.

The figure 5 shows the typical example of the water ingress through the delaminated region in the hydrophone. The water content highly affects the thermal capacity of the materials. The water diffusing in the material causes an increase in the specific heat capacity of the material, for example, specific heat capacity of the water is 4182 J/Kg/K which is 2-3 times higher than the specific heat capacity of the rubber encapsulant, and appropriate changes in the density and thermal conductivity of the material. Therefore, active infrared thermal inspection would be the most effective investigative procedure to detect the moisture content.
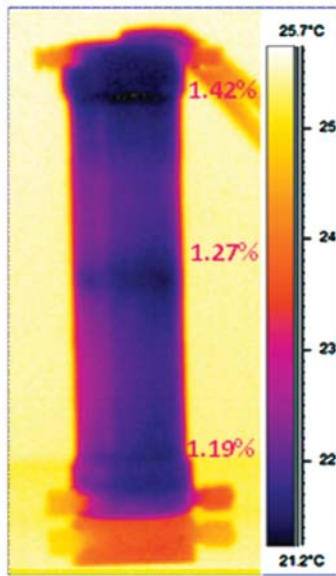
Fig. 5. The thermal image of the hydrophone indicating the water ingress through delaminated regions at the interface of the adhesive joints between the encapsulant and peizoceramic rings.
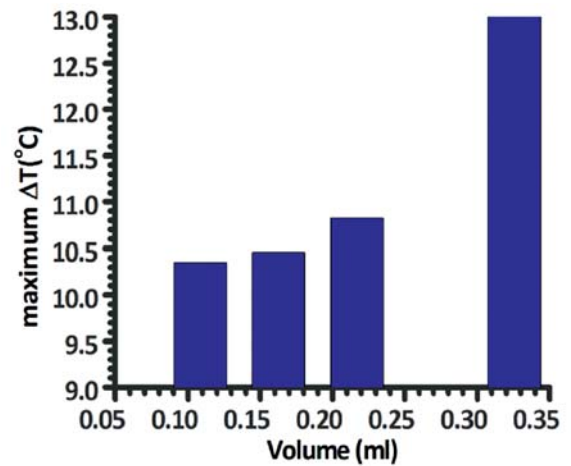
Fig. 6. The maximum thermal contrast as a function of the volume of the water present in the inspected structure.
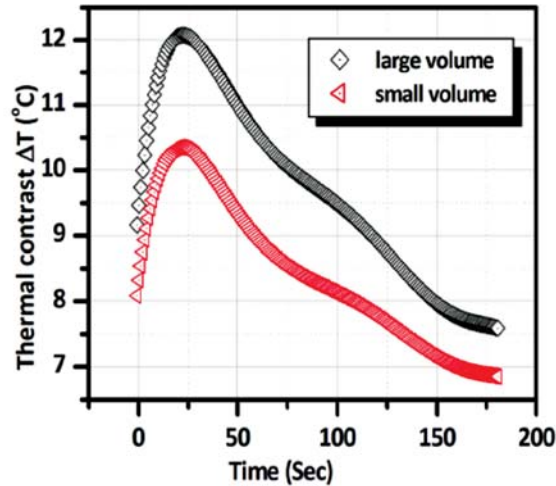
Fig. 7. The estimated thermal contrast as a function of different volume of the water.

Figure 6 shows the calculated thermal contrast as a function of the water. Figure 7 shows the thermal decay curves for the samples with different volume of the water content indicate that the maximum thermal contrast increases with increasing volume of the water content. It was found that water ingress equivalent to a volume not less than 2 drops (i.e. 0.03 ml) can be detected.

4. CONCLUSION

This work presents the results of infrared thermal imaging (IRT) based methodology for detecting and identifying water ingress through the delaminated regions of piezoelectric transducer. The measurement of the water ingress by infrared thermography assumes that high heat capacity region such as water appears cooler than its surrounding areas; hence, these regions can be easily monitored by means of an infrared camera. The developed method is based on the measurement and analysis of the thermal contracts of the IR thermal images of the rubber encapsulated hydrophones being inspected.

5. REFERENCES

[1] R.R. GOODMAN, H.P. BUCKER, I. DYER and J.A. SIMMEN, 2007. 'Monograph series in underwater transducers', *Springer Science + Business Media*, LLC.

[2] S. TOUZAIN, Q. LETHU and G. BONNET, 2005. *Prog. Org. Coat.*, **52** (4), 311-319.

[3] X.P. MALDAGUE, 2001. Theory and practice of infrared technology for nondestructive testing, in: K. Chang (Ed.), *Wiley Series in Microwave and Optical Engineering,* Wiley, New York, 684.

[4] H.S. CARSLOW and J.C. JAEGER, 'Conduction of heat in solids', 2nd Edition, Clerenden Press, Oxford .

[5] D. CHEN, Z. ZENG, N. TAI, C. ZHANG and Z. ZHANG, 2013. 'Liquid ingress recognition in honeycomb structure by pulsed thermography', *Eur. Phys. J. Phys.*

[6] C. IBARRA-CASTANEDO, D. GONZALEZ, M. KLEIN, M. PILLA,S. VELLERAND and X. MALDAGUE, 2004. 'Infra-red image processing and data analysis', *Infrared Physics and Technol,* **46,** 75-83.

A Morpho-Semantic Sound Description: "Semiotic Temporal Units"

Kaoutar El Ghali, Adil El Ghali and Charles Tijus
CHArt - Université Paris 8, Lutin Userlab, 39 avenue Corentin Cariou, 75019, Paris
e-mail: kaoutar.elghali@lutin-userlab.fr

ABSTRACT

Sound sample description often deals with sound source recognition. Synthetic sounds, noises, abstract sounds, that do not have an identifiable cause, can not be described in that context. We propose to elaborate a sound description that concentrates on the perceived sound morphology explaining the sound shape. Pierre Schaeffer was the first to propose a morphological description based on the evolution of the acoustical characteristics of sound over time on the basis of a reduced listening, ie an abstraction of sound origin or signification. Referring to Schaefferian theory, researchers and composers of the MIM (Laboratoire Musique et Informatique de Marseille) developed a method to analyze music in the form of a typology of 19 musical segments called the "Temporal Semiotic Units" (UST, from French, Unités Sémi-otiques Temporelles). These segments are sound figures carrying meaning through their morphological and kinetic structure. Our work consists in elaborating a sound description system based on the criteria identifying temporal semiotic units. In order to develop such a system, we need to choose an appropriate audio features and automatically index sound using this representation. Audio features numerically describe a specific property of an audio signal and are extracted by applying signal processing algorithms. Choosing discriminating and independent features is key to any efficient classification algorithm. Knowing that UST is a musicological model from electroacoustic music, choosing the right features implies understanding the exact meaning of this typology in terms of audio content. We analyze, in this paper, the definitions of the semantic criteria used to determine semiotic temporal units, and present a set of audio features matching those criteria.

1. INTRODUCTION

Research on audio description is often restricted the recognition of the sound source [1, 2], perceptual features [3], or music transcription [4]. We propose to investigate the existence of sonometric time figures [5] that allow us to characterize, identify and categorize a wide variety of sound events based the morphological and dynamic organization of a sound stream; the same way as geometric plane figures can characterize, identify and categorize a variety of delimited surfaces [6]. The work we are conducting aims to determine whether there are categories of sound events, summarized by a small number of sonometric figures that are hierarchically organized and defined by the morphological properties of the sound stream course; based on natural or taught procedures of segmentation, categorization of various sound events, formalization of sonometric figures and especially validation in terms of differentiation and composition of sonometric figures. Such considerations were pointed out by a diversity of composers and music theoreticians. The late 19th century marked a turn towards musical experience with the emergence of Gestalt psychology that focuses on perception as an identification of basic, characterized, complete figures. Ehrenfels [7] pointed that

transposing a melody does not change its melodic identity: the shape of melody is what matters in its perception. In his analysis of the 14th-century Italian madrigal, Schering [8] introduced the notion of melodic kernels that he defines as temporal figures baring an internal significance and acting as matrices of melodies. Becking [9] elaborated graphic curves to represent rhythmic invariants. Danckert [10] introduced the notion of primal symbols in melodic formation. In Schenker theory [11], composition is viewed as the elaboration of a basic contrapuntal design. Cooke [12] studied the idea of transposing linguistic theory into music analysis and claimed the existence of a finite musical vocabulary. Xenakis [13] proposed to substitute the traditional linear musical thought by an elementary analysis that treates sounds in the light of new characteristics such as density, order, and change. It was Pierre Schaeffer [14] that introduced a new vision of music centered on the sound material in a more tangible formulation.

On the basis of Schaeffer's work, the "Laboratoire Musique et Informatique de Marseille" created a morphosemantic typology of music segments called "SemioticTemporal Units" (UST, from French "Unités Sémiotiques Temporelles"). We propose to elaborate a sound description system based on this typology. In order to develop such a system, we need to choose an appropriate audio features and automatically index sound using this representation. Audio features numerically describe a specific property of an audio signal and are extracted by applying signal processing algorithms. Choosing discriminating and independent features is key to any efficient classification algorithm. Knowing that UST is a musicological model from electroacoustic music, choosing the right features implies understanding the exact meaning of this typology in terms of audio content. We present in this paper definitions of the different criteria used to determine temporal semiotic units, and audio features matching these criteria.

2. FRAMEWORK

2.1 Sound Objects

In Pierre Schaeffer's "Traité des Objets Musicaux" [9], typo-morphology, the initial two stages of the "program for a generalized solfeggio" (PROGREMU), focus on the immediate perception of sound that Schaeffer described by the means of the circuits of listening which are analyzed on the basis of two fundamental dualism of perceptive activities: "concrete/abstract" and "objective/subjective". Schaeffer proposes four listening functions to describe this circuit, namely the four French verbs: "ouïr", "entendre", "écouter" and "comprendre". "Écouter" is to index objects and events using sounds, ie taking sounds as representatives for sources or events. "Ouïr" refers to the passive listening experience as sounds strike the ear and is thus the lowest level of perception. "Entendre" represents the selection of sounds one can perceive showing an intention to listen. "Comprendre" designates the perception of sounds as communicative signs by referring to their meaning in a particular language or code. Schaeffer distinguishes two pairs of listening modes ordinary/ specialist and natural/cultural; and emphasizes that each mode, although specialized in a particular listening function, is always in relation with the 3 other functions.

Schaeffer preaches for a "relearning of the hearing" by defining a new listening intention that he refers to as "reduced listening". The concept of "reduced listening", in Schaefferian theory, consists in focusing on the sound itself and represents, in that, a breach with the natural and cultural listening that focuses on the source of sounds or the meaning they could bar rather than their inner perceptual properties. The correlate of that concept is the "sound object", that Michel Chion [10], in his synthesis of Schaeffer's work, defines as "any sound phenomena or event perceived as a coherent whole, and heard in a reduced listening that targets it for itself, independently from its origin or signification". The first task for sound object definition, typology, consists of isolating sound objects in all possible contexts (identification), and categorizing them into different types (classification). Schaeffer chooses three pairs of criteria to constitute this typology: a morphological pair, "Mass/Facture", a temporal pair, "Duration/Variation", and a structural pair, "Balance/Originality". A summary table of typology (TARTYP, table 1) summarizes the 29 types of sound objects discriminated by Schaeffer.

Two families of sound object types are distinguished: (i) balanced objects, found to be "a good compromise between the too structured and the too simple"; and (ii) unbalanced objects that could be either redundant (too regular and predictable) or excentric (too irregular and complex).

Table 1. Summary table for sound objects typology, TARTYP: TAbleau Récapitulatif de la TYPologie

		Disproportionate duration (macro-objects) of no temporal unity		measured duration temporal unity / reduced duration micro-objects			Disproportionate duration (macro-objects) of no temporal unity		
		unpredictable facture	non-existent facture	formed sustainment	impulse	formed iteration	non-existent facture		unpredictable facture
fixed mass	definite pitch	(En)	Hn	N	N'	N''	Zn		(An)
	complex pitch	(Ex)	Hx	X	X'	X''	Zx		(Ax)
not very variable mass		(Ey)	Tx Tn (special wefts)	Y	Y'	Y''	Zy (special pedals)		(Ay)
unpredictable variation of mass		E (general example)	T (general example)	W	φ	K	P (general example)		A (general example)

(Vertical labels: SAMPLES in left micro-object group; ACCUMULATIONS in right group. Row 4 spans: "— causal unity —" over E/T and "multiple but similar causes" over P/A.)

The second task for sound object definition, morphology, consists in describing the content of sound objects given a set of features. Schaeffer outlines 7 morphological features to perform this descriptive procedure: mass, harmonic timbre, grain, allure, melodic profile and mass profile. Mass generalizes the notion of pitch and describes the "pitch-space" surface. Harmonic timbre reflects the spectral distribution. Dynamic describes the dynamic evolution. Grain is the qualitative global perception of small irregularities in the sound's surface. Allure is the vibrato in the pitch, or the dynamic level. Melodic profile represents the trajectory of sound through the "pitch-space", ie the pitch variations. Finally mass profile characterizes the evolution of mass in time. Schaeffer classifies these features into matter criteria, shape criteria and variation criteria. This sound description scheme allows to describe any type of sound regardless to any information but the sound properties.

To sump up, Schaeffer's typo-morphology is consisted of two complementary and interdependent procedures that highlight a set of criteria to identify sound objects and describe them as a structure of these criteria. The following stages of PROGREMU are characterology, analysis and synthesis. Characterology consists in considering music, and sound in general, as a group of characteristic criteria linked in accordance to acoustic laws; this process aims to synthesize the musical. Analysis corresponds to the evaluation of the morphological criterion projection in the perceptual fields, ie defining discriminative positions for criteria in the perceptual fields. Synthesis, the final stage, aspires to create musical objects, based on rules drawn up from the results of the previous stages, that would be the basics of a "generalized solfeggio".

2.2 Semiotic Temporal Units

Referring to Schaeffer's concepts, artists and researchers of the "Laboratoire Musique et Informatique de Marseille" (MIM) elaborate a typology of 19 musical segments called the "Temporal Semiotic Units" [11] (UST, from French, Unités Sémiotiques Temporelles) based on empirical listening sessions. These segments are sound figures carrying meaning through their morphological and kinetic structure. A "UST" reflects the temporal evolution of a musical phenomena on a time scale ranging from a few seconds to a few minutes, indeed, it should be perceived as temporal process rather than a brief phenomena.

To determine a "UST", 4 morphological criteria are considered: duration, number of phases, reiteration and matter; as well as 2 kinetic criteria: velocity and acceleration, and 3 semantic criteria: direction, movement and energetic process. Duration expresses whether a "UST" is delimited in time (ie the begin and end are marked in time), or not (ie it consists in a pattern that can carry on in time). A phase is defined as the minimal sound segment clearly determinable, a "UST" can be composed of a unique phase, as well as multiple phases that can be delimited or not in time. Reiteration designates the varying repetition of a short sound figure dependent on regular temporal fulcra. Matter refers to sound functions related to timbre, grain, melodic profile and pitch distribution. Velocity characterizes the nature of the time course (from slow to fast) and acceleration indicates the nature of the variation in velocity (from negative to positive). Direction designates the predictable evolution of a variable or a coherent set of variables. Movement represents the perceived overall movement within a "UST" based on a set of morphological criteria. Energetic process is also based on a set of morphological criteria and describes the evolution of matter at a certain moment.

The 19 "UST" are: "Chute" (downfall), "Trajectoire inexorable" (inexorable trajectory), "Contracté-étendu" (contracted-extended), "Élan" (momentum), "Étirement" (streching), "En flottement" (floating), "Sans direction par divergence d'information" (without direction by divergence of information), "Lourdeur" (heaviness), "Freinage" (braking), "Obsessionnel" (obsessive), "Qui avance" (that moves forward), "Qui tourne" (that rotates), "Qui veut démarrer" (that wants to begin), "Sans direction par excès d'information" (without direction with excess of information), "Suspension-Interrogation" (suspensions-questioning), "En suspension" (in suspension), "Par vagues" (in waves), "Stationnaire" (steady), "Sur l'erre" (floating). The definitions of these "UST" are regrouped in sheets containing a morphological description and a semantic one, both qualitative and of a metaphoric nature.

Although the elaboration of a typology based on semantic criteria can be argued to be particularly related to the view of the group of persons conducting it, it is mainly related in this case to the concepts that are the basis of the methodology used. Moreover, studies on the perceptive pertinence of the "UST" show that the typology of "UST" is perceptively relevant [12], for musician and non-musician listeners, and demonstrate using an electrophysiological approach [13] that the temporal meaning of "UST" is indeed perceived by listeners.

3. AUDIO FEATURES FOR UST DESCRIPTION

The elaboration of a model for "UST" starts by selecting the discriminative audio features matching the different criteria used to determined a "UST". Due to the fact that some criteria used to determine a "UST" are subject to various interpretations and thus arduously definable, we choose to focus in the study of this paper on the semantic criteria, namely: movement, energetic process, and direction.

3.1 Energetic process

Energetic process describes the evolution of matter at a certain moment. It is for Marcel Frémiot [11] the essential and irreducible variable to describe an "UST". The energy in a "UST" can either be accumulated, converted, maintained, or retained. The energy of the signal x can be computed simply by taking the root average of the square of the amplitude, also called root-mean-square (RMS):

$$E = \frac{1}{N} \sum_{n=0}^{N-1} x^2(n) \tag{1}$$

The energetic process is represented as the short-time energy, ie the energy computed over successive 50%-overlaping frames of fixed length N:

$$E(n) = \frac{1}{N} \sum_{m0}^{N-1} x^2(m) \, w^2(n-m) \tag{2}$$

3.2 Movement

Movement is the perceived overall movement within a "UST", it can either express translation, or stillness by deformation or rotation. To model this criterion, we take interest in the signal spectral shape. A common

way to capture the spectral evolution is to consider the spectrum of each frame is considered as a distribution which frequencies are the values and normalized amplitudes the probabilities to observe the frequencies; and to compute its moments, ie spectral centroid, spectral spread, etc [14]. Based on the fact that a "UST" is a coherent spectral movement, we assume that the spectral shape would be best represented by considering the spectrum of each frame as a multivariate distribution and computing a similarity measure between each successive frames. We thus need to use multivariate distance measures suitable for spectral distributions that take on board the scale and the correlation between the distribution dimensions. The spectral distance measures used were:

– The spectral angle mapper is a spectral deterministic similarity measure defined as the angle between spectra considering them as vectors in a space with dimensionality equal to the number of bands.

$$SAM(X,Y) = arcos\left(\frac{\sum_{k=0}^{f_s/2} X(k)Y(k)}{\sum_{k=0}^{f_s/2} X(k) \sum_{k=0}^{f_s/2} Y(k)} \right) \tag{3}$$

– The symmetrical Kullback-Leiber distance is a measure of the difference between two distributions; it represents the information lost in the transformation, specifically, it is the expectation of the logarithmic difference between the two distributions.

$$KL(X,Y) = \frac{1}{2}\left(\sum_{k=0}^{f_s/2} X(k)\log\left(\frac{X(k)}{Y(k)}\right) + \sum_{k=0}^{f_s/2} Y(k)\log\left(\frac{Y(k)}{X(k)}\right) \right) \tag{4}$$

– The Kolmogorov-Smirnov distance is the maximal distance between the cumulated spectra. It compares areas under original distributions and therefore reflects spectral shape.

$$KS(X,Y) = \max_{k\ 0f,12}\left(\sum_{l=0}^{k} X(l) - Y(l) \right) \tag{5}$$

– The Mahalanobis distance is a measure based on correlations between variables defining different patterns. It accounts for the difference in variance in each dimension and the covariance between dimensions. Indeed, the multidimensional ellipsoid, that best represents the probability distribution, can be estimated through the covariance matrix of the samples. The Mahalanobis distance is simply the distance between two given points knowing their positions to the center of mass and the width of the ellipsoid, representing the distribution, in the direction of these points.

$$Mahal(X,Y) = \sqrt{\left((X-Y)^T \Sigma^{-1} (X-Y) \right)} \tag{6}$$

where Σ is the covariance matrix of the distribution.

4. EVALUATION

We dispose of 316 examples of "UST" from 3 main sources: excerpts of music pieces, sung examples, and melodies performed on piano ; all sounds proceed from the MIM works. The audio files are sampled at a rate of 44.1 kHz and have durations ranging from 0.771 s to 93.0481 s. We evaluate the proposed audio features by performing automatic classification of the semantic criteria using support machine vectors with a Gaussian kernel based on the features described above. Results are represented in tables 2 to 4.

We observe, in the results of the classification for the criterion "energetic process" (table III), that the classifier performs better for the class "converted energy" than the other classes. The short-time energy ought be combined to features representing spectral content. The classification results for the criterion "movement" (table IV) shows that the 4 spectral similarity measures perform roughly the same over the different categories

Table 2. Results of the classification for the criterion "Energetic Process".

	Precision	Recall	F1 Score
Accumulated energy	0.95	0.333952	0.478118
Converted energy	0.995	0.486236	0.636361
Maintained energy	0.986	0.279487	0.425812
Retained energy	0.324895	0.872424	0.472563

Table 3. Results of the classification for the criterion "Energetic Process".

	Spectral Angle Mapper	Kullback Leiber	Kolmogorov Smirnov	Mahalanobis
Translation	0.549982	0.567632	0.558369	0.656702
Stillness by deformation	0.600383	0.615273	0.599315	0.606586
Stillness by rotation	0.546774	0.49957	0.445528	0.692254

Table 4. Results of the classification for the criterion "Direction".

	Precision	Recall	F1 Score
With direction	0.5609	0.3702	0.446
Without direction	0.3759	0.4828	0.4127

with a preference for the Mahalanobis distance whose results present the smallest variance over the categories. The results of the classification for "direction" (table V) demonstrate that the sole loudness is insufficient to properly model this criterion; this could be explained by numerous variations in instantaneous loudness and can be improved by performing a polynomial approximation of the computed loudness.

5. CONCLUSION

In this exploratory work, we proposed a morpho-semantic approach for sound sample description based on the theory of semiotic temporal units. We tried to build a computational model describing the semantics of sound samples.

The main idea behind our approach is to establish a link between the audio descriptors and the UST. The audio features presented in this paper demonstrate promising performances for semantic criteria; that would be improve by combining the described features here to other "morphological" ones. Future works will include this improvement as well as models for the morphological and kinetic criteria.

6. REFERENCES

[1]   A. ERONEN, 2001. "Comparison of features for musical instrument recognition," *In Proc. IEEE Workshop on Applications of Signal Processing to Audio and Acoustics*.

[2]   K. MARTIN, 1999. "Sound source recognition: a theory and computational model", Ph.D. Thesis, MIT.

[3]   S. MCADAMS, S. WINSBERG, S. DONNADIEU, G. DE SOETE and J. KRIMPHOFF, 1995. "Perceptual scaling of synthesized musical timbres: common dimensions, specifities, and latent subject classes," *In: Psychological Research*, **58**, 177-192.

[4]   A. T. CEMGIL, H. J. KAPPEN and D. BARBER, 2006. "A generative model for music transcription," In: *IEEE Transactions on Speech and Audio Processing*, **14** (2), 679-694.

[5]   C. TIJUS, S. POITRENAUD, C. BELLISSENS, J. HENI and M. FRÉMIOT, 2004. "La spatialisation du temps musical : les Unités Sémiotiques Temporelles. In: Actes des 11èmes Journées CNRS de Ro-

chebrune : Rencontres Interdisciplinaires sur les systèmes complexes naturels et artificiels, "Le temps dans les systèmes complexes," S001, *École Nationale Supérieure des Télécommunications, Paris, France*. 341-351.

[6]   C. TIJUS and F. CORDIER, 2003. "Psychologie de la connaissance des objets: Catégories et propriétés, tâches et domaines d'investigation. *In: L'année psychologique, Éditions NecPlus, Vineuil, France.*" 103, 223-256.

[7]   C. VON EHRENFELS and U. GESTALTQUALITÄTEN, 1890. Vierteljahrsschrift für wissenschaftliche Philosophie 14.

[8]   A. SCHERING, 1911. Musikalische Bildung und Erziehung zum musikalischen Ho?ren.

[9]   G. BECKING, 1928. Der Musikalische Rhythmus als Erkenntnisquelle (Musical rhythm as a source of insight). *Benno Filser*, Augsberg, Germany.

[10] W. DANCKERT, 1931. Personale Typen des Melodiestils.

[11] H. SCHENKER, 1935. Der freie Satz. Neue Musikalische Theorien und Phantasien. Part 3. *Universal Edition*, Vienna, Austria.

[12] D. COOKE, 1963. The Language of Music, *Oxford University Press*, Oxford, United Kingdom (1959)

[13] Y. XENAKIS, Musiques formelles.

[14] P. SCHAEFFER, 1966. Traité des objets musicaux. *Éditions du Seuil*, Paris, France.

[15] M. CHION, 1983. Guide des objets sonores : *Pierre Schaeffer et la recherche musicale*. Bu-chet/Chastel, Paris, France.

[16] F. DELALANDE, M. FORMOSA, M. FRÉMIOT, P. GOBIN, P. MALBOSC, J. MANDELBROJT and E. PEDLER, 1996. Les unités sémiotiques temporelles, éléments nouveaux d'analyse musicale. *Laboratoire Musique et Informatique de Marseille*, Marseille, France.

[17] A. FREY, A. DAQUET, S. POITRENAUD, C. TIJUS, M. FRÉMIOT, M. FORMOSA, L. PROD'HOMME, J. MANDELBROJT, M. TIMSIT-BERTHIER, P. BOOTZ, X. HAUTBOIS and M. BESSON, 2009. "Pertinence cog-nitive des Unités Sémiotiques Temporelles," In: Musicæ Scientiæ, European Society for the Cognitive Sciences of Music, *Hannover*, Germany. **13** (2), 415-440.

[18] A. FREY, C. MARIE, L. PROD'HOMME, M. TIMSIT-BERTHIER, D. SCHÖN and M. BESSON, 2009. "Temporal Semiotic Units as Minimal Meaningful Units in Music? An Electrophysiological Approach," In Music Perception: *An interdisciplinary Journal, University of California Press*, Berkeley, CA, USA. **26** (3), 247-256.

[19] G. PEETERS, 2004. A large set of audio features for sound description (similarity and classification) in the CUIDADO project. Technical Report, *IRCAM*.

[20] S. S. STEVENS, 1956. "The direct estimation of the sensory magnitudes: loudness," In: The American *Journal of Psychology,* University of Illinois Press, Champaign, IL, USA. 69(1), 1-25.

[21] E. ZWICKER, G. FLOTTORP and S. S. STEVENS, 1957. "Critical band width in loudness summation," In: *Journal of the Acoustical Society of America*, Acoustical Society of America, Melville, NY, USA. **29** (5), 548-557.

Categorization of Tabla Strokes by Wavelet Analysis

Anirban Patranabis, Ranjan Sengupta, Kaushik Banerjee,
Tarit Guhathakurta and Dipak Ghosh
Sir C V Raman Centre for Physics and Music, Jadavpur University, Kolkata 700032,
e-mail: anir.thikana@gmail.com

ABSTRACT

Tabla is one of the most important percussion instruments in India popularly used for keeping rhythm. This percussion instrument consists of two drums played by two hands, structurally different and produces different harmonic sounds. Tabla strokes are commonly called as `bol', constitutes a series of syllables. Our main objective is to categorize these strokes and the tablas. Earlier work has done labeling tabla strokes from real time performances by testing neural networks and tree based classification methods. The current work extends previous work by C. V. Raman and S. Kumar in 1920 on spectrum modeling of tabla strokes. In this paper we have studied the timbre (spectral brightness, tristimulus, odd and even parameters, spectral irregularity and spectral centroid) and spectral characteristics (wavelet analysis by sub band coding method and using tollence wavelet tool) of nine strokes from each of five tablas using Wavelet transform. Wavelet analysis is now a common tool for analyzing localized variations of power within a time series and to find the frequency distribution in time-frequency space. Distribution of dominant frequencies at different sub-band of stroke signals, distribution of power and behavior of harmonics are the important features, leads to categorization of strokes and also the structure of tabla. This method also helps in synthesizing different new strokes.

1. INTRODUCTION

The ubiquity of tabla in the Indian Subcontinent is without dispute. Its variety of tonal colors gives it a flexibility seldom matched by other percussion instruments. Among the percussion instruments, tablas plays

[1]Parag chordia, "*Segmentation and recognition of tabla strokes*", CCRMA, Stanford university, Pchordia@ccrma.stanford.edu

[2]C V Raman, 1934. "*The Indian Musical Drums*", *Proc. Indian Acad. Sc.*, **1A**, 179-188.

[3]C V Raman and Sivakali Kumar "*Musical drums with harmonic overtones*", *Nature*, 104, (1920) 500.

[4]David Courtney "*Psychoacoustics of the Musical pitch of Tabla*" *Journal of SanGeet Research Academy, Calcutta, India,* **13**, (1999) 1.

[5]R N Ghosh, 1922. "*Note on Musical Drums*", Phys. Review, **20**, 526-527.

[6]K N Rao, 1938. "*Theory of the Indian Musical Drums*", *Proc. Indian Acad. Sci.* **7A**, 75-84.

[7]B S Ramakrishna, 1957. "*Modes of Vibration of the Indian Drum Dugga or left hand Thabala*", *J. Acoust. Soc. Am.* **29**, 234-238.

[8]T Sarojini and A Rahman, 1958. "*Variational Method for the Vibrations of Indian Drums*" *J. Acoust. Soc. Am.* **30**, 191-196.

[9]B M Banerjee and D Nag, 1991. "*The Acoustical Character of Sounds from Indian Twin Drums*", *ACUSTICA*, **75**, 206-208.

[10]C. Valens, 1999-2004. *"A Really Friendly Guide to Wavelets (C)"*, wavelets@polyvalens.com

[11]Robi Polikar, *"The Wavelet Tutorial"*, *Rowan University*, http://users.rowan.edu/polikar/wavelets/wtutorial.html

[12]N. Fletcher and T. Rossing, 1998. *"The physics of musical instruments"*, *Springer, New York.*

[13]Tae Hong Park, 2004. *"Towards Automatic Musical Instrument Timbre Recognition"*, *PhD thesis, Department of Music, Princeton University.*

[14]J.M. Grey, 1977 *"Multidimensional Perceptual Scaling of Musical Timbre"*, *Journal of the Acoustical Society of America* **61**, 1270-1277.

[15]Anirban Patranabis, Kaushik Banerjee, Ranjan Sengupta and Dipak Ghosh, 2011. *'Objective Analysis of the Timbral quality of Sitars having Structural change over Time'*, *Ninaad (Journal of ITC Sangeet Research Academy)*, **25**, 1-7.

[16]Christopher Torrence and Gilbert P. Compo. *"A Practical Guide to Wavelet Analysis"*, *University of Colorado, Boulder, Colorado.*

an important role in accompanying vocalists, instrumentalists and dancers in every style of music from classical to light in India. Tabla is comprised of a pair of drums, a treble drum, referred to as the tabla or *dayan*, and the bass drum called the *bayan*. The *bayan* is made of copper, brass, iron or terracotta (clay). The right-hand dayan is a tapering cylinder carved from a block of dense wood. Each of the drums is covered with goatskin. Undoubtedly the most striking characteristic of the *tabla* is the large black spot on each of the playing surfaces called the *syahi*. These black spots are a mixture of gum, soot, and iron filings. This is applied to the center of the *dayan*, and off-center on the *bayan*. Their function is to create the bell-like timbre that is characteristic of the instrument. The complexity of its construction accounts for its versatility. This complexity reaches such a degree that only trained craftsmen can create a tabla. When a membrane stretched over a resonating body is struck, there is generally no clear sense of pitch because the sound produced is rich in inharmonic overtones. In Parag Chordia's paper[1] he described a system that segments and labels tabla strokes from real performances. The work was done with large and diverse database includes the methodology of testing neural networks and tree based classification methods. Tabla strokes are typically inharmonic in nature but strongly pitched resonant strokes[2]. The sounds of most drums are characterized by strongly inharmonic spectra; however tablas, especially the dayan are an exception. This was pointed out as early as 1920 by C. V. Raman and S. Kumar[3] . Raman further refined the study in a later paper[2]. The classical model put forth by Raman represents the sound of tabla-dayan, as having a spectrum consisting of five harmonics; these are the fundamental with its four overtones[4]. Thereafter several theoretical and experimental studies were held on the dynamics of the instrument [5, 6, 7, 8, 9,4]. In this paper we studied the harmonic analysis and distribution of power within the time series of tabla strokes.

The two drums of the tabla produce many different timbres. Many of these sounds have been named, forming a vocabulary of timbres. The naming of strokes has facilitated the development and transmission of a sophisticated solo repertoire. In addition to the rhythmic complexity of tabla music, it is its timbral beauty and diversity that distinguish it from other percussion instruments[1]. In this paper we have considered five different tablas and nine single strokes from each table. Stroke 'Ta/Na' executes by lightly pressing the ring finger down in order to mute the sound while index finger strikes the edge. Stroke 'Ti' executes by striking the dayan on the 2nd circle with the index finger and by keeping the finger on that position causes more damping but after striking if the index finger release quickly to give an open tone it produces 'Teen'. Stroke 'Ghe' executes by striking the bayan with middle and index finger keeping the wrist on the membrane but after striking if released quickly it produces 'Ge'. Stroke 'Thun' executes by striking on the centre circle of dayan with index, middle, ring and little fingers together and by quickly releasing. Stroke 'Tu' executes by striking at the corner of centre circle of dayan with index finger only and immediately after striking finger will lift. Stroke 'Te' executes by striking the dayan with middle and ring finger at the centre of the circle. Stroke 'Re' executes by striking the dayan with index finger at the centre of the circle and by keeping the finger on that position causes more damping.

2. EXPERIMENTAL SETUP

All the strokes were played by eminent tabla players and the sound was recorded in a noise free acoustic room. Membrane of tabla 1, 2 and 3 have diameter 5", tabla 4 has a diameter 5.5" and tabla 5 has a diameter 6". Each of these sound signals was digitized with sample rate of 44.1 kHz, 16 bit resolution and in a mono channel. We then undertook iterated filter bank by sub-band coding for analyzing localized variations of amplitude within a time series and to find the frequency distribution in time-frequency space. We also used Torrence wavelet tool to observe distribution of power and behavior of harmonics. Timbre analysis was done by Long Term Average spectra (LTAS) of each signals.

3. WAVELET ANALYSIS

The whole purpose of wavelet analysis is to see the time-scale (frequency) distribution, i.e. how the power changes over time and to find the frequency distribution in time-frequency space. The idea behind these time-frequency joint representations is to cut the signal of interest into several parts and then analyze the parts separately. It is clear that analyzing a signal this way will give more information about the when and

where of different frequency components present[10] . The continuous wavelet transform or CWT. is written as:

$$\gamma(s,\tau) = \int f(t)\psi^*_{s,\tau}(t)dt$$

Where * denotes complex conjugation. This equation shows how a function f (t) is decomposed into a set of basic functions ψ_s, T (t) , called the wavelets. The variables s and τ are scale and translation, are the new dimensions after the wavelet transform. If we expand the wavelet transform into the Taylor series at $t = 0$ until order n (let = 0 for simplicity) we get :

$$\gamma(s,o) = \frac{1}{\sqrt{s}}\left[f(o)M_0 s + \frac{f^{(1)}(o)}{1!}M_1 s^2 + \frac{f^{(2)}(o)}{1!}M_2 s^3 ... + \frac{f^{(n)}(o)}{1!}M_n s^{n+1} + O(s^{n+2}) \right]$$

From the admissibility condition we already have that the 0th moment $M_0 = 0$ so that the first term in the right-hand side of the above equation is zero. If we now manage to make the other moments up to M_n zero as well, then the wavelet transform coefficients (s) will decay as fast as s^{n+2} for a smooth signal $f(t)$. This is known as the vanishing moments or approximation order. If a wavelet has N vanishing moments, then the approximation order of the wavelet transform is also N. The moments do not have to be exactly zero; a small value is often good enough. In fact, experimental research suggests that the number of vanishing moments required depends heavily on the application. Summarizing, the admissibility condition gave us the wave, regularity and vanishing moments gave us the fast decay, and put together they give us the wavelet[10].

The most important properties of wavelets are the admissibility and the regularity conditions and these are the properties which gave wavelets their name. It can be shown that square integral functions ψ (t) satisfying the admissibility condition,

$$\int \frac{|\psi(w)|^2}{|w|} dw < +\infty$$

This can be used to first analyze and then reconstruct a signal without loss of information. In ψ (ω) stands for the Fourier transform of ψ (t). The admissibility condition implies that the Fourier transform of ψ (t) vanishes at the zero frequency, i.e.

$$|\psi(w)|^2\big|_{w=0} = 0$$

This means that wavelets must have a band-pass like spectrum[10]. This is a very important observation, which we have used to build an efficient wavelet transform. Each signal is passed through a series of high pass filters to analyze the high frequencies, and it is passed through a series of low pass filters to analyze the low frequencies. A time compression of the wavelet by a factor of 2 will stretch the frequency spectrum of the wavelet by a factor of 2 and also shift all frequency components up by a factor of 2.

4. THE SUB-BAND CODING AND THE MULTI-RESOLUTION ANALYSIS

Here we split/filtered each of the signal spectrums in two (equal) parts, a low-pass and a high-pass part. Transition band width is kept minimum to 50 Hz and the offset information is negligible thus causing no artifact in the split signal. The first high-pass part contains no information. We now have two bands. However, the low-pass part still contains some details and therefore we split it again and again, until the last low-pass part contain no information. In this way we have created an iterated filter bank. This is done by sub-band coding/pyramidal coding algorithm using Nyquist's rule[11]. The Nyquist theorem states that perfect reconstruction of a signal is possible when the sampling frequency is greater than twice the maximum frequency of the signal being sampled or equivalently, when the Nyquist frequency (half the sample rate) exceeds the highest frequency of the signal being sampled. Why did we split the signal into several frequency bands? Energy of the signal varies with time. In this process a certain high frequency component can be located well in time while a low frequency component can be located better in frequency. In this process of

sub band coding each of the signals are divided into eight frequency sub bands of band width 7040 to 14080 rad/sec referred as 1st band or DWT 1st level, 3520 to 7040 rad/sec referred as 2nd band or DWT 2nd level, 1760 to 3520 rad/sec referred as 3rd band or DWT 3rd level, 880 to 1760 rad/sec referred as 4th band or DWT 4th level, 440 to 880 rad/sec referred as 5th band or DWT 5th level, 220 to 440 rad/sec referred as 6th band or DWT 6th level, 110 to 220 rad/sec referred as 7th band or DWT 7th level and less than 110 rad/sec referred as 8th band or DWT 8th level. From each of these sub bands number of harmonics, number of DWT coefficients and most prominent frequency (MPF) is measured. Fidelity factor Q^{11} here is ½. By this process the scale of each signal gets doubled, reducing the uncertainty in the frequency by half.

5. OBSERVATION

DWT 1st level (7040 to 14080 rad/sec), 2nd level (3520 to 7040 rad/sec) and DWT 8th level (55 to 110 rad/sec) reveals no information. All information lies within 3rd to 7th level of DWT. So Tabla sounds are harmonically best within the range of 0.1 kHz to 3 kHz. One of the most prominent features from spectral analysis has to do with the behavior of harmonics and indeed the knowledge of locations of harmonics. We can see that the harmonic number increases towards mid frequency range and an expansion of the harmonic locations can be observed in band 3. It is also possible to take into account the contraction (harmonic ratio<1) or expansion (harmonic ratio>1) of harmonics in all the spectrums. In band 5 ratio of 4th harmonic to 5th harmonic for all the strokes are less than 1, means spectral energy reduces at higher frequencies in that band. Mid frequency range dominates in band 5 while lower frequency ranges are dominating in band 6. According to Grey14, on the distribution of the harmonics, it has been suggested that no harmonics higher than the 5th to 7th, regardless of the fundamental frequency, are resolved individually. Studies have shown that the upper harmonics rather than being perceived independently are heard as a group.
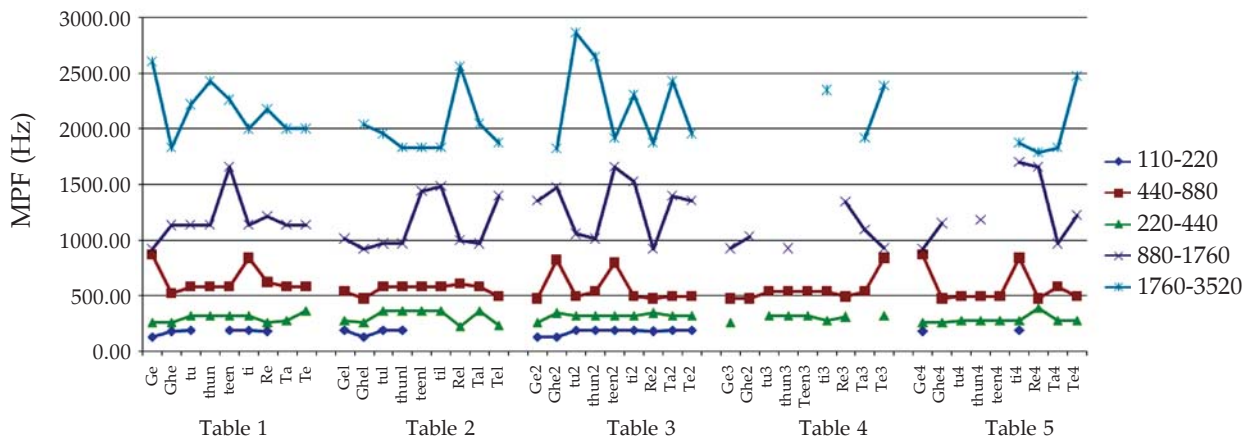

Fig. 1. Most prominent frequency (rad/sec) at different sub-bands

Fig. 1 reveals that the MPF corresponds to the highest peak of each sub-band, is uniform during the lower frequencies up to 900Hz, but varies in high frequency bands. At low frequency all tablas sounds same. Maximum harmonic information lies in the range 0.9 - 2.5 kHz. Although Tee and Teen, Ghe and Ge are similar strokes, a larger difference in MPF occurs for all the first three tablas. Such difference is due to the damping effect among the pair of strokes and is visible in 440 to 1760 Hz. But 4th and 5th tablas give a little information during these ranges. Such differences give rise to the fact that the production of harmonics is different for all tablas due to difference in their structure *i.e.* the resonant chamber.

Stroke Ta/Na (where the position of stroke and damping are different) of all tablas shows that the attack peak reaches very late compared to all other strokes. Attack peak of all strokes of 1st tabla delays to reach (found in the 6th of its band structure). Attack peak of all strokes of 2nd tabla immediately reaches (found in the 7th of its band structure). So the players of 1st and 2nd tablas made all the strokes consistently. No such

consistency is found in achieving attack peak for the rest of the three tablas because of their difference in stroke production. So the feature attack peak is an important cue to assess the learners about the accuracy of stroke both in terms of stroke intensity and also position. Attack peak also depend upon the stroke type and position viz. stroke Thun executes by striking on the centre circle with index, middle, ring and little fingers together and by quickly releasing, reaches the attack peak immediately while stroke Ta/Na executes by lightly pressing the ring finger down in order to mute the sound while index finger strikes the edge, reaches the attack peak delayed. It is also found that attack peak reaches faster in free strokes than damped strokes.

When a membrane stretched over a resonating body is struck, there is generally no clear sense of pitch because the sound produced is rich in inharmonic overtones. When properly applied, the syahi (outside the central part) causes the alignment of some of the inharmonic partials, giving the dayan a clear sense of pitch if struck correctly .

Also it is observed a shorter decay for Re, Te, Tu and Na while longer decay for Ghe, Ge, Tee and Teen. MPF of damped strokes show lesser time of occurrence compared to free strokes. Calculating the scale (frequency) and time of all the harmonics, it is observed that lower harmonics in the attack portion are always lagging. It is also observed that the higher energy bands are of shorter duration than the lower energy bands. In comparison to other strokes, Teen has longer duration of energy in all the bands. This proves that tabla produces different sounds with definite harmonic properties with the variation of stroke production and position.
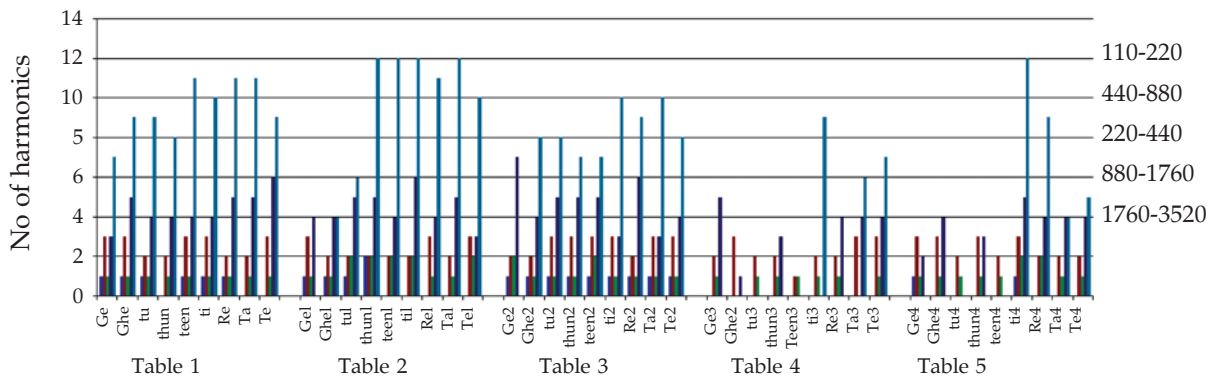

Fig. 2. Number of harmonics at different sub-bands

From fig. 2, Damped strokes have larger number of harmonics at high frequency ranges (band 3 and 4) for all the tablas compared to free strokes. Comparing the number of harmonics at higher frequency range we can categorize the stroke of tablas. For the 1st, 2nd and 3rd tablas (all are smaller in size), all strokes produce harmonics uniformly and equally in bands 5 and 6 but at higher frequency bands they show larger number of harmonics. For the 1st, 2nd and 3rd tabla, harmonics are present within band 3 to band 6. 4th and 5th Tabla (both are bigger in size) produces very less number of harmonics for the free strokes and they are found within band 4 and band 6 but the damped strokes produces harmonics within band 3 and band 6. So it is observed that tablas with smaller diameter produce more harmonics than tablas of larger diameter.

Again table 1 shows the standard deviation and average frequency of harmonics. It is observed that at low frequency range both the standard deviation and average frequency remains same but at higher frequency bands these values get scattered. This confirms that the randomness of energy of the partial increases at higher frequency bands. Hence uniqueness of table sound lies in the higher energy. From the data it is observed that 4th table is totally different compared to others. Such thing occurs due to differences in structure of the tabla as well as the intensity of strokes made by the player.

6. TIMBRE ANALYSIS

Timbre is defined in ASA (1960) as that quality which distinguishes two sounds with the same pitch, loudness and duration. This definition defines what timbre is not, not what timbre is. Timbre is generally assumed to

Table 1. Standard deviation and mean of tabla strokes at different sub-bands

	110-220		220-440		440-880		880-1760		1760-3520	
	Stdev	Mean	Stdev	Mean	Stdev	Mean	Stdev	Mean	Stdev	Mean
Tabla 1	24.341	178.732	36.927	302.998	124.346	640.864	195.905	1181.595	242.300	2170.102
Tabla 2	31.433	178.149	61.536	315.576	45.133	558.249	236.912	1130.017	245.908	1996.191
Tabla 3	27.200	178.310	23.820	321.220	139.530	565.568	253.916	1307.372	393.874	2228.098
Tabla 4			24.889	306.703	111.122	552.938	165.671	1043.175	261.962	2217.92
Tabla 5			40.109	288.843	159.109	580.582	309.175	1258.977	324.960	1991.757

be multidimensional, where some of the dimensions have to do with the spectral envelope, the time envelope, etc.[13, 14]. Many timbre parameters have been proposed to encompass the timbre dimensions. Among all timbre parameters important parameters are irregularity, tristimulus1 (T1), tristimulus 2 (T2), tristimulus 3 (T3), odd and even parameters, spectral centroid and brightness .

All the sound samples are normalized to 0 dB and of same length. From the LTAS of each signal above mentioned timbre features were measured of which some are harmonic and some perceptual features.

Correlation coefficient of the timbre parameters are shown in table 2. It is observed that tristimulus 2 (T2) and tristimulus 3 (T3) are highly correlated while tristimulus 1 (T1) is weakly correlated with T2 (corresponds to 2nd, 3rd and 4th harmonics) and T3 (corresponds to higher harmonics). This concludes the fact

Table 2. Correlation coefficients of various timbre parameters

	brightness	T1	T2	T3	odd	Even	irregularity	centroid
brightness	1	-0.1634	-0.6958	0.7314	0.2169	-0.1544	-0.5954	0.8293
T1		1	-0.2661	0.1582	-0.1359	-0.2269	-0.1771	0.0218
T2			1	-0.9939	-0.1634	0.2567	0.8948	-0.8412
T3				1	0.1830	-0.2370	-0.8964	0.8592
Odd					1	-0.9341	-0.4308	0.2121
Even						1	0.4873	-0.2164
irregularity							1	-0.7318
Centroid								1

that fundamental (corresponds to T1) of tabla stroke is weak compared to its harmonics. Also mid and higher frequency partials behave similarly. Odd and even harmonics are equally proportionate and are highly correlated and so tabla strokes are harmonically good to hear. T2 and T3 both have high correlation with spectral irregularity and spectral centroid. This concludes the fact that high frequency partials have higher order of irregularity among partials. Also brightness (i.e. centre of gravity of amplitude) and spectral centroid (i.e. centre of gravity of frequency) are highly correlated. It is also observed that stroke 'ta' and 'tu' have low brightness hence energy for all tablas. Since both strokes executes by striking index finger at the edge and such process of stroke cause weak resonance in the cavity of tabla. Comparing all strokes it is observed that irregularity among partials are higher for tabla 3 and 4 compared to other tablas.

Stroke 'Ge' of tabla 1 is different from others viz. brightness and centroid both are low and stronger 2nd, 3rd and 4th harmonics and low irregularity. Other tablas show uniformity in timbre for the stroke 'Ge'. Strokes 'Ghe', 'tu','teen' and 'ta' of tabla 3 and 4 are different from others viz. brightness and centroid are too low and stronger 2nd, 3rd and 4th harmonics and higher irregularity, while other three tablas show uniformity and all these four strokes are free stroke. For stroke 'thun', tabla 3 and 4 differ from other tablas only in brightness i.e. its CG of amplitude. Stroke 'ti' of tabla 3 is different from others viz. brightness and centroid both are low, stronger 2nd, 3rd and 4th harmonics and higher irregularity. For strokes 're' and 'te', tabla 3 and 4 differs from other tablas only in irregularity, in which both the strokes are made at the centre circle and both are damped strokes. Damped strokes have higher brightness and spectral centroid than the free strokes. So this

concludes the fact that style (nature and intensity) of strokes of player of 1st tabla is different than others. Also style of strokes is similar for the players of tabla 3 and 4. So the timbral quality of tabla strokes varies with position of the strokes and style of the stroke. Such timbral diversity makes this instrument so popular in Indian music.

Table 3. Power in dB^2, period in ms and time of occurrence in ms obtained from Torrence wavelet tool.

Stroke	Power (dB2) for thick contour of wavelet spectrum with 95% confidence level	Period (millisec)	Time (millisec)
Ge	2.5-23	8-16	8-40
	0-2.5	24-32	80-120
Ghe	0.82-17	8-16	40-80
Re	0-3	8-12	20-160
	3-32	12-48	80-160
Ta	1.3-25	8-32	100-200
Te	0-2.6	8-16	100-200
	0-2.6	32-64	80-160
	2.6-28	16-32	45-180
Teen	0.35-9.2	8-32	120-160
Thun	0.15-12	8-32	80-120
Ti	0-1.2	8-16	80-200
	1.2-31	16-32	80-160
Tu	0.095-17	8-24	320-480
Ge2	0.0077-7.3	8-24	20-80
Ghe2	0.094-16	8-24	20-80
Re2	0.13-45	8-48	60-160
Ta2	0.028-19	8-24	80-160
Te2	0.12-36	8-48	80-180
Teen2	0.059-22	8-32	40-160
Thun2	0.0058-8.4	8-16	20-160
Ti2	0.084-24	8-32	40-160
Tu2	0.0044-6.1	8-32	60-120
Ge3	0.17-38	8-48	20-160
Ghe3	0.038-29	8-24	20-200
Re3	0.048-18	8-48	40-160
Ta3	0.042-31	8-32	20-160
Te3	0.026-30	8-32	20-160
Teen3	0.0092-14	8-24	40-160
Thun3	0.097-29	8-32	40-160
Ti3	0.092-46	8-32	20-160
Tu3	0.053-30	8-24	20-160
Ge4	0.051-23	8-16	8-60
Ghe4	0.038-29	8-24	40-160
Re4	0.093-29	8-16	20-160
Ta4	0.021-12	8-16	80-120
Te4	0.031-19	8-24	80-160
Teen4	0.0058-9.1	8-16	40-120
Thun4	0.0073-7.8	8-16	40-80
Ti4	0.31-43	8-24	20-160
Tu4	0.0074-6.7	8-24	40-100
Ge5	0.12-22	8-24	20-100

Ghe5	0.0075-5.2	8-16	40-60
Re5	0.037-25	8-16	20-160
Ta5	0.0096-11	8-24	100-120
Te5	0.013-14	8-24	120-160
Teen5	1.3-86	8-24	0-40
Thun5	3.6-70	8-16	0-40
	0-3.6	8-16	40-60
Ti5	0.073-20	8-32	40-160
Tu5	1.4-39	8-16	8-40

7. SPECTRAL ENVELOPE

By decomposing a time series into time-frequency space, one is able to determine both the dominant modes of variability and how those modes vary in time. The spectral envelope, which embodies a wealth of information, is really a "zoomed-out" view of the power spectrum. What determines the shape of the envelope is basically the location of dominant peaks on the periodic scale[16] . For the Morlet, which has several smooth oscillations, the period is a well-defined quantity which measures the approximate Fourier period of the signal. With the help of Torrence wavelet tool we can locate the individual locations of high power. We also made contour plot using the Morlet wavelet of the wavelet power spectrum with white spectrum (with a flat Fourier spectrum) and colored spectrum (increasing power with decreasing frequency). By this we can know the time intervals in which certain band of frequencies exist. It involves a transform from a one-dimensional time series (or frequency spectrum) to a diffuse two-dimensional time-frequency image with statistical significance tests. Wavelet spectra of two tabla strokes ge and re only are shown in figure 3 here but power, period and time of occurrence for all strokes for all tablas are shown in table 3 and their confidence level were measured.
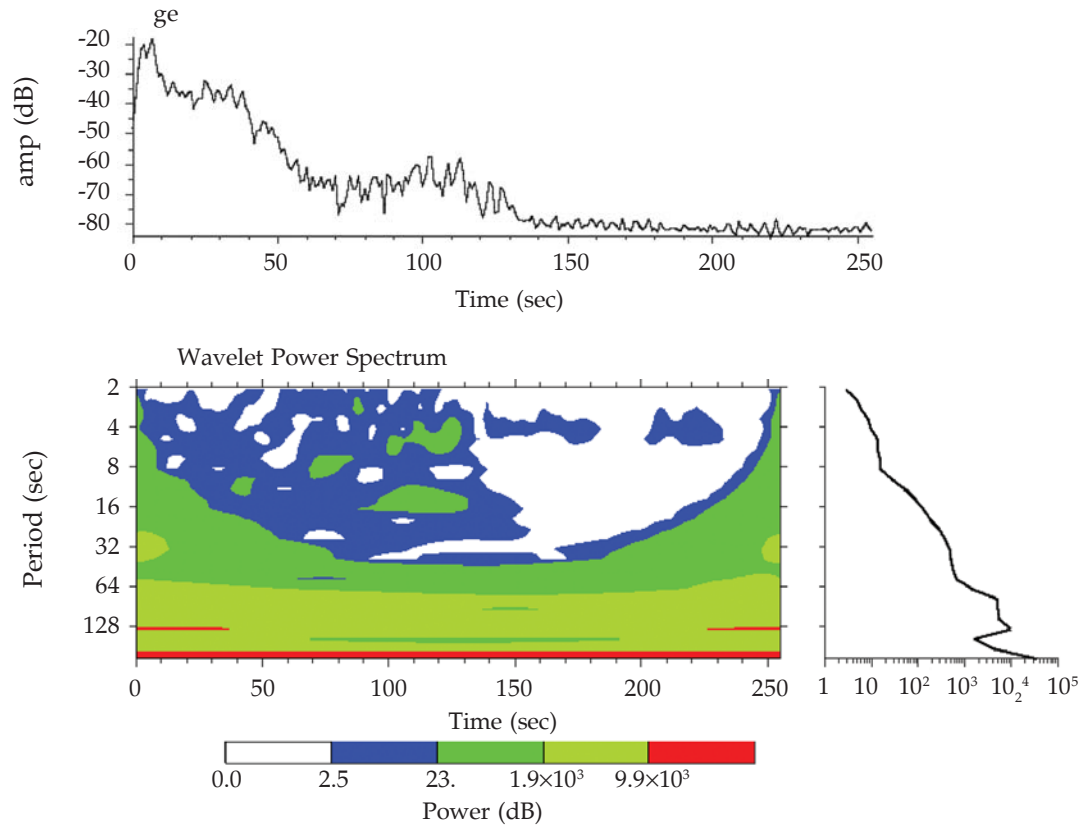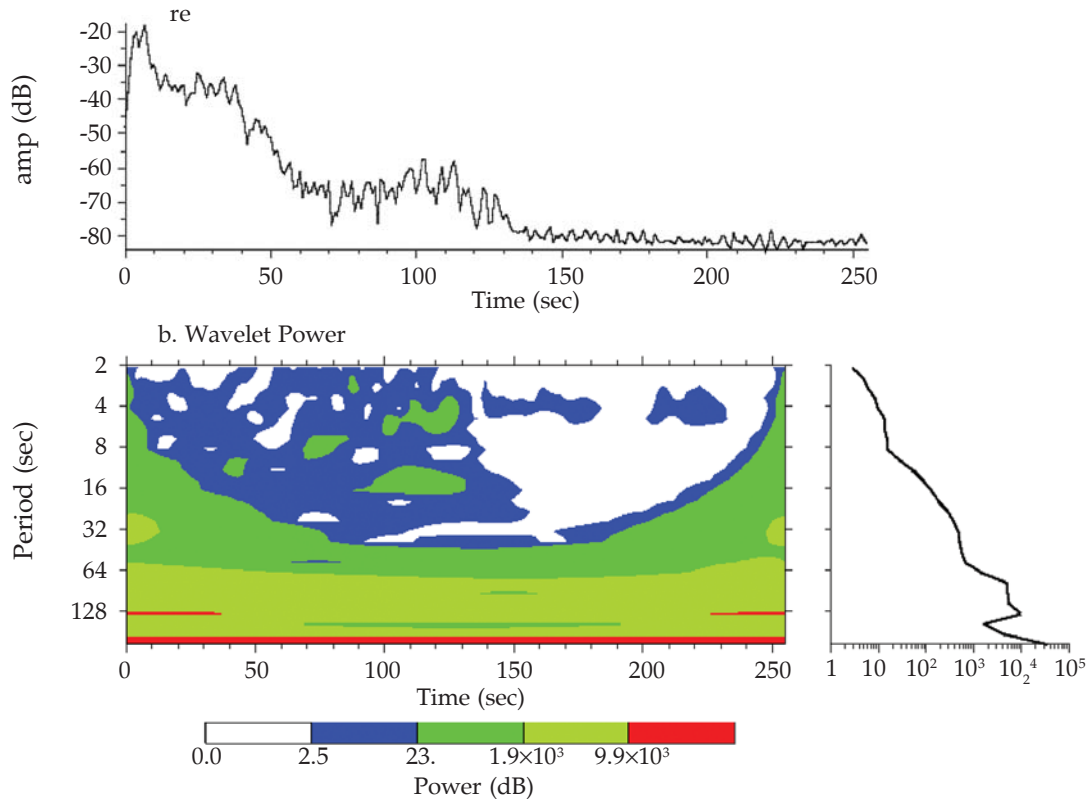
Fig. 3. Wavelet spectra of two tabla strokes ge and re

From table 3 it is clear that the most prominent power is not obtained immediately after strokes. This corroborated with the fact that tabla strokes have weak fundamental but strong mid frequency harmonics. Only Tabla 1 shows white contour of 95% confidence level while other tablas don't not show any white contour. Strokes of Tabla 1 are different from all others. Periodicity of change of power shows uniformity for all tablas. Difference in power and periodicity occur only due to stroke strength. Variance of power with period is more for free strokes than damped strokes.

8. CONCLUSION

With the help of wavelet tools we can precisely distinguish individual strokes which may lead to

(i) Categorization of tabla viz. (a) tabla 1 differs from other four tablas; (b) tablas with smaller diameter produce more harmonics than tablas of larger diameter; (c) stroke at the edge (3rd circle) produces weak resonance in the cavity of tabla and hence produce low energy sound while stroke at the 2nd circle produces strong resonance in the cavity of tabla and hence produce high energy sound .

(ii) Categorization of tabla strokes viz. (a) damped strokes are more powerful (energetic), higher irregularity in its harmonics and also posses larger number of harmonics than free strokes; (b) tabla strokes have weak fundamental. (c) attack peak reaches faster in free strokes than the damped strokes. (d) time to reach MPF is less for damped strokes compared to free strokes. Hence this percussion instrument is different from others.

(iii) Style of tabla player viz. (a) players of 1st and 2nd tablas made the strokes consistently; (b) style of strokes of player of 1st tabla is different than others. (c) also style of strokes is similar for the players of tabla 3 and 4. *So stroke technique plays a central* role in tabla repertoire, because it can be extensively elaborated, and because it is simpler to annotate than fully improvised sections. So table players make attempt to chose variety of strokes for improvisation.

(iv) Generate electronic tabla with synthesizing a wider variability of strokes.

(v) The two drums of the tabla produce many different timbres. Tabla strokes have unique harmonic and timbral characteristics at mid frequency range and have no uniqueness at low frequency ranges. This help it to facilitated the development and transmission of a sophisticated solo repertoire. In addition to the rhythmic complexity of tabla music, it is its timbral beauty and diversity that distinguish it from other percussion instruments.

(vi) It can be use for e-learning in which a amateur learner can compare their strokes with some standard strokes by analyzing the strokes.

ACKNOWLEDGEMENT

REFERENCE

[1] PARAG CHORDIA, "*Segmentation and recognition of tabla strokes*", CCRMA, Stanford university, Pchordia@ccrma.stanford.edu

[2] C.V. RAMAN, 1934. "The Indian Musical Drums", *Proc. Indian Acad. Sci.,* **1A**, 179-188.

[3] C.VRAMAN and SIVAKALI KUMAR, 1920. "Musical drums with harmonic overtones", *Nature*, **104**, 500.

[4] DAVID COURTNEY, 1999. "Psychoacoustics of the Musical pitch of Tabla" *Journal of SanGeet Research Academy*, Calcutta, India, **13** (1).

[5] R.N. GHOSH, 1922. "Note on Musical Drums", *Phys. Review*, **20**, 526-527.

[6] K.N. RAO, 1938. "Theory of the Indian Musical Drums", *Proc. Indian Acad. Sci.* **7A**, 75-84.

[7] B.S. RAMAKRISHNA, 1957. "Modes of Vibration of the Indian Drum Dugga or left hand Thabala", *J. Acoust. Soc. Am.* **29**, 234-238.

[8] T.S.AROJINI and A RAHMAN, 1958. "Variational Method for the Vibrations of Indian Drums" *J. Acoust. Soc. Am.,* **30**, 191-196.

[9] B.M. BANERJEE and D. NAG, 1991. "The Acoustical Character of Sounds from Indian Twin Drums", *ACUSTICA*, **75**, 206-208.

[10] C. VALENS, 1999-2004. "A Really Friendly Guide to Wavelets (C)", wavelets@polyvalens.com

[11] ROBI POLIKAR, 'The Wavelet Tutorial', Rowan University http://users.rowan.edu/polikar/wavelets/wttutorial.html

[12] N. FLETCHER and T. ROSSING, 1998. "The physics of musical instruments", *Springer, New York*.

[13] TAE HONG PARK, 2004. "Towards Automatic Musical Instrument Timbre Recognition", Ph.D. thesis, *Department of Music*, Princeton University.

[14] J. M. GREY, 1977. "Multidimensional Perceptual Scaling of Musical Timbre", *Journal of the Acoustical Society of America* **61**, 1270-1277.

[15] ANIRBAN PATRANABIS, KAUSHIK BANERJEE, RANJAN SENGUPTA and DIPAK GHOSH, 2011. "Objective Analysis of the Timbral quality of Sitars having Structural change over Time", *Ninaad (Journal of ITC Sangeet Research Academy)*, **25**, 1-7.

[16] CHRISTOPHER TORRENCE and GILBERT P. COMPO, "A Practical Guide to Wavelet Analysis", *University of Colorado, Boulder*, Colorado.

Engine Combustion Problem Diagnosis through Sound Power Measurement and Noise Analysis of the Diesel Engine

Aprajita Singh[1] and Mahavir Singh[2]
[1]*Krishna Institute of Engineering and Technology, Delhi Meerut Road, Ghaziabad*
[2]*CSIR-National Physical Laboratory, Dr. K. S. Krishnan Road, New Delhi*
e-mail: mahavir.acoustics@gmail.com

ABSTRACT

Noise reduction in an engine is the crucial phenomenon to have reduction in the pollution levels is the key parameter to investigate. In the noise prediction or reduction, sound power level; sound pressure, intensity mappings etc, are considered; however sound power level is of primary concern in diagnosing the combustion problem in an engine. Experimentation has been carried out on four stroke single cylinder water cooled diesel engine and investigations are made on sound power radiated by all its surfaces i.e., front, rear, left, right and top at various frequencies. The sound power level of the surfaces is noted at 1/3 octave frequency. From the sound power level sound power radiated by different surfaces at various frequencies are evaluated for three different load conditions. Maximum sound power is observed from our investigation in the frequency range of 200 Hz to 4 kHz. The 1/3 octave analysis elucidates maximum amplitude at 800 Hz, which is an indication of combustion problem generally, combustion problems fall in the band width from 600 Hz to 1200 Hz. Since combustion problem is a major problem in emanating noise, it usually reflects in all directions /sides of noise measurements around the engine.

1. INTRODUCTION

Noise is, to a great extent, purely subjective personal phenomena, perhaps an unwanted sound. Noise does, however, have two basic characteristics. The first is the physical phenomenon which can be measured and thus used in technical specification. The second is the psycho acoustical characteristic which attempts to judge the effect of noise on human beings. Sound and noise related aspects and the inherent relationship have been well discussed by earlier researchers. Engine combustion related noise and vibration aspects have been presented in literature.

Sound power radiated by various components of an engine are evaluated and ranked. The study is carried out to understand the engine noise characteristics of sound power radiation of the engine. The *two microphone sound intensity technique* has been used to locate major noise sources in an engine after ducting away the exhaust noise with the help of a long pipe.

Sound Power Level cannot be measured directly and evaluated from sound pressure measurements. Sound Power Level, since it is a measurement of noise unaffected by such factors as the engine's distance from the hearer, is used as the basic measurement for comparing noise levels of engines, as well as noise levels at different operating points of the same engine.

2. SOUND POWER LEVEL

In defining the noise generated by the engine, it is best to define the noise emanating from the source. This is called the Sound Power Level and is independent of the environment. Sound Power Level on a logarithmic scale is given as:

$$PWL = 10 \log (I/I_0)$$

where,

I = acoustic power of the source

I_0 = acoustic reference power i.e., 1 pW

Sound power of the control surfaces in different one-third octave frequency bands ranging from 200 Hz to 4 KHz and the percentage contribution of each frequency bands to the overall sound power of five surfaces are evaluated for all engine operating conditions. The magnitude of the sound power radiated from all surfaces of the engine in the 1/3 octave band center frequency range from 200 Hz to 500 Hz & 3150 Hz to 4000 Hz are low for all engine operating conditions compared with the frequency range 630 Hz to 2500 Hz. In this frequency range, acoustic power values are considerably higher at the frequency of 800 Hz in which the highest sound power values exist.

2. LITERATURE REVIEW

Physically, the sound intensity is energy vector that describes the amount of the sound energy passing through the observed surface as well as its direction. The sound intensity is the time-averaged product of the sound pressure (p) and particle velocity (v) [1, 2]

$$I = p. v$$

The acoustic diagnostics field, in which the sound intensity is applicable, was given as the examples whose results confirm the excused choice of the measurement method [3].

As an alternative to the sound pressure level measurement method, sound intensity was utilized to focus on the noise transmission through individual building elements.

Additionally, sound pressure measurements were conducted adjacent to the building elements, including windows, doors, walls and roof, to enable calculation of sound power levels. A comparison of the results achieved for the two methods is discussed [4].

4. EXPERIMENTATION

For the present study single cylinder four stroke water cooled direct injection diesel engine is used. It is installed in the engine test cell and is coupled with the eddy current dynamometer on a bed frame and the bed is mounted on the concrete floor. The exhaust line is ducted outside the room to isolate the aerodynamic noise so as to determine the engine surface radiation only in the experiment.

For three different loads, measurements are taken for investigating the effect of speed and load on sound intensity profile and sound power radiation of the test engine at the following load combinations at constant rated speed of 1500 rpm such as No load, 60% load & 90% load.

5. EXPERIMENTAL SETUP

Diesel engine with rated power 5.2 KW and rated speed of 1500 rpm is used for the present experiment shown in Fig.1. Since single cylinder DI diesel engine of about 0.661 liter capacity are widely used in stationary power sources in urban areas, powering agro-appliances in rural areas.

Two microphone instrument: The sound level meter B&K 2260 and the intensity probe used in the present experiment is B&K 2683 two- microphone intensity probe shown in Fig. 2. An 8 mm spacer is used.

It is required to develop the control surfaces, which enclose the sound source i.e. test engine in this case and make appropriate grids for intensity measurement.

Fig. 1. Experimental setup

Fig. 2. Two microphone instrument and Sound level meter.

Noise source identification :

Sound power of the control surfaces in different one-third octave frequency bands ranging from 200 Hz to 4 KHz and the percentage contribution of each frequency bands to the overall sound power of five surfaces were evaluated for all engine operating conditions.

6. RESULTS AND DISCUSSIONS

The summation of sound power in the specified frequency range contributes 82% to the total at 1500 rpm and no load condition and only the acoustic power in 800 Hz frequency band has 21% of total sound power produced by the test engine. This frequency range also contributes higher sound powers in other operating conditions showing the values of 85% at 1500 rpm & 60% load, 85% at 1500 rpm & 90% load condition. Out of these values, only the 800 Hz frequency band contributes 23% at 1500 rpm & 60% load, 24% at 1500 rpm & 90% load condition. These numerical figures indicate that almost all of the acoustic energy from the engine is released in this important frequency range from 630 Hz to 2.5 KHz and the critical frequency for the test engine is 800 Hz. The engine heterogeneity in combustion creates such a high order frequency which is source for the engine cylinder vibration. This frequency covers to 21 to 24% of total acoustic energy released by the engine in all operating conditions. Sound power distribution of different surfaces of test engine on this important frequency range at 1500 rpm & no load condition is shown in Fig. 3. And at 1500 rpm and 60% load operating conditions is shown in Fig. 4, and 1500 rpm and 90% load conditions is shown in Fig. 5 for clear comparison.

From figs. 3 to 5, it is observed that the critical frequency of all the five engine surfaces is 800 Hz and the significant frequency range of the engine lies in the frequency range between 630 Hz and 2500 Hz. In this range higher sound power values have been exhibited. For a particular frequency of 800 Hz, although the two main surfaces (engine front side and right side) produced the same acoustic power at idling condition (1500 rpm and no load), however, it is found that a great difference in sound power radiation between the two surfaces giving 162 μW by the front surface and 110 μW by the right side at 1500 rpm and 90% load condition. Results reveal that there is much difference of two surfaces it can be supposed that the sound power of front surface is more sensitive to the load than the right side at this critical frequency. It is noticed that the sound power radiation for the engine surfaces (Back side & Top side) is greatly increased from 1500 rpm & No load condition to 1500 rpm & 90% load condition, in the critical frequency range of 800 Hz. Sound power values of 42 μW & 21 μW are greatly increased to 135 μW and 58 μW respectively with an increase of 221% & 176%.
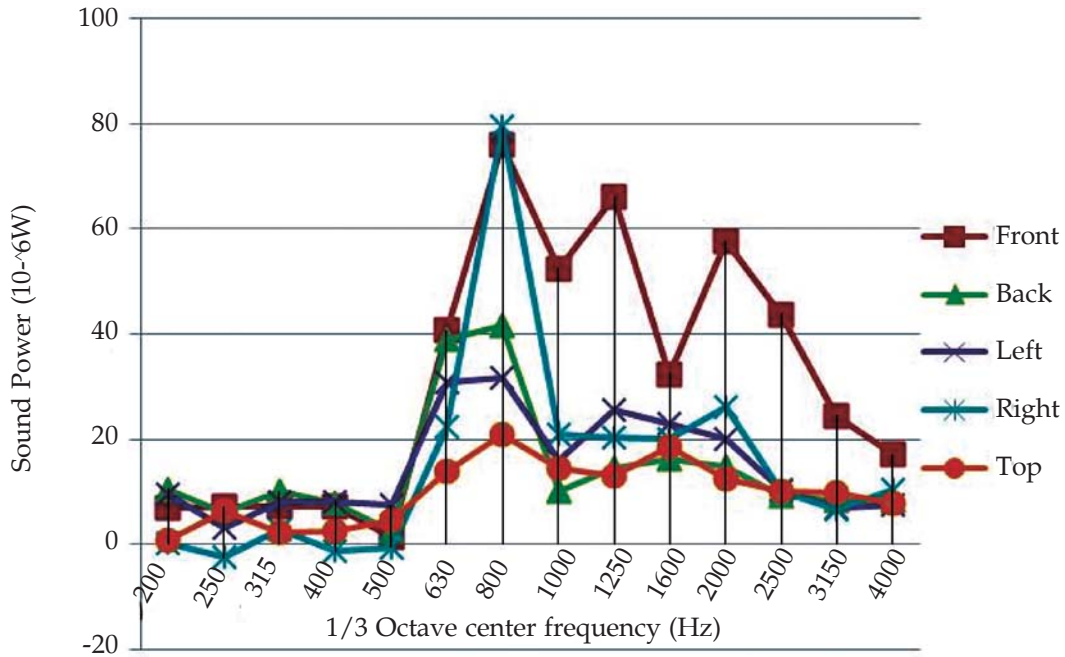
Fig. 3. Acoustic Power Distribution of Different Surfaces on
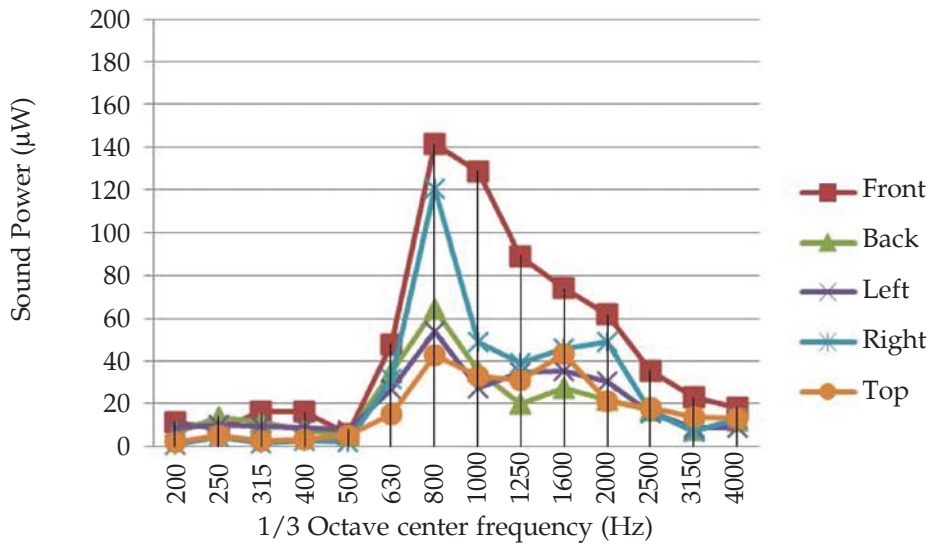1/3 octave band at 1500 rpm & No Load Torque
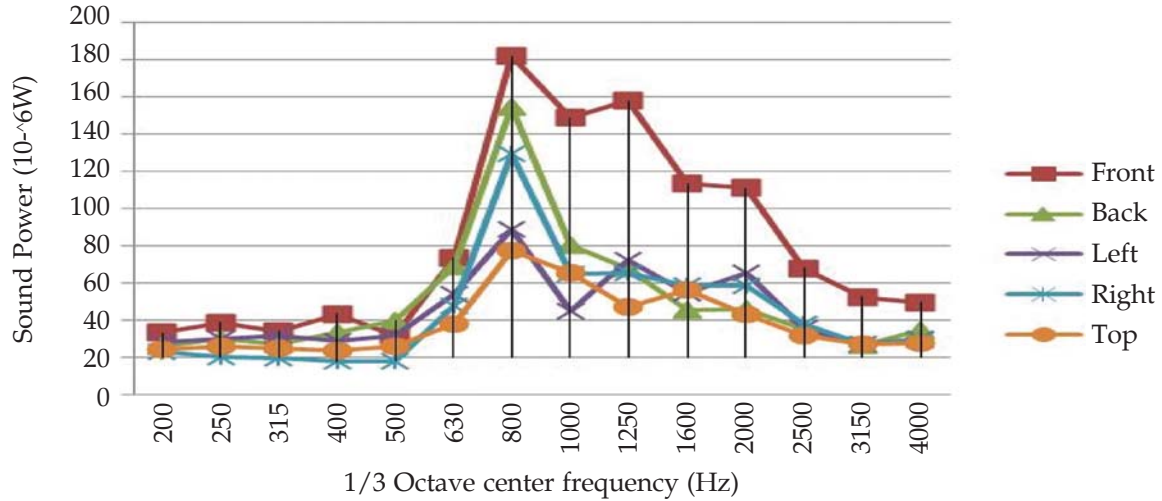

Fig. 4. Acoustic Power Distribution of Different Surfaces on 1/3 octave
Band at 1500 rpm & 60% Load Torque.

The total sound power radiated by the Diesel Engine in this frequency range at three different load conditions is plotted in Fig.6. Sound power in each frequency band represents summation of sound powers from five surfaces of the Diesel engine at the same frequency band. 800 Hz, 1/3 octave center frequency band is located as significant in its region both in Figs. 3, 4 & 5. Showing sound powers in this frequency are obviously higher, the significance is clearer in the overall engine sound power spectrum shown in Fig.6. especially at high load conditions (1500 rpm and 90% load).It can therefore be suggested that noise level of

Fig. 5. Acoustic Power Distribution of Different Surfaces on
1/3 octave band at 1500 rpm & 90% Load Torque

the test engine can be effectively reduced by tuning the structural vibrations of engine move away from the critical frequency mode (*i.e.* 800 Hz) and distribute to other frequency bands.
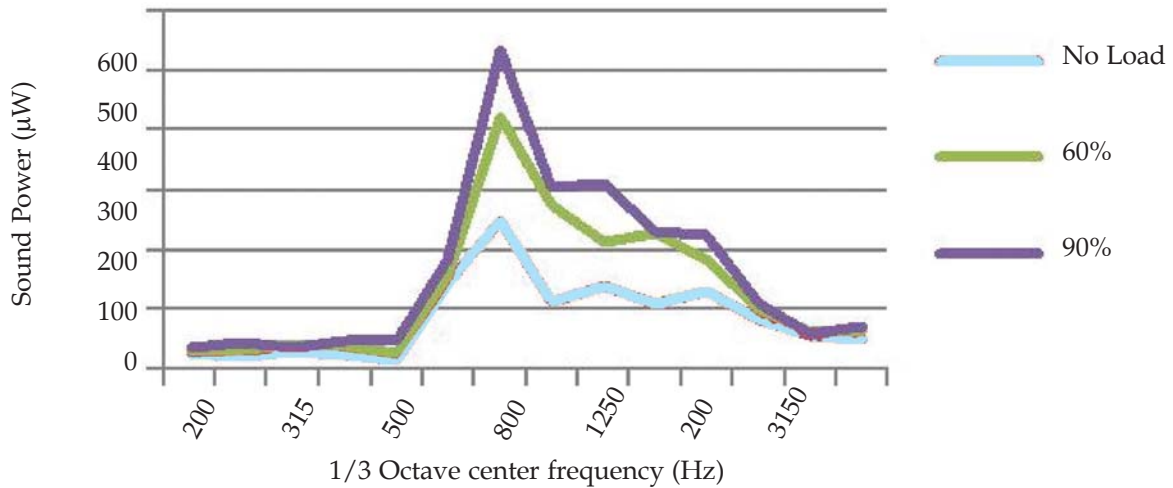

Fig. 6. Total Acoustic Power Distribution of Engine on 1/3 Octave
Band at 1500 rpm for various Load conditions.

7. CONCLUSIONS

From the investigations made it is found that:

■ Maximum spectral power is obtained at 800 Hz frequency, with the running condition of the engine has its frequency synchronizing with the 1/3 rd octave frequency of 800 Hz which may be a factor to cause failure of the engine component.

■ Care should be taken to overcome the synchronizing of the frequencies through its design or other factors.

8. ACKNOWLEDGMENTS

We thank the reviewers for their constructive suggestions which improved the paper considerably. Errors, omissions etc. that remain are, of course, our responsibility.

9. REFERENCES

[1] S. GADE, 1982. Sound Intensity (Part I). Technical Review No. 3, Bruel & Kjaer.

[2] S. GADE, 1982. Sound Intensity (Part II). Technical Review No. 4, Bruel & Kjaer.

[3] MOMIR PRAŠČEVIČ and DRAGAN CVETKOVIČ, 1997. Diagnostics of acoustic processes intensity measurement; *Working and Living Environmental Protection* **1** (2), 9 -16.

[4] LIU - YUE HUI, HAO - JI YONG, BI - FENG RONG and FU - LU HUA, 2002. HANG - Song Tao: Engine Noise Source Identification using Different Methods; Transactions of Tianjin University, **8** (3).

[5] L. CREMER and M. HECKL, 1988. Structure-borne sound - structural vibrations and sound radiation at audio frequencies - Second edition, *Springer-Verlag*.

[6] F.J. FAHY, 1998. Sound and structural vibration-radiation, transmission and response, Academic Press,1985 Genta, G., Vibrations of structures and machines; practical aspects Third Edition, *Springer Verlag, Berlin*.

[7] R. B. RANDALL, Y. REN and H. NGU, 1996. Diesel engine cylinder pressure recovery. Ren, Y. (1999) Detection of knocking combustion in diesel engines by inverse ?ltering of structural vibration signals. PhD dissertation, University of New South Wales. *Proceedings of ISMA21, KU Leuven, Belgium*, 847-856.

[8] Y. GAO and R. B. RANDALL, (1999) Reconstruction of diesel engine cylinder pressure using a time domain smoothing technique. *Mechanical Systems and Signal Processing*, **13** (5), 709-722.

[9] R. JOHNSSON, 2004. *Indirect measurement for control and diagnostics of IC engines*. Ph.D. thesis, Lule° a University of Technology.

Acoustical Society of India
(Regn. No. 65-1971)

Executive Council (2014 - 2016)

INFORMATION FOR AUTHORS

ARTICLES

The Journal of Acoustical Society of India (JASI) is a refereed publication published quarterly by the Acoustical Society of India (ASI). JASI includes refereed articles, technical notes, letters-to-the-editor, book review and announcements of general interest to readers.

Articles may be theoretical or experimental in nature. But those which combine theoretical and experimental approaches to solve acoustics problems are particularly welcome. Technical notes, letters-to-the-editor and announcements may also be submitted. Articles must not have been published previously in other engineering or scientific journals. Articles in the following are particularly encouraged: applied acoustics, acoustical materials, active noise & vibration control, bioacoustics, communication acoustics including speech, computational acoustics, electro-acoustics and audio engineering, environmental acoustics, musical acoustics, non-linear acoustics, noise, physical acoustics, physiological and psychological acoustics, quieter technologies, room and building acoustics, structural acoustics and vibration, ultrasonics, underwater acoustics.

Authors whose articles are accepted for publication must transfer copyright of their articles to the ASI. This transfer involves publication only and does not in any way alter the author's traditional right regarding his/her articles.

PREPARATION OF MANUSCRIPTS

All manuscripts are refereed by at least two referees and are reviewed by the Publication Committee (all editors) before acceptance. Manuscripts of articles and technical notes should be submitted for review electronically to the Chief Editor by e-mail or by express mail on a disc. JASI maintains a high standard in the reviewing process and only accept papers of high quality. On acceptance, revised articles of all authors should be submitted to the Chief Editor by e-mail or by express mail.

Text of the manuscript should be double-spaced on A4 size paper, subdivided by main headings-typed in upper and lower case flush centre, with one line of space above and below and sub-headings within a section-typed in upper and lower case understood, flush left, followed by a period. Sub-sub headings should be italic. Articles should be written so that readers in different fields of acoustics can understand them easily. Manuscripts are only published if not normally exceeding twenty double-spaced text pages. If figures and illustrations are included then normally they should be restricted to no more than twelve-fifteen.

The first page of manuscripts should include on separate lines, the title of article, the names, of authors, affiliations and mailing addresses of authors in upper and lowers case. Do not include the author's title, position or degrees. Give an adequate post office address including pin or other postal code and the name of the city. An abstract of not more than 200 words should be included with each article. References should be numbered consecutively throughout the article with the number appearing as a superscript at the end of the sentence unless such placement causes ambiguity. The references should be grouped together, double spaced at the end of the article on a separate page. Footnotes are discouraged. Abbreviations and special terms must be defined if used.

EQUATIONS

Mathematical expressions should be typewritten as completely as possible. Equation should be numbered consecutively throughout the body of the article at the right hand margin in parentheses. Use letters and numbers for any equations in an appendix: Appendix A: (A1, (A2), etc. Equation numbers in the running text should be enclosed in parentheses, i.e., Eq. (1), Eqs. (1a) and (2a). Figures should be referred to as Fig. 1, Fig. 2, etc. Reference to table is in full: Table 1, Table 2, etc. Metric units should be used: the preferred from of metric unit is the System International (SI).

REFERENCES

The order and style of information differs slightly between periodical and book references and between published and unpublished references, depending on the available publication entries. A few examples are shown below.

Periodicals:
[1] S.R. Pride and M.W. Haartsen, 1996. Electroseismic wave properties, *J. Acoust. Soc. Am.*, 100 (3), 1301-1315.
[2] S.-H. Kim and I. Lee, 1996. Aeroelastic analysis of a flexible airfoil with free play non-linearity, *J. Sound Vib.*, 193 (4), 823-846.

Books:
[1] E.S. Skudzryk, 1968. *Simple and Comlex Vibratory Systems*, the Pennsylvania State University Press, London.
[2] E.H. Dowell, 1975. *Aeroelasticity of plates and shells*, Nordhoff, Leyden.

Others:
[1]   J.N. Yang and A. Akbarpour, 1987. Technical Report NCEER-87-0007, Instantaneous Optimal Control Law For Tall Buildings Under Seismic Excitations.

SUMISSIONS

All materials from authors should be submitted in electronic form to the JASI Chief Editor: Dr Mahavir Singh, Acoustics, Ultrasonics & Vibration Section, CSIR-National Physical Laboratory, Dr. K. S. Krishnan Road, New Delhi-110 012 (email: mahavir@nplindia.org Tel: +91-11-4560.8317, Fax: +91-11-4560.9310). For the item to be published in a given issue of a journal, the manuscript must reach the Chief Editor at least twelve week before the publication date.

SUMISSION OF ACCEPTED MANUSCRIPT

On acceptance, revised articles should be submitted in electronic form to the JASI Chief Editor (mahavir@nplindia.org)